Antti Pitkäoja

ANALYSIS OF SORPTION-ENHANCED GASIFICATION FOR PRODUCTION OF SYNTHETIC BIOFUELS FROM SOLID BIOMASS

ACTA UNIVERSITATIS LAPPEENRANTAENSIS 996

Antti Pitkäoja

ANALYSIS OF SORPTION-ENHANCED GASIFICATION FOR PRODUCTION OF SYNTHETIC BIOFUELS FROM SOLID BIOMASS

Dissertation for the degree of Doctor of Science (Technology) to be presented with due permission for public examination and criticism in the Auditorium 1318 at Lappeenranta-Lahti University of Technology LUT, Lappeenranta, Finland on the 1st of December, 2021, at noon.

Acta Universitatis
Lappeenrantaensis 996

Supervisors Associate Professor (tenure track) Jouni Ritvanen
LUT School of Energy Systems
Lappeenranta-Lahti University of Technology LUT
Finland

Professor Emeritus Timo Hyppänen
LUT School of Energy Systems
Lappeenranta-Lahti University of Technology LUT
Finland

Reviewers Jukka Konttinen
Faculty of Engineering and Natural Sciences
Tampere University
Finland

Henrik Thunman
Department of Space, Earth and Environment
Chalmers University of Technology
Sweden

Opponent Jukka Konttinen
Faculty of Engineering and Natural Sciences
Tampere University
Finland

ISBN 978-952-335-746-4
ISBN 978-952-335-747-1 (PDF)
ISSN-L 1456-4491
ISSN 1456-4491

Lappeenranta-Lahti University of Technology LUT
LUT University Press 2021

Abstract

Antti Pitkäoja
Analysis of sorption-enhanced gasification for production of synthetic biofuels from solid biomass
Lappeenranta 2021
97 pages
Acta Universitatis Lappeenrantaensis 996
Diss. Lappeenranta-Lahti University of Technology LUT
ISBN 978-952-335-746-4, ISBN 978-952-335-747-1 (PDF), ISSN-L 1456-4491, ISSN 1456-4491

Anthrophonic greenhouse gas emissions have led to climate change. The transportation sector is one of the most significant greenhouse gas emitters. Mitigation of carbon dioxide (CO_2) emissions from transportation is a great challenge. Fossil CO_2 emissions of the transportation sector can be mitigated with the help of synthetic biofuels. Synthetic biofuels can be produced from biomass by combining the gasification process with the biofuel synthesis process. Sorption-enhanced gasification (SEG) is a promising indirect gasification process for the production of synthetic biofuels. The process has been demonstrated at a pilot-scale. However, a thorough understanding of the physical operation of the reactor still lacks. Establishing modelling capability is an essential step in the studying of new processes. Modelling enables cost-effective techno-economic feasibility evaluation of the process in different size scales before manufacturing the physical equipment.

In this thesis, the SEG is studied for the production of synthetic biofuels from biomass. The thesis consists of the development of modelling tools, a study of the physical operations of the process and the development of an industrial-scale reactor concept for the process. The goal of this thesis is to develop an industrial-scale SEG process for biofuel production. This goal is achieved by studying the process at a pilot-scale before the development of the industrial-scale reactor. A one-dimensional fluidised bed model frames were created for the pilot-scale and the industrial-scale processes. The models combine conservation of mass and energy with semi-empirical model equations for physical phenomena.

The model frame for the pilot-scale process was successfully validated against data from a 200kW_{th} pilot process and other studies in the literature. The model was applied to study balances of a dual fluidised bed SEG process. A quantitative understanding of the physical operation of the SEG process was obtained from the model validation. Based on this knowledge, an industrial-scale process concept was developed for synthetic dimethyl ether production. The designed industrial-scale reactor provides practical information to support industrial-scale plant design and assessing operational performance and cost.

Keywords: Sorption-enhanced gasification, gasification, biomass, fluidised bed, dual-fluidised bed, modelling

Acknowledgements

This work was carried out in LUT School of Energy Systems at Lappeenranta-Lahti University of Technology LUT, Finland, over the period of 2018–2021. The work was done in the scope of the "Flexible dimethyl ether production from biomass gasification with sorption-enhanced processes" project. The funding received from European Union's Horizon 2020 research and innovation programme is acknowledged.

I would like to express my special gratitude to my first supervisor, Professor Jouni Ritvanen, for his excellent guidance and support. I would like to express my sincere gratitude to Professor Timo Hyppänen for his guidance and for offering me the possibility for this research.

I would like to thank you, Professor Jukka Konttinen from the Tampere University and Professor Henrik Thunman from the Chalmers University of Technology, for reviewing this thesis and for valuable comments that helped improve this thesis.

I would also like to thank Mrs. Selina Hafner and Professor Günter Scheffknecht from the University of Stuttgart, and my colleagues, D.Sc. Kari Myöhänen, D.Sc. Markku Nikku, Mr. Eero Inkeri and Mr. Hannu Karjunen.

Finally, I would like to thank you, Anna, for your support, care and patience during the past years.

Antti Pitkäoja
December 2021
Lappeenranta, Finland

Contents

List of publications

Publication I
Ritvanen, J., Pitkäoja, A., Sepponen, S., Hyppänen, T., (2018). Modelling of Sorption-enhanced Biomass Gasification in Dual Fluidized Bed Process. *Proceedings of 23rd International Conference on Fluidized Bed Conversion*, pp. 528-535. Seoul.

Publication II
Pitkäoja, A., Ritvanen, J., Hafner, S., Hyppänen, T., Scheffknecht, G. (2020). Simulation of a sorbent enhanced gasification pilot reactor and validation of reactor model. *Energy Conversion and Management*, 204, 112318, pp. 1-14.

Publication III
Pitkäoja, A., Ritvanen, J., Hafner, S., Hyppänen, T., Scheffknecht, G. (2021). Numerical modelling of sorption-enhanced gasification: Development of a fuel decomposition model. *Fuel*, 289, 119868, pp. 1-10.

Publication IV
Ritvanen, J., Myöhänen, K., Pitkäoja, A., Hyppänen, T. (2021). Modeling of industrial-scale sorption enhanced gasification process: One-dimensional simulations for operation of coupled reactor system. *Energy*, 226, 120387, pp. 1-14.

Publication V
Pitkäoja, A., Ritvanen, J., Hafner, S., Hyppänen, T., Scheffknecht, G. (2021). Modeling of Sorbent Enhanced Gasification Utilizing Waste-Derived Fuel. *Proceedings of 13th International Conference on Fluidized Bed Technology*, pp. 479-484. Vancouver - Virtual conference.

Authors contribution

The author is the principal author and investigator in Publications II and III. The author participated in the model frame and sub-models development, conducted the simulations and model validation, interpreted the results, and wrote the manuscript and revised it. In Publication V, the author is the principal author and investigator. The author modified the model frame for the needs of the study, conducted the simulations and model validation, interpreted the results, and wrote the manuscript and revised it. Selina Hafner provided measurements for the pilot reactor in Publications II, III and V. The author participated in analysing data from the pilot reactor and analysis of other experiments used for modelling the system. In Publication I, the author conducted the simulations and post-processed the results. In Publication IV, the author participated in the development of the methodology

and preparing the manuscript. The author was the principal investigator of physical phenomena related publications (Publication II, III and V). The author's main contribution to Publication IV was transferring physical phenomena producing the physical operation characteristics of the SEG to the industrial-scale model. The understanding of the physical phenomena producing the physical operation of the process created the basis for the development of the industrial-scale process in this thesis.

Nomenclature

ΔH	reaction enthalpy	$\mathrm{J/mol}, \mathrm{J/kg}$
A	area	m^2
A_m	reaction surface area	m^2
C	concentration	$\mathrm{mol/m}^3$
c_p	specific heat capacity	$\mathrm{J/(kg \cdot K)}$
$C_{\mathrm{CO_2,eq}}$	CO_2 equilibrium concentration	$\mathrm{mol/m}^3$
D	dispersion coefficient	m^2/s
dW	mass fraction difference	$\mathrm{kg_i/kg_y}$
E	energy	W
h	enthalpy	$\mathrm{J/kg}$
J	interphase diffusion	$\mathrm{kg/(m}^3 \cdot \mathrm{s)}$
k	chemical reaction rate coefficient	$1/\mathrm{s}$
k'	chemical reaction rate coefficient	$\mathrm{m}^3/\mathrm{(mol \cdot s)}$
K_wgs	water-gas shift equilibrium coefficient	$-$
M	molar mass	$\mathrm{g/mol}$
n	mole	mol
p	pressure	Pa
Q	mass flow rate	$\mathrm{kg/(m}^3 \cdot \mathrm{s)}$
q_m	mass flow rate	$\mathrm{kg/s}$
R	chemical reaction rate	$\mathrm{kg/(m}^3 \cdot \mathrm{s)}$
R_i	ideal gas constant	$\mathrm{J/(mol \cdot K)}$
S	source term	$\mathrm{kg/(m}^3 \cdot \mathrm{s)}, \mathrm{kg/s}$
T	temperature	K
t	time	s
u	velocity	m/s
W	mass fraction	$\mathrm{kg_i/kg_y}$
y	mole fraction	$\mathrm{mol_i/mol_y}$
z	distance	m

Subcript

ar	as-received
b	bubble
$char$	char
$conv$	convection
daf	dry ash free
db	dry basis
$devol$	devolatilisation
e	emulsion
f	fuel
g	gas

hs	heat source or sink
ht	heat transfer
i	index
j	index
k	index
pg	permanent gas
r	reaction
s	solid
tar	tar
w	wake
x	index

Greek

γ	parameter	$-$
ρ	density	$\mathrm{kg/m^3}$

Abbreviations

1D	one-dimensional
3D	three-dimensional
AER	absorption-enhanced reforming
BFB	bubbling fluidised bed
C_xH_y	hydrocarbon
CFB	circulating fluidised bed
CGE	cold-gas efficiency
DME	dimethyl ether
LHV	lower heating value
S/C	steam-to-carbon
SEG	sorption-enhanced gasification
SNG	synthetic natural gas

1 Introduction

1.1 Background

Anthropogenic greenhouse gas emissions have led to climate change by increasing global average temperature. Warming of the climate has been estimated to be 1.5°C before 2050 with the current development of greenhouse gas emissions (IPCC, 2018). The Paris agreement, signed in 2015, mutual understanding among 190 countries reached that global warming should be kept well below 2°C compared to the pre-industrial levels, and the higher goal of 1.5°C should be pursued (European commission). Reduction of greenhouse gas emissions is necessary to accomplish the 2°C and 1.5°C targets. The CO_2 accounts for the largest share of all greenhouse gas emissions. The development of CO_2 emissions from the main sources is shown in Figure 1.1 from 1990 to 2018. In this timeline, transportation has been one of the most significant CO_2 emitters globally, with a steady yearly increase since 1990.

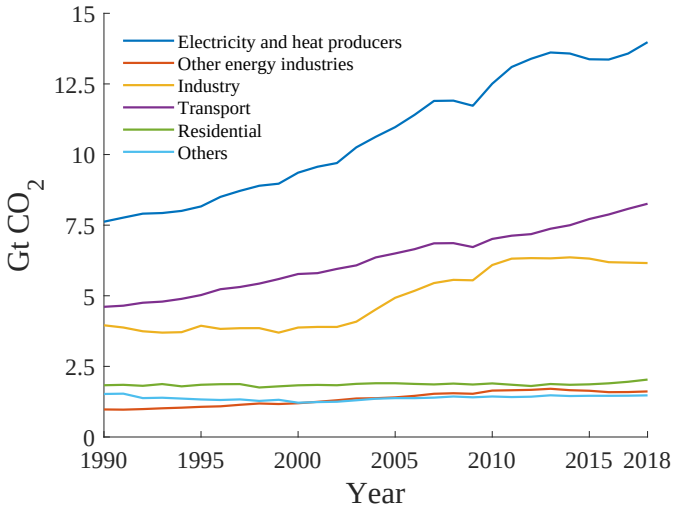

Figure 1.1: Global historic CO_2 emissions by sector (Data source: Energy data - CO_2 emissions by International Energy Agency (IEA)).

Transportation represented 30 % of the European Union's (EU-28) CO_2 emissions in 2018 (IEA). The CO_2 emissions in 2018 were 929 Mt. The CO_2 emissions from transportation in Finland were in the same year 12 Mt, representing a quarter of Finland's CO_2 emissions (IEA). By 2030, the European Union aims to reduce greenhouse gas emissions at least 40 % compared to the 1990 level (European Council, 2014). The current European Union's legislation requires Finland to reduce its greenhouse gas emissions from the effort sharing sector by 40 % before 2030 compared to 2005 (Ministry of Transport and Communications, 2020). On the national level, Finland has committed to reducing transportation's

greenhouse gas emissions (excluding aviation) by 50 % compared to 2005 (Ministry of Transport and Communications, 2020). Complying with the emission reduction target set by the government requires the use of biofuels and electric vehicles on road transportation (Nylund et al., 2015). The use of biofuels is essential for decreasing the emissions from heavy traffic, where broad electrification possibilities are limited.

A study made by Technical Research Centre of Finland (VTT) (Nylund et al., 2015) looked for possibilities to reduce CO_2 emissions by 40 % before 2030 in Finland. The study estimated that increased biofuel production could reduce emissions by the 40 %. The study estimated that an additional 600 ktoe/a biofuel production in Finland would be sufficient to reduce the emissions and the total consumption of biofuels in road transportation of 1000 ktoe/a would be needed. IEA report (IEA Bioenergy, 2020) evaluated the need for biofuels in Finland to be 1100 ktoe/a by the year 2030. The scenario accounted for the policies currently in action. The scenario assumed registration of electric vehicles to increase steadily and the share of electric vehicles to be 30 % of registered new vehicles at 2030. The report indicated the need for biofuels to decrease after the peak consumption at 2030 due to a steady increase in the electric vehicles fleet.

The biofuels can be produced from a great variety of biomass feedstocks. Based on the biomass feedstock, the biofuels are divided into different generations (Puricelli et al., 2021). Typical first-generation biofuels are ethanol and biodiesel (FAME) produced from edible biomass sources and energy crops, e.g. corn or palm oil. Second-generation synthetic biofuels possess a wide range of non-edible feedstocks (e.g., forest residues, straw and waste). Whereas first-generation biofuel production technologies are well established, second-generation technologies are under development. A study of the sustainability of various first and second-generation fuels was conducted by Volvo (Volvo, 2014). The sustainability analysis showed dimethyl ether (DME) as one of the most promising synthetic second-generation fuels for heavy road transportation. The fuels were evaluated based on climate impact, energy efficiency, efficiency of land use, fuel potential, vehicle adjustment, fuel costs, and based on the needed fuel infrastructure. The liquefied DME is a potential alternative for fossil diesel fuel. Diesel-powered vehicles can be converted for DME use with minor modifications of combustion technology.

The strong forest-based industry in Finland enables domestic synthetic biofuel production from forest industries side-streams. In 2019, the Finnish forest industry used 16.7 million m^3 of wood-based side-streams for energy production (Official Statistics of Finland (OSF)). The share of forest-residues was 3.2 million m^3. The available energy in the forest-residues for biofuel production is 600 ktoe/a based on the wood chips energy content (2.2 MWh/m^3, 35 % moisture content (Alakangas et al., 2016)). Consequently, the forest residues alone have potential to contribute to the future bioenergy demand in road transportation. The production potential of biofuels from forest industries side-streams, such as the forest-residues, can be expected to increase in the future due to possibilities for a sustainable increase in wood logging (Finnish Forest Industries).

The main process equipment of a biofuel synthesis are biomass dryer, gasifier, producer gas reformer or tar removal process, gas cleaning and conditioning processes, and synthesis reactor. Indirect steam gasification is a promising gasification technology as part of the synthesis processes. The technology has been investigated for production of the feed gas for Fischer-Tropsch liquids, synthetic natural gas (SNG) and H_2 synthesis from biomass (van der Meijden et al., 2013; Rauch et al., 2013; Thunman et al., 2018; Kurkela et al., 2019). A raw gas H_2/CO molar composition of the indirect process is around two or below (Kurkela et al., 2008, 2019). Therefore, synthesis applications with H_2/CO ratio requirement around two, e.g. production of Fischer-Tropsch liquids, are favourable for the process. Synthesis processes requiring a higher H_2/CO ratio, an additional gas conditioning after the gasifier is necessary with a separate water-gas shift reactor. When gasifier raw producer gas H_2/CO composition is below the requirements of the synthesis, gas modification with a separate water-gas shift reactor is required to increase the H_2/CO composition and control the gas composition for the synthesis. Sorbent-enhanced gasification (SEG) is an advanced indirect gasification process. The operation principle of the SEG process is similar to the indirect gasification process. The main difference between the traditional indirect process and the SEG is related to the bed material's behaviour in the process. In the SEG process, a bed material that absorbs CO_2 formed in the gasification is used. The CO_2 absorption enhances H_2 production of the water-gas shift reaction, and up to 75 vol-% content of hydrogen can be achieved for the producer gas (Hafner et al., 2021). Synergy exists between the CO_2 capture and the water-gas shift reaction. The synergy enables the adjustment of producer gas composition in the gasifier by adjusting the gasifier's operation parameters, such as the operating temperature. The synergy of the reactions enables tailoring of produce gas composition for different end-uses by altering process parameters. The module ($M = (y_{H_2} - y_{CO}) / (y_{CO} + y_{CO_2})$) is used to describe the gas composition. The appropriate gas module has been demonstrated for DME, methanol and SNG synthesis for the gasifier's raw gas (Hafner et al., 2021). Compared to indirect gasification, the production of synthetic fuels is possible at lower operating temperatures of the gasifier. Thus, making the SEG process more energy efficient. A part of the biomasses carbon is captured in the gasifier and transported to the combustor. This physical operation of the process allows for the production of carbon-negative biofuels when post-combustion carbon capture is utilised at the combustor's side.

Economic and technical challenges are related development of new technologies. The SEG process is aimed at the production of thermochemical biofuels. However, the economic competitiveness of fossil fuels is still better than that of biofuels (IEA Bioenergy, 2020). Nevertheless, in light of climate change, there is an urgent need for developing alternative fuel solutions for mitigating the CO_2 emissions of road transportation. In particular for the needs of heavy transportation (Nylund et al., 2015). The SEG concept has been proven in various pilot-scale reactors (Fuchs et al., 2019b). An industrial-scale demonstration of the SEG process still absences due to the economic and technical challenges. Technical challenges related to the scaling of the process. On the industrial-scale, there is the uncertainty of the SEG processes performance, the ambiguity of the suitable reactor design, uncertainty about the impact of process parameters on reactor's operation,

and many other similar challenges to be resolved before the demonstration. The modelling can be seen as a bridge between the pilot-scale and industrial-scale demonstrations of the process. The modelling allows studying the physical operation of the pilot-scale process and phenomena producing the operation characteristics. The observed physical phenomena can be transferred to the reactor's industrial-scale simulations. The simulation are essential in designing an industrial-scale reactor concept with a good performance for a wide range of operational conditions. The industrial-scale demonstration poses significant financial risks. The modelling plays a crucial role in the transition between the scales to minimise the demonstration's financial risks with a safe and cost-effective way to evaluate a process's technical and economical feasibility before manufacturing the physical equipment.

1.2 Objectives of the thesis

The development of a modelling tool is an essential step in the development of new processes. In this thesis, modelling capability to model physical operations in sorption-enhanced gasification is established. The developed models allow studying the process from the pilot-scale to the industrial-scale with typical process configurations. This capability enables studying the physical operation of the process from a pilot-scale reactor and allows developing the industrial-scale reactor concept for a DME production based on the pilot-scale studies. The modelling capability allows studying an industrial-scale process's performance to support more reliable cost estimates for financial arguments.

The following objectives have been set for this thesis:

- To establish modelling capability to study sorption-enhanced gasification with the physical phenomena-based approach. One-dimensional semi-empirical model frames for sorption-enhanced gasification are developed for bubbling fluidised bed (BFB) and circulating fluidised bed (CFB) reactors in which physical phenomena of sorption-enhanced gasification are included.

- To develop a pilot-scale model based on specifications of a pilot reactor to study physical operations in the sorption-enhanced gasification and to validate the model against measurements of the pilot reactor.

- To study the impact of the gasifier's operating parameters on gasifiers producer gas quality and the dual fluidised bed system's operation. To couple the validated gasifier model to a combustor model, and to simulate the dual fluidised bed gasification process. Impact of gasifier's operation parameters to overall performance of the dual fluidised bed system is studied.

- To develop an industrial-scale reactor concept for the sorption-enhanced gasification process based on studied physical phenomena. The performance of the industrial-scale gasifier is evaluated with the developed model for DME production.

1.3 Outline of the thesis

Contents of this thesis consist of three parts: (a) review of state-of-the-art (Chapter 2), (b) description of the applied methodology for reactor modelling (Chapter 3), and (c) discussion on results concerning physical phenomena based modelling of the process (Chapters 4, 5 and 6). Chapter 2 provides the theoretical background for this work. This chapter reviews the latest scientific knowledge regarding the sorption-enhanced gasification process. The review consists of experimental data and modelling methodologies applied for sorption-enhanced gasification. Chapter 3 describes the modelling methodology used in this thesis. Model frames developed for the sorption-enhanced gasification are described. Two model frames with BFB and CFB hydrodynamics implemented are described. These model frames are applied for modelling studies of pilot-scale and industrial-scale reactors. Chapter 4 presents the application of a model frame to the simulation of a pilot reactor. The BFB model frame described in Chapter 3 is applied for modelling. A pilot-scale model is developed based on the specification of the pilot gasifier. The model validation against measurements of the pilot reactor is presented. Based on the conducted model validation, analysis of physical operation of sorption-enhanced gasification processes are discussed. The simulations results are also compared against other studies available in the literature to obtain broader picture of the processes operation. Chapter 5 describes the application of models into studying of a pilot-scale dual fluidised bed system. The validated BFB gasifier model is coupled with a CFB combustor model to simulate balances of the dual fluidised bed reactor system. The impact of the gasifier's process parameters on producer gas quality is investigated. Also, the effect of the process parameters on the overall performance of the full-loop process is assessed. Chapter 6 presents the development of an industrial-scale reactor concept for the sorption-enhanced gasification process. The performance of the industrial reactor concept is evaluated for DME production. The CFB model frame described in Chapter 3 is applied for modelling. The reactor concept presented in this chapter is based on quantitative understanding of physical operation of the SEG reactors obtained by validation work presented in Chapter 4. Chapter 7 concludes the thesis, presents scientific contributions and gives recommendations for possible further research work.

2 State-of-the-art

This chapter begins by introducing sorption-enhanced gasification and the physical characteristics of the gasification process. The introduction is followed by a review of modelling approaches for fluidised bed reactors. Finally, state-of-the-art modelling of sorption-enhanced gasification is reviewed. This chapter's contents form an overall view of scientific knowledge related to sorption-enhanced gasification and fluidised bed reactor modelling approach to establish this thesis's research field.

2.1 Sorption-enhanced gasification

Sorbent-enhanced gasification is an indirect steam gasification process enhanced by in-situ CO_2 capture in the gasification reactor. The CO_2 capture enhances H_2 production of water-gas shift reaction. A simplified schematics of the coupled reactor process is shown in Figure 2.1.

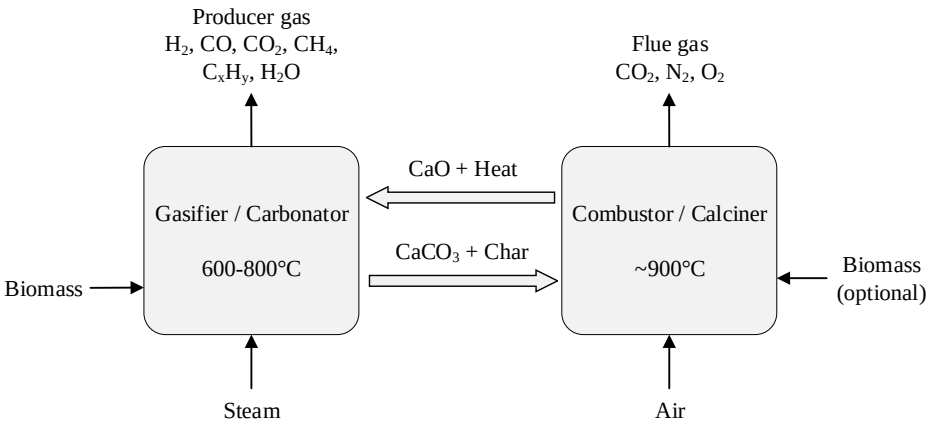

Figure 2.1: Sorption-enhanced gasification process.

The reactor system consists of two reactors, a gasifier and a combustor. Between the reactors, there is a continuous exchange of material flows. The SEG belongs to a family of looping processes and is closely related to the calcium looping process. The SEG process's physical operation is limited by the physical properties of the used sorbent. Likewise, in the calcium looping process, limestone (CaO) is used for CO_2 capture in the SEG process. Therefore, similar physical restrictions of the limestone are encountered in the SEG process as with the calcium looping process. Cyclic carbonation and calcination occur in the system. In the gasifier, limestone is carbonated and in the combustor calcined. In this cyclic process, the combustor's flue gas is enriched with CO_2, and the CO_2 content of gasifiers producer gas is decreased. The enhanced H_2 production is the result

of the synergy of water-gas shift and CO_2 capture. The synergy enables the tailoring of the producer gas for different end-uses by altering the gasifier's operating temperature and process parameters. At lower operation temperatures, over 75 % H_2 concentration for producer gas as a dry basis is achieved (Hafner et al., 2021), while increasing the temperature enables feed gas production for biofuel synthesis processes.

A review of the experimental data concerning the SEG is conducted. The chapter discusses process development phases, the main physical characteristics of the process, and the published experimental data. The review forms the experimental background for the model development and validation in this thesis.

2.1.1 Process development: A historical perspective

Curran et al. (1967) introduced the concept of sorption-enhanced gasification for coal gasification. The process concept was designed to produce a gaseous feed gas for SNG synthesis using CO_2 absorption in the presence of CaO. The study of the process concept was motivated by a need for developing an oxygen-free process, which can produce a high heat value gas from coal and substitute a part of the demand for natural gas. The process was operated with a bed formed from char and used steam as a gasification agent. The sorbent material was fed through the reactor in the vertical direction to capture the CO_2 from the producer gas. The used sorbent was transported to a separate regenerator and was regenerated by removing the CO_2 from it. Later, this same process concept was applied in the HyPr-Ring process for H_2 production from coal (Lin et al., 2005).

Curran's CO_2 acceptor process and the HyPr-Ring process were based on the use of coal as fuel and upgrading the quality of gas for CH_4 synthesis or producing H_2 from the coal. In both cases, the used fuel was fossil-based. The study of sorption-enhanced gasification processes with biomass has been conducted in Europe under various names: absorption-enhanced reforming process (AER), sorption-enhanced reforming (SER), and later sorption-enhanced gasification (SEG). The AER process based on dual fluidised bed gasification was introduced for biomass gasification at the Technical University of Wien (TUW) (Soukup et al., 2009). The process consisted of an interconnected gasifier and combustor. The process's gasifier is operated as a carbonator and the combustor as a regenerator (calciner). The AER concept was demonstrated to produce H_2 enriched producer gas compared to indirect gasification without the CO_2 capture (Soukup et al., 2009). The AER process achieved 71 % H_2 concentration as a dry basis for producer gas in the study. The experiment was conducted with the so-called classic 100 kW_{th} TUW process. At the University of Stuttgart, two AER concept-based pilot reactors in 20 kW_{th} and 200 kW_{th} thermal powers exist (Poboss et al., 2012; Hawthorne et al., 2012). The process design of these reactors is similar to the classic pilot in TUW. Data concerning producer gas composition on a wide temperature range was published by Poboss (2016) and Armbrust et al. (2014) from the University of Stuttgart reactors. Armbrust et al. (2014) in their study, discussed that the SEG process could be used as part of a wide range of applications, including gas production for fuels cells and production of synthetic chemicals and

fuels from it.

An advanced AER reactor design was introduced by Müller et al. (2017) from the 100 kW_{th} classic TUW process. A new freeboard design was introduced in the advanced gasification reactor. Demonstration of the AER concept with the advanced reactor design was done by Schmid et al. (2017). The authors studied producer gas composition change in a temperature range of 580°C to 800°C, obtaining similar composition to previous studies (Poboss, 2016; Armbrust et al., 2014). According to Fuchs et al. (2019b), in the advanced reactor the modified freeboard increases producer gas contact with the limestone, and therefore it decreases the tar concentration in the advanced reactor compared to the reactors similar to the classic TUW process. Fuchs et al. (2019b) demonstrated the difference by comparing tar concentrations.

The focus of the first AER studies was mainly on H_2 production from biomass (Pröll and Hofbauer, 2008; Pfeifer et al., 2009; Müller et al., 2011; Hawthorne et al., 2012). Armbrust et al. (2014) widened the discussion about AER's suitability as part of larger process concepts. A similar suggestion was made by Martínez and Romano (2016), who recognised the AER's potential as part of the biofuel production processes. Based on modelling, Martínez and Romano (2016) suggested that the process could be utilised to produce bio-SNG and Fischer-Tropsch liquids. Experimental demonstration in a pilot-scale facility followed (Hafner et al., 2018, 2021) where the process was demonstrated suitable for feed gas production for DME synthesis.

As discussed above, the AER process has been investigated in several pilot-scale reactors; however, continuously operating industrial-scale facility has not been developed. The concept has been briefly demonstrated on semi-industrial scale $8MW_{th}$ facilities in Gussing and Oberwart (Fuchs et al., 2019b). A dual fluidised bed gasifier is operated in both facilities as part of the gas engine cycle to produce combined heat and power. The facilities consist of a BFB gasifier and a fast fluidised combustor following similar design principles as the smaller dual fluidised bed facilities.

2.1.2 Lime-enhanced gasification

Sorbent-enhanced gasification requires using a bed material that can absorb CO_2 in the gasifier and be regenerated in the combustor. The use of sorbent to capture the CO_2 enhances H_2 production of the water-gas shift reaction in the gasifier. Limestone is often used as the bed material in the process. The limestone is low costs material, which has high mechanical stability (Koppatz et al., 2009). Calcined limestone is also known as a tar reforming catalyst in gasification, and therefore, it reduces producer gas tar concentration (Koppatz et al., 2009). Limestone is thermodynamically and kinetically good metal oxide candidate for CO_2 capture at high temperatures (Feng et al., 2007).

The operation range of the SEG process is around 600-800°C. Increasing the operating temperature from 600°C towards 800°C gradually alters the process's operating charac-

teristics towards indirect gasification. Sorbent-enhanced operation characteristics exist at the lower end of the temperature range in which the limestone carbonation reaction significantly decreases CO_2 concentration in the gasifier. The low CO_2 concentration affects the H_2 production of the water-gas shift reaction by changing the equilibrium's balance towards producing the reaction products:

$$H_2O + CO \longleftrightarrow CO_2 + H_2. \tag{2.1}$$

As a result, the H_2 production from the reaction is increased. At low operating temperatures, the most of the formed CO_2 is captured by limestone. The differences in producer gas composition between the SEG and the indirect gasification are shown in Table 2.1. In the SEG; the increased H_2 production also decreased CO concentration since the water-gas reaction consumes the CO.

Table 2.1: Comparison of producer composition of sorption-enhanced gasification and indirect gasification (Soukup et al., 2009)

Component	Indirect gasification	Sorption-enhanced gasification
H_2, vol-$\%_{db}$	36-42	55-71
CO, vol-$\%_{db}$	19-24	5-11
CO_2, vol-$\%_{db}$	20-25	7-20
CH_4, vol-$\%_{db}$	9-12	8-13
C_2H_4, vol-$\%_{db}$	2.0-2.6	1.4-1.8
C_2H_6, vol-$\%_{db}$	1.3-1.8	0.3-0.6
C_3, vol-$\%_{db}$	0.3-0.6	0.1-1.0
H_2O, vol-%	30-45	50-60

The change of SEG's operation characteristics towards indirect gasification is caused by thermodynamics of the sorbent. The limestone's reaction equilibrium determines, whether carbonation reaction or calcination reaction occurs in the process. At low operation temperatures, the CO_2 captures occurs by the limestone carbonation. At elevated operating temperatures, the CO_2 capture is reduces because of higher equilibrium concentration for the CO_2. The carbonation reaction in the increased temperatures is possible if the local CO_2 concentrations in the gasifier are higher than the equilibrium concentration. Therefore, a relatively high CO_2 concentrations are commonly observed at higher operating temperatures, where the equilibrium limits the CO_2 capture. The decreased CO_2 capture inhibits H_2 production of water-gas shift reaction. Consequently, the sorbent-enhancement requires operating the process in a temperature region where the carbonation reaction is active. This temperature region for the limestone is in Figure 2.2 on the left side of the CO_2 equilibrium at low operating temperatures.

The limestone enhances H_2 production by CO_2 capture and acts as a reforming catalyst for tars. The tars are a typical product of biomass gasification. The tars in a biomass

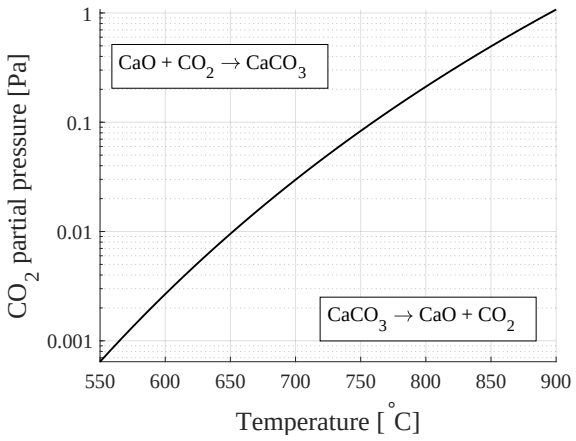

Figure 2.2: Equilibrium concentration of CO_2 for limestone (Stanmore and Gilot, 2005).

gasification process are formed from various hydrocarbon species, and often, the word tar refers to benzene and other high molar mass hydrocarbon species. The tars can be harmful substances for downstream processes because they can condense on cold surfaces and can cause blockages. The downstream processes often require high purity of the producer gas, and the tars are typically removed from the producer gas by catalytic reforming.

Calcined limestone has been demonstrated to influence the tar concentration in a post-gasifier gas cleaning section (Delgado et al., 1997) and when used as the bed material in the gasifier (Koppatz et al., 2009; Udomsirichakorn et al., 2013, 2014). However, after the limestone is carbonated, the material's catalytic influence is inhibited (Simell et al., 1995). The impact of limestone as bed material is highlighted in a study by Soukup et al. (2009). Focus of this study was on investigating the effect of limestone-containing bed materials in the AER process on tar production. Despite the lower gasification temperatures in the AER process, the tar content was observed five times lower compared to indirect gasification operated at higher temperatures. Though, the tar content of the producer gas is typically higher at lower operating temperatures (Mayerhofer et al., 2012). Typical tar amounts of different biomass gasifiers are listed in Table 2.2.

Table 2.2: Tar concentration in various biomass gasifiers.

	Indirect gasification (Soukup et al., 2009)	Sorption-enhanced gasification (Soukup et al., 2009)	Steam-blown BFB gasification (Gil et al., 1999)	Air-blown BFB gasification (Gil et al., 1999)	Steam-oxygen blown CFB gasification (Kurkela et al., 2014)
Fuel	Wood pellets	Wood pellets	Pine wood chips	Pine wood chips	Bark
Bed material	Olivine	Limestone	Silica	Silica	Dolomite + sand
Gravimetric tar, g/Nm^3	8-4	3.0-0.3	-	-	-
Tar, g/Nm^3	-	-	80-30	20-2	5.7

The limestone's physical behaviour under recurring calcination and carbonation cycles has been studied for the calcium looping processes. Extensive research has been conducted to investigate the physical behaviour of the material (Abanades, 2002; Abanades and Diego, 2003; Wang and Anthony, 2005; Grasa and Abanades, 2006; Grasa et al., 2009; Arias et al., 2012). In several studies, the limestone has been observed to lose parts of its CO_2 carrying capacity due to change in materials physical properties. During each high-temperature carbonation-calcination cycles, the porous structure of the lime particle sinters. The sintering weakens the limestone's ability to capture CO_2. This phenomenon cuts the looping process's performance, as shown in Figure 2.3. To compensate this loss of carrying capacity, a make-up flow of fresh limestone is needed to counteract the limestone's sintering.

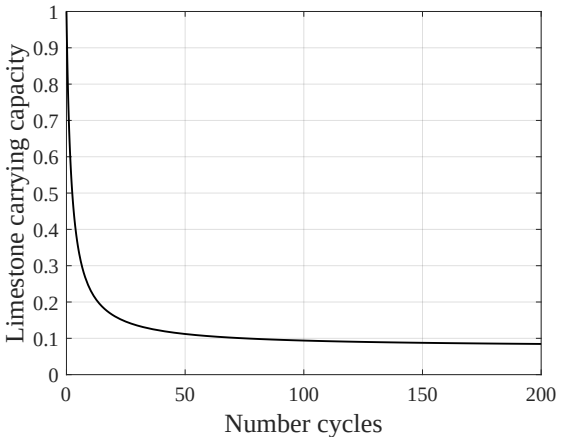

Figure 2.3: Carrying capacity of limestone as a function of carbonation-calcination cycles (Grasa and Abanades, 2006).

2.1.3 Experimental data

Various experimental studies have been published concerning sorption-enhanced gasification (Soukup et al., 2009; Poboss et al., 2012; Hawthorne et al., 2012; Armbrust et al., 2014; Diem et al., 2014; Poboss, 2016; Schmid et al., 2017; Müller et al., 2017; Hafner et al., 2018; Martínez et al., 2020a,b; Hafner et al., 2021). The process has been mainly demonstrated on pilot-scale facilities ranging from 20 kW_{th} to 200 kW_{th}. A review of experimental data has been conducted by Fuchs et al. (2019b). Based on the review, Fuchs et al. (2019a) presented typical gas yield and gas composition range for the SEG process. This data is shown in Figure 2.4.

The presented range is a general overview of the experiments, and it does not distinguish different operation parameters or hydrodynamic operation conditions. Data regarding process parameters of solid circulation rate (Poboss et al., 2012; Fuchs et al., 2018; Hafner et al., 2021), steam-to-carbon (S/C) ratio (Hafner et al., 2021), and different fuel qualities (Schmid et al., 2017; Fuchs et al., 2019b) are available in the literature.

The producer gas composition depends on the operating temperature. The temperature-dependent characteristic of the process allows the tailoring of the producer gas for different end-uses. Figure 2.5 (a) presents the H_2/CO ratio of the producer gas. Around 775°C, the molar ratio of H_2 and CO is 3. This molar ratio is an appropriate composition for a methane synthesis process's feed gas based on the stoichiometry of the steam-methane reforming reaction. Fischer–Tropsch process requires a molar ratio of CO/H_2 = 2, and to achieve this value, gasifier operation temperatures must exceed 800°C. Therefore, the molar ratio is obtainable only by the indirect gasification mode.

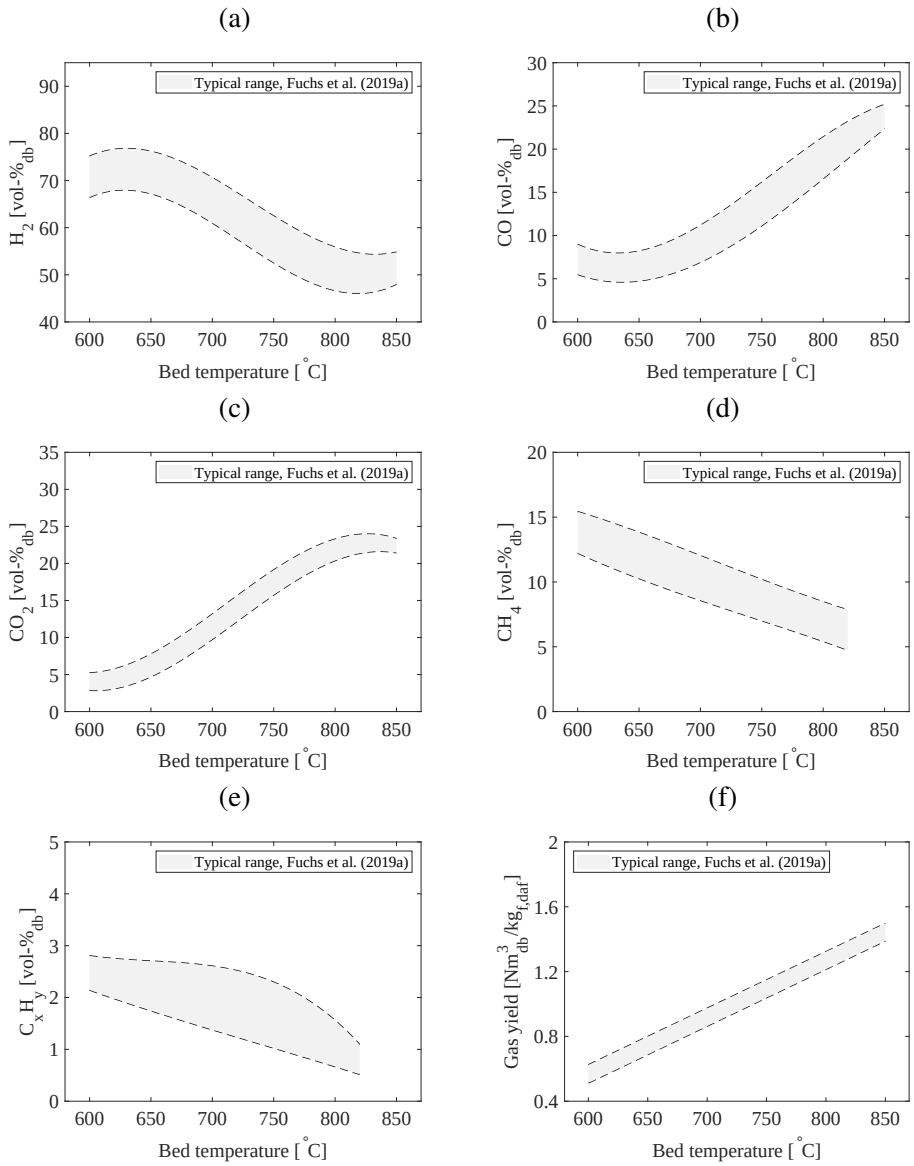

Figure 2.4: Producer gas volume fractions and gas yield of gas species (a) H_2, (b) CO, (c) CO_2, (d) CH_4, (e) C_xH_y and (f) gas yield are presented. The typical range for the measurements is presented based on various SEG experiments (Fuchs et al., 2019a). The data has been adapted from the source. The range is based on data of Soukup et al. (2009); Armbrust et al. (2014); Poboss (2016); Schmid et al. (2017). C_xH_y represents the concentration of lower hydrocarbon species (C_2-C_4) of which individual concentrations are typically low.

The module of producer gas is calculated from the composition of producer gas according to the equation:

$$M = \frac{y_{H_2} - y_{CO_2}}{y_{CO} + y_{CO_2}}. \tag{2.2}$$

The module of producer gas is shown in Figure 2.5 (b) according to Hafner et al. (2021). Module 2 is the optimal composition of the producer gas for DME synthesis and methanol synthesis process (Hafner et al., 2021). This module can be achieved with an operating temperature of around 750°C. Module 3 is obtained around 730°C temperature, which is an appropriate gas composition of producer gas with CO_2 for SNG synthesis (Wix et al., 2007; Hafner et al., 2021).

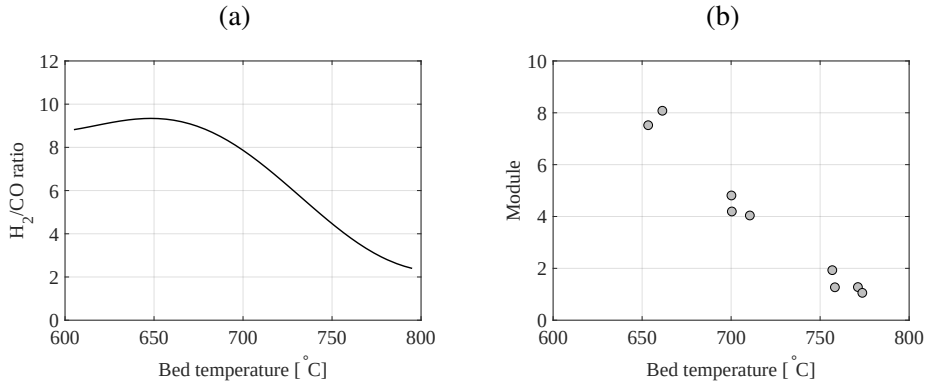

Figure 2.5: (a) H_2/CO ratio (Fuchs et al., 2019b) and (b) module (Hafner et al., 2021) of producer gas.

2.2 Fluidised bed reactor modelling

The development of a reactor model is an essential step in the study of new processes. A reactor model can be developed by combining physical phenomena occurring in a fluidised bed process. The reactor modelling enables studying how different process parameters affect physical operation of the reactor. In this chapter review of modelling approaches of fluidised bed gasification is conducted. The study's primary focus is on semi-empirical models, which have been regularly applied for modelling fluidised bed processes. This modelling approach combines empirical data with fundamental conservation equations. Hence, it provides a sound basis for studying new fluidised bed processes. A state-of-the-art of semi-empirical models for fluidised bed gasification and the SEG process is established.

2.2.1 Fluidised bed reactor modelling approaches

Fluidised bed reactor modelling approaches can be divided into three categories based on the number of physical dimensions of the model:

- 0-dimensional
- 1-dimensional and 1.5-dimensional
- 3-dimensional

Dimensionless models (0D) are based on fundamental mass and energy balances for the complete reactor. Often chemical equilibrium is presumed for producer gas (de Souza-Santos, 2010). Two main approaches to equilibrium modelling are stoichiometric and non-stoichiometric methods. An equilibrium model is very useable for the first estimation of the process but it commonly overestimates relations between gas species of producer gas (Ahmed et al., 2012). The simplest of the dimensional approaches are 1D-approach and 1.5D-approaches. The 1D modelling includes the formulation of mass and energy balances for the discretised domain representing the reactor. The reactor is typically discretised in the vertical direction as control volumes in which the fundamental balance equations are applied. The method separates the reactor into distinguishable sections, making it possible to investigate the extent of phenomena in different parts of the reactor. The 1D-approach suffers the drawback of averaging phenomena in the lateral direction of the reactor. Therefore, it is not suitable for reactors with significant lateral dimensions, or it requires sub-models to consider the lateral direction. The 1.5D-approach refers to the implementation of lateral mixing into the model. This particular case refers to a CFB reactor's core-annulus model in which mixing between wall and core sections takes place in the lateral direction. The 1D-approach is most appropriate for pilot-scale reactors since the impact of lateral mixing in the reactor is not significant due to the small lateral dimensions. The full-dimensional approach is often based on applying mass, momentum, and energy conservation for a three-dimensional domain. The approach is usually based on computational fluid dynamics (CFD) or semi-empirical approach. In the three-dimensional approach, uneven mixing in a fluidised bed reactor can be resolved.

2.2.2 Fluidised bed gasification reactor models

Various models have been proposed in the literature for modelling the fluidised bed gasifiers. Several models using the 0D chemical equilibrium approach (Li et al., 2001; Altafini et al., 2003; Mahishi and Goswami, 2007; Baratieri et al., 2008) have been proposed. The semi-empirical approach has been very commonly applied for modelling the biomass gasification process (Jennen et al., 1999; Fiaschi and Michelini, 2001; Corella and Sanz, 2005; Mahinpey and Nikoo, 2008; Kaushal et al., 2010; Myöhänen, 2011; Bates et al., 2017). Detailed CFD analysis of gasification reactor has been presented in several papers (Ku et al., 2015; Liu et al., 2016; Yang et al., 2019). The semi-empirical models are often developed for specific hydrodynamics conditions, e.g. bubbling fluidised bed or circulating fluidised bed conditions. Several one-dimensional bubbling fluidised bed models

have been proposed for bubbling fluidised bed gasification (Fiaschi and Michelini, 2001; Mahinpey and Nikoo, 2008; Kaushal et al., 2008; Bates et al., 2017). A fewer number of one-dimensional models have been proposed for modelling circulating fluidised bed gasification (Jennen et al., 1999; Corella and Sanz, 2005). The semi-empirical 3D-approach has been used for modelling CFB gasifiers in two studies (Petersen and Werther, 2005b; Myöhänen, 2011). Various one-dimensional models have been proposed for indirect gasification (Kaushal et al., 2011; Noubli et al., 2015; Yan et al., 2016; Aghaalikhani et al., 2019; Wojnicka et al., 2019). Some of the studies focus on the modelling of gasification reactors (Kaushal et al., 2011; Noubli et al., 2015; Yan et al., 2016; Aghaalikhani et al., 2019; Wojnicka et al., 2019) and only in a few studies the dual fluidised bed system is simulated (Yan et al., 2016).

The semi-empirical approach incorporates semi-empirical models to describe physical phenomena, such as fluidised bed hydrodynamics. In literature, several semi-empirical models for bubbling fluidised bed hydrodynamics exists. The models are often categorised as Davidson and Harrison model (Davidson, J.F. and Harrison, 1963), Kunii and Levenspiel model (Kunii and Levenspiel, 1968), counter-current back-mixing model (Fryer and Potter, 1972) and bubble assemblage model (Kato and Wen, 1969). Also, several variants of the models have been published (Werther, 1980; Jain et al., 2014). The fluidisation models were mostly created the 1970s or before. These models were reviewed by Chavarie and Grace (1975), who claimed Kunii and Levenspiel (1968) and Kato and Wen (1969) approaches as the most suitable approach for modelling bubbling fluidised bed hydrodynamics. These two hydrodynamic approaches have been often used for the modelling of bubbling fluidised bed processes (Matsui et al., 1985; Bilodeau et al., 1993; Pre et al., 1998).

In semi-empirical circulating fluidised bed models, the riser is separated into vertical sections. Separation of the the reactor to different vertical sections is done to account for variation of vertical concentration of solids (Johnsson and Leckner, 1995). Models considering the vertical solid concentration profiles has been published by Corella and Sanz (2005) and Krzywanski et al. (2010). Solids downflow close to the wall is observed in large-scale CFB's. A core-annulus approach has been applied for modelling the downflow and back-mixing induced by the flow in several models (Adánez et al., 1995; Jennen et al., 1999; Huilin, 2000; Gungor, 2009; Myöhänen, 2011).

2.2.3 Sorption-enhanced gasification reactor models

The semi-empirical approach has been well established for modelling of fluidised bed gasification. In literature, there are only a few models presented for modelling sorption-enhanced gasification. One of the first models was proposed by Florin and Harris (2007), who used the 0D equilibrium approach to model the process. Later a 0D dual fluidised bed model for the sorption-enhanced gasification was presented by Hejazi et al. (2014). Detchusananard et al. (2017) applied chemical equilibrium approach to model dual fluidised bed process using Aspen process simulator. The semi-empirical approach has been

applied on several papers (Inayat et al., 2010; Hejazi, 2017; Hejazi et al., 2019; Yan et al., 2018; Beirow et al., 2020; Hejazi and Grace, 2020). Inayat et al. (2010) developed a semi-empirical model for an SEG reactor. The presented model focused on the modelling of chemical reactions without reactor hydrodynamics. Recently, Hejazi (Hejazi, 2017; Hejazi et al., 2019; Hejazi and Grace, 2020) has proposed several 1D models for sorption-enhanced gasification. Hejazi (2017) utilised the traditional two-phase approach in which gas exists in bubble and emulsion phases. Davidson's bubble theory (Davidson, J.F. and Harrison, 1963) is used for modelling the rise of the bubble. The bubble size grow is modelled by correlation of Darton et al. (1977). The hydrodynamic model used resembles the bubble-assemblage model by Kato and Wen (1969). The model assumes solids in emulsion to be perfectly mixed without internal mixing of the bed. In the paper of Hejazi et al. (2019), the authors modelled the gasification process with gasification kinetics and without hydrodynamics. In the paper of Hejazi and Grace (2020), Aspen built-in fluidised bed model was applied for modelling a SEG reactor. Most of the published models concern the gasification reactor. The whole dual fluidised bed process has been accounted for in Hejazi et al. (2019) and Beirow et al. (2020) with the combustor's 0D balance. A dual fluidised bed model has been published by Yan et al. (2018). The model is based on a 1D-approach implemented within the Aspen process simulator. The model is used to compare a single-stage fluidised bed and a two-stage gasifier with a separate reforming section. The model uses the bubble-assemblage model (Kato and Wen, 1969) for bubbling fluidised bed hydrodynamics and assumes solids in the bed as perfectly mixed.

Table 2.3 summarises details of published model for the SEG process and compares them for the models of this thesis. The published models have been developed mainly for pilot-scale processes and no models exist for an industrial-scale process. The comparisons summarises semi-empirical models for the SEG process. The published models are very similar based on the listed details. Common for most of the models is that they take into account the temperature-dependency of the process. At low operating temperatures, the temperature influences on products yield of the fuel pyrolysis. The studies of (Di Blasi et al., 1999; Fagbemi et al., 2001; Neves et al., 2017) highlights the temperature-dependent nature of the pyrolysis process. The BFB hydrodynamics approach adapted for the models reassembles bubble-assemblage model. Chemical reactions that are applied for modelling are mostly consistent. However, study of Hejazi and Grace (2020) neglects char gasification reactions. In addition, pyrolysis is not modelled. The models in the literature commonly assume the bed as ideally mixed and no mixing model for internal mixing of solid phase is applied. The ideally mixing assumes even distribution of solid fractions (i.e. CaO, $CaCO_3$ and ash) for the whole bed. The approach naturally neglects the formation of vertical distribution profiles for each solid fraction and the influence of local process conditions on the solid fractions. Such models cannot accurately estimate the local CO_2 capture, and its possible limitations in the process, such as local equilibrium conditions. For studying physical operation of the process, implementation of the necessary details of the physical phenomena is important. There currently appears to be few published models with the necessary details implemented from the perspective of bed material conversion in the reactor. In the other models, the impact of the simplification to

processes physical operation is uncertain. The models developed in this thesis considers this important detail.

Table 2.3: Comparison of semi-empirical 1D models for sorption-enhanced gasification.

	Inayat et al. (2010)	Hejazi (2017)	Yan et al. (2018)	Hejazi et al. (2019)	Beirow et al. (2020)	Hejazi and Grace (2020)	This work
Model details							
Model type	In-house	In-house	Aspen	In-house	In-house	Aspen	In-house
Reactors	G	G	G-C	G-C/0D	G-C/0D	G	G-C
Hydrodynamics							
Reactor type	-	BFB	BFB-CFB	BFB	BFB	BFB	BFB-CFB CFB-CFB
Hydrodynamic model	-	BAM	BAM	-	BAM	K-L	BAM C-W
BFB solids mixing	-	Ideal	Ideal	Ideal	Mixing model	n.a.	Mixing model
Fuel model							
Pyrolysis type	-	Kin-TD-PM	Emp-TD	Kin-TD	Kin-TD	-	Emp-TD
Tar included	-	x	x	x	x	-	x
Char gasification reactions							
Water-gas	x	x	x	x	x	-	x
Boudouard	x	x	x	x	x	-	x
Methanation	x	x	-	x	-	-	x
Sorbent reactions							
Carbonation	x	x	x	x	x	x	x
Calcination	-	-	x	-	-	-	x
Sulphatation	-	-	-	-	-	-	x
Direct-sulphatation	-	-	-	-	-	-	x
De-sulphatation	-	-	-	-	-	-	x
Homogenous reactions							
Water-gas shift	x	x	x	x	x	x	x
Steam-methane reforming	x	x	-	x	-	-	-
Hydrocarbon reforming reactions	-	x	x	x	x	-	-
Tar reforming	-	x	-	x	-	-	-

Abbreviations: (x) included, (-) not included, (n.a.) information not available, (G) gasifier, (C) combustor, (0D) 0D balance, (BAM) bubble-assemblage type model, (K-L) Kunii & Levenspiel type model, (C-W) Core-Wall layer, (Ideal) no bed internal mixing, (Mixing model) bed internal mixing is modeled, (Emp) semi-empirical model, (Kin) kinetic model, (TD) temperature-dependent, (PM) particle model.

3 Model descriptions

The main research methods used in this thesis are presented in this chapter. This chapter describes model frames applied for studying the SEG process. Two model frames for BFB and CFB reactors are described in Chapters 3.1 and 3.2. Fuel decomposition model developed for a low temperature gasification process is described in Chapter 3.3. The BFB model was developed in Publication II, the CFB model in Publication I / Publication IV, and fuel decomposition model in Publication III / Publication V. The developed reactor models are comprehensive models, including the main phenomena relevant to the SEG process. The models can be used as stand-alone reactor models for an individual reactor, or they can be connected to form the full-loop dual fluidised bed process. The model frames were mainly developed for the fluidised bed gasification. However, it is possible to operate the models as fluidised bed combustors.

3.1 Two-phase BFB reactor model frame

A semi-empirical 1D BFB model frame was developed for modelling of the SEG process. A general description of the reactor model is presented in Figure 3.1. The reactor is discretised into several 1D control volumes. The governing equations are applied in each control volume to resolve local mass and energy balances for the reactor. Physical phenomena are implemented in the model by semi-empirical correlations. By combining the governing equations with the semi-empirical correlations, the influence of the physical phenomena on local mass and energy balances are resolved. Consequently, the 1D semi-empirical approach enables studying reactor operation from local and global perspectives.

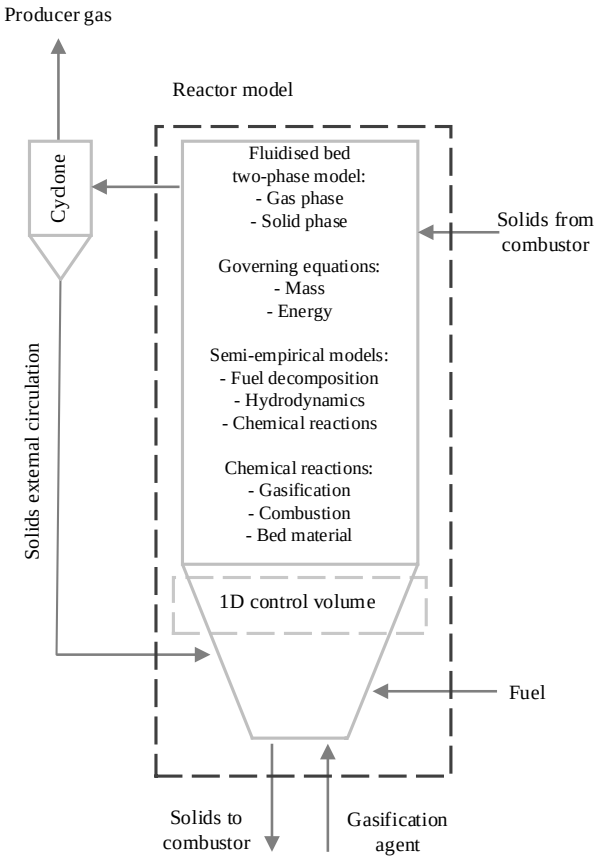

Figure 3.1: General description of BFB model frame.

The reactor model is discretised into multiple 1D control volumes at the vertical direction. The dimensions of the model are set by defining the cross-section's dimensions and height of the reactor. The reactor's geometry consists of two sections, a sloped frustum and a cylindrical body with constant cross-section. The sloped section's height and the grid's size at the reactor's bottom are defined in the reactor configuration. The locations for connections, e.g. solids flow from the combustor and cyclone's loop seal and gas inputs, are set in the reactor configuration. The reactor configuration also includes properties of solids and gases based on fixed values or correlations.

The main boundary conditions of the reactor are shown in Figure 3.2. Mass boundary conditions are applied for flows across the reactor boundaries; for each material flow, mass flow is assigned or computationally resolved in the reactor code. The material flows hold a temperature and composition based on assigned values or computed values. The primary gas feed and the solids exit to combustor from the reactor are fixed into the low-

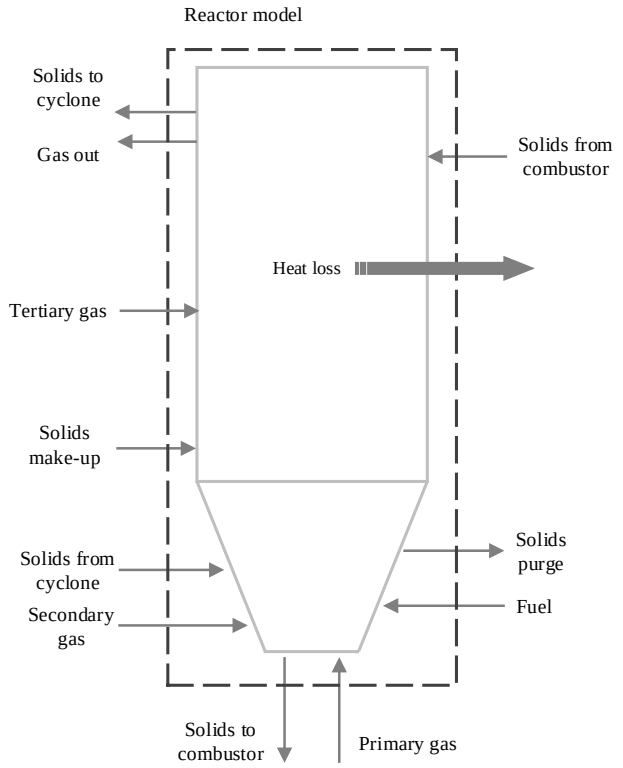

Figure 3.2: Boundary conditions of BFB model frame.

est control volume. Gas and solids exit flows to the cyclone from the reactor are assigned to the top control volume. Fuel decomposition is modelled according to Chapter 3.3. The fuel feed in the reactor can be assigned into an arbitrary control volume or divided between several control volumes. The fuel decomposition occurs in the assigned control volumes. Often, the decomposition is assumed to occur at the bottom of the reactor within 2-4 bottom control volumes.

Transient continuity and energy equations are implemented in the model frame. Mass and energy balances are resolved in each control volume with every time step. The control volumes are assumed as perfectly mixed in terms of mass and energy. The model frame includes two-phases, gas and solid. The continuity equation is separately resolved for both phases, and one common energy equation is resolved for gas and solid phases. In the bed, separate mass balances are computed for bubble and emulsion within the control volume. The description of the modelling routine for each time step is shown in Figure 3.3. Time derivatives are resolved using the forward Euler method. The first-order upwind scheme is used to differentiate spatial derivatives. Simulink's ordinary difference

equations solvers (ODE) are used to resolve differential equations.

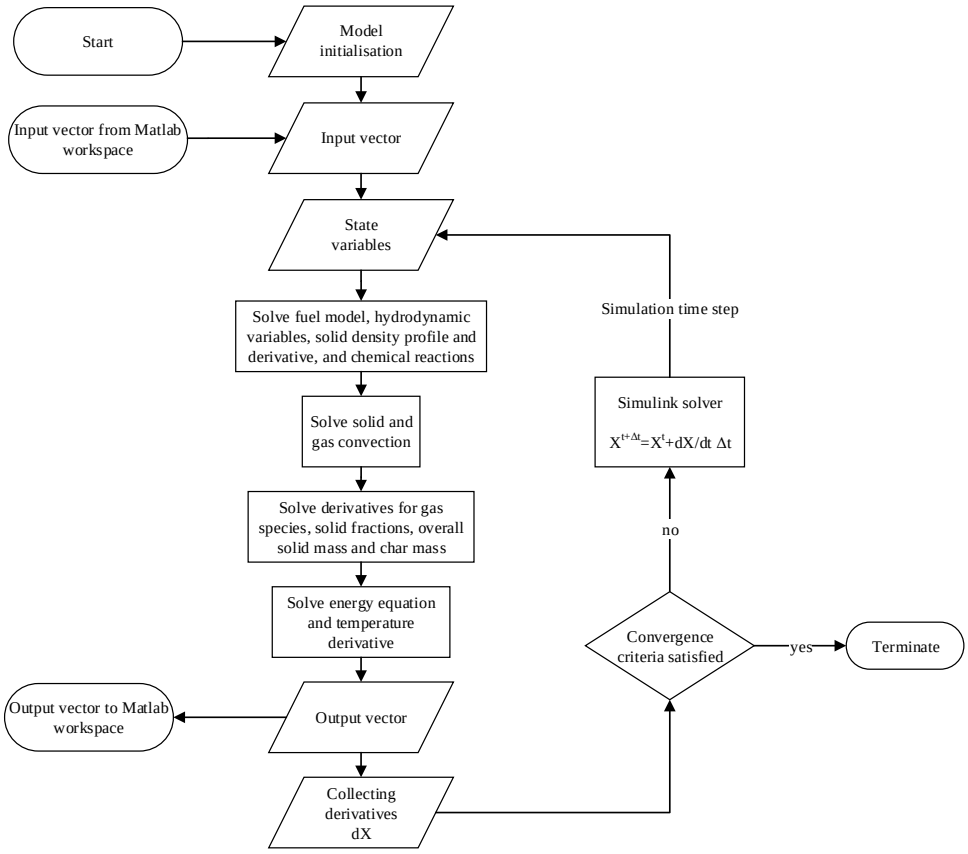

Figure 3.3: Simulation steps in BFB model.

3.1.1 Bubbling fluidised bed hydrodynamics

Semi-empirical hydrodynamic equations are employed to close the governing equations. A bubble-emulsion approach is used to model reactor hydrodynamics. The hydrodynamic model produces solid and gas phase movement in the bed. The description of the model is shown in Figure 3.4. The semi-empirical hydrodynamic model equations applied for modelling are described in Publication II.

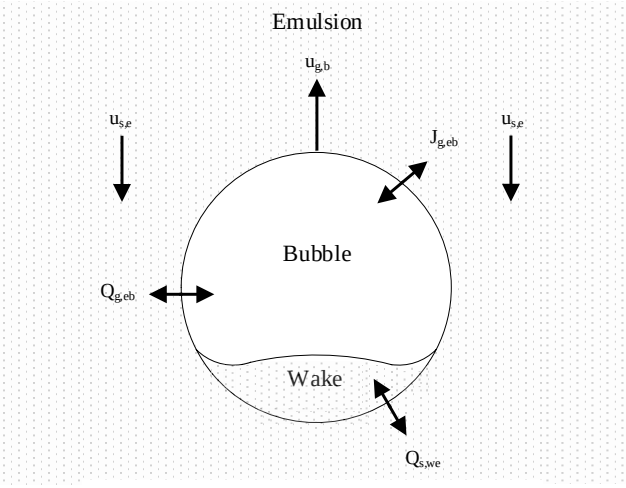

Figure 3.4: Bubble-emulsion model of dense bed. Notations: u_b is velocity of bubble gas, $u_{s,e}$ is velocity of solids in emulsion, $J_{g,eb}$ is interface mass transfer between emulsion and bubble, $Q_{g,eb}$ is gas net flow between emulsion and bubble and $Q_{s,we}$ is net flow of solids between wake and emulsion.

The bubble-emulsion model is applied at the bottom of the reactor where the dense bed is situated. The bubbling fluidised bed hydrodynamics model uses internal mixing approach of Kunii and Levenspiel (1968) for the bed, which enables in-bed distribution of limestone's material fractions (CaO, $CaCO_3$ and $CaSO_4$) to form. In the reactor model, the freeboard is treated as a dilute region, where small quantities of solids are present, and a two-phase flow exists. A transition zone from the dense bed to the freeboard is modelled above the bed. Solids concentration in this region is between the dense region and the freeboard. Solid entrainment to gas flow is modelled in this zone, impacting local mass and energy balances.

3.1.2 Solid-phase balances

The solid continuity equations are resolved in each control element of the reactor. Separate continuity equations have been formulated for the dense bottom and dilute freeboard. The bubbling bed is a dense two-phase zone separated as the wake of the bubble and the emulsion. The solid bed material is formed from discrete material fractions (CaO, $CaCO_3$, $CaSO_4$, and ash). The continuity equation is resolved for each material fraction, and the dense bed can retain different material fraction distributions for the wake and the emulsion in each control volume. Solid (s) continuity equations is resolved separately for

the wake and the emulsion in the bed

$$\frac{\partial \rho_s}{\partial t} + \frac{\partial u_s \rho_s}{\partial z} = Q_{s,we} + \sum R_s + \sum S_s, \tag{3.1}$$

which can be written for each material k as follows

$$\frac{\partial W_{s,k} \rho_s}{\partial t} + \frac{\partial W_{s,k} u_s \rho_s}{\partial z} = W_{s,k} Q_{s,we} + \sum R_{s,k} + \sum S_{s,k}, \tag{3.2}$$

where $W_{s,k}$ is material fraction of k, ρ_s is density of solids, u_s is velocity of solids, $Q_{s,ew}$ is net flow of solids between wake and emulsion, chemical reaction term $\sum R$ describes the chemical reactions of material k according to Table 3.1, while the term $\sum S$ considers local mass changes of material k due to local sinks and sources. The freeboard is treated as a dilute flow region with low concentration of solids present. Continuity equation for solid phase in the freeboard is

$$\frac{\partial \rho_s}{\partial t} + \frac{\partial u_s \rho_s}{\partial z} = \sum R_s + \sum S_s. \tag{3.3}$$

Material fraction distribution is resolved in the freeboard with the following equation

$$\frac{\partial W_{s,k} \rho_s}{\partial t} + \frac{\partial W_{s,k} u_s \rho_s}{\partial z} = \sum R_{s,k} + \sum S_{s,k}. \tag{3.4}$$

A separate continuity equation for char is resolved for the whole reactor. The char has been separated from the other material fraction and it is assumed to be uniformly mixed within the bed material. The char's mass in the reactor is resolved from continuity equation for the reactor

$$\frac{\partial \rho_{char}}{\partial t} = \sum R_{char} + \sum S_{char}, \tag{3.5}$$

where ρ_{char} is density of char, $\sum R_{char}$ describes the char chemical reactions according to Table 3.1, and the term $\sum S_{char}$ considers local sinks and sources of the char, and formation from the fuel. The char is formed from C, H, O, N and S elements. Average elemental distribution for reactor is resolved for each element (x) with equation

$$\frac{\partial W_{char,x} \rho_{char}}{\partial t} = \sum R_{char,x} + \sum S_{char,x}, \tag{3.6}$$

where $W_{char,x}$ is mass fraction of x element.

3.1.3 Gas-phase balances

The gas species O_2, N_2, CO_2, CO, NO, H_2O, H_2S, NH_3, CH_4, C_2H_4, H_2, SO_2 and C_7H_8 are considered. The continuity equation is resolved separately for each component in each control volume. In the bed section, equations for bubble gas and emulsion gas have

Table 3.1: Chemical reactions of sorption-enhanced gasification process.

Reaction	Equation	ΔH_{298K} [kJ/mol]
Boudouard	$C + CO_2 \rightarrow 2\,CO$	172.4
Water-gas	$C + H_2O \rightarrow CO + H_2$	131.3
Methanation	$C + 2\,H_2 \rightarrow CH_4$	-75.0
Char combustion	$C + 0.5\ O_2 \rightarrow CO$	-110.5
Char combustion	$C + O_2 \rightarrow CO_2$	-393.5
Water-gas shift	$CO + H_2O \leftrightarrow H_2 + CO_2$	-41.1
C_2H_4 combustion	$C_2H_4 + 3\,O_2 \rightarrow 2\,CO_2 + 2\,H_2O$	-1323.2
CH_4 combustion	$CH_4 + 2\,O_2 \rightarrow CO_2 + 2\,H_2O$	-802.6
H_2S combustion	$H_2S + 1.5\,O_2 \rightarrow SO_2 + H_2O$	-518.0
CO combustion	$CO + 0.5\,O_2 \rightarrow CO_2$	-283.0
H_2 combustion	$H_2 + 0.5\,O_2 \rightarrow H_2O$	-241.8
C_7H_8 combustion	$C_7H_8 + 9\,O_2 \rightarrow 7\,CO + 4\,H_2O$	-3772.0
NH_3 combustion	$NH_3 + 1.25\,O_2 \rightarrow NO + 1.5\,H_2O$	-902.1
Calcination	$CaCO_3 \rightarrow CaO + CO_2$	178.3
Carbonation	$CaO + CO_2 \rightarrow CaCO_3$	-178.3
Sulphation	$CaO + SO_2 + 0.5\,O_2 \rightarrow CaSO4$	-502.1
De-sulfation	$CaSO_4 + CO \rightarrow CaO + SO_2 + CO_2$	219.2
Direct sulfation	$CaCO_3 + SO_2 + 0.5\,O_2 \rightarrow CaSO_4 + CO_2$	-323.8

been formulated. The emulsion and the bubble can retain different concentration for gas species. Continuity equation for the gas in the emulsion and the bubble in the bed is

$$\frac{\partial \rho_g}{\partial t} + \frac{\partial u_g \rho_g}{\partial z} = \sum R_g + \sum S_g + Q_{g,eb} + J_{g,eb}, \tag{3.7}$$

where total mixture's spatial density derivative is considered to be small and to not have significant impact in the equation. The gas density of the total mixture is resolved from the ideal gas approach. Continuity equation for each gas specie j is written as

$$\frac{\partial W_{g,j}}{\partial t}\rho_g + \frac{\partial W_{g,j} u_g}{\partial z}\rho_g = \sum_j R_{g,j} + \sum_j S_{g,j} + Q_{g,eb,j} + J_{g,eb,j}, \tag{3.8}$$

where $\sum R$ describes the chemical reactions of each specie j according to Table 3.1 and the source term $\sum S$ considers local mass changes of each specie due to formation of volatiles, drying of fuel, char gasification and local sinks and sources. Biomass devolatilisation and drying is taking place in the emulsion. There is always net gas flow $Q_{g,eb}$ from the emulsion to the bubble, since the minimum fluidisation state must apply in the emulsion. Thus, the excess gas is assumed to appear as gas bubbles. Interface mass transfer $J_{g,eb}$ between the emulsion and the bubble is induced by concentration difference for gas species. Continuity equations Eq. 3.3 and Eq. 3.4 are applied for gas phase to model gas flow and gas species concentrations in the freeboard.

3.1.4 Energy balance

The energy balance for each control volume is solved at each time step. The control volumes are assumed to be fully mixed; thus, uniform temperature for the control volume is assumed. The general form of the energy equation applied to a control volume is

$$\frac{\partial U}{\partial t} = E_{conv} + E_r + E_{hs} + E_{ht}, \tag{3.9}$$

where U is internal energy, E_{conv} is convection of energy, E_r is energy from chemical reactions, E_{hs} is local energy source due to discharge or feed of mass into the reactor and E_{ht} is related to heating or cooling of the reactor. The change of internal energy U of a control volume can be separated into change of the internal energy due to energy transfer by solid and gas phases

$$\begin{aligned}\frac{\partial U_s}{\partial t} + \frac{\partial U_g}{\partial t} &= \rho_s \frac{\partial h_s}{\partial t} + h_s \frac{\partial \rho_s}{\partial t} + \rho_g \frac{\partial h_g}{\partial t} + h_g \frac{\partial \rho_g}{\partial t} \\ &= \frac{\partial \rho_s u_s h_s}{\partial z} + \frac{\partial \rho_g u_g h_g}{\partial z} + E_{s,r} + E_{g,r} + E_{s,hs} + E_{g,hs} + E_{ht}. \end{aligned} \tag{3.10}$$

The chemical reaction of solid and gas phase, release of volatiles, and evaporation of moisture are accounted in $E_{s,r}$ and $E_{g,r}$ terms

$$E_{s,r} + E_{g,r} = \sum_k \Delta H_{s,k,r} S_{s,k} + \sum_j \Delta H_{s,j,r} S_{s,j} + \Delta H_{\mathrm{devol}} S_{\mathrm{devol}} + \Delta H_{\mathrm{lat,H_2O}} S_{\mathrm{lat,H_2O}}, \tag{3.11}$$

where ΔH is reaction enthalpy (J/kg), S is mass source or sink term (kg/s), and $\Delta H_{\mathrm{lat,H_2O}} S_{\mathrm{lat,H_2O}}$ is evaporation of fuel's water.

3.2 Circulating fluidised bed model frame

A transient semi-empirical 1D CFB model frame was developed for the sorption-enhanced gasification process. The model frame is described in Figure 3.5. The model is a comprehensive reactor model including the main aspects of reactor hydrodynamics and chemical reactions.

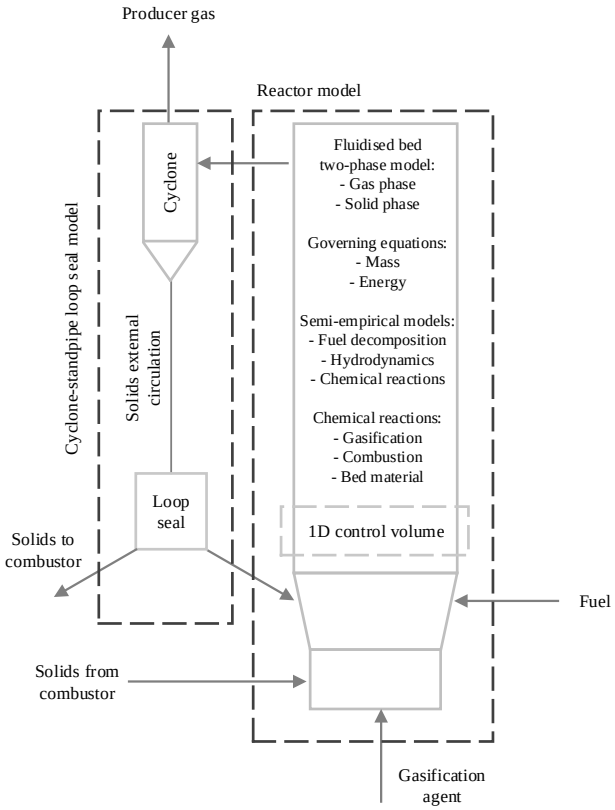

Figure 3.5: General description of CFB model frame.

The reactor is discretised into multiple 1D control volumes at the vertical direction of the reactor. The dimensions of the model are set by defining the cross-section's dimensions and height of the reactor. The geometry is divided into cylindrical bottom and riser, and conical frustum between the bottom and the riser. The cross-section of the reactor is constant at the bottom and the freeboard. The height of the bottom, frustum and riser are set in reactor configuration. The position of connections, e.g. solid flow from the combustor, solids flow from cyclone's loop seal and secondary airs, is set in the reactor configuration. The exit channel's height determines the control volumes where the gas and solids exit from the reactor.

The main boundary conditions are shown in Figure 3.6. Mass boundary conditions are applied for flows across the reactor boundaries; for each material flow, mass flow is assigned or computationally resolved in the reactor code. Each material flow holds a temperature and composition based on assigned values or computed values. The primary gas feed is fixed into the lowest control volume. Fuel decomposition is modelled according to Chap-

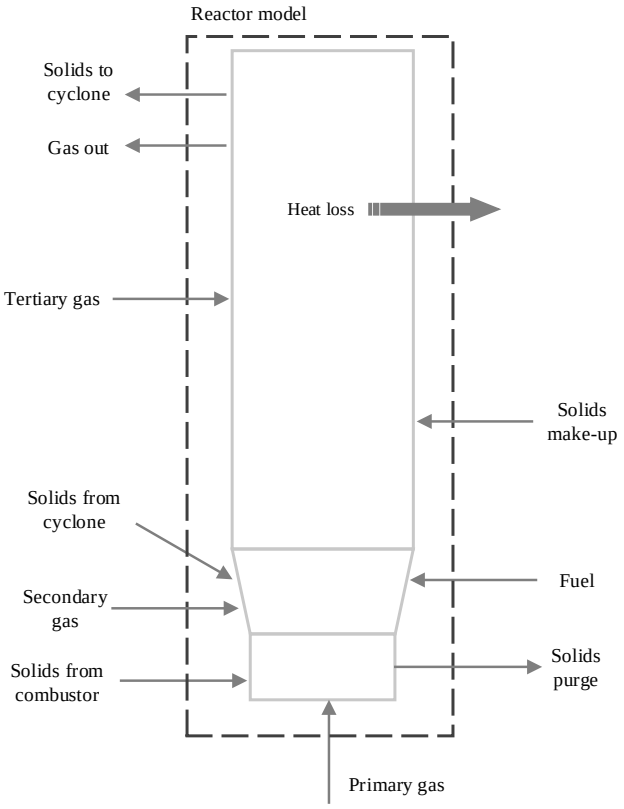

Figure 3.6: Boundary conditions of CFB model frame.

ter 3.3. The fuel feed's location can be assigned in an arbitrary control volume or divided between several the control volumes. In the assigned control volumes where the fuel is fed, the fuel decomposition occurs. Often, the decomposition is assumed to occur at the bottom of the reactor within 2-4 bottom control volumes.

Transient continuity and energy equations are implemented in the model frame. Mass and energy balances are resolved in each control volume with every time step. The control volumes are assumed as perfectly mixed in terms of mass and energy. The model frame includes gas and solid phases. The continuity equation is separately resolved for both phases, and one common energy equation is resolved for gas and solid phases. A core-annulus model for hydrodynamics is applied to model solids movement. The balance equations are separately resolved for the core and wall regions. The description of the modelling routine for each time step is shown in Figure 3.7. Time derivatives are resolved using the forward Euler method in the model. The first-order upwind scheme is used to differentiate spatial derivatives, and diffusion of energy is differentiated with the

central difference method. Simulink's ordinary difference equation solvers are applied to resolve differential equations.

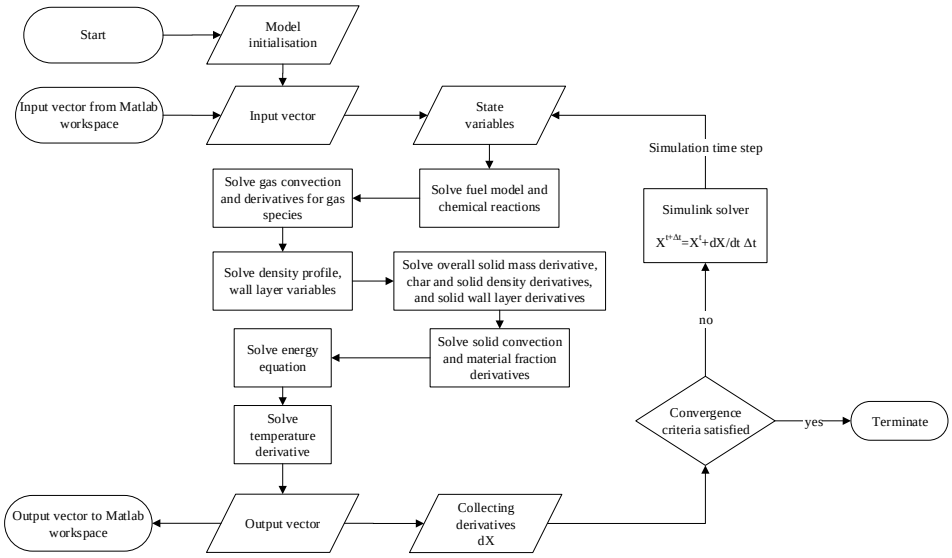

Figure 3.7: Simulations steps in CFB model.

3.2.1 Circulating fluidised bed hydrodynamics

The core-annulus model is applied to model solids movement in the rector. The model is described in Figure 3.8. The flow scheme produces internal circulation of the solids within the reactor. The semi-empirical hydrodynamic model equations applied for modelling are described in Publication IV.

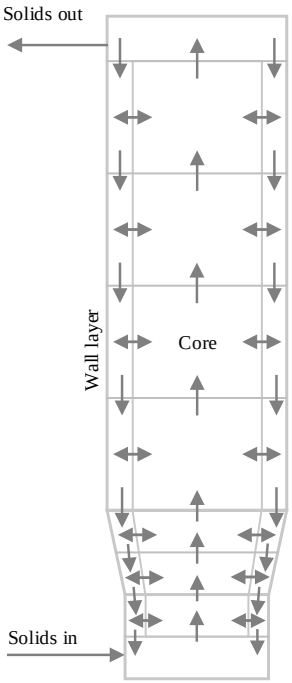

Figure 3.8: CFB core-annulus flow scheme.

3.2.2 Solid-phase balances

The model solves solid and gas phase mass balances for each element at each time step. The solid bed material is formed from discrete material fractions (CaO, $CaCO_3$, $CaSO_4$, and ash). The continuity equation for solid phase (s) is

$$\frac{\partial \rho_s}{\partial t} + \frac{\partial u_s \rho_s}{\partial z} = \sum R_s + \sum S_s. \tag{3.12}$$

The continuity equations for each material k is

$$\frac{\partial W_{s,k} \rho_s}{\partial t} + \frac{\partial W_{s,k} u_s \rho_s}{\partial z} = \sum R_{s,k} + \sum S_{s,k}, \tag{3.13}$$

where $W_{s,k}$ is material fraction of k, ρ_s is density of solids, u_s is velocity of solids, chemical reaction term $\sum R$ describes the chemical reactions of material k according to Table 3.1, while the term $\sum S$ considers local mass changes of material k due to sinks and sources. The continuity equation is resolved separately for the core and the wall layer. A

separate continuity equation for char is resolved for the whole reactor according to Eq. 3.5 and Eq. 3.6.

3.2.3 Gas-phase balances

The gas species O_2, N_2, CO_2, CO, NO, H_2O, H_2S, NH_3, CH_4, C_2H_4, H_2, SO_2 and C_7H_8 are considered. The continuity equation is resolved separately for each component in each control element. The continuity equations for the gases (g) is

$$\frac{\partial \rho_g}{\partial t} + \frac{\partial u_g \rho_g}{\partial z} = \sum R_g + \sum S_g, \tag{3.14}$$

where total mixtures spatial density derivative is considered to be small and to not have significant impact in the equation. The gas density of the total mixture is resolved from the ideal gas approach. The gas density of the total mixture is resolved from the ideal gas law. The continuity equation for each gas specie j is written as

$$\frac{\partial W_{g,j}}{\partial t}\rho_g + \frac{\partial W_{g,j} u_g}{\partial z}\rho_g = \sum_j R_{g,j} + \sum_j S_{g,j}, \tag{3.15}$$

where $\sum R$ describes the chemical reactions of each specie j (according to Table 3.1) and the source term $\sum S$ considers local mass changes of each species due to formation of volatiles, drying of fuel, char gasification and local sinks and sources.

3.2.4 Energy balance

The energy balance for each control volume is solved at each time step. Separate energy balances are resolved for the core and the wall layer. The control volumes are assumed to be fully mixed; thus, uniform temperature for the control volume is assumed. The general form of the energy equation is

$$\frac{\partial U}{\partial t} = E_{conv} + E_r + E_{hs} + E_{ht} + E_{disp}, \tag{3.16}$$

where U is internal energy, E_{conv} is convection of energy, E_r is energy from chemical reactions,E_{hs} is local energy source due to sinks and sources of mass, E_{ht} is heat source or sink related to heating or cooling and E_{disp} is a dispersion of energy. The change of internal energy U of a control volume can be separated into change of the internal energy due to energy transfer by solid and gas phases

$$\begin{aligned}\frac{\partial U_s}{\partial t} + \frac{\partial U_g}{\partial t} &= \rho_s \frac{\partial h_s}{\partial t} + h_s \frac{\partial \rho_s}{\partial t} + \rho_g \frac{\partial h_g}{\partial t} + h_g \frac{\partial \rho_g}{\partial t} \\ &= \frac{\partial \rho_s u_s h_s}{\partial z} + \frac{\partial \rho_g u_g h_g}{\partial z} + E_{s,r} + E_{g,r} + E_{s,hs} + E_{g,hs} + E_{ht} + E_{disp}.\end{aligned} \tag{3.17}$$

The energy terms $E_{s,r}$ and $E_{g,r}$ accounting for chemical reactions are resolved from Eq. 3.11. The dispersion of energy represents the mixing of energy between adjacent control volumes, and it is written by applying the central difference method to Fick's law of diffusion

$$E_{disp} = -D_s c_{p,s} A_b \rho_{av}^{-} \frac{\partial T_i^{-}}{\partial z} - D_s c_{p,s} A_t \rho_{av}^{+} \frac{\partial T_i^{+}}{\partial z} \tag{3.18}$$

where D_s is the dispersion coefficient [m^2/s], A_b and A_t are the cross-sections of the bottom and top boundary of the control volume. The average density between the calculation and sliding control volume is represented by ρ_{av}^{-} and ρ_{av}^{+}. The temperature gradient $\partial T_i/\partial z$ is the driving force for energy dispersion.

3.3 Fuel decomposition model

A fuel decomposition model was formulated for a low temperature biomass gasification process. Conventionally, fuel decomposition products have been modelled by using standard proximate analysis. In gasification processes operated well below the conventional operating temperatures, such as the SEG process, the fuel decomposition products are expected to differ from those observed under standard characterisation conditions. Temperature-dependency for the distribution of decomposition products has been observed from various decomposition experiments (Neves et al., 2011). Therefore, the temperature-dependent characteristic must be considered in the analysis of low-temperature gasification systems.

3.3.1 Fuel decomposition balances

The fuel decomposition model applied for modelling is described in Figure 3.9. The fuel decomposition model is used for modelling the primary conversion step of biomass in the gasifier, often referred as the pyrolysis step. The fuel model is based on mass balances described in Publication III. The balances are formulated based on proximate and ultimate analyses of the fuel. The fuel model requires conducting the fuel analysis in several temperatures to incorporate the temperature-dependency of the fuel decomposition process into the fuel model. The empirical data obtained from the fuel analyses are used to close the model's balances and determine permanent gas species released from the fuel. The following simplifications for the model have been made. The model uses ash and moisture fractions based on the standard proximate analysis. Lower hydrocarbons (C_2–C_4) in the permanent gas fraction are lumped under the C_2H_4 model component. Tar species are lumped under the single model component C_7H_8. The modelling assumes that all hydrocarbons are formed upon the fuel decomposition. The fuel decomposition is also assumed to be instantaneous. The elemental composition of hydrocarbons (CH_4, C_2-C_4 and tars) measured from producer gas are directly assigned to the fuel decomposition model without modelling reaction paths or kinetics. The approach assures the elemental distribution of producer gas in the simulations is divided according to the measurements between hydrocarbons and other gas species at the outlet of the gasifier. The fuel decomposition in the reactors models can be set in arbitrary control volumes. The selection is

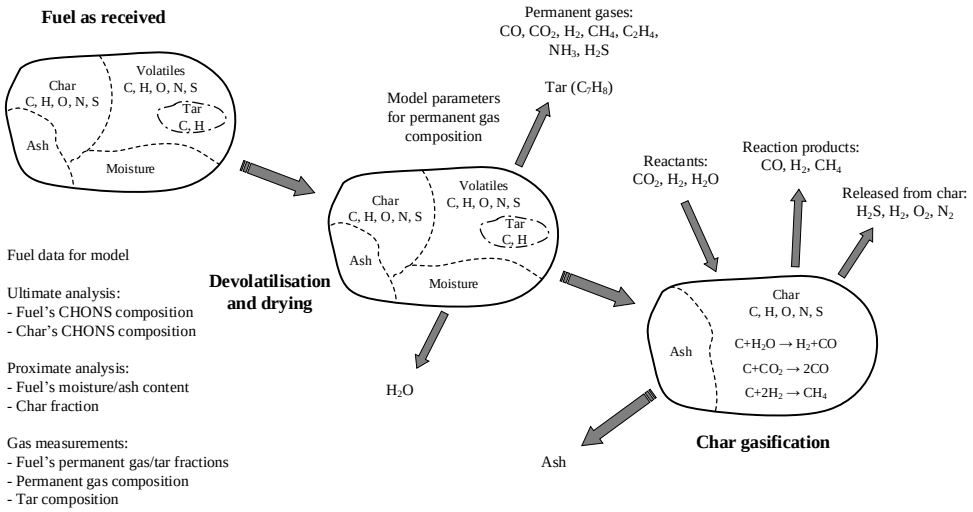

Figure 3.9: Fuel decomposition model.

based on reactor design. In the BFB model, the devolatilised gas species are accounted in the reactor's local mass balances (Eq. 3.7 and Eq. 3.8) for the emulsion gas. For the CFB reactor model, the devolatilised gas species are accounted in the gas phase in local mass balances (Eq. 3.14 and Eq. 3.15). The amount of char formed at the fuel decomposition is added to the reactor's balances (Eq. 3.5 and Eq. 3.6) in both models.

The volatiles released from the fuel in the devolatilisation process consists of permanent gases species and tar species. Consequently, the fuel can be separated into five main fractions in the fuel decomposition process

$$W_f = W_{pg} + W_{tar} + W_{char} + W_{ash} + W_{moist}, \tag{3.19}$$

which has elemental composition according to Figure 3.9. The char's elemental composition is modelled according to Neves et al. (2011) and Myöhänen (2011). Correlations for the C and H compositions of the char are according to Neves et al. (2011)

$$W_{char,\mathrm{C}} = 0.93 - 0.92\exp(-0.0042T) \tag{3.20}$$

$$W_{char,\mathrm{H}} = -0.0041 + 0.1\exp(-0.0024T), \tag{3.21}$$

where T is fuel decomposition temperature in °C. Elements N and S are assumed to follow correlations by Myöhänen (2011).

$$W_{char,\mathrm{N}} = 0.088 W_{f,\mathrm{N}} W_{char,daf}^{0.6} \left(\frac{W_{f,\mathrm{N}}}{W_{f,\mathrm{C}}}\right)^{-0.6} \tag{3.22}$$

$$W_{char,\mathrm{S}} = 0.14 W_{f,\mathrm{S}} W_{char,daf}^{0.2} \left(\frac{W_{f,\mathrm{H}}}{W_{f,\mathrm{C}}}\right)^{-0.6}, \tag{3.23}$$

where $W_{f,i}$ is the fraction of an element of the char's parent fuel according to the ultimate analysis. Oxygen in char is resolved from difference and the other elements from the correlations.

3.3.2 Volatile composition

Elemental composition of volatiles is resolved from elemental mass balances by removing the char and the tar from the fuel's elemental composition. The volatilised gas species are formed from the elemental leftover, which follows stoichiometry

$$\begin{aligned} y_{\mathrm{C}} + y_{\mathrm{H}} + y_{\mathrm{O}} + y_{\mathrm{N}} + y_{\mathrm{S}} &= y_{pg} \\ &= y_{NH_3} + y_{H_2S} + y_{CO} + y_{CO_2} + y_{CH_4} + y_{C_2H_4} + y_{H_2}. \end{aligned} \tag{3.24}$$

The stoichiometry can be altered with parameters γ_1 and γ_2

$$\gamma_1 = \frac{n_{CO}}{n_{CO} + n_{CO_2}} \tag{3.25}$$

$$\gamma_2 = \frac{n_{CH_4,C}}{n_{CH4,\mathrm{C}} + n_{C_2H_4,\mathrm{C}}} \tag{3.26}$$

The parameters influence on molar relations of the formed gas.

3.3.3 Energy balance

The energy balance of the fuel decomposition is formulated based on theoretical reaction energies. The energy balance is modelled according to:

$$E_{reaction} = E_{LHV} + E_{H_2O} + E_{devol} \tag{3.27}$$

in which E_{LHV} is the lower heating value of fuel, E_{H_2O} is evaporation of fuel's water, E_{devol} is an external heat required by the fuel decomposition and $E_{reaction}$ is theoretical reaction energy of the decomposition products according to the equation:

$$\begin{aligned} E_{reaction} = q_{m,f} \sum_x W_{char,x} \Delta H_{char,x} + q_{m,f} \sum_j W_{pg,j} \Delta H_{pg,j} \\ + q_{m,f} W_{tar} \Delta H_{tar} \end{aligned} \tag{3.28}$$

in which $q_{m,f}$ is mass flow rate of fuel $W_{char,k}$ is the mass fraction of a char element, $W_{pg,j}$ is mass fraction of a gas specie, $\Delta H_{char,k}$, $\Delta H_{pg,j}$ and ΔH_{tar} are reaction heats of char elements, permanent gases and tar, respectively.

4 Modelling of pilot-scale reactor and model validation

Validation of the BFB model presented in Chapter 3.1 is conducted. The model is validated against measurements of a 200 kW_{th} pilot-scale SEG reactor. The modelling aims to investigate the gasification phenomena producing the physical operation of the pilot-scale SEG process. This section of the thesis focuses on summarising the main results of the model validation discussed in Publication II and Publication III. The model frame was developed, and the modelling approach was established in Publication II. Further improvements of the model frame were introduced in Publication III including fuel decomposition model. In Publication II, the fuel decomposition phenomenon was modelled as temperature-independent, tar-free, and hydrocarbon devolatilisation was simplified. A more detailed fuel decomposition approach was introduced in Publication III, which improved the modelling results and enabled more accurate modelling. The validation of the reactor model included reactor hydrodynamics, heat balance of the reactor and producer gas composition. However, the discussion in this chapter focuses on the main modelling results concerning the gasification phenomena of the SEG process.

4.1 Process description and simulation setup

The gasification experiments were conducted at a 200 kW_{th} dual fluidised bed (DFB) pilot facility at the Institute of Combustion and Power Plant Technology (IFK) at the University of Stuttgart. The pilot facility consisted of a bubbling fluidised bed gasifier and a circulating fluidised bed combustor connected to each other. The process configuration IFK's dual fluidised bed process is shown in Figure 4.1. The main dimensions of the gasifier are described in Table 4.1.

Table 4.1: The main dimensions of the gasifier (Publication II).

Parameter	
Gasifier diameter, m	0.33
Grid diameter, m	0.136
Height of the sloped section, m	0.35
Gasifier outlet elevation, m	5.35
Loop seal inlet elevation, m	0.5
Solid inlet elevation, m	1.7

The experimental work focused on varying the temperature of the SEG pilot by altering the bed material circulation rate from the combustor to the gasifier. More information regarding the experiments is available in Hafner et al. (2018). During the experiments, gasifier fuel feed and steam feed were kept constant and the gasifier was operated with steam-to-carbon ratio of 1.5. The model geometry is prepared based on the dimensions of the pilot gasifier. The conducted study focused on the gasification reactor. Applied boundary conditions are described in Table 4.2.

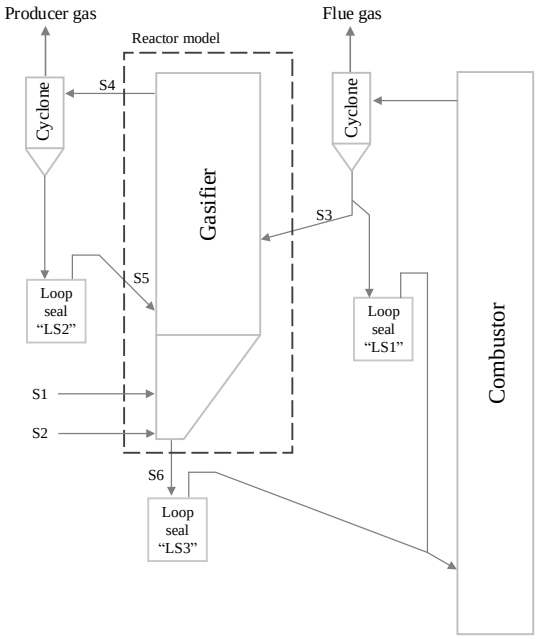

Figure 4.1: Schematics of IFK dual fluidised bed process, adapted from Hafner et al. (2018).

Table 4.2: Operation parameters and simulation boundary conditions (Publication II). Studied cases are referred as operation points (OP).

Parameter	S#	OP1.1	OP1.2	OP1.3	OP1.4
Biomass feed, kg/h	1		30		
Steam flow, kg/h	2		30.3		
Steam temperature, °C	2		146		
Solids flow, kg/h	3	341	498	570	694
Solids temperature, °C	3	716	734	787	809
Solids composition					
CaO, wt-%	3	85.2	93.3	91.2	96.0
$CaCO_3$, wt-%	3	9.6	2.0	4.7	0.4
Ash, wt-%	3	5.2	4.7	4.1	3.6
Bed temperature, °C		634	711	757	773

The boundary conditions were directly measured from the pilot or determined later by analysis of solid samples. Solids flow rate and temperature were measured from the pilot from between gasifier and combustor (S3). The composition of the solid flow was

measured from a sample extracted from combustor loop seal "LS1". In the experiments, wood pellets were used as the fuel. The properties of the used fuel are shown in Table 4.3. Fuel model parameters were obtained from experiments. The char fraction of fuel was determined experimentally for the used fuel for a temperature range of 650 to 800°C by proximate analysis. Tar fraction and γ_2 were obtained from hydrocarbon measurements of the pilot gasifier (Hafner et al., 2018). Average value for the γ_2 is used. Parameter γ_1 was determined from methane measurements of the pilot (Hafner et al., 2018). The methodology for determining the parameters is discussed in Publication III. Reaction kinetics of chemical reactions applied for modelling are shown in Table 4.4.

Table 4.3: Properties of used wood pellets and semi-empirical fuel model parameters.

Parameter	
Fuel properties	
Moisture fraction, wt-%,ar	6.0
Ash fraction, wt-%,db	0.2
C, wt-%,daf	50.8
H, wt-%,daf	6.1
N, wt-%,daf	0.2
S, wt-%,daf	0.1
O, wt-%,daf	42.8
LHV, MJ/kg,ar	17.36
Semi-empirical fuel composition	
Char fraction (°C), $\mathrm{kg_{char}/kg_{f,db}}$	$-1.72 \times 10^{-4}T + 0.3037$
Tar fraction (°C), $\mathrm{kg_{tar}/kg_{f,db}}$	$2.0 \times 10^{-5}T + 2.92 \times 10^{-2}$
Semi-empirical fuel model parameters	
γ_1 (°C), -	$2.448 \times 10^{-4}T + 0.565$
γ_2, -	0.65

Table 4.4: Chemical reaction kinetics.

Reaction	Ref.
Calcination	Martínez et al. (2012)
$R_{calc} = \rho_s k'_{calc} W_{\mathrm{CaCO_3}}^{2/3} (C_{\mathrm{CO_2,eq}} - C_{\mathrm{CO_2}})$	Fang et al. (2009)
$k'_{calc} = 2057 \exp(-\frac{112400}{R_i T})$	Stanmore and Gilot (2005)
Carbonation	Shimizu et al. (1999)
$R_{carb} = \rho_s k'_{carb} (W_{\max} - W_{\mathrm{CaCO_3}})(C_{\mathrm{CO_2}} - C_{\mathrm{CO_2,eq}})$	Alonso et al. (2009)
$k'_{carb} = 30$	Stanmore and Gilot (2005)
Sulphation	
$R_{sulph} = \rho_s k_{sulp} W_{\mathrm{CaO}} W_{\mathrm{SO_2}} W_{\mathrm{O_2}}$	Rajan and Wen (1980)
$k_{sulph} = 4.0(-3.843T + 5640) \exp(-\frac{8810}{T})$	
De-sulphation	
$R_{desulph} = \rho_s k'_{desulp} W_{\mathrm{CaSO_4}} C_{\mathrm{CO}}$	Myöhänen (2011)
$k'_{desulph} = 0.005 \exp(-\frac{10000}{T}) A_{\mathrm{m,CaSO_4}} M_{\mathrm{CaSO_4}}$	
Direct sulphation	
$R_{disulph} = \rho_s k'_{disulp} W_{\mathrm{CaCO_3}} C_{\mathrm{SO_2}}^{0.9} C_{\mathrm{CO_2}}^{-0.75} C_{O_2}^{0.001}$	Myöhänen (2011)
$k'_{disulph} = 0.01 \exp(-\frac{3031}{T}) A_{\mathrm{m,CaCO_3}} M_{\mathrm{CaCO_3}}$	
Boudouard	
$R_{boud} = k_{boud} \rho_{char} W_{char}$	Risnes et al. (2001)
$k_{boud} = 2.11 \times 10^7 \exp(-\frac{219000}{R_{\mathrm{i}} T}) p_{\mathrm{CO_2}}^{0.36}$ [bar]	
Water-gas	
$R_{wg} = k_{wg} \rho_{char} W_{char}$	Hemati and Laguerie (1988)
$k_{wg} = 1.23 \times 10^7 \exp(-\frac{198000}{R_{\mathrm{i}} T}) p_{\mathrm{H_2O}}^{0.75}$ [atm]	
Methanation	
$R_{meth} = k_{meth} \rho_{char} W_{char}$	Hejazi et al. (2017)
$k_{meth} = 16.4 \exp(-\frac{94800}{R_{\mathrm{i}} T}) p_{\mathrm{H_2}}^{0.93}$ [MPa]	
Water-gas shift	
$R_{wgs} = M_{\mathrm{CO}} k'_{wgs} ((C_{\mathrm{CO}} C_{\mathrm{H_2O}}) - (C_{\mathrm{CO_2}} C_{\mathrm{H_2}}) / K_{\mathrm{wgs}})$	Biba et al. (1978)
$k'_{wgs} = 2.78 \exp(-\frac{1510}{T}) f_{wgs}$	de Souza-Santos (1989)
$f_{wgs} = 1.0$	

4.2 Simulation results

The model validation is conducted against measurements of the IFK pilot reactor and other studies in the literature. The main results of the validation are reported. The focus of the discussion is on the physical phenomena producing the operation of the reactor. Understanding the physical phenomena is of value in the designing of an industrial-scale reactor.

4.2.1 Producer gas yield

The typical gas yield range of various SEG experiments is presented in Figure 4.2 based on Fuchs et al. (2019a). The simulations are compared against this typical range. The simulations results are consistent with the typical gas yield range of the process. The producer gas yield in the figure is affected by the fraction of volatiles in the fuel, its composition and chemical reactions, such as char gasification and CO_2 capture. The producer gas composition at the simulated operating points against measurements of the IFK's pilot gasifier from Hafner et al. (2018) are shown in Figure 4.3 with a range from various experiments based on Fuchs et al. (2019a). The presented range was obtained from three different gasifiers and covers various operating conditions. The presented measurement ranges do not distinguish different operation parameters of the gasifier. Therefore, it is possible that experimental data (In Figure 4.2, CO_2) or simulations could diverge from the measurement ranges.

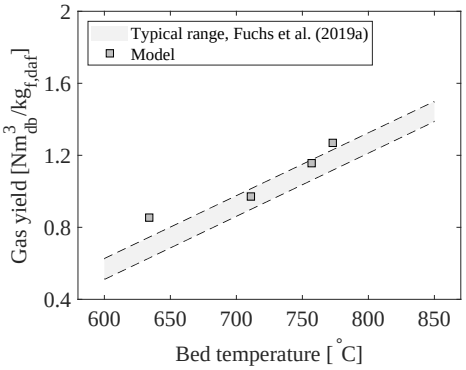

Figure 4.2: Gas yield of various SEG experiments and simulated producer gas yield. The gas yield range is based on Fuchs et al. (2019a). The data has been adapted from the source.

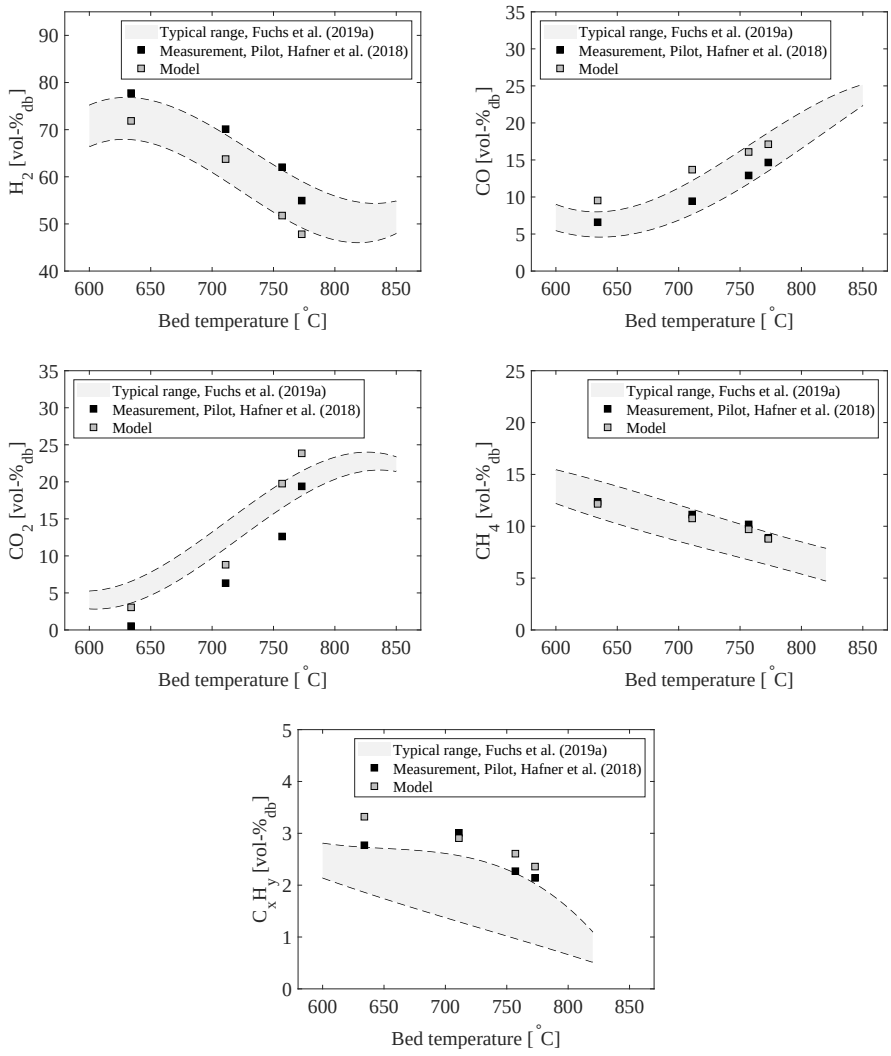

Figure 4.3: Volume fractions of H_2, CO, CO_2, CH_4, and C_xH_y gas species of producer gas at the studied operating points of 200 kW_{th} pilot gasifier (Hafner et al., 2018). The typical range of the measurements is based on various SEG experiments Fuchs et al. (2019a). The data has been adapted from the source. In the simulations, C_2H_4 component represents C_2-C_4 hydrocarbon species described in the figure with C_xH_y.

4.2.2 Carbon balances of the reactor

Carbon balances of the reactor are formulated from the simulations. The data is compared against carbon balance data from Fuchs et al. (2019a) in Figure 4.4. The carbon balance is presented as carbon transported to the combustor from the gasifier. The total carbon transport in Figure 4.4 is divided among char (solid carbon in char) and $CaCO_3$. The distribution of char and $CaCO_3$ is similar to Fuchs et al. (2019a). Char formed in fuel decomposition is also shown in the figure. Comparison of char transport and char formed from fuel shows almost complete transport of the formed char to the combustor. The low conversion is caused by a relatively low residence time of char in the gasifier. Consequently, the elemental carbon concentration of producer gas mainly originates from the devolatilised carbon.

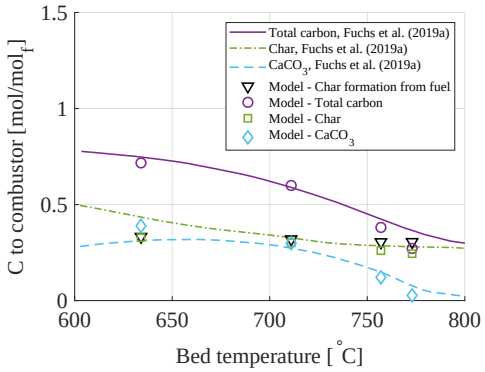

Figure 4.4: Carbon transport to the combustor. The simulated carbon transport is presented against balances from an SEG balance study Fuchs et al. (2019a). The overall carbon transport to the combustor is divided among char and $CaCO_3$. The char fraction of the fuel is shown for comparison.

4.2.3 Bed material's CO_2 capture

The operating temperature is the main process parameter to define the amount of carbon capture in the gasifier. The influence of temperature on bed material's $CaCO_3$ fraction change within the gasifier is shown in Figure 4.5. The CO_2 capture decreases with increasing operating temperature and vice versa. The bed material $CaCO_3$ fraction profiles are shown in Figure 4.6 at the bed material feeding point and below it. In each case $CaCO_3$ fraction of limestone is below the maximum carrying capacity ($W_{\max} = 0.3$). High mixing rates causes uniform solid profiles for the bed. Above the bed, entrainment of particles from the bed, solids feed composition from the combustor, and local reactions conditions affects the $CaCO_3$ fraction.

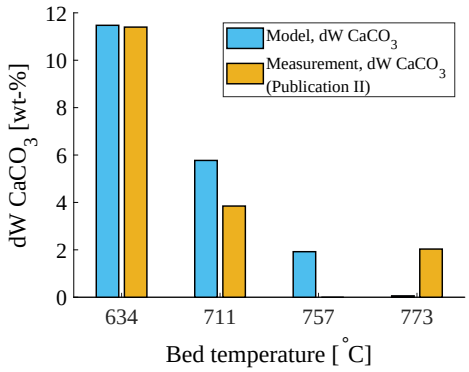

Figure 4.5: Bed material $CaCO_3$ mass fraction change within the gasifier. The change is calculated from the difference between "S6" and "S3" streams. For the pilot, the change is calculated based on difference of solid samples $CaCO_3$ fraction from loop seals "LS3" and "LS1".

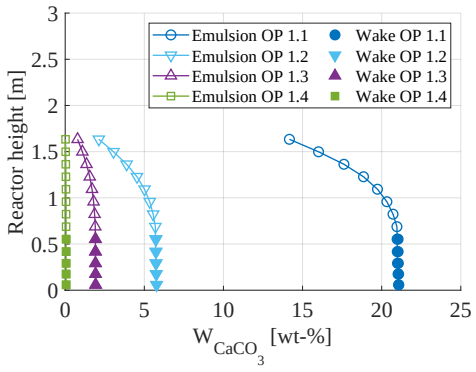

Figure 4.6: $CaCO_3$ profiles of model for emulsion and wake.

In Figure 4.7, the local CO_2 concentrations within the bed in respect of limestone's reaction equilibrium for carbonation and calcination reactions are shown. The figure shows the bed of the gasifier to operate close to the reaction equilibrium. At 770°C, the bed of the reactor operates on the calcination side of the equilibrium. The reaction kinetics of carbonation were fast enough, and local CO_2 concentrations were sufficient to set the bed operating close to the equilibrium at OP 1.1, OP 1.2 and OP 1.3. When the bed of the gasifier operates on the reaction equilibrium, the carbonation reaction is no longer occurring. Therefore, limestone's maximum transfer capacity for the CO_2 to the combustor can be attained below the maximum carrying capacity ($W_{\max}$). In the simulated cases OP 1.2 and 1.3, the bottom of the gasifier operated close to the equilibrium. In these cases, the equilibrium limited the CO_2 transfer capacity to the combustor. Although the maximum carrying capacity was not achieved.

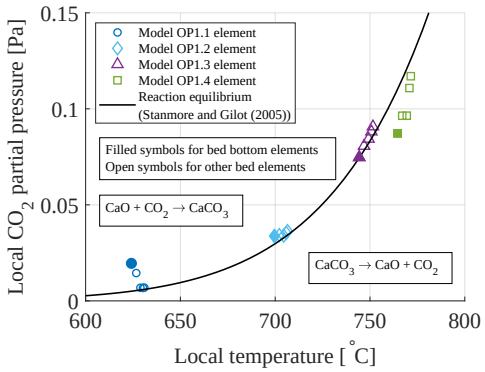

Figure 4.7: Simulated local CO_2 partial pressure in the bed elements with respect to the local temperature and thermodynamic reaction equilibrium according to Stanmore and Gilot (2005) is shown. The pressure in emulsion is presented.

4.2.4 Water-gas shift equilibrium

The water-gas shift reaction is enhanced by CO_2 capture in the reactor. The CO_2 capture enhances production of H_2 from the reaction by influencing the balance reaction products and reactants. The reaction's equilibrium constant ($K_{\text{wgs}} = \frac{y_{\text{H}_2}\, y_{\text{CO}_2}}{y_{\text{H}_2\text{O}}\, y_{\text{CO}}}$) determined from the simulated operation points is shown in Figure 4.8. The equilibrium of the reaction is shown in comparison. Commonly, in biomass BFB steam gasification processes the producer gas composition is well below the equilibrium at similar operation temperatures as with the SEG process. A comparison of the modelling, a steam-blown gasification experiments (Maniatis and Buekens, 1982; Herguido et al., 1992; Gómez-Barea et al., 2005) and an indirect gasifier experiments (Aghaalikhani et al., 2019) is shown in Figure 4.8.

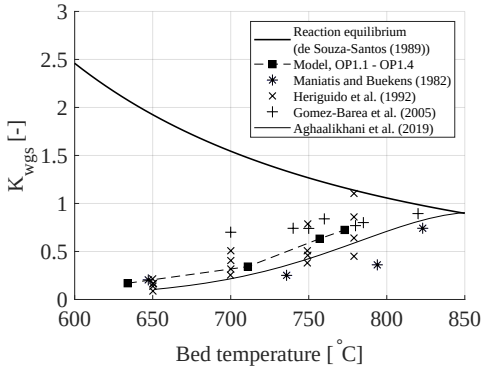

Figure 4.8: Water-gas shift reaction constant (K_{wgs}) of simulations compared against experimental data from literature (Maniatis and Buekens, 1982; Herguido et al., 1992; Gómez-Barea et al., 2005; Aghaalikhani et al., 2019).

4.2.5 Synergy of water-gas shift and carbonation reactions

The main chemical reactions of the gasifier are shown in Figure 4.9. The figure shows two distinctive operation regions for the gasifier, low-temperature and high-temperature regions. At low operation temperatures, the operation of the gasifier is carbonation dominated. When the temperature increases over 700°C, the operation characteristics change to a so-called steam gasification region. Limestone carbonation is still active in this region. However, its role is not as significant as with the lower operating temperatures. At the low operational temperatures, the vigorous CO_2 capture enhances the H_2 production from the water-gas shift reaction. The water-gas shift and the limestone carbonation in this region are the most dominant reactions.

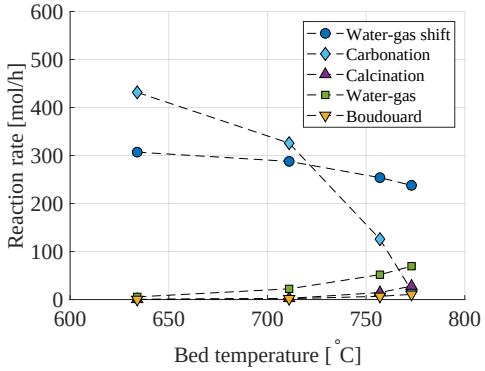

Figure 4.9: Reaction rates of main chemical reactions from simulations for the reactor.

At the steam gasification region above 700°C, the reaction rate of limestone carbonation and water-gas shift are decreased. The decline of CO_2 capture at higher temperatures (Figure 4.9) can be observed from Figure 4.3 as increasing CO_2 concentration of producer gas. The reaction rate of the water-gas shift is decreased as temperature increased. Char conversion by water-gas reaction increases most significantly from the char gasification reactions at the higher operating temperatures.

At the low operation temperatures, enhanced water-gas shift produced high H_2/CO ratios. The ratio decreases with increasing operating temperatures since H_2 production from the water-gas shift is reduced. At 770°C, the reaction rate of limestone calcination surpasses the carbonation reaction in the reactor. At this point, the gasifier operates similarly to a conventional indirect steam gasifier, and H_2/CO ratio below three is obtained from the simulations. A similar ratio can be obtained from indirect gasification processes operated on comparable process conditions.

4.3 Discussion

The BFB reactor model for the sorbent-enhanced gasification process was developed in this thesis based on the specifications of a 200 kW_{th} pilot plant. The developed

model takes into account the most important aspects required for comprehensive one-dimensional modelling of SEG processes. The developed model is based on the conservation of mass and energy. Reactor hydrodynamics and chemical reaction are based on semi-empirical correlations. The model is used for studying the SEG process at steady-state conditions.

The developed model allows studying of physical operation of SEG processes. In this study, data from the pilot reactor was used. The model was validated against the data from the IFK pilot reactor and other studies in the literature. The model predicted gas yield and producer gas composition typically observed for the SEG processes. The carbon balance of the model was consistent with the literature data. The carbon balance of the model indicated char transport to the combustor to be equal to char that was formed from the fuel. Due to a relatively low residence time of char in the gasifier and low reaction rates, the char conversion was low. In the simulations, almost all char was transported to the combustor. The result indicates the gaseous carbon in the producer gas to be mainly formed at fuel devolatilisation. Therefore, fuel decomposition modelling has a significant role in the precise modelling of the process. The modelling of the traditional processes is commonly done by assuming the fuel decomposition to follow the standard proximate and ultimate analyses. The approach is valid for a high-temperature processes. At lower temperatures, the process conditions of the reactor and the influence of the process conditions on the fuel decomposition should be regarded. Therefore, the precise modelling of low-temperature processes requires considering the temperature's influence on the main fractions of the fuel (permanent gas, char, tar), its impact on the elemental composition of the char, and the formed gas species.

The temperature also has a significant impact on chemical reactions. The reaction kinetics of limestone carbonation was sufficiently fast to set local CO_2 concentrations within the bed of the gasifier close to the reaction equilibrium of limestone. Consequently, the carbon transport to the combustor by $CaCO_3$ was close to the maximum carbon transport at temperatures over 700°C for the studied cases. The results imply the role of the equilibrium to be significant for the process's physical operation. Water-gas shift reaction has a strong coupling to the CO_2 capture. The coupling is formed via a balance of reaction products and reactants. The carbon capture removes CO_2 from the reaction products side of the balance, which sets the balance towards reaction products, and enhances the production of the H_2 from the reaction.

The work presented improved the current understanding of the physical phenomena governing the SEG processes. The developed model was able to capture the sorbent-enhanced characteristics of the SEG process. The validated model can be used for further studies of the process. The validated semi-empirical correlations for the physical phenomena were obtained from the model validation. The gained knowledge can be utilised in studying the industrial-scale reactor system.

5 Study of dual fluidised bed sorption-enhanced gasification process

Analysis of a pilot-scale dual fluidised bed system is conducted. The reactor system's mass and energy balances are analysed for the production of synthetic biofuels. The study of the SEG process with coupled reactors has been previously presented with equilibrium model (Hejazi et al., 2014) and with 1D semi-empirical reactor models for BFB-CFB (Yan et al., 2018) and CFB-CFB (Publication IV) systems. In this work, a dual fluidised bed system is created by coupling the pilot-scale BFB gasifier and the CFB combustor models. The validated BFB gasifier used for the study is described in Chapter 4 and the CFB combustor was designed based model frame presented in Chapter 3. The analysis presented in this chapter for the dual fluidised bed system consists of two studies. In the first modelling study, the mass and energy balances of the dual fluidised bed system are examined by altering processes operation temperature. The system is studied in a temperature range of 650°C to 775°C. An influence of the gasifier's S/C ratio on the mass and energy balances of the dual fluidised bed system is investigated in the second study. The second study is conducted on the temperature range of 700°C to 775°C, where producer composition shows suitability for synthetic biofuel production. Analysis of dual fluidised bed processes balances in two case studies is presented. The conducted modellings studies aimed to strengthen the understanding of system's mass and energy balances. Analysis of adiabatic reactor system with the comprehensive semi-empirical model has not been conducted before. The understanding of the processes operation is of value in the design of an efficient industrial-scale system.

5.1 Process description and simulation setup

A dual fluidised bed system with BFB and CFB reactors was created. The system configuration is shown in Figure 5.1. The system is created by coupling solid streams from the reactor to another. The dimensions of the reactor system are given in Table 5.1. Dimensions of the gasifier are according to Chapter 4. The combustor is designed for the system. The design point for the system is gasifier operation temperature of 775°C and S/C ratio of 1.0. The selected design point represents conditions where the gasifier's endothermicity is the highest in this study. Therefore, the highest solids flow rate into the gasifier is required to obtain the gasifier operation temperature. The combustor is designed to operate on the design point without solids internal circulation (S10). The selected design point assures a wide operation range for the system. The system is designed with perfectly insulated reactors.

The simulation studies in this chapter include analysis of the dual fluidised bed system's mass and energy balances for the temperature range of 650°C to 775°C. In addition, the impact of the S/C ratio on the mass and energy balances for the temperature range of 700 °C to 775°C is investigated. The variation of the S/C ratio is studied on the higher temperature range where producer composition shows suitability for synthetic biofuel production. Applied boundary conditions for the studies are described in Table 5.2. In the first

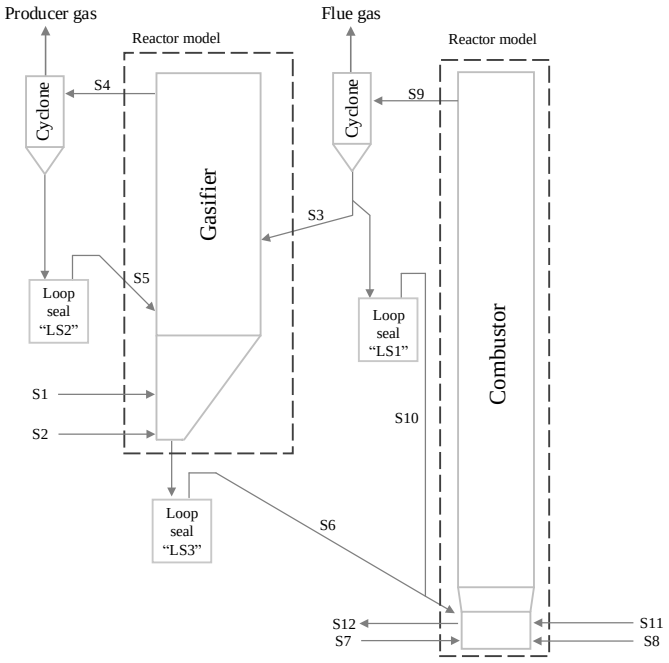

Figure 5.1: Dual fluidised bed system configuration.

Table 5.1: Dimensions of the dual fluidised bed system.

	Gasifier	Combustor
Height of the bottom section, m	-	0.5
Height of the conical section, m	0.35	1
Height of the reactor, m	5.35	11
Diameter of the grid, m	0.136	0.125
Diameter of the freeboard, m	0.33	0.14
Number of nodes in bottom section	-	2
Number of nodes in conical section	3	4
Number of nodes in freeboard section	37	34
Elevation of secondary gas feed, m	-	0.50
Elevation of tertiary gas feed, m	-	1.50
Elevation of input solid flow channel, m	0.50	0.375
Elevation of external circulation channel, m	1.70	0.375
Solid exit to another reactor, m	0	11

study, gasifier temperature and solid flow from the combustor are varied. The operating temperature of the gasifier is adjusted by altering the solids flow rate from the combustor.

In addition, the energy balance of the system is adjusted based on the gasifier's producer gas composition. The combustor is operated using constant operational parameters, e.g. temperature of reactor top, flue gas oxygen concentration and grid pressure. The system is studied with the gasifier's S/C ratio of 1.5. In the second study, the impact of the S/C ratios of 1.0 and 2.0 for 700 °C to 775°C range are investigated. The ratio is adjusted by altering fuel feed to the gasifier. Altering the S/C ratio by fuel feed has a beneficial influence on system balances since additional char fed to the combustor substitutes a part of the combustor's additional fuel.

The properties of the fuel are according to Table 4.3. Fuel model parameters for γ_1 is used according to Table 4.3. Parameter γ_2 is used based on Publication IV/Chapter 6 where higher number of experimental data points were available for determining the parameter. The methodology used for determining fuel model parameters is based on Publication III.

Table 5.2: Boundary conditions for the simulations. Stream numbers (S#) refers to numbering in Figure 5.1.

	S#	650°C	675°C	700°C	725°C	750°C	775°C
S/C, mol/mol		1.5	1.5	1.0/1.5/2.0	1.0/1.5/2.0	1.0/1.5/2.0	1.0/1.5/2.0
Fuel feed to gasifier, kg/h	1	30	30	42/30/25	42/30/25	42/30/25	42/30/25
Fuel to combustor, kg/h	7	2.85	2.52	1.47/2.51/3.04	1.50/2.34/2.92	2.31/3.15/3.56	3.47/3.92/4.21
Combustor temperature[1], °C					880		
Steam, °C	2				146		
O_2, vol $-$ $\%_{\mathrm{db}}$	9				3.0		
Air, °C	8				250		
$CaCO_3$, kg/h	11				1.5		
$CaCO_3$, °C	11				25		
Grid over pressure[2], kPa					5.0		
Bed surface height[3], m					0.75		
Solid purge, kg/h	12	0.93	0.93	0.96/0.93/0.91	0.96/0.92/0.91	0.95/0.92/0.91	0.94/0.92/0.91
Cooling power[4], kW		9.9	6.6	3.3	0	0	0

1) At top of the combustor.

2) Pressure difference caused by solid material in the combustor.

3) Gasifier bed height from the bottom.

4) Cooling is applied to gasifier bed.

5.2 Simulation results

The operation of the dual fluidised bed system is studied. In the first part of this chapter, simulations results in the temperature range of 650°C to 775°C are discussed. The study focuses on mass and energy balances of the dual fluidised bed process. The second part discusses the influence of gasifier S/C ratio on producer gas composition. The study is conducted in 700°C to 775°C temperature range, where producer gas composition is favourable for biofuel synthesis. The results show the effect of operating parameters on producer gas composition and balances of the system. The suitability of the SEG as part of biofuel synthesis processes is discussed. The presented modelling studies aimed to strengthen the understanding of the processes operational balances. The understanding

of the processes operation is of value in the design of an efficient industrial-scale scale system.

5.2.1 Analysis of dual fluidised bed system's balances: Temperature variation

The operation of the dual fluidised bed system is studied. The study focuses on the temperature range of 650°C to 775°C, where six operation points are studied. The producer gas composition and gas yield at the simulated temperatures are shown in Figure 5.2. The simulation results are compared against the typical range of measurements for the process (Fuchs et al., 2019a). The simulation results are consistent with the measurements.

In Figure 5.3 (a), solids flow rates from the combustor to the gasifier are shown for the simulated temperature range. Gasifier operation temperature is varied by altering the solid flow rate from the combustor. The solids flow rate to the gasifier depends on the combustor's solids inventory and gas velocity. The gas velocity varied from 5.4 to 6.9 m/s depending on the feed flows. Figure 5.3 (b) shows the fuel feed to combustor and cooling of the gasifier. The system can partly self-sustain its operation by using a part of the gasifier's fuel feed (char) to produce the heat for the process. However, additional fuel feed to the combustor is required in the simulated cases. This fuel feed is shown Figure 5.3 (b). The share of the fuel feed from the total combustion energy is 22-34 %. The cooling of the gasifier is required at lower temperature operating points. The cooling is needed to maintain the set-point temperature of the combustor. However, to operate the system effectively, additional cooling is necessary. The simulations indicated the producer gas composition at the lower temperature operation temperatures (at 700°C and below) to depend on the solid flow rate into the gasifier. A too low solids flow rate is observed to limit the CO_2 capture in the reactor, and consequently, to reduce H_2 production of the gasifier. Due to the high concentration of H_2 at lower operating temperatures, the process can be used for producing H_2 from biomass. Hence, the system balances are analysed from this perspective below 700°C. The energy balance is used to adjust producer gas CO_2 concentration on the lower boundary of the typical measurement range (Fuchs et al., 2019a). A steadily increasing heat loss is applied to maintain sufficient CO_2 capture and production of H_2 by water-gas shift reaction.

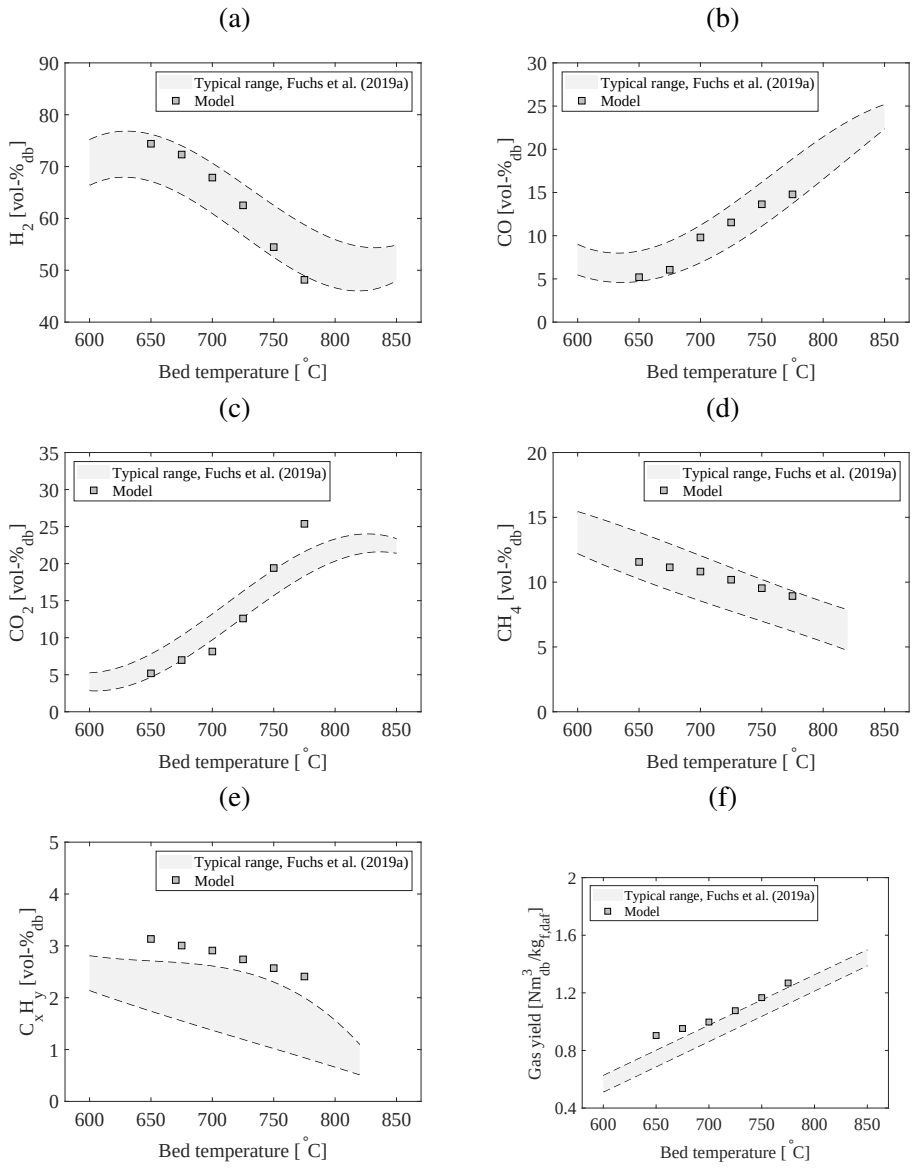

Figure 5.2: (a) Producer gas volume fractions of gas species (a) H_2, (b) CO, (c) CO_2, (d) CH_4, (e) C_xH_y and (f) gas yield are presented. The typical range of the measurements is presented based on various SEG experiments Fuchs et al. (2019a). The data has been adapted from the source.

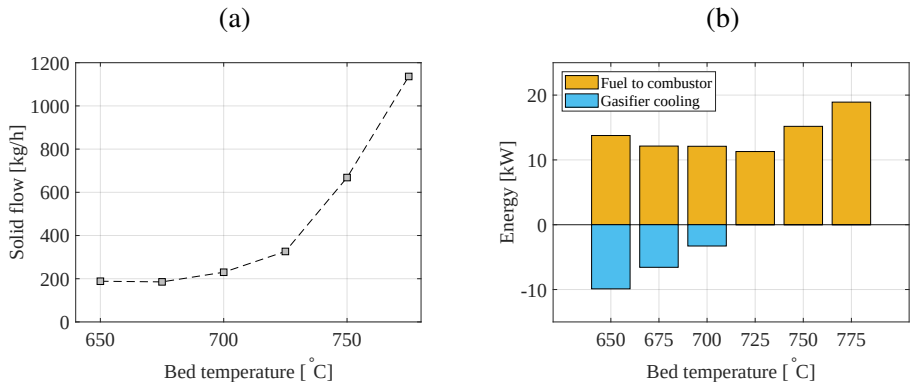

Figure 5.3: (a) Solids mass flow rate to gasifier from combustor and (b) fuel feed to the combustor and cooling of the gasifier.

The cooling of the gasifier increases the solid flow rate from the combustor to the gasifier when the set-point temperatures are maintained for both reactors. At the low operation temperatures, the CO_2 concentration of producer gas could be adjusted by cooling the gasifier and the solids circulation rate. Over 700°C temperatures, the cooling of the gasifier could not be used for increasing the CO_2 capture since the gasifier's bed operated in the proximity of limestone's reaction equilibrium. In these process conditions, no further CO_2 capture is possible by increasing the cooling. Average CO_2 partial pressure in the bed of the simulated cases is shown in Figure 5.4 with the reaction equilibrium.

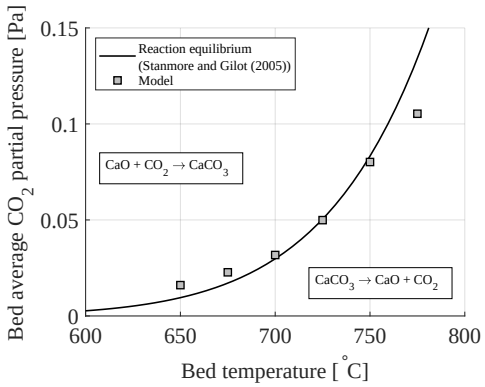

Figure 5.4: Simulated average CO_2 partial pressure and thermodynamic reaction equilibrium according to Stanmore and Gilot (2005) is shown. The pressure in emulsion is presented.

5.2.2 Analysis of dual fluidised bed system's balances: Steam-to-carbon ratio variation

The influence of the gasifier's S/C ratio on producer gas composition is studied in the range of 700°C to 775°C in four operation points. The S/C ratio of 1.0 and 2.0 are used. The system is operated with process parameters similar to the study with an S/C ratio of 1.5. In the temperature range of this study, raw producer gas is suitable for downstream DME synthesis (Hafner et al., 2018).

The influence of the S/C ratio on producer gas composition and gas yield is shown in Figure 5.5. Operating the gasifier with the S/C ratio of 2.0 produces higher hydrogen concentration for the producer gas, increases CO_2 concentration and decreases CO concentration. The gas yield of the process increased with the higher S/C ratio. The change of gas species relations in the studied operation points is attributed to the synergy of water-gas shift reaction and CO_2 capture and also the S/C ratio. The adjustment of the S/C ratio in this study is made by fuel feed, and H_2O feed to the gasifier is kept at a constant value. The higher S/C ratio increases the concentration of H_2O and lowers the concentration of the other species involved in the water-gas shift reaction. The higher H_2O concentration can be suspected to increase the water-gas shift's yield.

The influence of the S/C ratio on H_2 production can be observed as a higher H_2/CO ratio of gas species in Figure 5.6 (a). Higher the operation temperature decreases the ratio since CO_2 capture reduces. The CO_2 capture by limestone carbonation has a synergistic influence on the water-gas shift reaction, and when the CO_2 capture reduces, the H_2 production by water-gas shift reduces. In Figure 5.6 (b) and Figure 5.6 (c), the H_2/CO_2 ratio and module of producer gas are shown, respectively. The module for producer gas is determined from Eq. 2.2. The optimal composition of producer gas for DME synthesis as module-based is 2 (van Kampen, 2021). For CO_2-based conversion, the value of H_2/CO_2 in the range of 1 to 3 is preferred the DME synthesis (Dieterich et al., 2020). The simulations indicate producer gas H_2/CO composition to be too high for H_2/CO-based conversion in which H_2/CO = 2 or less is preferred (Dieterich et al., 2020). Based on the simulations, the producer gas shows applicability for methanol and SNG production as well as DME production. For methanol and DME synthesis, requirements of the producer gas composition are similar (Dieterich et al., 2020). Production of synthetic natural gas from gasifier raw gas requires the gas composition of module 3 (Wix et al., 2007). The production of SNG is possible around 700°C operating temperatures of this study.

For the studied cases, cold-gas efficiency (CGE) is shown in Figure 5.7. The cold-gas efficiency is calculated based on producer gas chemical energy content and lower heat value of fuel

$$\mathrm{CGE} = \frac{q_{m,pg} \sum W_j \mathrm{LHV}_j}{P_f} \tag{5.1}$$

where $q_{m,pg}$ is the producer mass flow rate, W is the mass fraction of gas specie j, LHV_j is the lower heating value of the specie j, and P_f is fuel power in LHV basis. Operating

the gasifier with different S/C ratios has a minor impact on the CGE.

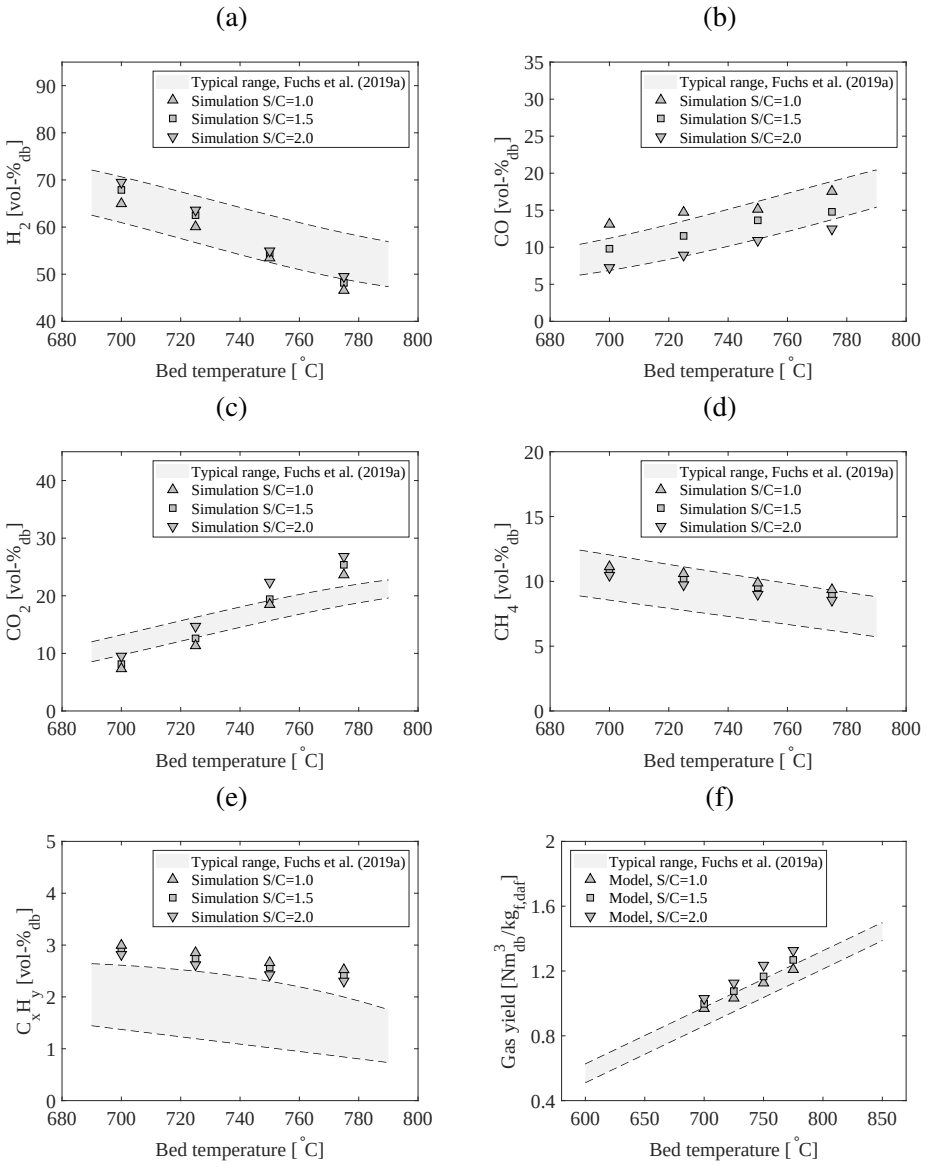

Figure 5.5: (a) Volume fractions of gas species (a) H_2, (b) CO, (c) CO_2, (d) CH_4 and (e) C_xH_y and (f) gas yield are presented. The typical range of the measurements is presented based on various SEG experiments Fuchs et al. (2019a). The data has been adapted from the source.

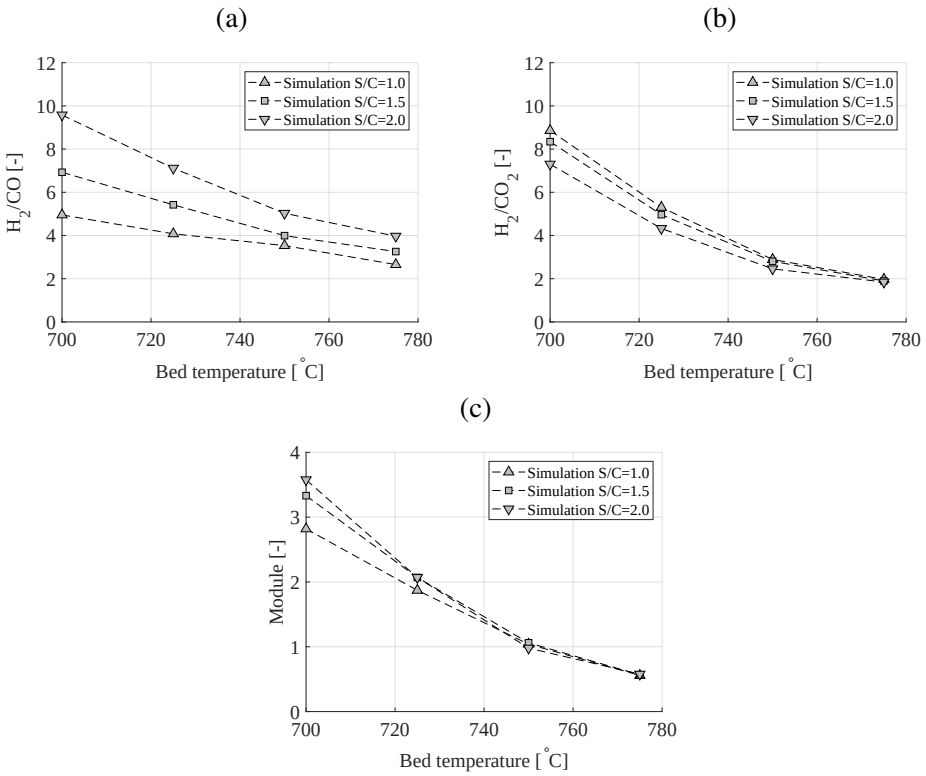

Figure 5.6: (a) H_2/CO ratio, (b) H_2/CO_2 ratio and (c) module of producer gas.

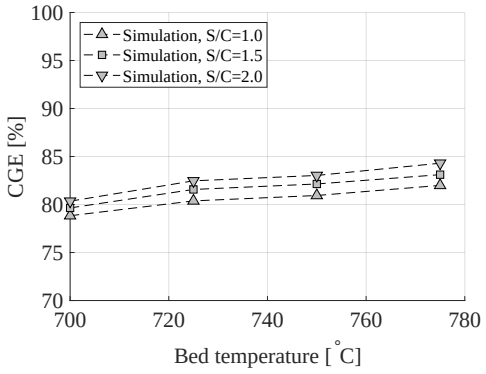

Figure 5.7: Cold-gas efficiency.

Figure 5.8 (a) shows the influence of the S/C ratio on the solid flow rate into the gasifier. Operating the gasifier with the S/C ratio of 1.0 increases the endothermicity of the reactor, and thus, higher solids flow rates are required. Operating the gasifier with a low S/C ratio has a beneficial effect on the system's energy balance. Figure 5.8 (b) shows the energy

required for heating the system. Operating the system with a lower S/C ratio lowers the need for additional fuel to the combustor by increasing fuel feed into the gasifier and increasing the amount of char used in the combustor. The decreased need for additional fuel increases the system's overall efficiency since less fuel is required to maintain the system's operation.

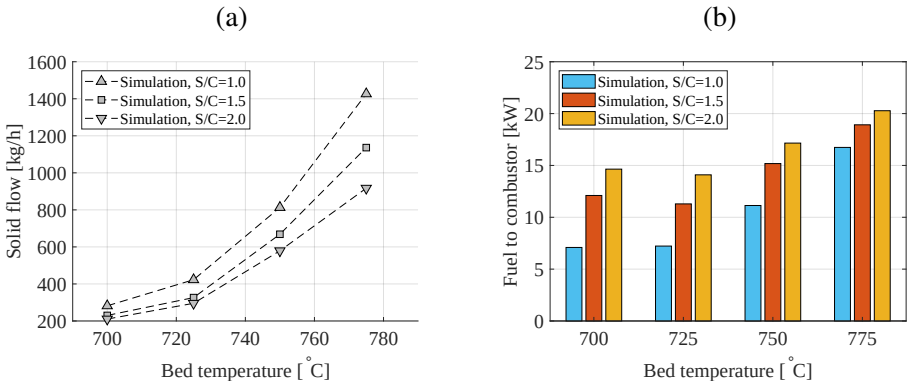

Figure 5.8: (a) Mass flow rates of solid to gasifier from combustor and (b) fuel feed to the combustor.

5.3 Discussion

The model for the dual fluidised bed sorption-enhanced gasification process was developed in this work. The model was created by coupling 1D BFB and 1D CFB reactor models to each other by material flows. The connected reactor system forms a comprehensive 1D dual fluidised bed model for sorption-enhanced gasification. The developed model allowed studying the balances of the pilot-scale dual fluidised bed system.

The operation of the dual fluidised bed system was studied. A system without heat losses was designed. The gasifier presented in Chapter 4 was used, and the combustor was designed to allow a wide operation range for the system. The dual fluidised bed system was studied in the temperature range of 650°C to 775°C. Mass and energy balances of the system were investigated. The model showed that the system could not be operated without additional fuel feed into the combustor in the studied operation points. At lower operating temperatures, cooling of the gasifier was required. The cooling was needed to keep the combustor's operation temperature on the set-point and maintain adequate solid flow through the gasifier. Additional cooling was applied to increase the solid flow. The higher solid flow enabled operating the system effectively at 650-700°C operating temperatures.

The simulation study evaluated how operating the gasifier with different S/C ratios impacted producer gas composition and balances of the dual fluidised bed system. The

simulation results indicated the cold-gas efficiency of the gasifier to stay relatively independent of the S/C ratio. Operating the gasifier with a lower S/C ratio was beneficial from the perspective of the overall balances of the system. The higher fuel feed into the gasifier increased the thermal fuel power of the gasifier. The higher thermal power increased the quantity of char used in the combustor and substituted a part of the additional fuel for heating the system.

Synthetic biofuels fuels could be refined from producer gas. Producer gas suitable for downstream synthesis processes was obtained by operating the gasifier over 700°C temperatures. The study indicated DME, methanol and SNG as possible synthesis products based on the gasifier's raw gas composition. The raw gas H_2/CO and H_2/CO_2 ratios were changed by gasifier operation parameters. However, only minor changes to the module occurred on the temperatures, where the module was optimal for DME synthesis.

The work presented improved the current understanding of the dual fluidised bed system's balances. The results showed how the gasifier operational parameters influence the gasifier's performance and the system's balances. The work evaluated possible synthesis processes that the sorption-enhanced gasification can be combined with based on the gasifier raw gas composition. The understanding of system's operation is of value in the design of the efficient industrial-scale systems.

6 Modelling of an industrial-scale sorption-enhanced gasification process

An industrial-scale SEG process is designed for the production of DME from biomass. The thermal power of the designed reactor system is 100 MW_{th}. The system was designed by a model-based approach. A 1D circulating dual fluidised bed reactor model was developed for this task. The modelling work presented in this chapter is based on pilot-scale model validation (Chapter 4). Quantitative understanding of physical operation of the SEG reactors was obtained from the validation. The acquired knowledge was used in the development of the industrial-scale process. The model used in this study is described in Chapter 3.2 and Publication IV. This chapter presents the developed industrial-scale reactor concept and summarises the main modelling results.

6.1 Process description and simulation setup

A dual fluidised bed system with two CFB reactors was formed by coupling solid streams from the reactor to another. The system configuration is shown in Figure 6.1. The dimensions of the reactor system are given in Table 6.1. The system was designed to operate with a gas velocity of 5 m/s and a steam-to-carbon ratio of 1.5.

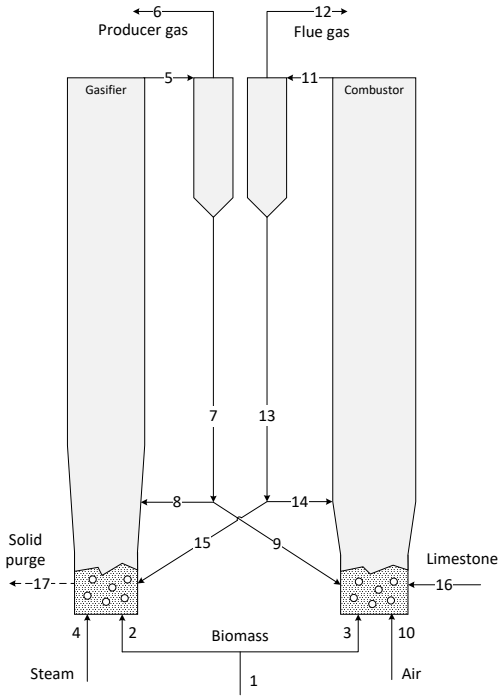

Figure 6.1: Reactor configuration for the process.

Table 6.1: Dimensions of the SEG reactors and solid material properties.

	Gasifier	Combustor
Height of the bottom section, m	2.3	2.2
Height of the cone section, m	4.00	2.00
Height of the reactor, m	20.00	20.00
Diameter of the grid, m	2.35	2.51
Diameter of the freeboard, m	2.88	3.09
Number of nodes in bottom section	5	5
Number of nodes in cone section	8	4
Number of nodes in freeboard section	27	31
Elevation of secondary gas feed, m	1.0	1.0
Elevation of tertiary gas feed, m	2.0	2.0
Elevation of input solid flow channel, m	0-0.9	0-0.9
Elevation of external circulation channel, m	0-0.9	0-0.9
Solid exit to another reactor, m	18.00	18.00

A simulation study was conducted to investigate the operation of the dual fluidised bed system. The undertaken study included ten operation points with producer gas module varying between 2 and 0.7 (module definition in Eq. 2.2). Module value 2 represents a case where producer gas is directly suitable for DME synthesis without downstream conditioning of the gas. Boundary conditions for the conducted study are presented in Table 6.2. A constant heat loss of 20.0 kW/m was applied to model the heat loss of the reactors.

Table 6.2: Boundary conditions for the simulations. Stream numbers (S#) refers to numbering in Figure 6.1. Studied cases are referred as operation points (OP).

	S#	OP1	OP2	OP3	OP4	OP5	OP6	OP7	OP8	OP9	OP10
Fuel feed, kg/s	1	6.644									
Fuel feed, MW	1	108.8									
Fuel to combustor, %	3	1	2	3	4	5	6	6	6	6	6
S/C, mol/mol	4/2	1.5									
CO_2 feed[1], kg/s	4	0.2									
CO_2 feed[1], °C	4	25									
Steam, °C	4	200	200	200	200	200	200	300	400	400	400
O_2, vol $-\ \%_{\mathrm{db}}$	12	3.0	3.0	3.0	3.0	3.0	3.0	3.5	4.7	4.7	4.7
Air, °C	10	250									
$CaCO_3$, kg/s	16	0.5									
$CaCO_3$, °C	16	20									
Grid over pressure[2], Pa	4,10	4500	4500	4500	4500	4500	4500	4500	4750	5000	5250
Exit pressure, kPa	6,12	143									
Solid purge, kg/s	17	0.163	0.156	0.150	0.144	0.138	0.131	0.122	0.097	0.088	0.080

1) At top of the combustor.

2) Pressure difference caused by solid material in the combustor.

Properties of the used fuel are described in Table 6.3. Release of hydrocarbons from the fuel was set based on a pilot reactor's measurements presented in Publication IV. The char fraction of fuel was determined experimentally for the used fuel for a temperature range of 650 to 800°C. Chemical reaction kinetics applied for the modelling of the gasifier are

summarised in Table 4.4. On the contrary to the table, carbonation reaction kinetics in this study was used according to Grasa et al. (2009) and for water-gas shift kinetics a parameter of $f_{wgs} = 0.075$ was applied based on Petersen and Werther (2005a).

Table 6.3: Properties of used wood pellets and semi-empirical fuel model parameters.

Parameter	
Fuel properties	
Moisture fraction, wt-%,ar	15.0
Ash fraction, wt-%,db	1.2
C, wt-%,daf	51.8
H, wt-%,daf	6.2
N, wt-%,daf	0.2
S, wt-%,daf	0.02
O, wt-%,daf	41.8
LHV, MJ/kg,ar	16.37
Semi-empirical fuel composition	
Char fraction (°C), $kg_{char}/kg_{f,db}$	$-1.72 \times 10^{-4}T + 0.3037$
Tar fraction (°C), $kg_{tar}/kg_{f,db}$	$2.0 \times 10^{-5}T + 2.92 \times 10^{-2}$
Semi-empirical fuel model parameters	
γ_1 (°C), -	$1.626 \times 10^{-4}T + 0.703$
γ_2 (°C), -	$-4.38 \times 10^{-8}T^2 + 8.142 \times 10^{-5}T + 0.612$

6.2 Simulation results

The industrial-scale reactor design was created for the SEG process. The presented simulation results focus on the main balances of the reactor system. The physical operation characteristics, performance of the designed reactor system and process integration of the gasifier as part of DME production are discussed in this chapter. The presented operating values of an industrial-scale plant provide essential information to support plant design and assess plant operating performance and cost.

6.2.1 Solid circulation and operation temperatures

Simulated temperature range and solids circulation rates in the SEG system are shown in Figure 6.2 (a) and Figure 6.2 (b), respectively. The presented range is obtained by altering the fuel feed ratio according to Table 6.2 and controlling system hydrodynamics. An increase in solid circulation rate from the combustor to the gasifier increased the operating temperature of the gasifier.

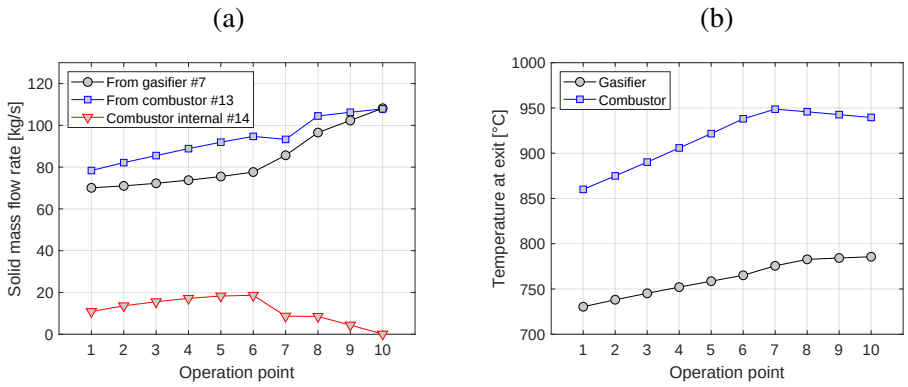

Figure 6.2: (a) Mass flow rates of gasifier and combustor and (b) temperatures at the top of the reactors.

6.2.2 Producer gas yield

The producer gas yield of the simulations is shown in Figure 6.3 (a). The simulations are compared against the typical gas yield range of various SEG experiments (Fuchs et al., 2019a). An increase in the operating temperature of the gasifier increases the gas yield of the process. The obtained gas yield is consistent with the presented range. The composition of the producer gas at the simulated operating points is shown in Figure 6.3 (b) - Figure 6.3 (f) against a range from various SEG experiments (Fuchs et al., 2019a). Module of producer gas for the simulated range is shown in Figure 6.3 (g). The simulation results show consistency with the experimental results obtained similar kind systems. Operation temperature of 730°C, where module 2 is obtained for the producer gas composition is suitable for DME production.

6.2.3 Chemical energy conversion

Chemical energy conversion efficiency in the gasifier is described with cold-gas efficiency (CGE). The CGE describes conversion of fuel's chemical energy to chemical energy of the producer gas. The CGE is calculated from Eq. 5.1. A distribution of chemical energy bound to the gas species of producer gas is shown in Figure 6.4 (a). According to the figure, hydrocarbons species comprise a significant portion of the chemical energy of the producer gas. The DME production cannot utilise the hydrocarbon species. Therefore, the share of the total energy utilised for the DME production depends on how effectively hydrocarbon species can be used in downstream processes. Without retaining the chemical energy of the hydrocarbons, the overall synthesis process suffers a significant energy penalty due to loss of the chemical energy of the hydrocarbon species. The total chemical energy production of the gasifier is shown in Figure 6.4 (b). The chemical energy production is relatively constant in the simulated operation range. The figure indicates the chemical energy content of the producer gas to be higher at lower operating temperatures compared to higher operating temperatures.

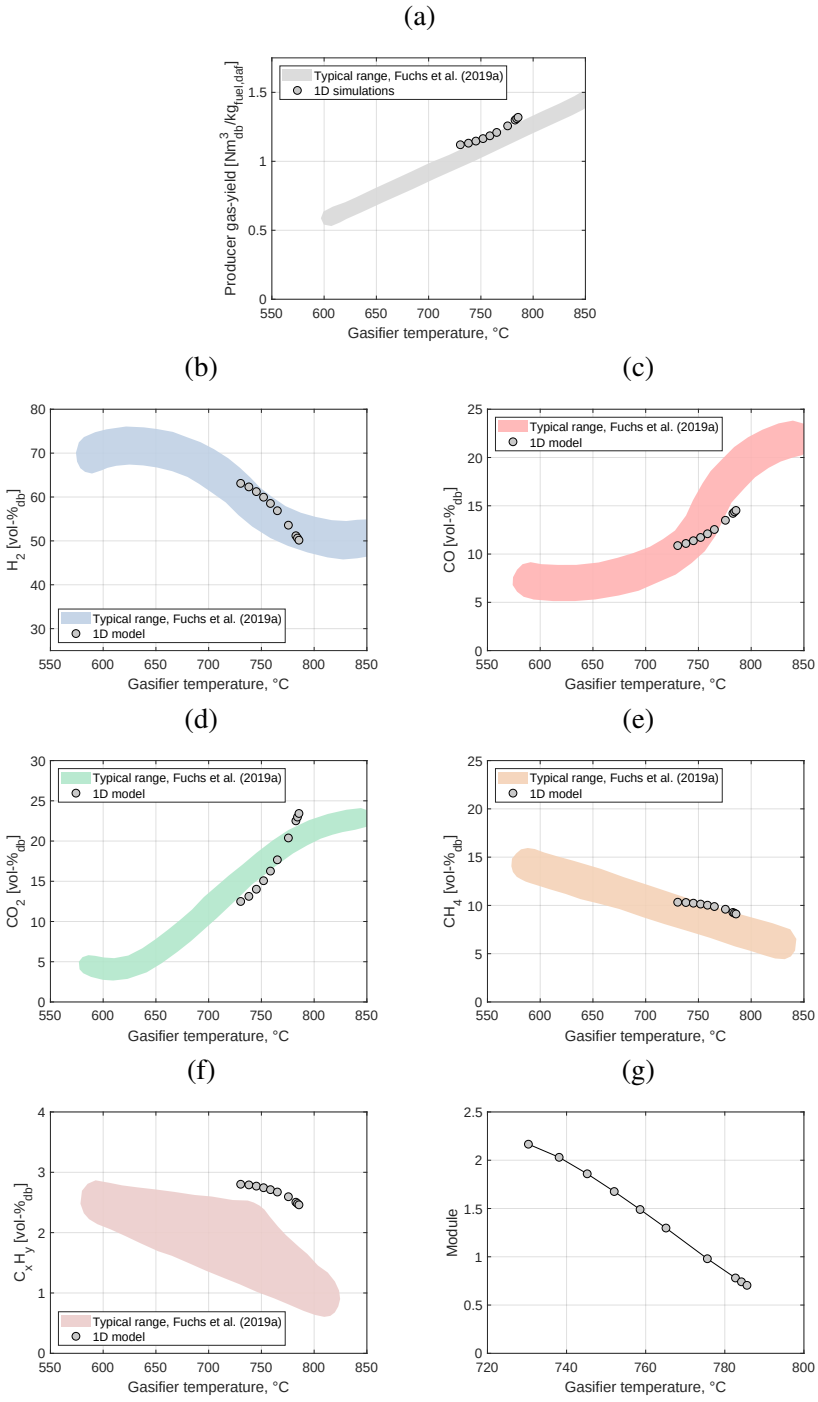

Figure 6.3: (a) Producer gas yield and volume fractions of gas species (b) H_2, (c) CO, (d) CO_2, (e) CH_4, (f) C_xH_y and (g) module are presented. The typical range for the measurements is presented based on various SEG experiments Fuchs et al. (2019a). The data has been adapted from the source. In the simulations, C_2H_4 component represents C_2-C_4 hydrocarbon species described in the figure with C_xH_y.

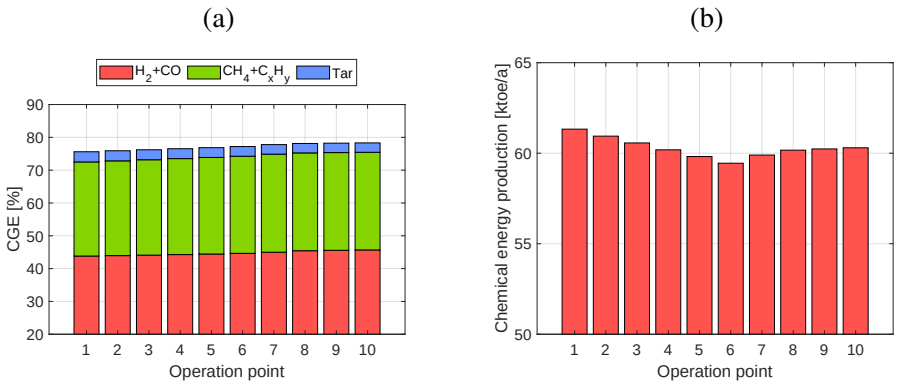

Figure 6.4: (a) Cold-gas efficiency (CGE) of gasifier and (b) total chemical energy production at the simulated operation points. The figure (a) shows chemical energy content of different gas species in producer in relation to fuel feed to the gasifier and (b) total energy of producer gas including H_2, CO, CH_4, C_xH_y and tar species at yearly basis production. The total energy production is calculated based on mass flow and lower heating value of producer gas.

6.2.4 Carbon balance of the gasifier

The carbon balance of the gasifier is investigated. Carbon conversion of the fuel and carbon transport to the combustor for the reactor is shown in Figure 6.5 (a) and Figure 6.5 (b), respectively. The carbon conversion describes the reformation of fuel's solid carbon in the gasifier. According to the figure, increasing operation temperature increases the carbon content of producer gas. The increase is owed to the decrease of carbon in the other carbonaceous constituents. The increase in operating temperature reduces the quantity of formed char and increases char's conversion. Less CO_2 is captured at elevated temperatures. Carbon transport from the gasifier to the combustor is shown in Figure 6.5 (b). The carbon transport to the combustor is decreased with increased temperatures due to higher conversion of carbon to producer gas and decreased CO_2 capture.

6.2.5 Water-gas shift equilibrium and reaction equilibrium of limestone

The gasifier operates below equilibrium conditions for water-gas shift and limestone carbonation in studied operation points. In Figure 6.6, the simulation results and the equilibrium conditions for (a) water-gas shift and (b) limestone's carbonation and calcination reactions are shown. The simulations results show the gasifier to approach equilibrium conditions at higher operation temperatures. For limestone, the equilibrium conditions are reached around 780°C. The water-gas shift stays below the equilibrium conditions in each studied operating temperature. A comparison of the water-gas shift equilibrium constants from the modelling is shown against a steam-oxygen blown gasification experiments (Hannula and Kurkela, 2012) and an indirect gasifier experiments (Kurkela et al., 2019). Conversion of producer gas in the SEG reactor by water-gas shift is similar to the

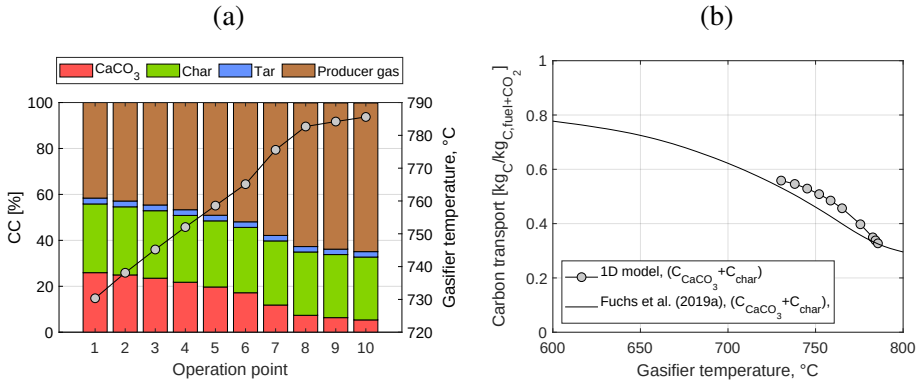

Figure 6.5: Carbon balance of the gasifier. (a) Carbon conversion and (b) carbon transport are shown. The carbon conversion is divided between carbonaceous constituents, where carbon of fuel can take residence. The carbon transport of the model is compared against carbon transport of various experiments (Fuchs et al., 2019a).

CFB steam gasification experiments.

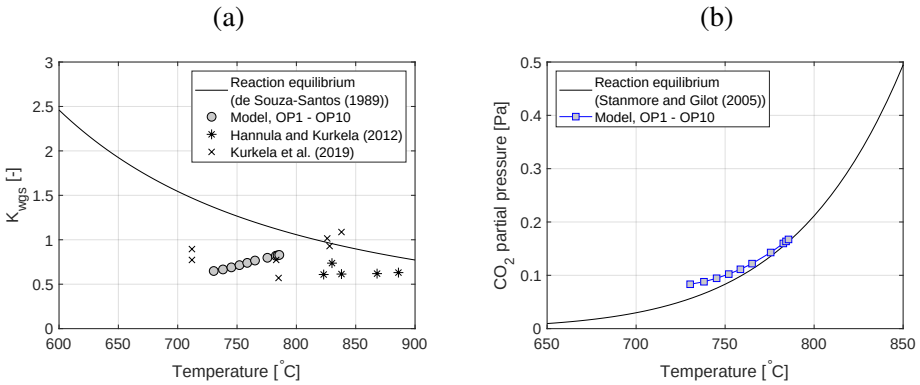

Figure 6.6: (a) Simulated equilibrium constant of water-gas shift reaction and (b) CO_2 partial pressure at the top of the reactor with respect to the temperature at the top of the reactor. Equilibrium is shown as comparison. For water-gas shift reaction, experimental equilibrium coefficients for similar type process (Hannula and Kurkela, 2012; Kurkela et al., 2019) are shown.

6.3 Discussion

In the presented work, sorption-enhanced biomass gasification of industrial-scale was studied. A reactor concept to operate with 100 MW_{th} thermal power was created. The proposed reactor design enables gas production of 61 ktoe/a with module 2 for DME production from biomass. A 1D modelling tool was developed. The tool was used to

design and investigate the performance of the reactor concept. A wide operating range was demonstrated in which the producer gas was suitable for downstream DME synthesis.

The SEG CFB reactor concept was designed based on the quantitative understanding of the physical processes of the SEG process. Validated sub-models for gasification phenomena were obtained from validation of the pilot-scale model. For developing the CFB reactor concept, the physical sub-models for the gasification phenomena were transferred to the industrial-scale reactor model, and the model was used to develop the industrial-scale design for the process.

The simulation results of the reactor concept were consistent with experiments in the literature for similar processes. The presented work demonstrated the suitability of CFB-CFB configuration for the SEG process. DME production from biomass was possible at 730°C operation temperature. The work demonstrated flexible adjustment of the producer gas composition. The flexibility enables the use of various fuel feedstocks, and the adjustment capability of the reactor allows for the production of favourable process conditions for the gasifier to production of DME.

The presented work evaluated the performance of the developed SEG reactor concept. The performance of the process is often denoted with cold-gas efficiency, which describes fuels chemical energy conversion. At 730°C with the module value of 2, the cold-gas efficiency of the gasifier was 76 %. Hydrocarbons in this operation point contain 32 % of the chemical energy of fuel, of which tars hold 3 % share. Synthesis of DME can utilise CO and H_2 gasses. The unuse of hydrocarbons energy causes a significant energy penalty for the chemical energy use of the overall synthesis process. Therefore, after the gasifier, a hydrocarbon reforming section is highly recommendable. By equipping the DME production process with a reforming process, the concentration of the hydrocarbons in the producer gas can be lowered. The reforming of the producer gas affects the H_2/CO ratio of the producer gas, leading to the need for producer gas composition adjustment in the gasifier and studying new optimal operation point for the gasifier.

The developed process model for the industrial-scale SEG process enables evaluating the process operation under various process conditions. Modelling enables the development of process control scenarios for different operational cases. The operating values of an industrial-scale plant presented in this work provide essential information to support plant design and assess plant operating performance and costs.

7 Conclusions

Anthropogenic greenhouse gas emissions have led to climate change by increasing global average temperature. Globally, road transportation has a significant share of the total emissions. In Finland, the fossil CO_2 emissions of road transportation account for a quarter of the total CO_2 emissions. The fossil CO_2 emissions can be reduced by use renewable fuels. Forest-industries side-streams in Finland show potential in future as a source of wood-based the synthetic biofuels. Indirect gasification processes, such as sorption-enhanced gasification, shows promise for the production of synthetic biofuels.

In this thesis, an analysis of sorption-enhanced gasification for synthetic biofuel production was conducted. Modelling tools for the process were developed. An industrial-scale reactor concept to estimate the performance of the industrial-scale sorption-enhanced gasification for synthetic biofuel production was created. The industrial-scale gasification process was designed for DME production due to its potential as fuel for road transportation. The development of the industrial-scale process was carried out by means of modelling. To gain the ability for modelling the industrial-scale SEG process several objectives had to be accomplished. The objectives aimed for a quantitative understanding of the physical operations of the SEG processes. The objectives included validation of a pilot-scale process model and a concept study of the dual fluidised bed process using the validated gasifier model. The main focus of this thesis was an analysis of the gasification process for DME production. However, possibilities for the production of other synthetic fuels was also studied. This thesis forms a comprehensive study of the sorption-enhanced gasification process, where the process was studied at pilot and industrial scales. Broad discussion concerning physical phenomena producing physical operation of the reactor was given in this thesis based on implications of the presented modelling results. In the literature, there are very few modelling studies addressing this topic.

7.1 Contributions and implications of the results

This chapter presents the contributions of this thesis and summarises the implications of the simulations results. In the previous sections, a thorough discussion concerning the results was presented. The main contributions of this work are

- Development of comprehensive model frames for the SEG process including validated main physical phenomena producing physical operation of the process.
- The development of an industrial-scale reactor concept for the SEG and analysis of the reactor for synthetic biofuel production.

The contribution of this thesis to scientific knowledge by chapter are as follows.

In Chapter 3, two comprehensive reactor model frames for the SEG processes was introduced: BFB and CFB model frames. The model frames combine various physical phenomena together to form comprehensive reactor models. The model frames can be

coupled to each other to form models for a dual fluidised bed process. The models include the main physical phenomena producing the physical operation of the process. The models enable physical phenomena based estimates for the operation of the dual fludised bed process. Validation of the developed modelling approach was conducted in this thesis.

In Chapter 4, a pilot-scale model was developed using the BFB model frame. Validation of the BFB model was conducted against data from a 200kW$_{\mathrm{th}}$ pilot reactor and other studies in the literature. The physical operation of the pilot reactor was studied. The study revealed essential aspects regarding the physical operation of the reactor not discussed or inadequately addressed in the literature, such as the role reaction equilibrium of carbonation/calcination reactions and fuel decomposition.

- The pilot-scale BFB reactor model was successfully validated against data from a pilot reactor and literature studies. Mass balances of the simulations were analysed against data from the pilot and the literature.
- The analysis of the process showed the physical operation of the process to be highly temperature-dependent. The temperature had a significant influence on producer gas composition. The simulations revealed aspects concerning the physical mechanisms causing the temperature-dependency of the producer gas composition.
- Solid flow through the bed of the gasifier caused high mixing rates for the bed with the 1D solids mixing approach. The simulations indicated the solid mixing to cause uniform profiles in the bed for different bed material solid fractions. The result implies that an ideal mixing assumption for the bed could apply in the studied cases. However, the approach would significantly simplify the CO_2 capture in the bed, one of the main physical phenomena of the process. Implementing the ideal mixing approach would directly influence the CO_2 capture in the bed since it dismisses the influence of local process conditions.

In Chapter 5, a dual fluidised bed process was investigated. The validated pilot-scale reactor model was used in this study. The BFB gasifier model was combined with a CFB combustor to form the BFB-CFB dual fluidised bed process. The study investigated the mass and energy balances of the process. The study showed the influence of gasifiers operation parameters on producer gas composition and balances of the system. The study also evaluated SEG processes suitability for the production of various synthetic fuels based on the simulation results. Analysis of adiabatic BFB-CFB SEG system's balances with the semi-empirical model has not been presented in the literature. The system without heat losses is thermally the most efficient system possible. The understanding of the balances is of value in the design of efficient industrial-scale systems.

- Modelling tool for BFB-CFB dual fluidised bed SEG process was created. Pilot-scale dual fluidised bed system was developed and balances of the system were analysed.
- The study showed that external fuel to combustor was required in the studied balances at a temperature range of 650-775°C. The simulations also indicated that need

for the external fuel could be reduced by increasing gasifier's thermal fuel power. The studied system was perfectly insulated, and consequently, without heat losses.

- At lower operating temperatures (below 700°C), an excess heat produced by the system required cooling of the process to maintain the good operating performance. This should be considered when the dual fluidised bed system is designed. Too good insulation of the gasifier could negatively impact the processes performance, although system's overall energy efficiency would be increased.

- The impact of gasifier S/C ratio on producer gas composition and balances of the system was investigated. The S/C ratio was adjusted by gasifier fuel feed. The simulations showed the S/C ratio's influence on the need for additional fuel for the combustor. The higher fuel feed to the gasifier reduced the combustor's requirement for the additional fuel since more char from the gasifier was used in the combustor. The overall energy efficiency of the dual fluidised bed system improved with reduced fuel feed to the combustor. Based on the S/C ratio variation, the study evaluated the suitability of producer gas for the production of synthetic biofuels. The study indicated DME, SNG and methanol as possible synthesis products.

In Chapter 6, an industrial-scale concept for the SEG process was developed, and the performance of the process was investigated. DME was selected as the synthesis product. The developed reactor concept and simulated balances provide essential information supporting plant design and assessing plant operating performance and costs. The presented approach with CFB-CFB reactors and the industrial-scale reactor design for the SEG process have not been presented before.

- A modelling tool for CFB-CFB dual fluidised bed SEG process was developed. An industrial-scale SEG reactor concept was created for the production of DME and balances of the dual fluidised bed system were analysed.

- The process integration of the gasifier to the synthetic biofuel production process was discussed. The simulations results show the significance of effective utilisation of hydrocarbon gas species at downstream processes before the biofuel synthesis.

- The simulation results demonstrate the CFB reactor system's flexible controllability over a broad operating range. The system can be flexibly adjusted for the production of synthetic biofuels of regionally and seasonally changing fuel feedstocks.

- Simulation results show producer gas composition to stay below reaction equilibrium of water-gas shift. The equilibrium of concentration of CO_2 approaches the equilibrium conditions at the top of the reactor as operating temperature increases. These details should be accounted for with analysis of the process by simplified reaction equilibrium models.

The sorption-enhanced gasification was studied with BFB-CFB and CFB-CFB reactor configurations. Although the processes were physically different, the processes had SEG's

operational characteristics. Both reactor configurations showed similar flexibility for tailoring producer gas composition by adjusting processes operation parameters. Producer gas composition in the studied cases was similar. The main control parameters and control methods for the process are alike in both reactor configurations. However, the CFB has process control options, which are not possible in the BFB, such as gasifier internal circulation or altering process conditions in the riser. Also, from a technology perspective, the CFB-CFB process can utilise the standard CFB reactor technology already demonstrated in various scales in different applications. The technological readiness of the CFB's is high when most of the experiments from BFB-CFB configuration are from a few pilot-scale and semi-industrial scale processes. More investigation of BFB-CFB configuration physical operation is needed for developing its technological readiness for industrial-scale demonstration.

7.2 Suggestions for further research

The analysis of the SEG process revealed various topics that have not yet gained thorough research attention and could be investigated in future.

- The literature lacks a thorough investigation of water-gas shift reaction kinetics for biomass gasification processes under different process conditions. The reactions kinetics used in this work was based on kinetics applied in the literature for conventional gasification processes. The role of the reaction in the SEG is very significant compared to the conventional processes. Therefore, its accurate estimation is very important.

- More detailed hydrocarbon reaction paths should be investigated. The implementation of more complex hydrocarbon reaction paths would improve the estimation capability of developed models.

- The dynamics of the dual fluidised bed process have not been examined. The investigation of the dynamic behaviour of the process is of value on the continuous operation of the process, where changes of gasification agent feed and fuel loads could occur during the operation. Understanding the transient behaviour of the process enables a more effective operation of the process when its response to changes of process conditions can be estimated.

- Hydrodynamics of the BFB gasifier could be investigated by applying the CFD approach. A more accurate description of fluidised hydrodynamics could be obtained by the method. The CFD also enables studying the mixing of solids and fuel in the reactor. The ideal mixing of the bed was estimated in this study. The CFD could be used for studying the accuracy of this estimation.

- Hydrodynamics of the CFB reactors could be studied by the CFD approach in different process conditions. The study would enable to obtain a more accurate estimation of solid transfer between the fluidised bed reactors. In a large-scale CFB,

inhomogeneous process conditions are caused by the local feeding of fuel, gasification agent, and other materials and the limited mixing rate of different reactive substances. The influence of mixing for the physical operation of the SEG should be investigated.

References

Abanades, J. and Diego, A. (2003). Conversion limits in the reaction of CO_2 with lime. *Energy and Fuels*, 17(2), pp. 308–315.

Abanades, J.C. (2002). The maximum capture efficiency of CO_2 using a carbonation/calcination cycle of $CaO/CaCO_3$. *Chemical Engineering Journal*, 90(3), pp. 303–306.

Adánez, J., de Diego, L., Gayán, P., Armesto, L., and Cabanillas, A. (1995). A model for prediction of carbon combustion efficiency in circulating fluidized bed combustors. *Fuel*, 74(7), pp. 1049–1056.

Aghaalikhani, A., Schmid, J.C., Borello, D., Fuchs, J., Benedikt, F., Hofbauer, H., Rispoli, F., Henriksen, U.B., Sárossy, Z., and Cedola, L. (2019). Detailed modelling of biomass steam gasification in a dual fluidized bed gasifier with temperature variation. *Renewable Energy*, 143, pp. 703–718.

Ahmed, T., Ahmad, M., Yusup, S., Inayat, A., and Khan, Z. (2012). Mathematical and computational approaches for design of biomass gasification for hydrogen production: A review. *Renewable and Sustainable Energy Reviews*, 16(4), pp. 2304–2315.

Alakangas, E., Hurskainen, M., Laatikainen-Luntama, J., and Korhonen, J. (2016). *Properties of indigenous fuels in Finland (Suomessa käytettävien polttoaineiden ominaisuuksia) (In Finnish)*. Espoo: VTT Technology 258.

Alonso, M., Rodríguez, N., Grasa, G., and Abanades, J. (2009). Modelling of a fluidized bed carbonator reactor to capture CO_2 from a combustion flue gas. *Chemical Engineering Science*, 64(5), pp. 883–891.

Altafini, C., Wander, P., and Barreto, R. (2003). Prediction of the working parameters of a wood waste gasifier through an equilibrium model. *Energy Conversion and Management*, 44(17), pp. 2763–2777.

Arias, B., Grasa, G., Abanades, J.C., Manovic, V., and Anthony, E.J. (2012). The Effect of Steam on the Fast Carbonation Reaction Rates of CaO. *Industrial & Engineering Chemistry Research*, 51(5), pp. 2478–2482.

Armbrust, N., Schweitzer, D., Gredinger, A., Beirow, M., Beisheim, N., Poboss, N., Hawthorne, C., Dieter, H., and Scheffknecht, G. (2014). Gasification of Biomass with In-Situ CO_2 Capture and Separation in a 200 kW_{th} Pilot Plant. In: *Gasification Technologies*.

Baratieri, M., Baggio, P., Fiori, L., and Grigiante, M. (2008). Biomass as an energy source: Thermodynamic constraints on the performance of the conversion process. *Bioresource Technology*, 99(15), pp. 7063–7073.

Bates, R., Ghoniem, A., Jablonski, W., Carpenter, D., Altantzis, C., Garg, A., Barton, J., Chen, R., and Field, R. (2017). Steam-Air Blown Bubbling Fluidized Bed Biomass Gasification (BFBBG): Multi-Scale Models and Experimental Validation. *AIChE Journal*, 63(5), pp. 1543–1565.

Beirow, M., Parvez, A.M., Schmid, M., and Scheffknecht, G. (2020). A Detailed One-Dimensional Hydrodynamic and Kinetic Model for Sorption Enhanced Gasification. *Applied Sciences*, 10, 6136.

Biba, V., Macák, J., Klose, E., and Malecha, J. (1978). Mathematical Model for the Gasification of Coal under Pressure. *Industrial and Engineering Chemistry Process Design and Development*, 17(1), pp. 92–98.

Bilodeau, J., Therien, N., Proulx, P., Czernik, S., and Chornet, E. (1993). A Mathematical Model of Fluidized Bed Biomass Gasification. *The Canadian Journal Of Chemical Engineering*, 71, pp. 549 – 557.

Chavarie, C. and Grace, J.R. (1975). Performance Analysis of a Fluidized Bed Reactor. II. Observed Reactor Behavior Compared with Simple Two-Phase Models. *Industrial & Engineering Chemistry Fundamentals*, 14(2), pp. 79–86.

Corella, J. and Sanz, A. (2005). Modeling circulating fluidized bed biomass gasifiers. A pseudo-rigorous model for stationary state. *Fuel Processing Technology*, 86(9), pp. 1021–1053.

Curran, G., Fink, C., and Gorin, E. (1967). CO_2 Acceptor Gasification Process. *Fuel Gasification*, (1), pp. 141–165.

Darton, R., LaNauze, R., Davidson, J., and Harrison, D. (1977). Bubble-growth due to coalescence in fluidized beds. *Trans Inst Chem Eng*, 55, pp. 274 – 280.

Davidson, J.F. and Harrison, D. (1963). *Fluidized particles*. Cambridge University Press.

Delgado, J., Aznar, M.P., and Corella, J. (1997). Biomass Gasification with Steam in Fluidized Bed: Effectiveness of CaO, MgO, and CaO-MgO for Hot Raw Gas Cleaning. *Industrial and Engineering Chemistry Research*, 36(5), pp. 1535–1543.

Detchusananard, T., Ponpesh, P., Saebea, D., Authayanun, S., and Arpornwichanop, A. (2017). Modeling and Analysis of Sorption Enhanced Chemical Looping Biomass Gasification. *Chemical Engineering Transactions*, 57, pp. 103–108.

Di Blasi, C., Signorelli, G., Di Russo, C., and Rea, G. (1999). Product Distribution from Pyrolysis of Wood and Agricultural Residues. *Ind. Eng. Chem. Res.*, 38, pp. 2216–2224.

Diem, R., Mueller, S., Fuchs, M., Schmid, J.C., and Hofbauer, H. (2014). Sorption-enhanced reforming with limestone from iron production. *Biomass Conversion and Biorefinery*, 5, p. 95–102.

Dieterich, V., Buttler, A., Hanel, A., Spliethoff, H., and Fendt, S. (2020). Power-to-liquid via synthesis of methanol, DME or Fischer–Tropsch-fuels: a review. *Energy & Environmental Science*, 13(10), pp. 3207–3252.

European commission. *European commission climate action - Paris agreement*. url: `https://ec.europa.eu/clima/policies/international/negotiations/paris_en`. [retrieved: 25.8.2021].

European Council (2014). *2030 climate & energy framework - EUCO 169/14 European Council (23 and 24 October 2014) – Conclusions EUCO 169/14* .

Fagbemi, L., Khezami, L., and Capart, R. (2001). Pyrolysis products from different biomasses. *Applied Energy*, 69(4), pp. 293–306.

Fang, F., Li, Z.S., and Cai, N.S. (2009). Experiment and Modeling of CO_2 Capture from Flue Gases at High Temperature in a Fluidized Bed Reactor with Ca-Based Sorbents. *Energy & Fuels*, 23(1), pp. 207–216.

Feng, B., An, H., and Tan, E. (2007). Screening of CO_2 Adsorbing Materials for Zero Emission Power Generation Systems. *Energy & Fuels*, 21(2), pp. 426–434.

Fiaschi, D. and Michelini, M. (2001). A two-phase one-dimensional biomass gasification kinetics model. *Biomass and Bioenergy*, 21(2), pp. 121–132.

Finnish Forest Industries. *Forest resources statistics*. url: `https://www.metsateollisuus.fi/tilastot`. [retrieved: 10.03.2021].

Florin, N. and Harris, A. (2007). Hydrogen production from biomass coupled with carbon dioxide capture: The implications of thermodynamic equilibrium. *International Journal of Hydrogen Energy*, 32(17), pp. 4119–4134.

Fryer, C. and Potter, O.E. (1972). Countercurrent Backmixing Model for Fluidized Bed Catalytic Reactors. Applicability of Simplified Solutions. *Industrial & Engineering Chemistry Fundamentals*, 11(3), pp. 338–344.

Fuchs, J., Schmid, J.C., Müller, S., Mauerhofer, A.M., Benedikt, F., and Hofbauer, H. (2019a). The impact of gasification temperature on the process characteristics of sorption enhanced reforming of biomass. *Biomass Conversion and Biorefinery*, 10, p. 925–936.

Fuchs, J., Schmid, J.C., Müller, S., and Hofbauer, H. (2019b). Dual fluidized bed gasification of biomass with selective carbon dioxide removal and limestone as bed material: A review. *Renewable and Sustainable Energy Reviews*, 107, pp. 212–231.

Fuchs, J., Schmid, J.C., Benedikt, F., Müller, S., Hofbauer, H., Stocker, H., Kieberger, N., and Bürgler, T. (2018). The impact of bed material cycle rate on in-situ CO_2 removal for sorption enhanced reforming of different fuel types. *Energy*, 162, pp. 35–44.

Gil, J., Corella, J., Aznar, M.P., and Caballero, M.A. (1999). Biomass gasification in atmospheric and bubbling fluidized bed: Effect of the type of gasifying agent on the product distribution. *Biomass and Bioenergy*, 17(5), pp. 389–403.

Gómez-Barea, A., Arjona, R., and Ollero, P. (2005). Pilot-Plant Gasification of Olive Stone: a Technical Assessment. *Energy & Fuels*, 19(2), pp. 598–605.

Grasa, G., Murillo, R., Alonso, M., and Abanades, J.C. (2009). Application of the random pore model to the carbonation cyclic reaction. *AIChE Journal*, 55(5), pp. 1246–1255.

Grasa, G.S. and Abanades, J.C. (2006). CO_2 Capture Capacity of CaO in Long Series of Carbonation/Calcination Cycles. *Industrial & Engineering Chemistry Research*, 45(26), pp. 8846–8851.

Gungor, A. (2009). One dimensional numerical simulation of small scale CFB combustors. *Energy Conversion and Management*, 50(3), pp. 711–722.

Hafner, S., Schmid, M., and Scheffknecht, G. (2021). Parametric Study on the Adjustability of the Syngas Composition by Sorption-Enhanced Gasification in a Dual-Fluidized Bed Pilot Plant. *Energies*, 14, 399.

Hafner, S., Spörl, R., and Scheffknecht, G. (2018). Sorption Enhanced Gasification : Process validation and investigations on the syngas composition in a 200 kW_{th} dual fluidized bed facility. *Proceeding of 23rd International Conference on Fluidized Bed Conversion*, pp. 826–832.

Hannula, I. and Kurkela, E. (2012). A parametric modelling study for pressurised steam/O_2-blown fluidised-bed gasification of wood with catalytic reforming. *Biomass and Bioenergy*, 38, pp. 58–67.

Hawthorne, C., Poboss, N., Dieter, H., Gredinger, A., Zieba, M., and Scheffknecht, G. (2012). Operation and results of a 200-kW_{th} dual fluidized bed pilot plant gasifier with adsorption-enhanced reforming. *Biomass Conversion and Biorefinery*, 2(3), pp. 217–227.

Hejazi, B., Grace, J., Bi, X., and Mahecha-Botero, A. (2017). Kinetic Model of Steam Gasification of Biomass in a Bubbling Fluidized Bed Reactor. *Energy and Fuels*, 31(2), pp. 1702–1711.

Hejazi, B. (2017). *Modeling of biomass steam gasification in a dual fluidized bed reactor with/without lime-based CO_2 capture*. Vancouver: University of British Columbia. Doctoral Dissertation. 222 p.

Hejazi, B. and Grace, J.R. (2020). Simulation of tar-free biomass syngas enhancement in a calcium looping operation using Aspen Plus built-in fluidized bed model. *International Journal of Greenhouse Gas Control*, 99, 103096, pp. 1–9.

Hejazi, B., Grace, J.R., Bi, X., and Mahecha-Botero, A. (2014). Steam gasification of biomass coupled with lime-based CO_2 capture in a dual fluidized bed reactor: A modeling study. *Fuel*, 117, pp. 1256–1266.

Hejazi, B., Grace, J.R., and Mahecha-Botero, A. (2019). Kinetic Modeling of Lime-Enhanced Biomass Steam Gasification in a Dual Fluidized Bed Reactor. *Industrial & Engineering Chemistry Research*, 58(29), pp. 12953–12963.

Hemati, M. and Laguerie, C. (1988). Determination of the kinetics of the sawdust steam-gasification of charcoal in a thermobalance. *Entropie*, 142, pp. 29 – 40.

Herguido, J., Corella, J., and González-Saiz, J. (1992). Steam Gasification of Lignocellulosic Residues in a Fluidized Bed at a Small Pilot Scale. Effect of the Type of Feedstock. *Industrial and Engineering Chemistry Research*, 31(5), pp. 1274–1282.

Huilin, L. (2000). A coal combustion model for circulating fluidized bed boilers. *Fuel*, 79(2), pp. 165–172.

IEA. *International Energy Agency data and statistics, Energy data - CO_2 emissions*. url: `https://www.iea.org/data-and-statistics/data-browser/?country=WORLDfuel=CO2%20emissionsindicator=CO2BySource`. [retrieved: 25.8.2021].

IEA Bioenergy (2020). *The Role of Renewable Transport Fuels in Decarbonizing Road Transport*. IEA Bioenergy: Task 41-10.

Inayat, A., Ahmad, M.M., Yusup, S., and Mutalib, M.I.A. (2010). Biomass Steam Gasification with In-Situ CO_2 Capture for Enriched Hydrogen Gas Production: A Reaction Kinetics Modelling Approach. *Energies*, 3(8), pp. 1472–1484.

IPCC (2018). Global warming of 1.5°C: an IPCC Special Report on the impacts of global warming of 1.5°C above pre-industrial levels and related global greenhouse gas emission pathways, in the context of strengthening the global response to the threat of climate change, sustainable development, and efforts to eradicate poverty. Masson-Delmotte, V. and Zhai, P. and Pörtner, H.-O. and Roberts, D. and Skea, J. and Shukla, P.R. and Pirani, A. and Moufouma-Okia, W. and Péan, C. and Pidcock, R. and Connors, S. and Matthews, J.B.R. and Chen, Y. and Zhou, X. and Gomis, M.I. and Lonnoy, E. and Maycock, T. and Tignor, M. and Waterfield, T., (eds.).

Jain, M., Sathiyamoorthy, D., and Rao, V.G. (2014). A new model for bubbling fluidized bed reactors. *Chemical Engineering Research and Design*, 92(3), pp. 471–480.

Jennen, T., Hiller, R., Köneke, D., and Weinspach, P. (1999). Modeling of gasification of wood in a circulating fluidized bed. *Chemical Engineering and Technology*, 22(10), pp. 822–826.

Johnsson, F. and Leckner, B. (1995). Vertical distribution of solids in a CFB-furnace. In: *13th International Conference on Fluidized Bed Combustion*, pp. 671–679.

van Kampen, J. (2021). *Efficient carbon utilization to dimethyl ether by steam adsorption enhancement*. Eindhoven: Technische Universiteit Eindhoven. Doctoral Dissertation. 220 p.

Kato, K. and Wen, C. (1969). Bubble assemblage model for fluidized bed catalytic reactors. *Chemical Engineering Science*, 24(8), pp. 1351–1369.

Kaushal, P., Abedi, J., and Mahinpey, N. (2010). A comprehensive mathematical model for biomass gasification in a bubbling fluidized bed reactor. *Fuel*, 89(12), pp. 3650–3661.

Kaushal, P., Pröll, T., and Hofbauer, H. (2008). Model for biomass char combustion in the riser of a dual fluidized bed gasification unit: Part 1 - Model development and sensitivity analysis. *Fuel Processing Technology*, 89(7), pp. 651–659.

Kaushal, P., Pröll, T., and Hofbauer, H. (2011). Application of a detailed mathematical model to the gasifier unit of the dual fluidized bed gasification plant. *Biomass and Bioenergy*, 35(7), pp. 2491–2498.

Koppatz, S., Pfeifer, C., Rauch, R., Hofbauer, H., Marquard-Moellenstedt, T., and Specht, M. (2009). H_2 rich product gas by steam gasification of biomass with in situ CO_2 absorption in a dual fluidized bed system of 8 MW fuel input. *Fuel Processing Technology*, 90(7-8), pp. 914–921.

Krzywanski, J., Czakiert, T., Muskala, W., Sekret, R., and Nowak, W. (2010). Modeling of solid fuels combustion in oxygen-enriched atmosphere in circulating fluidized bed boiler. *Fuel Processing Technology*, 91(3), pp. 290–295.

Ku, X., Li, T., and Løvås, T. (2015). CFD-DEM simulation of biomass gasification with steam in a fluidized bed reactor. *Chemical Engineering Science*, 122, pp. 270–283.

Kunii, D. and Levenspiel, O. (1968). Bubbling Bed Model. Model for Flow of Gas through a Fluidized Bed. *Industrial & Engineering Chemistry Fundamentals*, 7(3), pp. 446–452.

Kurkela, E., Kurkela, M., and Hiltunen, I. (2014). The effects of wood particle size and different process variables on the performance of steam-oxygen blown circulating fluidized-bed gasifier. *Environmental Progress & Sustainable Energy*, 33(3), pp. 681–687.

Kurkela, E., Simell, P., McKeough, P., and Kurkela, M. (2008). *Production of synthesis gas and clean fuel gas (In Finnish)*. Espoo: VTT publications 682.

Kurkela, E., Kurkela, M., Tuomi, S., Frilund, C., and Hiltunen, I. (2019). *Efficient use of biomass residues for combined production of transport fuels and heat*. Espoo: VTT Technology 347.

Li, X., Grace, J., Watkinson, A.P., Lim, C.J., and Ergüdenler, A. (2001). Equilibrium modeling of gasification: A free energy minimization approach and its application to a circulating fluidized bed coal gasifier. *Fuel*, 80(2), pp. 195–207.

Lin, S., Harada, M., Suzuki, Y., and Hatano, H. (2005). Process analysis for hydrogen production by reaction integrated novel gasification (HyPr-RING). *Energy Conversion and Management*, 46(6), pp. 869–880.

Liu, H., Cattolica, R., and Seiser, R. (2016). CFD studies on biomass gasification in a pilot-scale dual fluidized-bed system. *International Journal of Hydrogen Energy*, 41(28), pp. 11974–11989.

Mahinpey, N. and Nikoo, M. (2008). Simulation of biomass gasification in fluidized bed reactor using ASPEN PLUS. *Biomass and Bioenergy*, 32(12), pp. 1245–1254.

Mahishi, M. and Goswami, D. (2007). Thermodynamic optimization of biomass gasifier for hydrogen production. *International Journal of Hydrogen Energy*, 32(16), pp. 3831–3840.

Maniatis, K. and Buekens, A. (1982). Fluidized bed gasification of biomass. *EPE*, 17, pp. 35 – 43.

Martínez, I. and Romano, M. (2016). Flexible sorption enhanced gasification (SEG) of biomass for the production of synthetic natural gas (SNG) and liquid biofuels: Process assessment of stand-alone and power-to-gas plant schemes for SNG production. *Energy*, 113, pp. 615–630.

Martínez, I., Grasa, G., Murillo, R., Arias, B., and Abanades, J. (2012). Kinetics of calcination of partially carbonated particles in a Ca-looping system for CO_2 capture. *Energy and Fuels*, 26(2), pp. 1432–1440.

Martínez, I., Kulakova, V., Grasa, G., and Murillo, R. (2020a). Experimental investigation on sorption enhanced gasification (SEG) of biomass in a fluidized bed reactor for producing a tailored syngas. *Fuel*, 259, 116252.

Martínez, I., Grasa, G., Callén, M.S., López, J.M., and Murillo, R. (2020b). Optimised production of tailored syngas from municipal solid waste (MSW) by sorption-enhanced gasification. *Chemical Engineering Journal*, 401, 126067.

Matsui, I., Kunii, D., and Furusawa, T. (1985). Study of fluidized bed steam gasification of char by thermogravimetrically obtained kinetics. *Journal of Chemical Engineering of Japan*, 18(2), pp. 105–113.

Mayerhofer, M., Mitsakis, P., Meng, X., de Jong, W., Spliethoff, H., and Gaderer, M. (2012). Influence of pressure, temperature and steam on tar and gas in allothermal fluidized bed gasification. *Fuel*, 99, pp. 204–209.

van der Meijden, C., Könemann, J.W., Sierhuis, W., van der Drift, B., and Rietveld, B. (2013). *Wood to Bio-Methane demonstration project in the Netherlands*. url: https://www.milenatechnology.com/fileadmin/milenatechnology/user/documents/reports/ Wood_to_Bio-Methane_demonstration_project_in_the_Netherlands.pdf. [retrieved: 18.10.2021].

Ministry of Transport and Communications (2020). *Road map for fossil-free transport. Working group final report (In Finnish)*. Helsinki: Publications of the Ministry of Transport and Communications 2020:18.

Müller, S., Fuchs, J., Schmid, J., Benedikt, F., and Hofbauer, H. (2017). Experimental development of sorption enhanced reforming by the use of an advanced gasification test plant. *International Journal of Hydrogen Energy*, 42(50), pp. 29694–29707.

Müller, S., Stidl, M., Pröll, T., Rauch, R., and Hofbauer, H. (2011). Hydrogen from biomass: large-scale hydrogen production based on a dual fluidized bed steam gasification system. *Biomass Conversion and Biorefinery*, 1(1), pp. 55–61.

Myöhänen, K. (2011). *Modelling of Combustion and Sorbent Reactions in Three-Dimensional Flow Environment of a Circulating Fluidized Bed Furnace*. Lappeenranta: Acta Universitatis Lappeenrantaensis. Doctoral Dissertation. 164 p.

Neves, D., Thunman, H., Matos, A., Tarelho, L., and Gómez-Barea, A. (2011). Characterization and prediction of biomass pyrolysis products. *Progress in Energy and Combustion Science*, 37(5), pp. 611–630.

Neves, D., Matos, A., Tarelho, L., Thunman, H., Larsson, A., and Seemann, M. (2017). Volatile gases from biomass pyrolysis under conditions relevant for fluidized bed gasifiers. *Journal of Analytical and Applied Pyrolysis*, 127, pp. 57–67.

Noubli, H., Valin, S., Spindler, B., and Hemati, M. (2015). Development of a modelling tool representing biomass gasification step in a dual fluidized bed. *The Canadian Journal of Chemical Engineering*, 93(2), pp. 340–347.

Nylund, N.O., Sipilä, K., Laurikko, J., Tamminen, S., Sipilä, E., Mäkelä, K., Hannula, I., and Honkatukia, J. (2015). *How to Reach 40% Reduction in Carbon Dioxide Emissions from Road Transport by 2030: Propulsion Options and their Impacts on the Economy (Tieliikenteen 40 %:n hiilidioksidipäästöjen vähentäminen vuoteen 2030: Käyttövoimavaihtoehdot ja niiden kansantaloudelliset vaikutukset) (In Finnish)*. Espoo: VTT report (VTT-R-00752-15).

Official Statistics of Finland (OSF). *Total wood consumption 2019*. Helsinki: Natural Resources Institute Finland (Luke). url: https://stat.luke.fi/en/total-wood-consumption. [retrieved: 10.03.2021].

Petersen, I. and Werther, J. (2005a). Experimental investigation and modeling of gasification of sewage sludge in the circulating fluidized bed. *Chemical Engineering and Processing: Process Intensification*, 44(7), pp. 717–736.

Petersen, I. and Werther, J. (2005b). Three-dimensional modeling of a circulating fluidized bed gasifier for sewage sludge. *Chemical Engineering Science*, 60(16), pp. 4469–4484.

Pfeifer, C., Puchner, B., and Hofbauer, H. (2009). Comparison of dual fluidized bed steam gasification of biomass with and without selective transport of CO2. *Chemical Engineering Science*, 64(23), pp. 5073–5083.

Poboss, N. (2016). *Experimentelle Untersuchung der sorptionsunterstützten Reformierung*. Stuttgart: Universität Stuttgart. Doctoral Dissertation. 181 p.

Poboss, N., Swiecki, K., Charitos, A., Hawthorne, C., Zieba, M., and Scheffknecht, G. (2012). Experimental investigation of the absorption enhanced reforming of biomass in a 20 kW_{th} dual fluidized bed system. *International Journal of Thermodynamics*, 15(1), pp. 53–59.

Pre, P., Hemati, M., and Marchand, B. (1998). Study on natural gas combustion in fluidized beds. *Chemical Engineering Science*, 53(16), pp. 2871–2883.

Pröll, T. and Hofbauer, H. (2008). H_2 rich syngas by selective CO_2 removal from biomass gasification in a dual fluidized bed system — Process modelling approach. *Fuel Processing Technology*, 89(11), pp. 1207–1217.

Puricelli, S., Cardellini, G., Casadei, S., Faedo, D., van den Oever, A.E., and Grosso, M. (2021). A review on biofuels for light-duty vehicles in Europe. *Renewable and Sustainable Energy Reviews*, 137, 110398, pp. 1–19.

Rajan, R. and Wen, C. (1980). A comprehensive model for fluidized bed coal combustors. *AIChE Journal*, 26(4), pp. 642–655.

Rauch, R., Kiennemann, A., and Sauciuc, A. (2013). Fischer-Tropsch Synthesis to Biofuels (BtL Process). In: Triantafyllidis, K., Lappas, A., and Stöcker, M., eds, *The Role of Catalysis for the Sustainable Production of Bio-fuels and Bio-chemicals*, pp. 397–443. Elsevier.

Risnes, H., Sorensen, L., and Hustad, J. (2001). CO_2 reactivity of chars from wheat, spruce and coal. In: Bridgewater, A., ed., *Progress in Thermochemical Biomass Conversion*, pp. 61 – 72. Oxford: Blackwell Science.

Schmid, J.C., Fuchs, J., Benedikt, F., Mauerhofer, A.M., Muller, S., Hofbauer, H., Stocker, H., Kielberger, N., and Burgler, T. (2017). Sorption Enhanced Reforming With The Novel Dual Fluidized Bed Test Plant At TU Wien. In: *25th European Biomass Conference and Exhibition*, pp. 421–428.

Shimizu, T., Hirama, T., Hosoda, H., Kitano, K., Inagaki, M., and Tejima, K. (1999). A Twin Fluid-Bed Reactor for Removal of CO_2 from Combustion Processes. *Chemical Engineering Research and Design*, 77(1), pp. 62–68.

Simell, P., Leppälahti, J., and Kurkela, E. (1995). Tar-decomposing activity of carbonate rocks under high CO_2 partial pressure. *Fuel*, 74(6), pp. 938–945.

Soukup, G., Pfeifer, C., Kreuzeder, A., and Hofbauer, H. (2009). In Situ CO_2 Capture in a Dual Fluidized Bed Biomass Steam Gasifier - Bed Material and Fuel Variation. *Chemical Engineering & Technology*, 32(3), pp. 348–354.

de Souza-Santos, M.L. (2010). *Solid fuels combustion and gasification*. CRC Press. 508 p.

de Souza-Santos, M. (1989). Comprehensive modelling and simulation of fluidized bed boilers and gasifiers. *Fuel*, 68(12), pp. 1507–1521.

Stanmore, B. and Gilot, P. (2005). Review—calcination and carbonation of limestone during thermal cycling for CO_2 sequestration. *Fuel Processing Technology*, 86(16), pp. 1707–1743.

Thunman, H., Seemann, M., Berdugo Vilches, T., Maric, J., Pallares, D., Ström, H., Berndes, G., Knutsson, P., Larsson, A., Breitholtz, C., and Santos, O. (2018). Advanced biofuel production via gasification – lessons learned from 200 man-years of research activity with Chalmers' research gasifier and the GoBiGas demonstration plant. *Energy Science & Engineering*, 6(1), pp. 6–34.

Udomsirichakorn, J., Basu, P., Abdul Salam, P., and Acharya, B. (2014). CaO-based chemical looping gasification of biomass for hydrogen-enriched gas production with in situ CO_2 capture and tar reduction. *Fuel Processing Technology*, 127, pp. 7–12.

Udomsirichakorn, J., Basu, P., Salam, P.A., and Acharya, B. (2013). Effect of CaO on tar reforming to hydrogen-enriched gas with in-process CO_2 capture in a bubbling fluidized bed biomass steam gasifier. *International Journal of Hydrogen Energy*, 38(34), pp. 14495–14504.

Volvo (2014). *Sustainability Report 2013: Our Progress Towards Sustainable Transport Solutions*. Gothenburg. 85p. url: `www.volvogroup.com/sustainabilityreport`. [retrieved: 25.08.2021].

Wang, J. and Anthony, E.J. (2005). On the Decay Behavior of the CO_2 Absorption Capacity of CaO-Based Sorbents. *Industrial & Engineering Chemistry Research*, 44(3), pp. 627–629.

Werther, J. (1980). Modeling and scale-up of industrial fluidized bed reactors. *Chemical Engineering Science*, 35(1-2), pp. 372–379.

Wix, C., Dybkjær, I., and Udengaard, N. (2007). Coal to SNG – The Methanation Process. *Proceedings of 24th Annual International Pittsburgh Coal Conference*.

Wojnicka, B., Sciazko, M., and Schmid, J.C. (2019). Modelling of biomass gasification with steam. *Biomass Conversion and Biorefinery*, 1, pp. 1–19.

Yan, L., Jim Lim, C., Yue, G., He, B., and Grace, J. (2016). One-dimensional modeling of a dual fluidized bed for biomass steam gasification. *Energy Conversion and Management*, 127, pp. 612–622.

Yan, L., Cao, Y., He, B., and Li, X. (2018). Calcium Looping Enhanced Biomass Steam Gasification in a Two-Stage Fluidized Bed Gasifier. *Energy & Fuels*, 32(8), pp. 8462–8473.

Yang, S., Wang, H., Wei, Y., Hu, J., and Chew, J.W. (2019). Particle-scale modeling of biomass gasification in the three-dimensional bubbling fluidized bed. *Energy Conversion and Management*, 196, pp. 1–17.

Publication I

Ritvanen, J., Pitkäoja, A., Sepponen, S. and Hyppänen, T.
Modelling of Sorption enhanced Biomass Gasification in Dual Fluidized Bed Process

Reprinted with permission from
Proceedings of 23rd International Conference on Fluidized Bed Conversion,
Seoul, Korea, 13.-17.05.2018,
© 2018, 23rd International Conference on Fluidized Bed Conversion

B4-2

Modelling of Sorption-enhanced Biomass Gasification in Dual Fluidized Bed Process

Jouni Ritvanen*, Antti Pitkäoja, Simo Sepponen, Timo Hyppänen

Lappeenranta University of Technology, LUT School of Energy Systems,
P.O. Box 20, 53851 Lappeenranta, Finland.

**Telephone: +358 400 416 106, e-mail: jouni.ritvanen@lut.fi*

Abstract

One of the key target of EU's "*Strategy on Climate Change for 2020 and Beyond"* is to produce at least 10% of transport fuel of all EU countries from renewable sources by the year 2020. Therefore, there is a need for more efficient and cost effective ways to produce renewable transport fuels.

Sorption-enhanced gasification (SEG) offers a promising and renewable path for creating hydrogen-rich product gas from biomass with in-situ CO_2 removal. The product gas can be further processed into a renewable transport fuel. The concept of SEG uses a calcium based sorbent as a bed material and two interconnected circulating fluidized bed reactors: steam gasifier (carbonator) and combustor (calciner). In the gasifier, the sorbent absorbs the CO_2 as soon as it has been formed shifting the equilibrium of the water-gas shift reaction towards the production of H_2. In the combustor, the sorbent is regenerated and heated up by the biomass char combustion. Based on the biomass properties, the char combustion can provide the necessary heat for the calcination in the combustor and for the gasification reactions in the gasifier. For a low char biomass, additional biofuel can be fed in to the combustor to obtain required heat for the process.

To understand the dual fluidized bed SEG and its feasibilities, the fundamentals of the process needs to be studied. Computational modeling offers means for process design and prediction of operation behavior. In this work, one-dimensional model for the dual fluidized bed SEG is introduced with process sensitivity studies in 100 MW_{th} scale. Based on the modelling results, the syngas composition can be adjusted with process parameters. In this study, the additional biofuel is fed in to the combustor and combustor's recirculation effect is investigated. These two methods are possible options for adjusting the composition of syngas.

Keywords: Sorption-enhanced gasification, biomass, in-direct gasification, 1D modelling, dual fluidized bed.

1. Introduction

The use of renewable energy in the EU has been sped up by the "*Strategy on Climate Change for 2020 and Beyond".* One of the key target of this strategy is to produce at least 10% of transport fuel of all EU countries from renewable sources by the year 2020. Therefore, there is a need for more efficient and cost effective ways to produce renewable transport fuels.

Sorbent-enhanced gasification (SEG) is a promising way to produce hydrogen-rich syngas with *in-situ* removal of carbon dioxide. The process combines indirect gasification with calcium looping. The circulating bed material acts as a heat carrier, but also has an influence in the gasification process by acting as a carbon dioxide (CO_2) transporting agent. The bed material absorbs CO_2 in the gasifier and releases the gas in the combustor. The removal of CO_2 from the gasifier also enhances the hydrogen (H_2) production through the water-gas shift reaction. The hydrogen content in the product gas can be up to 80 % [1]. A schematic of the process is presented in Figure 1.

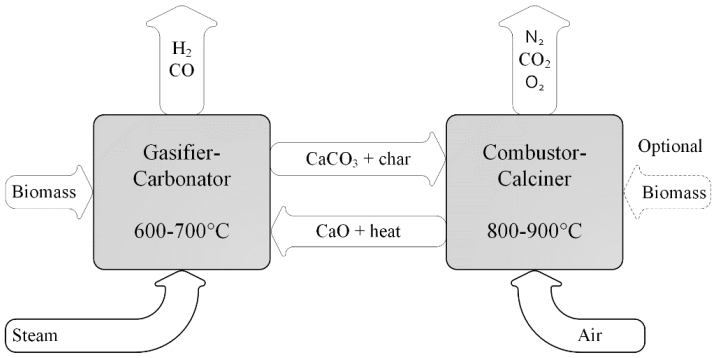

Figure 1. Basic principle of sorbent-enhanced gasification.

The main idea behind the SEG process is the ability to control the hydrogen-to-carbon monoxide (H_2/CO) ratio to be suitable for downstream fuel synthesis process. This will intensify the traditional biofuel production chain by reducing the units needed for syngas conditioning. So far, SEG process utilizing dual circulating fluidized bed (CFB) technology hasn't been reported. SEG operation have been studied with simple models, which do not take the process hydrodynamics and local concentrations of reacting components into account. These phenomena are critical to evaluate the operation of the interconnected CFB reactor system, such as SEG. In this study, the dual CFB SEG process will be investigated by 1D modelling approach in 100 MW_{th} scale with CFB hydrodynamics and local reaction kinetics.

2. Model description

The model frame used for modeling in this work solves one-dimensional conservation equations of mass and energy for gas and solid material fractions. Semi-empirical closure models for hydrodynamics and reactions are used. Hydrodynamics is modelled according to Johnsson and Leckner [2] model with 1D implementation by Ylätalo [3]. Fuel reaction path is according to Myöhänen and Hyppänen [4]. Evaporation and devolatilization rates, and the composition of devolatilized gases are determined by empirical correlations by Myöhänen [5]. The model equations are solved with a built-in solver within Matlab/Simulink. In the model frame, both of the reactors are vertically discretized into control volumes and they are connected together through cyclone-standpipe-loop models. The model frame is illustrated in the Figure 2. The 1D control volumes are assumed to be ideally mixed. Gas and solid phases are treated separately, using locally the same average temperature.

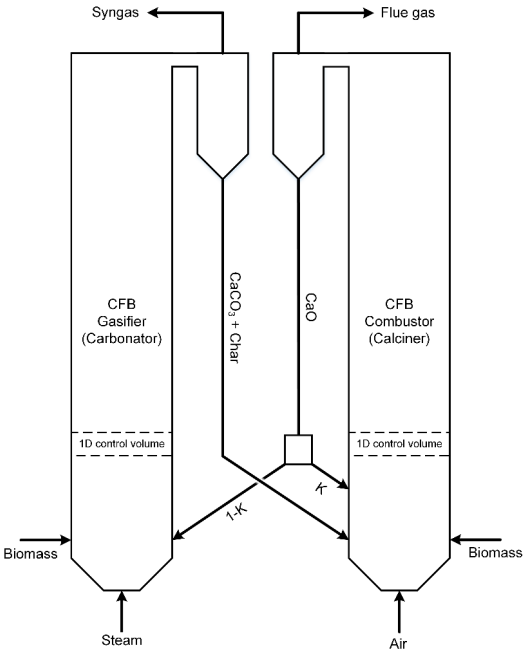

Figure 2. Model frame of the 1D SEG model. CaO flow from combustor recirculated by factor K.

The original calcium looping model frame developed by Ylätalo [3,6] was modified to be suitable for the SEG process. Original model includes reactions for evaporation of moisture in the fuel, devolatilization, char

and volatile combustion, carbonation, calcination and indirect sulphation.

To model the SEG process, the following gasification reactions were implemented into the original model frame:

$C+CO_2 \rightarrow 2CO$	Boudouard	(R1)
$C+H_2O \rightarrow H_2+CO$	Water-gas	(R2)
$C+2H_2 \rightarrow CH_4$	Methane formation	(R3)
$CO+H_2O \leftrightarrow CO_2+H_2$	Water-gas-shift	(R4)

In addition to the gasification reactions, direct sulphation and desulphation were also implemented into the model. The reaction rate equations found from the literature were used to model the reactions. The used reaction rate equations are presented in the Table 1.

Table 1. Reaction rate equations for the main gasification reactions.

Reaction	R'''	k	Reference
R1	$kc_{char}c_{CO_2}$; [kg m^{-3}s^{-1}]	$7.69 \cdot 10^6 \exp\left(-\frac{30600}{T}\right)$	[5]
R2	$kc_{char}c_{H_2O}$; [kg m^{-3}s^{-1}]	$235.3 \exp\left(-\frac{15500}{T}\right)$	[5]
R3	$kc_{char}p_{H_2}^{0.93}$; [kg m^{-3}s^{-1}]	$16.4 \exp\left(-\frac{11400}{T}\right)$	[7]
R4	$k\left(c_{CO}c_{H_2O} - \frac{c_{CO_2}c_{H_2}}{K_{WGS}}\right)$; [mol m^{-3}s^{-1}]	$k = 2.78 \exp\left(-\frac{1515}{T}\right)$ $K_{WGS} = 0.0265 \exp\left(\frac{3965}{T}\right)$	[8]

3. Simulation case

Another objective of this work was to build a 100 MW_{th} simulation case to demonstrate the SEG process. It has to be noted that the model is not yet validated against experimental data, however the simulation cases are providing an operational insight of the SEG process. Wood pellets has been used as a fuel and the properties of the fuel are shown in the Table 2.

Table 2. Proximate analysis, ultimate analysis and calorific value of wood pellets.

Proximate analysis				Ultimate analysis					
Moisture	Ash	Volatiles	Fixed Carbon	C	H	N	S	O	LHV
wt%,ar	wt%,ds			wt%,daf					MJ/kg
5.55	0.38	83.43	16.19	49.28	6.30	0.10	0.02	40.77	17.59

The reactors in the model were defined as perfectly insulated. In the model, the fuel ash was removed from the system at the calciner return leg to avoid ash accumulation. For the limestone material the maximum carbonate content X_{max} was selected as 0.3.The kinetic coefficients of carbonation and calcination were based on the previous study of calcium looping [6]. The design fluidization velocity for both reactors was selected as 6 m/s. The gasifier was dimensioned with a sloped section to compensate the increase in gas flow due to the volatile and moisture released from the fuel. The combustor was set to have a constant cross section without the sloped section. The dimensions of the reactors and the main boundary conditions are presented in Table 3.

Table 3. Dimensions of the reactors and the main boundary conditions.

	Gasifier/Carbonator	Combustor/Calciner
Height of the sloped section, m	2	-
Height of the reactor, m	18	18
Elevation of exit channel, m	16	16
Width and depth of the grid, m	2.2	2.5
Width and depth of the freeboard, m	2.7	2.5
Number of nodes	40	40
Primary gas	Steam	Air
Primary gas temperature, °C	300	25
Primary gas mass flow rate, kg/s	5.931	11.42…17.43
Steam to Carbon ratio, -	1.5	-
Biomass mass flow, kg/s	5.685	0.14…1.14
Thermal power, MW_{th}	100	2.5…20
Limestone particle diameter, µm	180	180
Char particle diameter, µm	300	300
Limestone solid density, kg/m^3	3000	3000
Char solid density, kg/m^3	550	550
Solid recirculation coefficient K, -	0	0.2…0.7

The primary air mass flow rate to the combustor was determined by setting excess oxygen of flue gas as 1vol-%,db. Total amount of the solid mass in the system was about 4500 kg.

4. Results

One dimensional simulation results for the 100 MW_{th} reference case with 10 MW_{th} additional fuel feeding to the combustor are illustrated in Figure 3. In this simulation case, the combustor solid recirculation coefficient of K=0.521 was used to achieve solid mass of 3000 kg for the gasifier. The main results of the reference case is illustrated in Table 4.

Table 4. Main results of the reference case.

Syngas and flue gas data		
	Gasifier	Combustor
Gas outlet flow rate, kg/s	7.5	19
H_2, vol-%,db	72.1	0.3
CO_2, vol-%,db	11.7	30.0
CO, vol-%,db	5.9	1.0
CH_4, vol-%,db	10.3	0.0
O_2, vol-%,db	0.0	1.0
N_2, vol-%,db	0.0	68.6
H_2O, vol-%	47.1	3.1
LHV, MJ/m_n,db	11.4	0.0
Module M = $(H_2-CO_2)/(CO+CO_2)$	3.4	
H2/CO ratio	12.3	
Reactor data		
Solid mass, kg	3000	1540
Average temperature, °C	687	869
CaO in, kg/s	27.6	

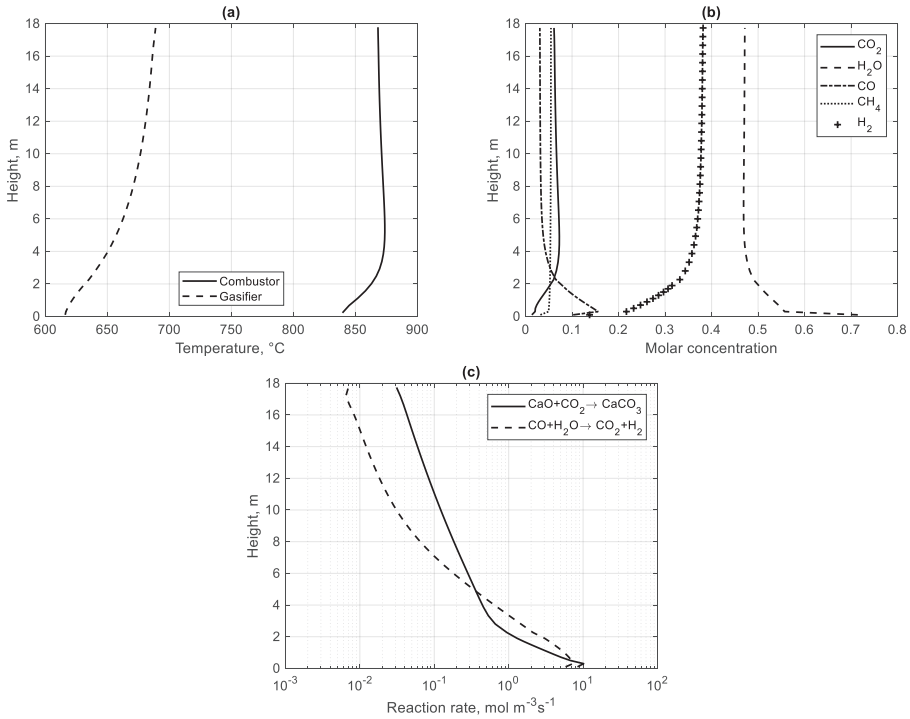

Figure 3. 1D profile data for the reference case. (a) Temperature profiles for both reactors. (b) Gasifier gas concentration profiles. (c) Carbonation and water-gas-shift reaction rates in the gasifier.

In order to study the process operation, two sensitivity studies were conducted. At first, the fuel feeding into the combustor was varied to obtain different temperature levels for the reactors. At the same time the primary air feed was adjusted to achieve excess oxygen of 1vol-%,db. Also, the combustor solid recirculation rate was adjusted to maintain constant mass of 3000 kg in the gasifier. In Figure 4, the mass averaged temperatures and syngas composition as a function of fuel feeding in to the combustor are presented. There is a strong influence of the temperature levels on the CO_2 and H_2 concentrations. CO_2 concentration is mainly defined by the carbonation reaction of the limestone. With a low fuel feeding the combustor temperature is limiting the calcination reaction and therefore there is not enough CaO available in the gasifier for an effective CO_2 capture. A high fuel feeding will increase the gasifier temperature close to the carbonation equilibrium and due to the reason CO_2 capture will be slower. Temperature values with carbonation equilibrium at different fuel feeding are presented in Figure 5.

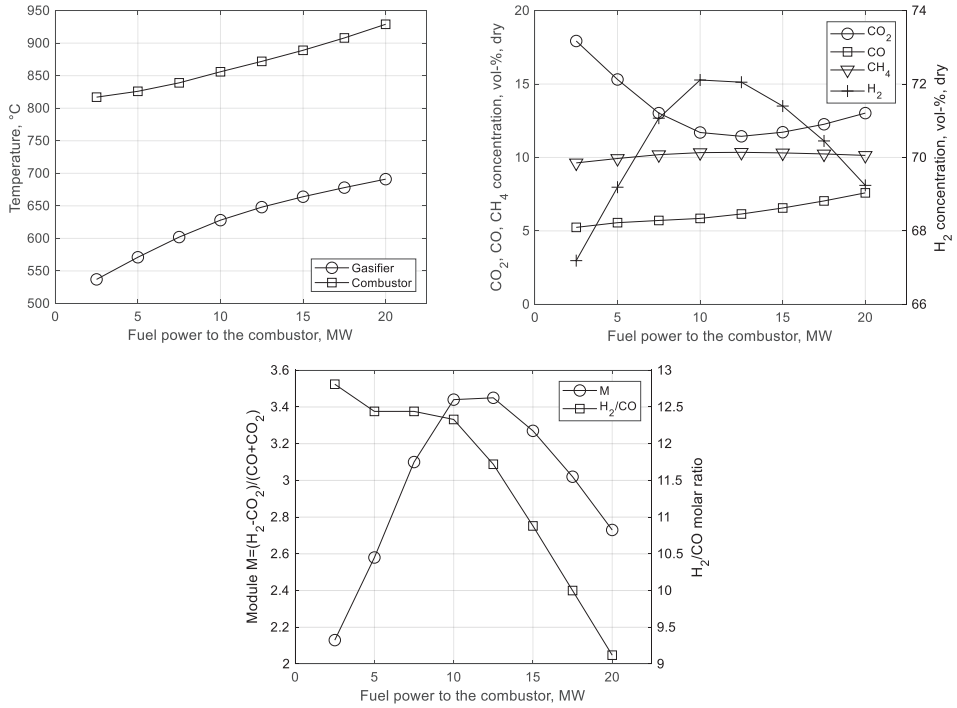

Figure 4. Temperature profiles of the reactors and syngas composition in a function of fuel feeding to the combustor.

In the second study, the combustor recirculation ratio K was altered. With the K value, the solids leaving from the combustor could be altered, and the amount, which was fed back in to the combustor to be determined. Solid flow with factor 1-K was directed to the gasifier. By adjusting the K value, the solid distribution between the reactors and actual CaO flow in to the gasifier was changed. The limestone circulating between the combustor and gasifier will act as a heat carrier and due to this reason, adjusting the K value has an impact on the temperature levels in the reactors. Solid distribution between the reactors and average temperatures of the reactors are presented in the Figure 6(a). Syngas composition, module M and H_2/CO ratio are presented in the Figure 6(b-c).

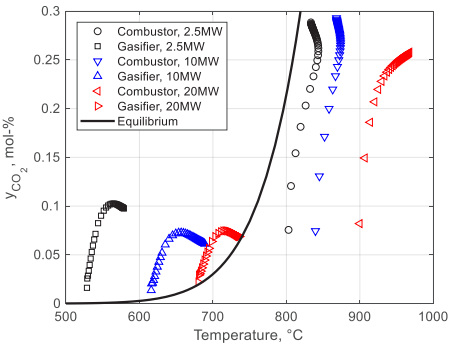

Figure 5. CO_2 molar concentration as a function of local temperature for the fuel powers 2.5 MW, 10 MW and 20 MW to the combustor. Equilibrium according to Silcox et al. [9].

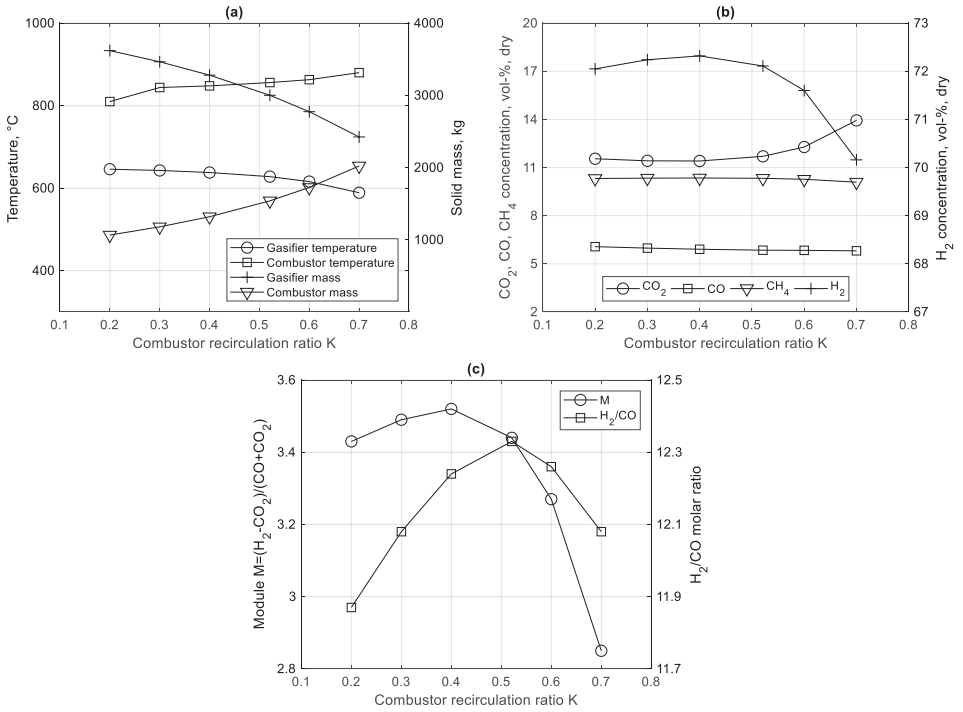

Figure 6. Combustor recirculation ratio K effect to (a) reactor average temperatures and solid distribution between reactors (b) syngas composition and (c) syngas module and H_2/CO ratio.

5. Conclusions

The objective of this work was to study SEG process, by introducing the one-dimensional model frame for the process and use the model to simulate the 100 MW_{th} reference case. The objective was achieved by implementing the most important gasification reactions into an existing calcium looping model frame. The reference case was built to base on the selected biofuel and steam to carbon ration (SCR). One-dimensional temperatures, reaction rates and gas concentration profiles were achieved. The effect of temperature and circulation rate were studied and it was found out that they can be used to control the syngas composition. The SCR was kept as a constant value in this work, but the effect of SCR should be studied in future research, as it is one of the key parameter in SEG.

The study of SEG is at its early stages when compared to traditional gasification processes. No SEG process utilizing dual circulating fluidized bed (CFB) technology has been reported and so far, the models reported in the literature have been so called 0D models, which do not take the process hydrodynamics and local concentrations of reacting components into account. The model in this work is the first reported 1D SEG model for the dual CFB system and it gives a starting point for the development of the SEG process. The model frame used in this study is capable for transient simulations, which provides an option for further operational and control studies.

Acknowledgement

This work in FLEDGED project has received funding from the European Union's Horizon 2020 research and innovation programme under grant agreement No 727600 .

References

[1] Pfeifer C, Sorbent-enhanced gasification, in Fluidized bed technologies for near-zero emission combustion and gasification. Woodhead Publishing; 2013.
[2] Johnsson F, Leckner B, Vertical distribution of solids in a CFB-furnace. In: Proceedings of the 13th International Conference on Fluidized Bed combustion, Orlando, USA, 1995, pp. 671–679.
[3] Ylätalo J, Ritvanen J, Arias B, Tynjälä T, Hyppänen T, 1-Dimensional modelling and simulation of the calcium looping process, International Journal of Greenhouse Gas Control 9, 2012, p. 130-135.
[4] Myöhänen K, Hyppänen T, A three-dimensional model frame for modelling combustion and gasification in circulating fluidized bed furnaces, International Journal of Chemical Reactor Engineering 9, 2011, A25.
[5] Myöhänen K, Modelling of combustion and sorbent reactions in three-dimensional flow environment of a circulating fluidized bed furnace, DSc Thesis, Lappeenranta University of Technology, 2011, http://urn.fi/URN:ISBN:978-952-265-161-7.
[6] Ylätalo J, Model based analysis of the post-combustion calcium looping process for carbon dioxide capture, DSc Thesis, Lappeenranta University of Technology, 2013, http://urn.fi/URN:ISBN:978-952-265-521-9.
[7] Hejazi B, Grace JR, Bi X, Mahecha-Botero A, Kinetic Model of Steam Gasification of Biomass in a Bubbling Fluidized Bed Reactor, Energy & Fuels 31, 2017, pp. 1702-1711.
[8] Biba V, Macak J, Klose E, Malecha J, Mathematical model for gasification of coal under pressure, Industrial & Engineering Chemistry Process Design and Development 17, 1978, pp. 92-98.
[9] Silcox GD, Kramlich JC, Pershing DW, A mathematical model for the flash calcination of dispersed CaCO3 and Ca(OH)2 particles, Industrial & Engineering Chemistry Research 28, 1989, pp. 155-160.

Publication II

Pitkäoja, A., Ritvanen, J., Hafner, S., Hyppänen, T. and Scheffknecht, G.
Simulation of a sorbent enhanced gasification pilot reactor and validation of reactor model

Reprinted with permission from
Energy Conversion and Management
Vol. 204, 112318, pp. 1-14, 2020.
© 2020, Elsevier

Energy Conversion and Management 204 (2020) 112318

Contents lists available at ScienceDirect

Energy Conversion and Management

journal homepage: www.elsevier.com/locate/enconman

Simulation of a sorbent enhanced gasification pilot reactor and validation of reactor model

Antti Pitkäoja[a,*], Jouni Ritvanen[a], Selina Hafner[b], Timo Hyppänen[a], Günter Scheffknecht[b]

[a] LUT School of Energy Systems, Lappeenranta – Lahti University of Technology, PO. Box 20, FI-53851 Lappeenranta, Finland
[b] Institute of Combustion and Power Plant Technology (IFK), University of Stuttgart, Pfaffenwaldring 23, 70569 Stuttgart, Germany

ARTICLE INFO

Keywords:
Sorbent enhanced gasification
Gasification
Biomass thermochemical conversion
Simulation
Limestone
Hydrodynamics

ABSTRACT

Sorption enhanced gasification (SEG) is a promising technology for production of a renewable feedstock gas for biofuel synthesis processes. The technology has been previously demonstrated at pilot scale. Scaling of the technology to an industrial size requires knowledge from governing phenomena. One-dimensional bubbling fluidized bed (BFB) reactor model was developed and validated against experimental data from 200kW_{th} dual fluidized bed facility. Sub-models for biomass gasification, reactive bed material and fluidized bed hydrodynamics were incorporated into the model frame. The model gave satisfactory predictions for bed material conversion, temperature profiles and gas composition of the producer gas. The conducted validation improved understanding of bed material conversion, water–gas shift reaction and hydrodynamics and their role in SEG reactors. Further refinement and comprehensive validation of the model with additional data from the pilot is required. The knowledge from the comprehensive validation can be utilized in simulation of an industrial size reactor.

1. Introduction

EU strategy for transition to a low-carbon economy sets out a framework and mechanisms to address climate change. The aim of the EU strategy is to keep average global warming below 2 °C compared to the pre-industrial temperatures [1]. Greenhouse gas emissions from transportation account for almost a quarter of Europe's greenhouse gas emissions and transportation is the main source of air pollution in European cities [2]. A target of 14% renewable fuels usage in the transportation sector by 2030 has been set and, consequently, there is a pressing need to develop effective and cost-efficient ways to produce transportation fuels from renewable sources [3].

Fossil liquid fuels, such as petroleum and diesel have been used for transportation for decades due to high energy density. The majority of emissions from the traditional fuels comprises CO_2, NO_X and small particulate emissions. From the localized pollution perspective, gaseous fuel grades, such as dimethyl ether (DME) are considered attractive alternative fuels, since combustion of gas is free from small particulate emissions. DME can be used in diesel-powered vehicles without any major modification to the combustion technology by liquidizing the gas [4]. DME synthesized from a renewable feedstock, for instance biomass, can be considered to be renewable fuel.

DME can be synthesized from a gaseous feedstock, which is containing a suitable ratio of CO, H_2, CO_2 and hydrocarbons. The gas required for DME synthesis can be produced by a number of different methods, of which gasification of biomass is one alternative. In recent decades, considerable research attention has been devoted to study of conventional biomass gasification, but in recent years, more advanced processes, such as dual fluidized bed gasifiers, have become the subject of increased research interest [5]. Sorbent enhanced gasification (SEG) is dual fluidized bed technology that improves the quality of the producer gas compared to conventional gasification [6]. The producer gas from indirect H_2O gasification processes, such as SEG process, contains less non-combustible gas species (CO_2 and N_2) compared to the conventional gasification processes without CO_2 capture.

The conventional fluidized bed gasification process is operated at elevated temperatures around 800–900 °C, where in oxygen depleted sub-stoichiometric conditions, biomass thermal degradation fractionates the biomass as gas species, tars and char [7]. Sorbent enhanced gasification is indirect steam gasification process operated at temperatures between 600 and 800 °C and the process is enhanced by limestone, which captures CO_2 from the process.

The actual processes governing the biomass gasification are difficult to model, since the conversion process is complicated and modeling all details might not be even possible. Therefore, extent and rate of chemical conversion processes are commonly simplified as unambiguous

* Corresponding author.
E-mail address: antti.pitkaoja@lut.fi (A. Pitkäoja).

https://doi.org/10.1016/j.enconman.2019.112318
Received 27 August 2019; Received in revised form 15 November 2019; Accepted 16 November 2019
Available online 27 November 2019
0196-8904/ © 2019 Elsevier Ltd. All rights reserved.

Nomenclature

a	coefficient [−]
A	area of control element [m^2]
A_r	reaction surface area [m^2/kg]
Ar	Archimedes number [−]
c	mass ratio constant [−]
c_p	specific heat capacity [J/(kgK)]
C	concentration [mol/m^3]
d	diameter [m]
D	binary diffusion coefficient [cm^2/s]
E	energy [W/m^3]
f_{exbed}	bed expansion coefficient [−]
f_w	wake volume ratio [−]
g	gravity [m/s^2]
h	enthalpy [J/kg]
H	reaction enthalpy [J/kg]
h_{bed}	bed height [m]
h_{TDH}	TDH height [m]
J	diffusion [kg/(m^3s)]
k	chemical reaction rate coefficient [1/s]
$kg_{G,C}/kg_{F,C}$	elemental carbon conversion from daf fuel to producer gas [−]
k'	chemical reaction rate coefficient [m^3/(mols)]
K_d	lateral mixing coefficient [−]
K_m	total mass transfer coefficient [1/s]
K	reaction equilibrium [−]
$\dot{m}$	mass flow rate [kg/s]
M	molar mass [mol/kg]
p	pressure [Pa]
Q_{hs}	heat source [W]
$Q_{s,w}$	flow of wake [kg/(m^3s)]
$Q_{g,eb}$	net flow [kg/(m^3s)]
$Q_{s,ew}$	net flow [kg/(m^3s)]
R	chemical reaction rate [kg/(m^3s)]
R_i	ideal gas constant [J/(molK)]
S	source term [kg/(m^3s)]
t	time [s]
T	temperature [K]
TDH	transport disengaging height [m]
u	velocity [m/s]
U	internal energy [W/m^3]
V	volume [m^3]
W	mass fraction [kg_i/kg_y]
y	mole fraction [mol_i/mol_y]
z	distance [m]

Greek

γ	CO and CO_2 ratio [−]
ϵ	void fraction [−]
μ	dynamic viscosity [Pas]
ρ	density [kg/m^3]
σ	collision diameter [m]
Ω	diffusion parameter [−]

Indices

b	bubble, bubble gas
bed	bubble bed
br	single bubble
$conv$	convection
$char$	char (fixed carbon)
C	carbon
e	emulsion
eq	equilibrium
fb	freeboard
g	gas
hs	heat source/sink
i	index
j	index
k	index
lat	latent
max	maximum conversion limit for sorbent
mf	minimum fluidization
p	particle
r	reaction
s	solid
$surface$	surface of dense bed
vol	volatiles
w	wake
0	superficial

reaction equations and chemical kinetics are describing the rate of conversion from one substance to another. Fluidized bed reactor modeling methods can be divided into different approaches based on the number of physical dimensions of the model. Selection of the number of physical dimensions is done according to the required level of details and generally involves a choice between 0D, 1D and 3D-approaches. Dimensionless models (0D) are based on fundamental mass and energy balances of a control volume for the complete reactor [8]. An equilibrium model is useable for first estimation, however development of new processes generally requires more detailed information. Modeling of the additional details requires implementation of dimensional approach with fluidized bed hydrodynamics and chemical reaction kinetics. 1D-approach is the simplest from the dimensional approaches. In 1D-approach simulation domain is vertically discretized as control elements. The method separates the reactor into distinguishable sections making it possible to investigate the extent of phenomena in different parts of the model. 1D modeling approach for bubbling fluidized bed (BFB) gasification has been widely implemented [9–13], but suffer the drawback of averaging of phenomena in lateral direction of the reactor. Therefore, it is not suitable for reactors with significant dimensions or it requires sub-models for considering the lateral direction. The model is most suitable for pilot scale reactors, since impact of lateral mixing in the reactor is not significant due to the small lateral reactor dimensions. To take into account the lateral mixing, 3D-approach is required. In literature there are modeling paper with various levels of details [12,14–16], however for the current need 1D-approach is the most suitable.

Most published 1D models have been developed for conventional gasification and are not suitable for modeling of the SEG process. The SEG process requires use of a chemically active bed material (formed from individual material fractions, such as ash, CaO and $CaCO_3$), since the sorbent bed material reacts with the gases formed from biomass, and these reactions must be included in the model. A comprehensive 1D SEG process model has been developed by Hejazi [17]. A drawback with this model is that 0D balance is used for modeling sorbent conversion in the bed instead of 1D balances. The assumption makes the bed as perfectly mixed without considering local solid fraction differences. Although, there can be mixing and diffusional limitations in the bed if reacting gas species are locally depleted.

There currently appears to be very few published 1D SEG or 1D biomass gasification models that implement non-ideal mixing with sufficient accuracy. The model developed in this study considers the

mixing issue by separating in-bed solid phase as emulsion and wake, and conversion of bed material fractions separately for the emulsion and the wake.

Development and scaling of technology requires thorough understanding of all relevant phenomena. The main outcome from reactor process modeling are correlations describing different phenomena occurring in the reactor. These correlations could be used in development of the technology by implementing the correlations in semi-empirical 3D simulation of an industrial scale reactor.

The goal of this paper is to develop a 1D BFB gasification model suitable for SEG gasification that be coupled with previously developed SEG circulating fluidized bed combustor model [18]. Previously published empirical equations for gas–solid interaction and gasification chemistry are employed in the model. The model is based on general accepted principles and is extended with chemically reactive bed material. With the developed model in-bed and freeboard operation conditions of the gasifier can be investigated.

The model developed in this work is one of very few 1D models developed for SEG processes and enables study of the gasification reactor at steady-state operation and during transient change of operation. Preliminary validation of the developed model is carried out by steady-state simulations against experimental data published by Hafner et al. [19] from a dual fluidized bed facility located at the Institute of Combustion and Power Plant Technology (IFK) of the University of Stuttgart.

2. Modeling approach

The model frame for the BFB SEG process was developed based on a semi-empirical 1D-approach. The model frame consists of a gasification reactor which can later be coupled with a previously published complete model of a SEG process with CFB reactors [18]. Ideal fundamental balance equations for mass and energy are implemented in the gasification model frame. Transport phenomena and chemical reactions are modeled using empirical model equations. The model frame is implemented in Matlab's Simulink environment, where reactor code is resolved using Simulink's embedded computational engine. The reactor model is written with C-programming language. Spatial derivatives of the reactor model are discretized using a first order upwind scheme for convection terms and time derivatives are resolved using an explicit solver in Simulink.

2.1. Two-phase model

A hydrodynamic model was developed for the BFB SEG process. The bubble bed model was derived based on well-known principles of fluidization [20,21]. Simplifications have been made for BFB hydrodynamics. The hydrodynamic scheme includes important solid dynamics of the BFB reactor. The two-phase model is based on following assumptions:

- Bubbling bed contains gas and solid phases,
- the gas is situated in bubble and emulsion and the gases are called as bubble gas and emulsion gas,
- the solids are situated in emulsion and wake,
- the solids situated in the wake are rising upwards with gas bubble,
- the emulsion and the wake are assumed to be at the minimum fluidization state,
- the solids in the emulsion move downwards,
- heterogeneous chemical reactions occur between the wake solid and the bubble gas and the emulsion solids and the emulsion gas,
- the solid and the gas phases are resolved by using the average temperature of reactor element for both phases, and
- elutriated particles are added into the emulsion at the freeboard, which has an impact on energy and mass balances.

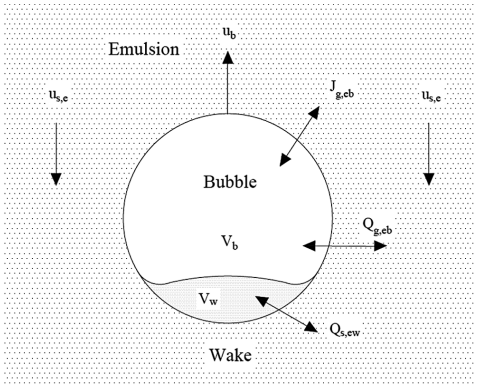

Fig. 1. Bubble-emulsion model of dense bed. Notations: u_b is velocity of bubble gas, $u_{s,e}$ is velocity of solids in emulsion, V_b is volume of bubble, V_W is volume of wake, $J_{g,eb}$ is diffusion between emulsion and bubble, $Q_{g,eb}$ is gas net flow between emulsion and bubble and $Q_{s,ew}$ is net flow of solids between emulsion and wake.

The computational domain is divided into three sections: bed, surface and freeboard, of which the bed and the freeboard are divided into multiple 1D elements. The surface element is the boundary of the bed and the freeboard, where mixing of gases and solids takes place. Upward of surface element an emulsion is used for mixture of solid and gas. The bubble-emulsion model of the bed follows simplified approach shown in Fig. 1. The freeboard sections is hydrodynamically treated as dilute two-phase flows where dispersion of solids is high. The freeboard section is assumed to hold small quantities of solid material entrained in the gas flow. The freeboard is divided amongst emulsion gas and emulsion solids. Solids are circulated from the combustor to the gasifier with continuous flow and are added in the freeboard to the emulsion at the feed location. Respectively, solids are discharged from the emulsion at the bottom of the reactor.

2.2. Solid phase balances

Solid phase is resolved in dense bed, bed's surface and freeboard sections. The bubbling bed is dense (high density of solid) two-phase zone separated physically as the wake of bubble and the emulsion. The bed zone's physical and mathematical separation is required, since solids are rising upwards in the wake of the bubble and moving downwards in the emulsion. Solids in-bed circulation and mixing is caused by this movement. Emulsion solids movement to downwards is caused by reactor configuration in which the solids are fed to the surface of the bed and are discharged at the bottom of the bed.

The solid bed material is formed from discrete material fractions (CaO, $CaCO_3$, $CaSO_4$, and ash). Char have been separated from the other material fraction and is assumed to be uniformly mixed with the bed material in each control element. The continuity equation is resolved for each material fraction in each control element and the dense bed can retain different material fraction distributions for the wake and the emulsion. Formulation of separate continuity equations for the wake and the emulsion is shown in Appendix A. General continuity equation for material fraction k can be written as:

$$\frac{\partial}{\partial t}(W_{s,k}\rho_s) + \frac{\partial}{\partial z}(W_{s,k}u_s\rho_s) = W_{s,k}Q_{s,ew} + \sum R_{s,k} + \sum S_{s,k} \quad (1)$$

where $W_{s,k}$ is material fraction of k, ρ_s is density of solids, u_s is velocity of solids, $Q_{s,ew}$ is net flow of solids between emulsion and wake, chemical reaction term $\sum R$ describes the chemical reactions of material k

according to Table 1, while the term $\sum S$ considers local mass changes of material k due to local feeds and discharges of the solids. Maximum $W_{s,k}$ for $CaCO_3$ is selected as 30 m-% based on previous studies of the calcium looping process [22], which is caused by aging of the limestone [23]. In each control element, the effect of chemical reaction into the material fractions is resolved using balance equations. Solid mixing $Q_{s,ew}$ from the wake to the emulsion and net flow of solids to the opposite direction is resolved with equation

$$Q_{s,ew} = K_d Q_{s,w} \tag{2}$$

within each dense bed control element. The solid mixing $Q_{s,ew}$ between wake and emulsion is modeled using K_d of 0.15 from mass transported by the wake. The magnitude of the mixing is selected based on experimental work of Chiba and Kobayashi [24].

2.3. Gas phase balances

Two simplifications have been made to simplify gas phase balances. The first, on the interface of the bubble and the emulsion region, there is no area called as cloud. The second, gas species balance of the emulsion is resolved first, and it will define the amount of gas situated in the bubble. The gas species O_2, N_2, CO_2, CO, NO, H_2O, H_2S, NH_3, CH_4, C_2H_4, H_2, and SO_2 are considered in the model and the total gas flow is the sum of individual gas species. Mass balances are resolved separately for each component in each control element, however at the bed section, there is a division between bubble gas and emulsion gas with separate balance equation, which are described in Appendix A. The emulsion and the bubble can retain different concentration of gas species. General continuity equation for individual gas specie j is written as:

$$\frac{\partial W_{g,j}}{\partial t}\rho_g + \frac{\partial W_{g,j} u_g}{\partial z}\rho_g = \sum R_{g,j} + \sum S_{g,j} + Q_{g,eb,j} + J_{g,eb,j} \tag{3}$$

where $\sum R$ describes the chemical reactions of each specie j and are summarized in Table 2 and the source term $\sum S$ considers local mass changes of each species due to formation of volatiles, drying of fuel, char gasification and local feeds and discharges of the gas. However, biomass devolatilization and drying is taking place only in the emulsion. There is always net gas flow $\sum Q_{g,eb,j}$ from the emulsion to the bubble, since the minimum fluidization state must apply at the emulsion. Thus, the excess gas is assumed to appear as gas bubbles. Diffusion $\sum J_{g,eb,j}$ between the emulsion and the bubble is taking place and different concentrations between the bubble and the emulsion gas induces mass transfer $J_{g,eb,j}$. The mass transfer is modeled using Chapman-Enskog theory with parameters of Cussler [31] and a mixture approach of Fairbanks and Wilke [32] to resolve the diffusion in a correlation of Sit and Grace [33]. Gas phase mass balances at the freeboard section are resolved according Eq. (3) without the mass transfer.

Devolatilization process is modeled according to Myöhänen [30] and Ylätalo [22]. The model formulation makes possible to freely define devolatilization profile for the process. Gases released at the devolatilization from the fuel are CO, CO_2, H_2, CH_4 and C_2H_4. The devolatilization model parameter γ influences in distribution of volatiles. Ratio of CO and CO_2 is adjusted with the parameter. All volatile O elements in the fuel are spend and distributed as CO and CO_2 according to the coefficient. The leftover volatilized elements are distributed to NH_3, H_2S, H_2, CH_4 and C_2H_4 gases. Other gas species NO, H_2S and NH_3 are formed during combustion (not taking place) and char gasification. Drying of the fuel produces H_2O.

2.4. Bubbling bed hydrodynamics

Empirical hydrodynamic equations are employed to close the above defined constitutive equations. These equations are based on measurements and observations of fluidization phenomena. The empirical hydrodynamic equations cannot be often used directly, since the equations are based on measurements done with specific operating conditions. Therefore, the empirical equations are needed to be tuned to make the equations valid on pilot conditions, or modified otherwise, if the equations are not directly valid on the operation conditions of interest. The empirical hydrodynamic equations described in Table 3 are implemented in the reactor model. Additional information is provided in Appendix A.

2.5. Energy balance

Energy balance is required in order to resolve time dependent temperatures in the reactor. The energy balance is resolved in the control element for two-phase flow. The general uniform energy balance for gas and solid phases can be written as:

Table 1
Limestone chemical reactions.

Reaction	Equation	H (at 25 °C)	Refs.
Calcination	$CaCO_3(s) \rightarrow CaO(s) + CO_2(g)$	178300	[25]
	$R_{calc} = \rho_s k'_{calc} W_{s,CaCO_3}^{\frac{2}{3}} (C_{CO_2,eq} - C_{CO_2})$		
	$k'_{calc} = a_{calc}\ 2057 \exp\left(-\frac{112400}{RT}\right)$		
Carbonation	$CaO(s) + CO_2(g) \rightarrow CaCO_3(s)$	−178300	[26,27]
	$R_{carb} = \rho_s k'_{carb} (W_{s,max} - W_{s,CaCO_3})(C_{CO_2} - C_{CO_2,eq})$		
	$k'_{carb} = 30\ a_{carb}$		
Limestone thermodynamic reaction equilibrium	$C_{CO_2,eq} = \frac{4.137 \times 10^{12}}{R_i T} exp\left(-\frac{20474}{T}\right)$		[28]
Sulphation	$CaO(s) + SO_2(g) + 0.5\ O_2(g) \rightarrow CaSO_4(s)$	−502100	[29]
	$S_{sulp} = \rho_s W_{s,CaO} k_{sulp} W_{g,SO_2} W_{g,O_2}$		
	$k_{sulp} = a_{sulp} 4.0(-3.843T + 5640) exp\left(-\frac{8810}{T}\right)$		
De-sulphation	$CaSO_4(s) + CO(g) \rightarrow CaO(s) + SO_2(g) + CO_2(g)$	219200	[30]
	$R_{desulp} = \rho_s W_{s,CaSO_4} k'_{desulp} C_{CO} A_{r,CaSO_4} M_{CaSO_4}$		
	$k'_{desulp} = a_{desulp} 0.005 exp\left(-\frac{10000}{T}\right)$		
Direct sulphation	$CaCO_3(s) + SO_2(g) + 0.5\ O_2(g) \rightarrow CaSO_4(s) + CO_2(g)$	−323800	[30]
	$R_{disulp} = \rho_s W_{s,CaCO_3} k'_{disulp} C_{SO_2}^g C_{O_2}^b C_{O_2}^s A_{r,CaCO_3} M_{CaCO_3}$		
	$k'_{disulp} = a_{disulp} 0.01 \exp\left(-\frac{3031}{T}\right)$		
	$a = 0.9,\ b = -0.75,\ c = 0.001$		

Table 2
Gasification reactions.

Reaction	Equation	H (at 25 °C)	Refs.
Boudouard	C (s) + CO_2 (g) → 2 CO (g) $R_{boud} = a_{boud} k_{boud} \rho_{char} W_{char,C}$ $k_{boud} = 2.34 \times 10^4 \exp\left(-\frac{166200}{RT}\right) p_{CO_2}^{0.83}$ [kPa]	172400	[34]
Water-gas	C (s) + H_2O (g) → H_2 (g) + CO (g) $R_{wg} = a_{wg} k_{wg} \rho_{char} W_{char,C}$ $k_{wg} = 2.14 \times 10^5 \exp\left(-\frac{164000}{RT}\right)$	131300	[35]
Methanation	C (s) + 2 H_2 (g) → CH_4 (g) $R_{meth} = a_{meth} k_{meth} \rho_{char} W_{char,C}$ $k_{meth} = 16.4 \exp\left(-\frac{94800}{RT}\right) p_{H_2}^{0.93}$[MPa]	−75000	[36]
Water-gas shift	CO (g) + H_2O (g) ↔ CO_2 (g) + H_2 (g) $R_{wgs} = a_{wgs} M_{CO} k'_{wgs} \left(C_{CO} C_{H_2O} - \frac{C_{CO_2} C_{H_2}}{K_{wgs}}\right)$ $k'_{wgs} = 2.78 \exp\left(-\frac{12560}{RT}\right)$	−41100	[37]
Shift thermodynamic reaction equilibrium	$K_{wgs} = 0.0265 \exp\left(-\frac{3965}{T}\right)$		[38]
Steam methane reforming	CH_4 (g) + H_2O (g) ↔ CO (g) + H_2 (g) $R_{smr} = a_{smr} M_{CH_4} k'_{smr} (C_{CH4} C_{H_2O} - \frac{C_{CO} C_{H_2}^3}{K_{smr}})$ $k'_{smr} = 3.05 \times 10^5 \exp\left(-\frac{125000}{RT}\right)$	206200	[39]
Reforming thermodynamic reaction equilibrium	$K_{smr} = 6.14 \times 10^{13} \exp\left(-\frac{28116}{RT}\right)$		[39]

Table 3
Hydrodynamic equations.

Name	Equation	Refs.
Minimum fluidization velocity	$u_{mf} = \frac{\mu_g}{\rho_g d_p} (\sqrt{27.2^2 + 0.0408 Ar} - 27.2)$	[40,41]
Bed expansion 1)	$f_{exbed} = a_{exbed} (1 + \frac{14.31 (u_0 - u_{mf})^{0.738} d_p^{1.006} \rho_p^{0.376}}{\rho_g^{0.126} u_{mf}^{0.937}})$ $a_{exbed} = 0.85$	[42]
Bubble gas velocity	$u_b = u_0 - u_{mf} + u_{br}$	[20]
Single bubble rise velocity	$u_{br} = 0.711 \sqrt{g d_b}$	[20]
Bubble diameter 2)	$d_b = a_{bd} 0.54 (u_0 - u_{mf})^{0.4} (h + 4\sqrt{A})^{0.8} g^{-0.2}$ $a_{bd} = 0.1$	[43]
Entrainment mass flow 3)	$\dot{m}_{fb} = a_{elutriation} \dot{m}_{s,w,surface} exp(-a_{decay} h_{TDH}) = c$ $c = 0.01$, $a_{decay} = 3.5$, $a_{elutriation} = 0.5$	[44]
Wake volume ratio	$f_w = \frac{V_w}{V_b} = 0.3$	[45]
Mass transfer coefficient 4)	$K_{m,be,j} = a_{diff} \left(\frac{2 u_{mf}}{d_b} + 12 \sqrt{\frac{D_{g,j} \epsilon_{mf} u_b}{\pi d_b^3}}\right)$ $a_{diff} = 0.03$, for $CO_2 a_{diff,CO2} = 0.5$	[33]

1) Bed expansion for the pilot was determined against pressure measurements.
2) A bubble size coefficient of 0.1 was determined as appropriate model coefficient value after a bubble size study.
3) h_{TDH} is calculated according Appendix A. Model coefficient $a_{elutriation}$ is selected based on the data provided by Wen and Chen [44].
4) $a_{diff} = 0.03$ is based on experiments of Chiba and Kobayashi [46] and $a_{diff,CO_2} = 0.5$ for CO_2 based on experiments of Wakabayash and Kunii [47].

$$\frac{dU}{dt} = E_{conv} + E_r - E_{hs} \tag{4}$$

where U is internal energy, E_{conv} convection of energy, E_r energy from chemical reactions, E_{hs} is heat source or sink. In Appendix A, detailed formulation of the energy balance is presented. One element wise temperature is resolved from the uniform energy equation (Eq. (4)) that is used by gas and solid phase in the model.

3. Experimental work and modeling setup

Experimental investigations of the SEG process was conducted at a 200 kW_{th} dual fluidized bed facility at the Institute of Combustion and Power Plant Technology (IFK) at the University of Stuttgart (Fig. 2). The facility consists of a bubbling (BFB) and a circulating fluidized bed (CFB) reactor that are connected to each other.

BFB reactor is 6 m in height, has an inner diameter of 0.33 m, and is operated as gasifier/carbonator. The CFB reactor has a height of 10 m, an inner diameter of 0.2 m, and is operated as a combustor/calciner. Biomass is gravimetrically fed via a rotary valve and screw conveyor

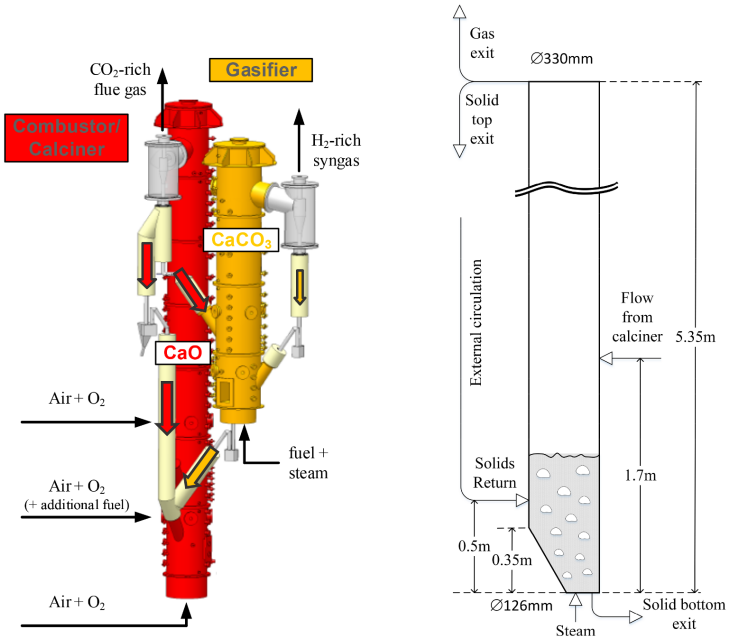

Fig. 2. 200 kW_{th} dual fluidized bed facility at IFK, University of Stuttgart and main model dimensions of the gasifier.

directly into the bed of the gasifier. Steam is fed via two gas spargers at the bottom of the gasifier and the steam acts as both a gasification and fluidizing agent. The gasifier is equipped with a primary cyclone for particle separation and internal recirculation of entrained bed material and char particles. In the producer gas line, there is a secondary cyclone for further particle reduction before the gas is combusted in a flare.

Bed material and char particles leave the gasifier via the bottom loop seal and enter the calciner at the lower part of the reactor. In the calciner, char particles are combusted together with additional biomass (if needed) and oxygen enriched air to provide the heat that is required for the calcination of the bed material. To maintain the activity of the bed and for compensation of losses due to attrition, fresh limestone is fed to the calciner.

Solids are separated from the flue gas in the primary cyclone of the calciner. A part of the separated solids is transferred back to the gasifier via a screw conveyor, while the rest of the material is sent back to the calciner. The solid circulation rate is controlled by the rotational speed of the screw. For further reduction of the particle concentration in the flue gas, the calciner is provided with a secondary cyclone and a bag filter.

In the gasifier, gas samples for different measurements can be taken after the primary cyclone and/or after the secondary cyclone. Standard gas components such as H_2, CO, CO_2 and CH_4 were measured continuously after the primary cyclone using an ABB AO2020 gas analyzer after fine filtration, washing in isopropanol (for tar removal) and condensation. Low hydrocarbons (C_2H_4, C_2H_6, C_3H_6, C_3H_8 and C_4H_{10}) were measured with a Varian CP-4900 Micro GC analyzer.

Experiments in this work have been conducted with wood pellets as fuel and limestone from Germany with a nominal particle size distribution of 100 µm–300 µm as active bed material. The chemical composition of the wood pellets is given in Table 4. During the experiments, the steam-to-carbon ratio was kept constant at 1.5 mol_{H2O}/mol_C. Gasification temperature was increased by variation of the circulation rate and the calcination temperature was between 910 °C and 935 °C. Each experimental point was kept at steady-state conditions for a minimum of 1 h and a maximum of 3 h.

Modeling setup was done based on the specification of the pilot gasifier. The main dimensions of the gasifier are shown in Fig. 2. For modeling, the reactor was divided into 40 discrete elements from which 3 were place on the conical bottom section of the gasifier. The gasifier was operated with constant operational parameters during the experiments and the parameters are summarized in Table 5. Simulation boundary conditions were determined based on online process measurements and samples of solid material extracted from loop seals. The main boundary conditions are summarized in Table 6 and solid properties are presented in Table 7.

Simulations included the dense bed and the freeboard section. Gas and solid flows entering or exiting from the reactor were modeled as balances adding or removing the material. Primary gas fed from the bottom of the reactor was assumed to be perfectly mixed and the gas was fed in the bubble gas at the bottom element of the reactor. The fuel was fed into the reactor at the conical section above the bottom boundary (at the two lowest bed elements). The top boundary at the

Table 4
Chemical composition of wood pellets used in experimental investigations of the SEG process.

Proximate analysis				Ultimate analysis					
Moisture	Ash	Volatiles	Fixed carbon	C	H	N	S	O	LHV
m-%, ar		m-%, ds		m-%, daf					MJ/kg,ar
6.0	0.2	82.5	17.3	50.8	6.1	0.2	0.1	42.8	17.36

Table 5
Operating conditions of experimental balances.

Parameter	
Fuel feed [kg/h]	30
Primary gas [kg/h]	30.3
Primary gas temperature [°C]	146
S/C [mol/mol]	1.5

Table 6
Simulation boundary conditions.

Parameter	OP 1.1	OP 1.2	OP 1.3	OP 1.4
Solid flow from combustor [kg/h]	341	498	570	694
Char from combustor [kg/h]	0	0	0.003	0
Material mass fractions at circulation [%]				
CaO	85.21	93.33	91.24	95.97
$CaCO_3$	9.55	1.99	4.68	0.42
$CaSO_4$	0.00	0.00	0.00	0.00
Ash	5.24	4.68	4.08	3.61
Temperature of solid flow [°C]	716	734	787	809
N_2 feeds total [kg/h]	10.50	10.94	15.05	14.63
N_2 feeds temperature [°C]				
Dense bed	550	650	650	650
Freeboard	200	200	200	200

Table 7
Solid properties.

Parameter	
Bed material particle diameter [μm]	180
Char particle diameter [μm]	300
Solid ρ [kg/m^3]	3000
Char ρ [kg/m^3]	550
Solid c_p [J/(kg K)]	1000
Reaction surface of $CaCO_3$ [m^2/kg]	300
Reaction surface of $CaSO_4$ [m^2/kg]	100

freeboard was set below the cyclone connecting pipe, where the gas flow was assumed to be steady, and it was assumed that there were no effects from the connecting pipe. Chemical reactions between the top simulation boundary and the cyclone were assumed to be small due to the small distance between the simulation boundary and the measurement points. Solids internal circulation from the primary and secondary cyclones were modeled by returning elutriated solids from the top element back to the bed. Totally eight N_2 feed positions were situated in the simulation domain. The N_2 feeds were modeled as secondary air feeds. The N_2 in the reactor was used for various purposes such as: fluidizing bottom and cyclone loop seals, sealing rotary valve and purging pressure sensors. Part of the total N_2 feed leaked outside the reactor through rotary valve and loops seals without entering into the reactor.

4. Results

Modeling activities in this paper focus on modeling the gasification reactor of the dual fluidized bed facility. Totally six operation points were experimentally investigated by Hafner et al. [19], and four of the operation points are modeled. The aim of the modeling is to gain the knowledge required to model hydrodynamics, chemical kinetics and energy transfer in the process. The role of in-bed chemical reactions, particularly bed material conversion and water–gas shift were found important. The developed model is capable to model the aforementioned important characteristics of the SEG process. Temperature dependency of fuel conversion were found important for precise modeling capability of lower temperature operation points. Validation of the reactor model focused on higher temperatures, where favourable gas composition for DME synthesis is produced. Detailed knowledge of the physical and chemical phenomena in a SEG reactor is of value in scale-up of the SEG process from a pilot to an industrial scale.

4.1. Model validation

Validation of the developed reactor model was conducted by introducing the measured operation parameters into the model with appropriate model equations for physical and chemical phenomena. Hydrodynamics and gasification chemistry were modeled using literature correlations and parameters. The experimental work shows that higher operating temperatures to be more significant for the model validation than lower operating temperatures, since gas composition on the higher temperatures is more favourable for DME synthesis [19]. The precise prediction capability on the higher temperatures was used as the basis of the model validation and to produce the favourable gas composition on the higher temperatures equilibrium of limestone carbonation was adjusted. The equal shift of the equilibrium was applied for each operation. The fitting of the employed hydrodynamic correlations to the measurements was done first. The hydrodynamics were adjusted against pressure measurements with experimental parameters from literature. Gasification chemistry was set after the hydrodynamics. Char reactivity was investigated using literature correlations, since reactivity data were not available for in-bed conditions of the pilot reactor. Information for different chars was collected based on literature reviews [48,49], and the most representative correlations were selected as preliminary models by considering an influence of biomass quality [50]. The preliminary correlation for water–gas reaction was according to Hemati and Laquerie [51], and for Boudouard reaction, according to Risnes et al. [52]. The kinetics of the selected preliminary correlations were set based on balances and new correlations having a good fit with the fitted correlations were selected from the reactivity library. The methodology provided direct literature correlations for char reaction kinetics, which are presented in Table 2.

Biomass devolatilization is modeled using standard proximate analysis. This is a common modeling assumption made for conventional processes operating on temperatures around 900 °C. However, at lower temperatures such as where the SEG process is operated, the quantity of formed volatiles, char and hydrocarbons depends on devolatilization temperature [53]. Heavy hydrocarbons “tars” are not directly considered in the used devolatilization model. The implemented devolatilization model assumes all oxygen in the fuel to be volatilized and no leftover oxygen remains in the formed char. The assumption might have a slight impact on how the elements are distributed as different volatiles species in the model compared to the actual formation of volatiles in the gasifier. Formation of volatile gas species H_2, CO, CO_2, CH_4 and C_2H_4 gas species are considered in the devolatilization model. However, C_2H_4 gas was not formed in the fuel decomposition. In the selected approach, light hydrocarbon species are assumed to be assimilated into CH_4, since formation of lower hydrocarbons (C_2, C_3 or C_4) were not considered. In general, the higher hydrocarbons are containing a smaller hydrogen to carbon ratio compared to CH_4, which causes the lumping of the elements overestimates CH_4 concentration and underestimates H_2 concentration in the reactor. The tars formed on biomass devolatilization can be assumed to be more severely cracked in SEG reactors compared to a conventional reactors, since bed material is mostly calcined limestone [54]. The effect of the calcined limestone to the tar conversion has been demonstrated experimentally [55,56]. The devolatilization was assumed to be the major source of hydrocarbons in the process [53]. The model was adjusted according to this assumption. CH_4 formation from char was assumed to be small and to not have a large contribution into the total amount of hydrocarbons [14]. Devolatilization parameter γ was selected as 0.53 for all cases based on the previous assumptions.

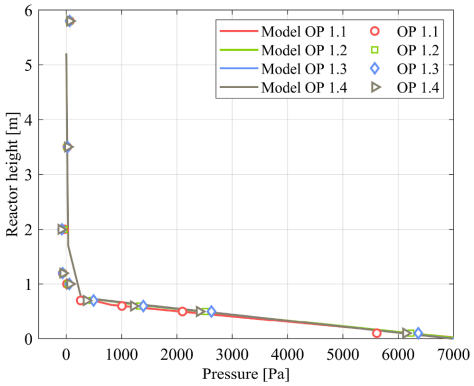

Fig. 3. Hydrostatic pressure profiles of the gasifier. The hydrostatic pressure profile of operation point 1.1 has minor deviation from the other profiles, since inventory of solids was slightly smaller in the gasifier during the experiments.

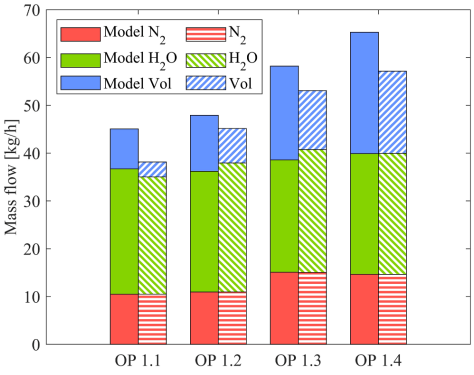

Fig. 4. The overall producer gas mass flow. The mass flow of the producer gas was determined based on the measurements. In the figure, at each operation point, the left bar represents simulation and the right bar the measurement. Abbreviation "Vol" in this instance denotes all gases except H_2O and N_2. The mass flow determined from measurements is not including tars, which will cause a difference between simulations and experimental mass flows.

4.2. Hydrodynamics

Hydrodynamics of the reactor were adjusted against vertical pressure measurements. The hydrodynamic scheme was formulated based on previously investigated correlations for physical phenomena. Good agreement between the model and the measurements was achieved using uniform hydrodynamic parametrization for the simulated operation points. The simulated hydrostatic pressure profiles compared to hydrostatic pressures determined from the pressure measurements are shown in Fig. 3.

4.3. Mass balance and heat balance

The producer gas flow from the pilot gasifier was measured before the gas was flared. The simulated gas mass flows compared to mass flows determined from the measurements are shown in Fig. 4. The simulations are following similar temperature trends as the measurements. Model prediction for gas mass flow on higher temperatures agrees with the measurements. Moreover, the difference between the mass flows is diminished as the temperature is increased. This suggest that the used modeling approach is adequate for modeling on the higher temperatures.

The measured producer gas composition against simulation results is shown in Fig. 5. Good agreement between the measured producer gas composition and the simulation is achieved on higher temperatures. Particularly at operation point 1.3, module 2 is achieved, which is the most favourable gas composition for DME synthesis [19]. The module is calculated from relations of gases:

$$M = \frac{y_{H_2} - y_{CO_2}}{y_{CO} + y_{CO_2}} \tag{5}$$

The favourable module should be applied as the target of process optimization, since additional process steps required for preparation of the feedstock gas can be reduced. Model performance is good on the higher temperatures, which can be seen from precise prediction capability of the module. On these operation points the simulation agrees with the measured mass flows (Fig. 4). However, on lower temperatures model prediction differs from the measurement, which influences in water–gas shift and carbonation reactions, since partial pressures of gases are not predicted precisely. The effect can be seen from relations of CO, CO_2 and H_2 of operation point 1.1 from Fig. 5.

Simulated gas concentration profiles in respect to the reactor height for emulsion gas and bubble gas are shown in Fig. 6. In example, N_2 gas is inert in the process. The gas is fed to the bubble at the bottom of the bed in the two lowest bed elements. In these elements, there is a large concentration difference for the N_2 between the emulsion and the bubble until the mixing evens the difference. The relatively high concentration difference for the N_2 is caused by three reasons: biomass devolatilization is taking place in the emulsion, primary gas is fed to the bubble and minimum fluidization state influences on gas exchange. The mixing of emulsion and bubble are limited at the bottom because of modeling assumptions.

Solid feed rate between the combustor and the gasifier was increased during the experimental runs. The increased feed elevated the bed temperature of the gasifier, since more heat was transferred from the combustor. The vertical process temperatures and the simulated temperature profiles are shown in Fig. 7. A heat source term was applied for bed of the reactor to match local temperatures. The heat balance adjustment according to Table 8 was applied for the bed. Constant heat loss of -2.4 kW/m was applied at freeboard in each simulations case. The freeboard heat loss is included in the adjustment in Table 8. The approach was used to compensate impact of uncertainties, such as devolatilization process, solid flow measurement and temperature measurements in the energy balance.

Good match was gained between simulated temperature profiles and temperature measurements with the used boundary conditions and applied heat balance adjustment term. It is important to gain good match between the simulated and the measured temperature profile, since the temperature affects the chemical reactions and the operation of the entire reactor.

4.4. Bed material conversion

Bed material carbonation is mainly influenced by bed temperature and as the bed temperature increases, bed material carbonation becomes more limited, which can be remarked from Fig. 5c), as increased CO_2 concentration, and from Fig. 4 as increased mass flow. The limited CO_2 capture decreases the bed material carbonation and the conversion reduced as function of the bed temperature, which is shown in Fig. 8. The simulated results are following the trend shown by measurements from operation point 1.1 and 1.4, which are reflecting a different behaviour of the reactor. Conversion of limestone was estimated precisely

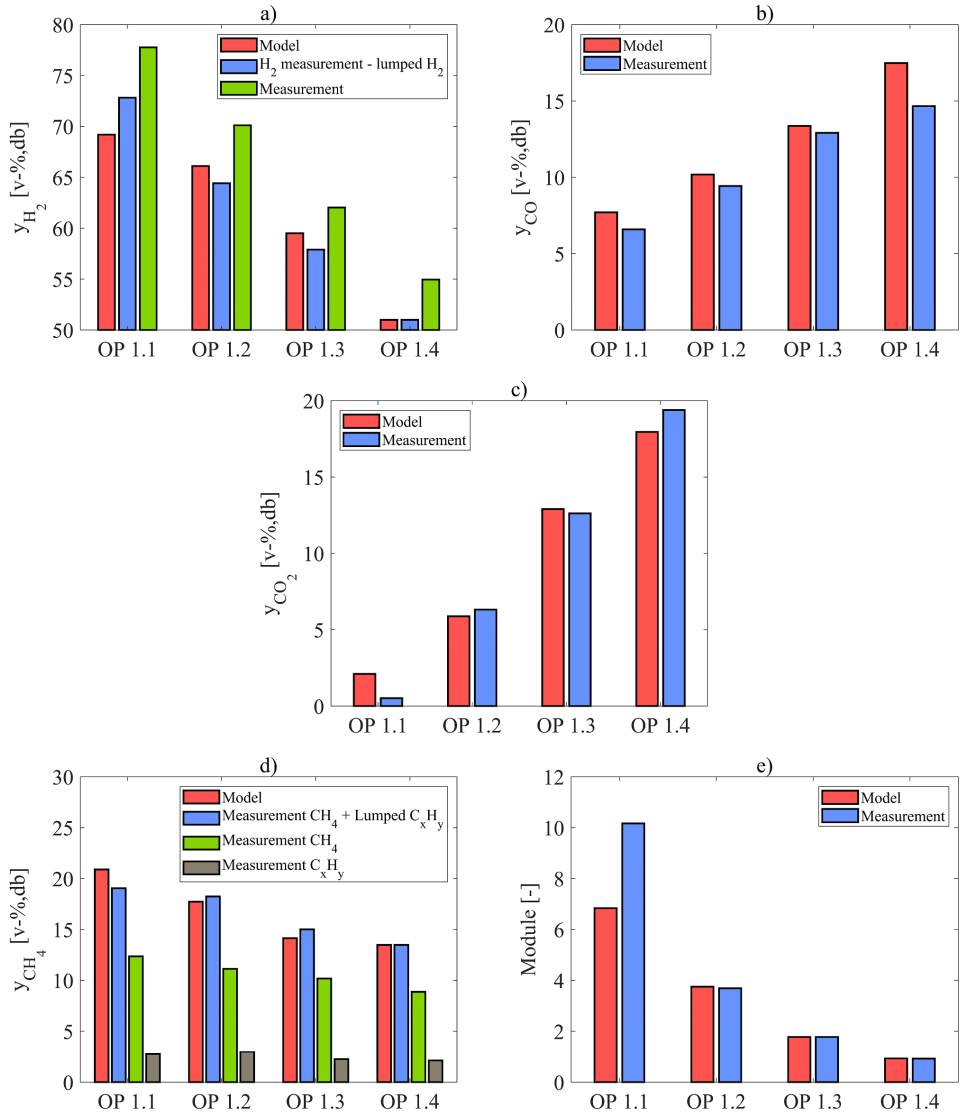

Fig. 5. Volume fractions of H_2, CO, CO_2 and CH_4 gas species and module of producer gas at the studied operation points. In Fig. 5 a) H_2, b) CO, c) CO_2, and d) CH_4 volume fractions of producer gas are shown. In Fig. 5 e) The producer gas module is presented.

at operation point 1.4. Moreover, the module of the producer gas and mass flow were precise at the operation point. The indications suggest the model to be precise on higher operating temperatures. The conversion of the limestone was over predicted on lower temperatures, which can be caused by modeling conversion of fuel as temperature independent. The model could not reproduce the lower conversion at operation point 1.2, since the devolatilization model overestimated the yield of CO_2. Previously investigated correlation for carbonation reaction was used and calcination was assumed to not take place in the reactor. Sulphation reactions of the bed material were not occurring, since SO_2 was not present.

The carbonation of limestone is influenced by factors such as temperature, limestone material fractions and difference between CO_2 equilibrium concentration and concentration of the process. Generally, as the temperature increases the limestone carbonation becomes limited due to elevated equilibrium concentration. In simulations,

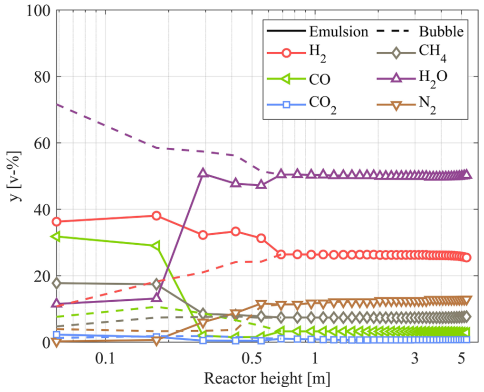

Fig. 6. Gas profiles of the major gas species in the bubble and the emulsion at operation point 1.1. Primary and secondary gas feeds are mixed into bubble gas in the bed. Gases formed on devolatilization are situated in the emulsion before mixing with the bubble gas. At the surface of the bed concentration differences disappear due to complete mixing.

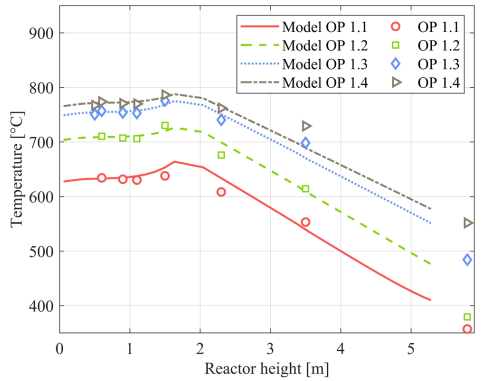

Fig. 7. Simulated temperature profiles and process measurements from the pilot gasifier.

Table 8
Heat source term of simulations.

Parameter	OP 1.1	OP 1.2	OP 1.3	OP 1.4
Heat balance adjustment [kW/kW$_{fuel}$]	−0.14	−0.09	−0.04	0.04

appropriate bed material conversion and CO_2 concentration according to gas measurements is attained by adjusting the thermodynamic reaction equilibrium of limestone. It is reasonable to assume that actual limestone does not follow exactly the theoretical reaction equilibrium in real process conditions because of impurities of the limestone. This remark can be determined from measurements of Hajaligol et al. [57]. The reaction equilibrium was set according to operation point 1.3, where favourable module for gas composition was attained by shifting the equilibrium. The equilibrium was shifted 22 °C towards calcination in each case.

The developed gasification model is capable of modeling differences in the bed material conversion between emulsion and wake. The feature

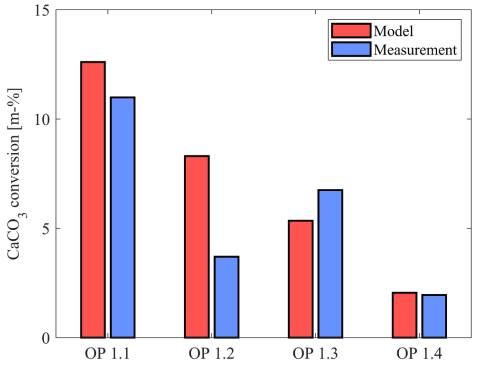

Fig. 8. Bed material conversion from CaO to $CaCO_3$ in the gasifier. The bed material conversion was determined from solid samples extracted from loops seals. The conversion is calculated as difference of $CaCO_3$ mass fraction between the loop seals.

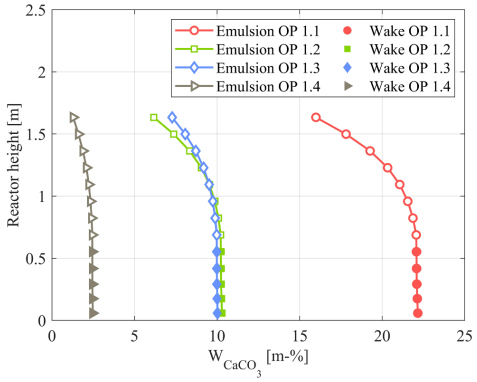

Fig. 9. Simulated solid profiles in the reactor below bed material feeding point for $CaCO_3$. The bed material feeding point and the surface of the bed are situated approximately at height of 1.7 m and 0.7 m, respectively.

has not been previously implemented into 1D gasification models according to the conducted literature review. However, the reactive bed material has been incorporated into the SEG model published by Hejazi [17]. Nevertheless, in the corresponding case, the bed has been assumed to be perfectly mixed (0D solid balance of the bed). By implementing 1D balances, modeling assumptions of 0D-approach, such as, uniform solid temperature and uniform $CaCO_3$ fraction of the bed are avoided. With 1D-approach the material conversion can be traced within the gasifier and the effect of local operation conditions are taken into account. The bed material conversion in the gasifier and local material fractions of $CaCO_3$ are shown in Fig. 9. High in-bed solid mixing is induced by pilot reactor design that evens differences in the solid material fractions on vertical direction of the dense bed. The high mixing of solids causes the bed to behave as ideally mixed bed without significant material fraction differences.

4.5. Water-gas shift reaction

Water in the reactor is consumed by water–gas shift, steam-methane

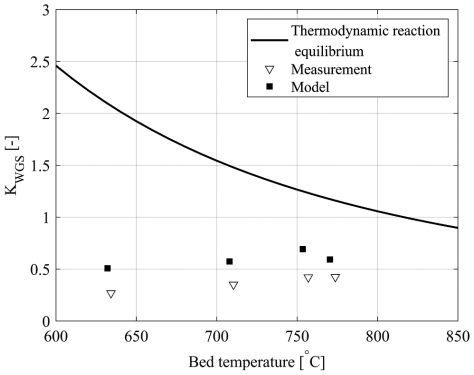

Fig. 10. Water-gas shift reaction equilibrium. The reaction is kinetically limited at the freeboard, which causes the gas composition stay below the thermodynamic reaction equilibrium. The equilibrium coefficient was determined from the relation of gas partial pressures with equation: $K_{wgs} = \frac{PCOPH_2}{PCOPH_2O}$ [38].

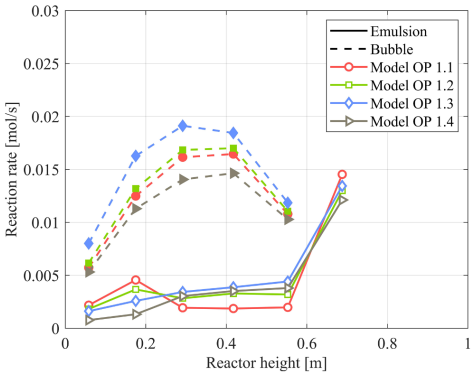

Fig. 11. In-bed and surface water–gas shift reaction rates. Separate reaction rates for emulsion and bubble are presented.

reforming and water–gas reaction. At low temperatures water–gas reaction rate remained slow. This is an indication that most of the water in the reactor was consumed by the water–gas shift reaction, since methane reforming was assumed to be slow due to absence of a catalyst [58,59]. The influence of water–gas shift reaction on producer gas composition can be observed from the relations of H_2, CO and CO_2 gas species concentrations presented in Fig. 5. The reaction is enhanced by limestone carbonation, which consumes CO_2 as gas conversion by water–gas shift reaction proceeds. Active in-bed CO_2 capture is the main cause for the low concentration in the reactor at operation point 1.1. The present signifies the water–gas shift reaction to be kinetically limited at the freeboard. The water–gas reaction has been reported to be catalyzed by ash of the fuel and in-organic substances in previous studies [58,14,49], and in the absence of the catalyst or the inorganic substances the reaction is kinetically limited. Modeling was done by considering reaction equilibrium of the water–gas shift and the catalytic effects [14,13]. In-bed and surface reaction rate was modeled according to Biba et al. [37] and freeboard reaction rate was set slow. The reaction produced satisfactory trends for the final composition of the producer gas as is shown in Fig. 5. Due to the slow reaction kinetics at the freeboard, the reaction conversion remained below reaction equilibrium, which is shown in Fig. 10. The same remark has been made in other experimental steam gasification studies conducted with a laboratory scale equipment [13,60,61].

Uniform parametrization was used for in-bed water–gas shift kinetics. The differences between the emulsion and the bubble reaction rates are shown in Fig. 11. The most of the reaction conversion took place in the bubble gas where high concentration of H_2O was available because of primary gas feed. CO required by the reaction was formed in the emulsion on biomass devolatilization and the CO was exchanged from the emulsion to the bubble by net flow. The influence of high CO_2 concentration at operation point 1.1 can be seen in Fig. 11 as decreased reaction rate.

4.6. Carbon conversion

Carbon conversion describes chemical energy conversion of a fuel in a gasification reactor. With the fuel, elemental carbon is supplied into the reactor, and in this instance, the carbon conversion describes conversion of the elemental carbon from the fuel to the producer gas. The carbon conversion is reflecting the chemical conversion taking place by fuel devolatilization, hydrocarbon cracking and reforming, and char gasification. The carbon conversion is lower in the case of SEG processes, if compared to conventional gasifiers, since bed material carbonation decreases the carbon in the producer gas. The carbon conversion in the simulated operation range is shown in Fig. 12. The conversion has been calculated from data shown in Figs. 4 and 5. The developed model was able to predict trend of the carbon conversion in the simulated temperature range.

5. Conclusions

A reactor model for the sorbent enhanced gasification (SEG) process was developed in this work. The model was formulated based on the specifications of a 200kW_{th} SEG pilot plant. The developed model takes into account the most important aspects required for comprehensive 1-dimensional modeling of SEG processes. The model formulation is based on a non-perfectly mixed bubble bed, where a bed material conversion degree can vary along vertical direction for solids situated in emulsion or wake. Biomass gasification has previously been modeled successfully using a two-phase approach similar to the one developed in this paper, however none of these models has been directly applicable

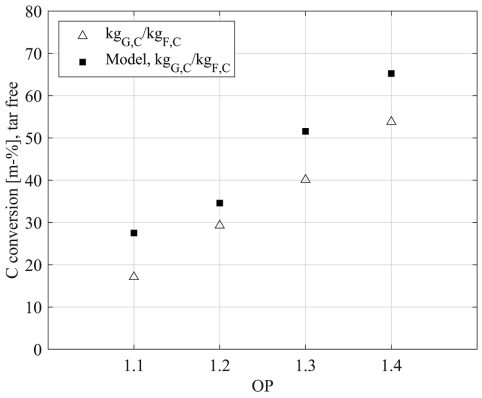

Fig. 12. Carbon conversion from fuel to producer gas on a tar free basis. The ratio $kg_{G,C}$ / $kg_{F,C}$ is determined directly from producer gas measurements. The ratio considers the full chemical conversion process taking place in the gasifier.

to SEG processes. The developed model is based on ideal fundamental mass and heat balances, and the model permits simulation of the SEG process at steady-state conditions. The developed gasification reactor model can be coupled with previously developed combustor model to simulate the full dual fluidized bed. The developed hydrodynamic model is not limited for the conditions of the SEG pilot, but can be applied for different hydrodynamic conditions using proper model equations.

Preliminary validation of the 1D BFB gasification model was done at steady-state conditions. The pilot reactor was operated with steam-to-carbon ratio of 1.5 [mol/mol] and temperature of the gasifier was varied between 630 and 770 °C. The developed model was capable of capturing important characteristics of the SEG process. The model was able to predict hydrodynamics and trends for temperatures, bed material conversion and producer gas composition. The model performed precisely in the temperature range, which is the most important for synthesising DME from the producer gas of the gasifier. The model performance is limited on lower operation temperatures and more detailed fuel conversion model including tars might be required for precise simulations on the lower temperatures. The indicated is less substantial on the higher temperatures, which can be observed as diminished difference between the simulations and the experiments, which makes the model capable of predicting the operation of the pilot on the higher temperatures.

Bed material carbonation and water–gas shift played an important role in the SEG pilot. Combined effect of the reactions had significant impact on the final yield of the gasifier. Yield of the water–gas shift is increased by low operating temperatures, where CO_2 capture of limestone is active. However, when the operation temperature limits the CO_2 capture capability of the bed, the gasifier starts to behave similarly as a conventional steam gasification process and decreased CO_2 capture limits the gas conversion by the water–gas shift.

The current model is based on literature correlations. However, the model prediction could be still further improved with better knowledge of reaction phenomena in the pilot reactor. Such information would require further experimental work focusing on specific phenomenon. The work conducted in this paper improved the current understanding of physical and chemical phenomena important in SEG processes.

The work presented in this study is a first step towards scaling the pilot SEG process to a industrial scale reactor. The model was developed based on the pilot reactor to simulate the SEG processes. The preliminary validation revealed important aspects about the behaviour of the SEG reactors. Further investigations of phenomena could be conducted with the developed model. Furthermore, investigations could include full loop 1D simulation of the dual fluidized bed facility. The knowledge of physical and chemical phenomena gained from the 1D simulations could be utilized in semi-empirical 3D simulations and scaling of the reactor technology. The capability to model phenomena in complex reactor systems is an important step towards scaling and commercialization of the SEG technology.

CRediT authorship contribution statement

Antti Pitkäoja: Methodology, Software, Validation, Formal analysis. **Jouni Ritvanen:** Methodology, Software, Formal analysis. **Selina Hafner:** Investigation. **Timo Hyppänen:** Supervision. **Günter Scheffknecht:** Supervision.

Declaration of Competing Interest

The authors declare that they have no known competing financial interests or personal relationships that could have appeared to influence the work reported in this paper.

Acknowledgements

This work in FLEDGED project has received funding from the European Union's Horizon 2020 research and innovation programme under grant agreement No 727600. The authors would like to acknowledge the financial support for this research from the Academy of Finland under Grant No. 278641.

Appendix A. Model formulation and additional model equations

A.1 Solid mass balances for wake and emulsion

General solid (s) mass balance equations at the wake (w) and the emulsion (e) can be written as:

$$\frac{\partial \rho_{s,w}}{dt} + \frac{\partial u_{s,w}\rho_{s,w}}{\partial z} = -Q_{s,ew} + \sum R_{s,w} + \sum S_{s,w} \tag{A.1}$$

$$\frac{\partial \rho_{s,e}}{\partial t} + \frac{\partial u_{s,e}\rho_{s,e}}{\partial z} = Q_{s,ew} + \sum R_{s,e} + \sum S_{s,e} \tag{A.2}$$

where ρ_s is density of solids, u_s is velocity of solids, $Q_{s,ew}$ is net flow of solids between emulsion and wake, chemical reaction term $\sum R$ includes mass change due to solid chemical reaction, while the term $\sum S$ includes the mass from other sources such as local feeds and discharges. The solid concentration depends on the material composition

$$\rho_s = \sum_k W_{s,k}\rho_s \tag{A.3}$$

in which $W_{s,k}$ is material fraction for each solid material k. The continuity equations for each material k in wake and emulsion are after substitution

$$\frac{\partial}{\partial t}(W_{s,w,k}\rho_{s,w}) + \frac{\partial}{\partial z}(W_{s,w,k}u_{s,w}\rho_{s,w}) = W_{s,w,k}Q_{s,ew} + \sum R_{s,w,k} + \sum S_{s,w,k} \tag{A.4}$$

$$\frac{\partial}{\partial t}(W_{s,e,k}\rho_{s,e}) + \frac{\partial}{\partial z}(W_{s,e,k}u_{s,e}\rho_{s,e}) = W_{s,e,k}Q_{s,ew} + \sum R_{s,e,k} + \sum S_{s,e,k} \tag{A.5}$$

The Eq. (A.5) is applied for the freeboard emulsion.

A.2 Gas phase mass balances for wake and emulsion

General mass balance for the gases in the emulsion and the bubble are according to equations:

$$\frac{\partial \rho_{g,e}}{\partial t} + \frac{\partial u_{g,e}\rho_{g,e}}{\partial z} = \sum R_e + \sum S_e - Q_{g,eb} - J_{g,eb} \tag{A.6}$$

$$\frac{\partial \rho_{g,b}}{\partial t} + \frac{du_{g,b}\rho_{g,b}}{\partial z} = \sum R_b + \sum S_b + Q_{g,eb} + J_{g,eb} \tag{A.7}$$

Time derivate is resolved from Eq. (A.6) and Eq. (A.7) according to the following equation:

$$\frac{\partial \rho_g}{\partial t} = \frac{\partial (W_{g,j}\rho_g)}{\partial t} = \frac{\partial W_{g,j}}{\partial t}\rho_g + \frac{\partial \rho_g}{\partial t}W_{g,j} \tag{A.8}$$

where the time derivate of gas mixture density is considered to be small and to not have significant impact in the equation. Gas density of the total mixture is resolved from ideal gas approach. After substitution the continuity equation for each individual gas specie j is written as:

$$\frac{\partial W_{g,j}}{\partial t}\rho_g + \frac{\partial W_{g,j}u_g}{\partial z}\rho_g = \sum R_{g,j} + \sum S_{g,j} + Q_{g,eb,j} + J_{g,j} \tag{A.9}$$

A.3 Bubbling bed hydrodynamics

The emulsion of dense bed is assumed to remain at the minimum fluidization state. Emulsion gas void fraction is resolved:

$$\epsilon_{g,e} = \frac{\epsilon_{g,mf}}{f_{exbed}} \tag{A.10}$$

where minimum fluidization voidage $\epsilon_{g,mf}$ is resolved from the Ergun equation [40] with empirical parameters of Grace [41] and the bed expansion factor f_{exbed} modeled according to Babu et al. [42].

Gas moves with the emulsion and the slip velocity between the emulsion gas and the emulsion solid is u_{mf}/ϵ_{mf}. When solids in the emulsion are moving with the velocity $u_{s,e}$, the emulsion gas velocity is:

$$u_{g,e} = \frac{u_{mf}}{\epsilon_{mf}} + u_{s,e} \tag{A.11}$$

It should be noted that the direction of the emulsion gas can be upwards or downwards, based on the velocity of the emulsion solids.

Particles transported by the wake of the bubble are ejected to the freeboard from the surface of the bubbling bed by bubble splashes. The finest particles entrained in the gas flow are pneumatically transported into the cyclone of the reactor. However, coarse particles do not exit from the freeboard region. One representative particle size is used for entrainment model. Transport disengaging height (TDH) is the limit, how far-off at the freeboard the coarse particles are transported

$$TDH = h_{bed} + h_{TDH} \tag{A.12}$$

A.4 Energy balance

General energy balance Eq. (4) is formed from separate balances for gas and solid phases, which have been conjoined as one equation:

$$\frac{dU_s}{dt} + \frac{dU_g}{dt} = E_{s,conv} + E_{g,conv} + E_{s,r} + E_{g,r} - E_{hs} \tag{A.13}$$

in which the terms are obtained from following set of equations:

$$\frac{\partial U_s}{\partial t} + \frac{\partial U_g}{\partial t} = \sum_k (\rho_{s,e}W_{s,e,k})c_{p,s}\frac{\partial T}{\partial t} + \sum_k (\rho_{s,w}W_{s,w,k})c_{p,s}\frac{\partial T}{\partial t} + \sum_j (\rho_{g,e}W_{g,e,j})\frac{\partial h_{g,e}}{\partial t} + \rho_{g,e}\sum_j (\frac{\partial W_{g,e,j}}{\partial t}h_{g,e,j}) + \sum_j (\rho_{g,b}W_{g,b,j})\frac{\partial h_{g,b}}{\partial t} + \rho_{g,b}\sum_j (\frac{\partial W_{g,b,j}}{\partial t}h_{g,b,j}) \tag{A.14}$$

$$E_{s,conv} + E_{g,conv} = \sum_k (\rho_{s,e}W_{s,e,k})u_{s,e}c_{p,s}\frac{\partial T}{\partial z} + \sum_k (\rho_{s,w}W_{s,w,k})u_{s,e}c_{p,s}\frac{\partial T}{\partial z} + \sum_j (\rho_{g,e}W_{g,e,j})u_{g,e}\frac{\partial h_{g,e}}{\partial z} + \sum_j (\rho_{g,b}W_{g,b,j})u_{g,b}\frac{\partial h_{g,b}}{\partial z} \tag{A.15}$$

$$E_{s,r} + E_{g,r} = \sum_k H_{s,e,k,r}R_{s,e,k} + \sum_k H_{s,w,k,r}R_{s,w,k} + \sum_j H_{g,e,j}R_{g,e,j} + \sum_j H_{g,b,j}R_{g,b,j} + H_{g,e,vol,j}S_{g,e,vol,j} + H_{g,e,lat,j}S_{g,e,lat,j} \tag{A.16}$$

where h is enthalpy, H is reaction enthalpy and $H_{g,e,lat,j}S_{g,e,lat,j}$ is latent heat of specie j. In the total mixture, only latent heat of H_2O is considered. Convection of energy in the system is resolved by using first order upwind scheme for the gas and the solid phases.

References

[1] Delbeke J, Vis P. EU climate policy explained 2016. https://ec.europa.eu/clima/sites/clima/files/eu_climate_policy_explained_en.pdf.

[2] European commission. A European Strategy for Low-Emission Mobility 2016. https://ec.europa.eu/transparency/regdoc/rep/1/2016/EN/1-2016-501-EN-F1-1.PDF.

[3] Pelkmans L. European Union – 2018 update, Bioenergy policies and status of implementation 2018:1–10. https://www.ieabioenergy.com/wp-content/uploads/2018/10/CountryReport2018_EU_final.pdf.

[4] Thomas G, Feng B, Veeraragavan A, Cleary MJ, Drinnan N. Emissions from DME combustion in diesel engines and their implications on meeting future emission norms: a review. Fuel Process Technol 2014;119:286–304. https://doi.org/10.1016/J.FUPROC.2013.10.018.

[5] Corella J, Toledo J, Molina G. A review on dual fluidized-bed biomass gasifiers. Ind Eng Chem Res 2007:6831–9. https://doi.org/10.1021/ie0705507.

[6] Pfeifer C. Sorption-enhanced gasification. In: Scala F, editor. Fluid. Bed Technol. Near-Zero Emiss. Combust. Gasif. 1st ed.,. Woodhead Publishing; 2013. p. 971–1001. doi: 10.1533/9780857098801.4.971.

[7] Boroson M, Howards J, Longwell J, Peters W. Product Yield and Kinetics from the Vapor Phase Cracking of Wood Pyrolysis Tars. AIChE J 1989;35:120–8.

[8] de Souza-Santos ML. Solid fuels combustion and gasification. CRC Press; 2010. doi: 10.1201/9781420047509.
[9] Bilodeau J, Therien N, Proulx P, Czernik S, Chornet E. A Mathematical model of fluidized bed biomass gasification. Can J Chem Eng 1993;71:549–57.
[10] Fiaschi D, Michelini M. A two-phase one-dimensional biomass gasification kinetics model. Biomass Bioenergy 2001;21:121–32. https://doi.org/10.1016/S0961-9534(01)00018-6.
[11] Radmanesh R, Chaouki J, Guy C. Biomass gasification in a bubbling fluidized bed reactor: experiments and modeling. AIChE J 2006;52:4258–72. https://doi.org/10.1002/aic.
[12] Yan L, Jim Lim C, Yue G, He B, Grace JR. One-dimensional modeling of a dual fluidized bed for biomass steam gasification. Energy Convers Manag 2016;127:612–22. https://doi.org/10.1016/j.enconman.2016.09.027.
[13] Bates RB, Ghoniem AF, Jablonski WS, Carpenter DL, Altantzis C, Garg A, et al. Steam-air blown bubbling fluidized bed biomass gasification (BFBBG): multi-scale models and experimental validation. AIChE J 2017;63:1543–65. https://doi.org/10.1002/aic.
[14] Gómez-Barea A, Leckner B. Estimation of gas composition and char conversion in a fluidized bed biomass gasifier. Fuel 2013;107:419–31. https://doi.org/10.1016/J.FUEL.2012.09.084.
[15] Beheshti SM, Ghassemi H, Shahsavan-Markadeh R. Process simulation of biomass gasification in a bubbling fluidized bed reactor. Energy Convers Manag 2015;94:345–52. https://doi.org/10.1016/J.ENCONMAN.2015.01.060.
[16] Yang S, Wang H, Wei Y, Hu J, Chew JW. Particle-scale modeling of biomass gasification in the three-dimensional bubbling fluidized bed. Energy Convers Manag 2019;196:1–17. https://doi.org/10.1016/J.ENCONMAN.2019.05.105.
[17] Hejazi B. Modeling of biomass steam gasification in a dual fluidized bed reactor with/without lime-based CO2 capture. Vancouver: University of British Columbia; 2017.
[18] Ritvanen J, Pitkäoja A, Sepponen S, Hyppänen T. Modelling of sorption-enhanced biomass gasification in dual fluidized bed process. 23rd Int Conf. Fluid Bed Convers 2018:528–35.
[19] Hafner S, Spörl R, Scheffknecht G. Sorption enhanced gasification: process validation and investigations on the syngas composition in a 200 kW th dual fluidized bed facility. 23rd Int Conf. Fluid Bed Convers 2018:826–32.
[20] Davidson JF, Harrison D. Fluidized particles. Cambridge University Press; 1963.
[21] Kunii D, Levenspiel O. Fluidization engineering. 2nd Butterwoth-Heinemann; 1991.
[22] Model Ylätalo J. Based analysis of the post- combustion calcium looping process for carbon dioxide capture lappeenranta. Acta Universitatis Lappeenrantaensis; 2013. Doctoral Dissertation.
[23] Abanades JC, Diego A. Conversion limits in the reaction of CO2 with lime. Energy Fuels 2003;17:308–15. https://doi.org/10.1021/ef020152a.
[24] Chiba T, Kobayashi H. Solid exchange between the bubble wake and the emulsion phase in a gas-fluidised bed. J Chem Eng Japan 1977;10:206–10. https://doi.org/10.1252/jcej.10.206.
[25] Martínez I, Grasa G, Murillo R, Arias B, Abanades JC. Kinetics of calcination of partially carbonated particles in a Ca-looping system for CO2 capture. Energy Fuels 2012;26:1432–40. https://doi.org/10.1021/ef201525k.
[26] Shimizu T, Hirama T, Hosoda H, Kitano K, Inagaki M, Tejima K. A twin fluid-bed reactor for removal of CO2 from combustion processes. Chem Eng Res Des 1999;77:62–8. https://doi.org/10.1205/026387699525882.
[27] Alonso M, Rodríguez N, Grasa G, Abanades JC. Modelling of a fluidized bed carbonator reactor to capture CO2 from a combustion flue gas. Chem Eng Sci 2009;64:883–91. https://doi.org/10.1016/J.CES.2008.10.044.
[28] Stanmore BR, Gilot P. Review—calcination and carbonation of limestone during thermal cycling for CO2 sequestration. Fuel Process Technol 2005;86:1707–43. https://doi.org/10.1016/J.FUPROC.2005.01.023.
[29] Rajan RR, Wen CY. A comprehensive model for fluidized bed coal combustors. AIChE J 1980;26:642–55. https://doi.org/10.1002/aic.690260416.
[30] Myöhanen K. Modelling of combustion and sorbent reactions in three-dimensional flow environment of a circulating fluidized bed furnace. Lappeenranta: Acta Universitatis Lappeenrantaensis; 2011. Doctoral Dissertation.
[31] Cussler EL. Diffusion, mass transfer in fluid systems. 1 ed. Cambridge University Press; 1984.
[32] Fairbanks DF, Wilke CR. Diffusion coefficients in multicomponent gas mixtures. Ind Eng Chem 1950;42:471–5. https://doi.org/10.1021/ie50483a022.
[33] Sit SP, Grace JR. Effect of bubble interaction on interphase mass transfer in gas fluidized beds. Chem Eng Sci 1981;36:327–35. https://doi.org/10.1016/0009-2509(81)85012-9.
[34] van den Aarsen F, Beenackers A, van Swaaij W. Wood pyrolysis and carbon dioxide char gasification kinetics in a fluidized bed. In: Overend RP, Milne TA, Mudge LK, editors. Fundam. Thermochem. Biomass Convers. Dordrecht: Springer; 1985. p. 1159. doi: 10.1007/978-94-009-4932-4_36.
[35] Nandi SP, Onischak M. Gasification of Chars Obtained from Maple and Jack Pine Woods. In: Overend RP, Milne TA, Mudge LK, editors. Fundam. Thermochem. Biomass Convers. Dordrecht: Springer; 1985. p. 1159. doi: 10.1007/978-94-009-4932-4_32.
[36] Hejazi B, Grace JR, Bi X, Mahecha-Botero A. Kinetic model of steam gasification of biomass in a bubbling fluidized bed reactor. Energy Fuels 2017;31:1702–11. https://doi.org/10.1021/acs.energyfuels.6b03161.
[37] Biba V, Macák J, Klose E, Malecha J. Mathematical model for the gasification of coal under pressure. Ind Eng Chem Process Des Dev 1978;17:92–8. https://doi.org/10.1021/i260065a017.
[38] de Souza-Santos ML. Comprehensive modelling and simulation of fluidized bed boilers and gasifiers. Fuel 1989;68:1507–21. https://doi.org/10.1016/0016-2361(89)90288-3.
[39] Jones WP, Lindstedt RP. Global reaction schemes for hydrocarbon combustion. Combust Flame 1988;73:233–49. https://doi.org/10.1016/0010-2180(88)90021-1.
[40] Ergun S. Fluid flow through packed columns. Chem Eng Prog 1952;48:89–94.
[41] Grace JF. Fluidized-Bed Hydrodynamics. In: Hetsroni G, editor. Handb. Multiph. Syst.,. Washington: Hemisphere; 1982. p. 1200.
[42] Babu SP, Shah B, Talwalkar A. Fluidization correlations for coal gasification materials-minimum fluidization velocity and fluidized bed expansion ratio. AIChE Sym Ser 1978;74:176–86.
[43] Darton RC, LaNauze RD, Davidson JF, Harrison D. Bubble-growth due to coalescence in fluidized beds. Trans Inst Chem Eng 1977;55:274–80.
[44] Wen CY, Chen LH. Fluidized bed freeboard phenomena: entrainment and elutriation. AIChE J 1982;28:117–28.
[45] Rowe PN, Partridge BA. An x-ray study of bubbles in fluidized beds. Trans Inst Chem Eng 1965:43.
[46] Chiba T, Kobayashi H. Gas exchange between the bubble and emulsion phases in gas-solid fluidized beds. Chem Eng Sci 1970;25:1375–85. https://doi.org/10.1016/0009-2509(70)85060-6.
[47] Wakabayash T, Kunii D. Contribution of solids dispersed in bubbles to mass transfer in fluidized bed. J Chem Eng JAPAN 1971;4:226–30. https://doi.org/10.1252/jcej.4.226.
[48] Klose W, Wölki M. On the intrinsic reaction rate of biomass char gasification with carbon dioxide and steam. Fuel 2005;84:885–92. https://doi.org/10.1016/J.FUEL.2004.11.016.
[49] Di Blasi C. Combustion and gasification rates of lignocellulosic chars. Prog Energy Combust Sci 2009;35:121–40. https://doi.org/10.1016/j.pecs.2008.08.001.
[50] Nzihou A, Stanmore B, Sharrock P. A review of catalysts for the gasification of biomass char, with some reference to coal. Energy 2013;58:305–17. https://doi.org/10.1016/j.energy.2013.05.057.
[51] Hemati M, Laguerie C. Determination of the kinetics of the sawdust steam-gasification of charcoal in a thermobalance. Entropie 1988;142:29–40.
[52] Risnes H, Sorensen LH, Hustad JE. CO2 reactivity of chars from wheat, spruce and coal. In: Bridgewater AW, editor. Prog. Thermochem. Biomass Convers. Oxford: Blackwell Science; 2001. p. 61–72.
[53] Neves D, Thunman H, Matos A, Tarelho L, Gómez-Barea A. Characterization and prediction of biomass pyrolysis products. Prog Energy Combust Sci 2011;37:611–30. https://doi.org/10.1016/J.PECS.2011.01.001.
[54] Simell PA, Leppälahti JK, Kurkela EA. Tar-decomposing activity of carbonate rocks under high CO2partial pressure. Fuel 1995;74:938–45. https://doi.org/10.1016/0016-2361(95)00012-T.
[55] Hawthorne C, Poboss N, Dieter H, Gredinger A, Zieba M, Scheffknecht G. Operation and results of a 200-kWthdual fluidized bed pilot plant gasifier with adsorption-enhanced reforming. Biomass Convers Biorefinery 2012;2:217–27. https://doi.org/10.1007/s13399-012-0053-3.
[56] Pfeifer C, Puchner B, Hofbauer H. Comparison of dual fluidized bed steam gasification of biomass with and without selective transport of CO2. Chem Eng Sci 2009;64:5073–83. https://doi.org/10.1016/j.ces.2009.08.014.
[57] Hajaligol MR, Longwell JP, Sarofim AF. Analysis and modeling of the direct sulfation of CaCO3. Ind Eng Chem Res 1988;27:2203–10. https://doi.org/10.1021/ie00084a002.
[58] Chen WJ, Sheu FR, Savage RL. Catalytic activity of coal ash on steam methane reforming and water-gas shift reactions. Fuel Process Technol 1987;16:279–88. https://doi.org/10.1016/0378-3820(87)90025-7.
[59] Gómez-Barea A, Leckner B. Modeling of biomass gasification in fluidized bed. Prog Energy Combust Sci 2010;36:444–509. https://doi.org/10.1016/j.pecs.2009.12.002.
[60] Maniatis K, Buekens A. Fluidized bed gasification of biomass. EPE 1982;17:35–43.
[61] Herguido J, Corella J, González-Saiz J. Steam gasification of lignocellulosic residues in a fluidized bed at a small pilot scale. Effect of the type of feedstock. Ind Eng Chem Res 1992;31:1274–82. https://doi.org/10.1021/ie00005a006.

Publication III

Pitkäoja, A., Ritvanen, J., Hafner, S., Hyppänen, T. and Scheffknecht, G.
Numerical modelling of sorption-enhanced gasification: Development of a fuel decomposition model

Reprinted with permission from
Fuel
Vol. 289, 119868, pp. 1-10, 2021.
© 2021, Elsevier

Fuel 289 (2021) 119868

Contents lists available at ScienceDirect

Fuel

journal homepage: www.elsevier.com/locate/fuel

Full Length Article

Numerical modelling of sorption-enhanced gasification: Development of a fuel decomposition model

Antti Pitkäoja [a,*], Jouni Ritvanen [a], Selina Hafner [b], Timo Hyppänen [a], Günter Scheffknecht [b]

[a] Lappeenranta-Lahti University of Technology, LUT School of Energy Systems, P.O. Box 20, FI-53851 Lappeenranta, Finland
[b] Institute of Combustion and Power Plant Technology (IFK), University of Stuttgart, 7 Pfaffenwaldring 23, 70569 Stuttgart, Germany

ARTICLE INFO

Keywords:
Sorption-enhanced gasification
Gasification
Biomass
Thermochemical conversion
Pyrolysis
Simulation

ABSTRACT

Sorption-enhanced gasification (SEG) is a promising technology for producing renewable feedstock gas to be used in biofuel synthesis processes, especially in dimethyl ether (DME) synthesis. To adopt the technology on a commercial scale, it is necessary to acquire knowledge about the related operational characteristics. The SEG process is carried out at lower temperatures than those employed in conventional gasifiers. A typical operating range is from 600 °C to 800 °C. Fuel decomposition experiments have shown distribution of the decomposition products to vary by the process temperature in this operating range, and thus, it is important to adapt this phenomenon for modelling the SEG process. To model the temperature dependence of the decomposition products, a fuel model was developed. Fuel decomposition experiments were conducted to obtain the boundary conditions for the fuel model. The developed fuel model was implemented to an SEG model frame, and the model prediction was compared against data from a 200 kW_{th} dual fluidised bed facility. The model gave satisfactory predictions for producer composition and temperature trends. Furthermore, the main balances of the model were in agreement with typical trends of the SEG process. The conducted simulations improved our understanding of material balances in SEG reactors. Knowledge from physical operations governing the process is of value in further development of the technology.

1. Introduction

Increased greenhouse gas emissions during the past few decades have induced the European Union (EU) to pursue a climate policy whose goal is to keep average global warming below 2 °C compared to pre-industrial temperatures [1]. To pursue this policy, the EU has set a target of 14% renewable energy usage for the transportation sector by 2030 [2]. Consequently, there is a pressing need to develop effective and cost-efficient ways for producing transportation fuels from renewable sources. The transportation sector has relied on liquid fossil oil-derived fuels, such as petroleum and diesel, for decades. A cost-efficient alternative is thus to replace fossil-based diesel fuel with liquefied renewable dimethyl ether (DME).

Sorption-enhanced gasification (SEG) has been recognised as a promising technology to produce renewable feedstock for the synthesis of DME. The SEG process operated within specific operating conditions can produce a feedstock gas from biomass that is almost directly suitable for the DME synthesis. This has been experimentally verified under a certain operating condition of the gasifier [3]. The benefit of the process is that additional downstream modification of the producer gas composition is not required. In the SEG process, the producer gas composition can be tailored to be suitable for the downstream DME synthesis in the gasification reactor.

However, experiments are usually limited to a finite number of experimental points; operations outside the experimental points or on a different scale cannot be evaluated with certainty. To overcome these experimental limitations, a process model can be developed. Process modelling can directly evaluate the impact of various process parameters on the operation of a gasifier. To develop a process model for this purpose, the main phenomena governing the operation of the process must be included in the model. Occasionally, a simplified gasification process model with only the most relevant characteristics has been sufficient to produce satisfactory prediction capability [4]. However, in other instances, more detailed modelling approaches have been developed, especially for fuel decomposition [5,6].

The fuel decomposition process is called pyrolysis, and it is the primary step of biomass gasification. During pyrolysis, the biomass is decomposed into solid and gaseous fractions. The gas fraction is formed from non-condensable and condensable gas species. The condensable

* Corresponding author.
E-mail address: antti.pitkaoja@lut.fi (A. Pitkäoja).

https://doi.org/10.1016/j.fuel.2020.119868
Received 20 August 2020; Received in revised form 13 November 2020; Accepted 25 November 2020
Available online 16 December 2020
0016-2361/© 2020 The Author(s). Published by Elsevier Ltd. This is an open access article under the CC BY license (http://creativecommons.org/licenses/by/4.0/).

Nomenclature

γ	parameter, [–]
ρ	density, [kg/m^3]
ar	as-received
C	concentration, [mol/m^3]
$C_{CO_2,eq}$	CO_2 equilibrium concentration, [mol/m^3]
ds	dry solid
dW	mass fraction difference, [kg$_i$/kg$_y$]
F	fuel
g	gas
H	reaction heat, [kJ]
i	index
j	index
k	chemical reaction rate coefficient, [1/s]
k′	chemical reaction rate coefficient, [m^3/(mol·s)]
K_{WGS}	water–gas shift equilibrium coefficient, [−]
M	molar mass, [g/mol]
n	mole, [mol]
PG	permanent gas
Q	energy, [J]
R	reaction rate, [kg/(m^3·s)]
R_i	ideal gas constant, [J/(mol·K)]
s	solid
T	temperature, [K]
W	mass fraction, [kg$_i$/kg$_y$]
y	mol fraction, [mol$_i$/mol$_y$]

fraction is mainly formed from heavy hydrocarbons, referred to as tars.

In the literature, there are several studies concerning fuel decomposition, and one of the main observations of these studies has been that the decomposition products vary by temperature [7]. A comprehensive literature review concerning fuel decomposition products was made by [8]. The authors thoroughly reviewed many experimental studies for various biomasses and provided many examples of how the fuel decomposition products are changed by the process temperature.

Conventionally, fuel decomposition products have been modelled by using standard proximate analysis. Standard proximate analysis represents the fuel decomposition products at 905 °C. The standard approach has been successfully applied for conventional gasification processes, which are carried out at temperatures around 850 °C. In gasification processes that are carried out well below the conventional operating temperatures, the fuel decomposition products are expected to differ from those observed under standard characterisation conditions. The distribution of decomposition products is temperature-dependent, and it varies with temperature. To analyse low-temperature systems, this characteristic must be considered, and thus, a temperature-dependent fuel decomposition model is needed.

The goal of this study is to develop a fuel decomposition model suitable for low-temperature biomass gasification and to implement the model into an SEG model frame. By introducing characteristics of the decomposition phenomena into the model frame, the fuel model development is premised on the main characteristics of the decomposition process. The major decomposition products, e.g. permanent gases, char, and tar, are included in the model. Elemental balances are formulated based on these main products. The effect of temperature on the distribution of the main products is considered to model the effect of temperature on the elemental balances.

The fuel model is implemented into a previously published SEG model frame [9], and the model prediction is compared against gasification experiments [3]. In addition, fuel decomposition experiments were conducted at a temperature range that is important for the SEG process. The experiments were carried out to obtain boundary conditions for the fuel decomposition sub-model.

2. Numerical model development

Gasification can be divided into three major steps: drying, decomposition, and gasification of the decomposition products. A simplified overview of the gasification process is shown in Fig. 1. The objective of this work is to develop a fuel model that considers the main aspects of fuel decomposition. Fuel decomposition is one of the main process steps of gasification, and hence, it impacts the final gasification products.

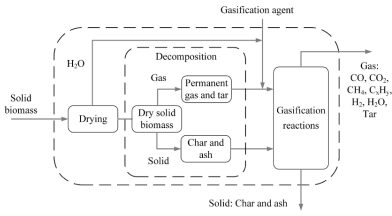

Fig. 1. Simplified process steps of gasification.

2.1. Drying

Biomass drying is carried out at low temperatures. The water bound in the biomass is analysed by drying the biomass. Determining the water fraction is a standard procedure belonging to the standard proximate analysis of the fuel.

2.2. Fuel decomposition

In fuel decomposition, the biomass is fractioned into solid and gas fractions. The gas fraction is formed from permanent gases (CO, CO_2, H_2, CH_4, and C_2–C_4 hydrocarbons) and condensable gas species, referred to as tars. The primary decomposition occurs at temperatures from 200 °C to 500 °C [8]. Typically, at temperatures around 500 °C, tar yield is maximised. At higher temperatures, the tar yield decreases owing to tar reformation reactions. The tars are decomposed to lower hydrocarbons, and in the process, additional permanent gases are released. This process continues until the decomposition temperature is approximately 905 °C. At this temperature, the fuel decomposition is free from the tars according to the standard proximate analysis.

A solid fraction is formed from biomass after the biomass is stripped from the volatile substances. The solid is formed from char and ash. The ash fraction of biomass is inert and is mainly formed from various trace elements. However, the char fraction varies by the process temperature [8]. The char inherits the same elements that were present in the parent fuel, and the elemental composition varies by the process temperature. According to [8], the char formed at decomposition is mostly formed from elemental carbon. However, there are still significant traces of hydrogen and oxygen present. In addition, low quantities of nitrogen and sulphur remain in the formed char [10].

2.3. Gasification reactions

The chemical reactions can be divided to reactions with char, permanent gases, and reaction with tars [11]. The main heterogenous reactions with the char are Boudouard, water–gas, and methanation reactions. The primary homogeneous reaction is water–gas shift reaction. Furthermore, there are various reaction paths for the decomposition of the tars. The tars are typically reduced to permanent gases by oxidation, dry reforming, steam reforming, hydrogenation, and thermal cracking reactions. These reactions can be homogeneous or heterogeneous, and they can take place inside or outside the biomass particles. The tar reactions are not commonly modelled owing to very complex reaction networks and uncertainty about the application of reaction networks to the fluidised bed process.

2.4. Main modelling assumptions and formulation of decomposition balances

A fuel model that considers the most significant fractions of the fuel and their temperature-dependent interrelations is developed. The main assumptions of the fuel decomposition model are as follows:

- Fuel is decomposed to permanent gases, tars, char, ash, and moisture.
- The relationship between permanent gases, tars, and char depends on temperature.
- The elemental composition of the main fractions are as follows:
  - Permanent gas (C, H, O, N, S)
  - Char (C, H, O, N, S)
  - Tar (C, H)
- Devolatilisation product gases from the fuel model are CO, CO_2, CH_4, C_2H_4, H_2S, NH_3, and H_2.
- Lower hydrocarbons (C_2–C_4) are lumped under the C_2H_4 model component.
- Tars are lumped under the single model component C_7H_8.
- All hydrocarbons are formed upon fuel decomposition, and are assumed as inert gas species without chemical reactions associated with the gases.
- Char gasification releases elements bound to the char as H_2S, H_2, O_2, and N_2.
- Fuel decomposition is instantaneous.
- Ash is an inert fraction.
- The ash and moisture fractions are based on the standard proximate analysis.

The hydrocarbons are assumed to be inert, and no reaction paths are associated with them. Elemental composition of hydrocarbons (CH_4, C_2-C_4 and tars) measured from producer gas is set into decomposition model for the hydrocarbon model components. This approach assures that the elemental distribution of hydrocarbons in the producer gas is according to measurements at the outlet of the gasifier. Fuel decomposition balances are formulated based on the assumptions presented above. According to the standard proximate analysis, the fuel is formed from four main fractions:

$$W_{F,ar} = W_{Vol,ar} + W_{Char,ar} + W_{Ash,ar} + W_{Moist,ar}, \quad (1)$$

where the fuel is the sum of the volatile, char, ash, and moisture fractions. The equation can be extended for a gasification process:

$$W_{F,ar} = W_{PG,ar} + W_{Tar,ar} + W_{Char,ar} + W_{Ash,ar} + W_{Moist,ar} \quad (2)$$

in which the tar fraction is separated from the volatile fraction. The fuel and the decomposition products can be divided into i elements:

$$\sum_i W_{F,daf,i} = \sum_i W_{PG,i} + \sum_i W_{Tar,i} + \sum_i W_{Char,i} \quad (i = C, H, O, N, S) \quad (3)$$

in which the sum of the elements makes up the main products and the fuel is formed from the sum of the main products or from the elements within the fuel. It should be noted that tar consists only of C and H elements. The char elemental composition is modelled according to [8] and [10]. Correlations for the C and H compositions of the char are according to [8]

$$W_{Char,C} = 0.93 - 0.92\exp(-0.0042T) \quad (4)$$

$$W_{Char,H} = -0.0041 + 0.1\exp(-0.0024T), \quad (5)$$

where T is fuel decomposition temperature in °C. Elements N and S are assumed to follow correlations by [10].

$$W_{Char,N} = 0.088 W_{F,N} W_{Char,daf}^{0.6} \left(\frac{W_{F,N}}{W_{F,C}}\right)^{-0.6} \quad (6)$$

$$W_{Char,S} = 0.14 W_{F,S} W_{Char,daf}^{0.2} \left(\frac{W_{F,H}}{W_{F,C}}\right)^{-0.6}, \quad (7)$$

where $W_{F,i}$ is the fraction of an element of the char's parent fuel according to the ultimate analysis. Oxygen represents the most uncertainty in data by [8], and therefore, O is resolved from the balance and the other elements from the correlations.

2.5. Tar fraction

The tar fraction is specified in the model as the mass fraction based on the tar measurement of the producer gas. Tar species that are measured from the producer gas are typically formed from elemental carbon and hydrogen [12]. Toluene (C_7H_8) was evaluated to represent the overall elemental composition of tars.

2.6. Volatile release

Volatile release is resolved from elemental mass balances by removing the char and the tar from the elemental composition of the fuel. The volatilised gas species are formed from the leftover elemental mass balance. The volatile composition follows stoichiome try.

$$y_C + y_H + y_O + y_N + y_S = y_{PG} = y_{NH_3} + y_{H_2S} + y_{CO} + y_{CO_2} + y_{CH_4} + y_{C_2H_4} + y_{H_2} \quad (8)$$

The volatile composition changes by temperature [8]. In the model, the stoichiometry can be altered with parameters γ_1 and γ_2.

$$\gamma_1 = \frac{n_{CO}}{n_{CO} + n_{CO_2}} \quad (9)$$

$$\gamma_2 = \frac{n_{CH_4,C}}{n_{CH_4,C} + n_{C_2H_4,C}} \quad (10)$$

The parameter γ_1 divides volatilized oxygen between CO and CO_2.

$$y_{O,CO} = \gamma_1 y_O \quad (11)$$

$$y_{O,CO_2} = 2(1-\gamma_1) y_O \quad (12)$$

The amount of oxygen determines carbon consumed by CO and CO_2 gases. The remaining carbon is consumed by CH_4 and C_2H_4 gases.

$$y_{C,rem} = y_C - y_{C,CO} - y_{C,CO_2} \quad (13)$$

$$y_{C,CH_4} = \gamma_2 y_{C,rem} \quad (14)$$

$$y_{C,C_2H_4} = (1-\gamma_2) y_{C,rem} \quad (15)$$

Elemental balances for the volatilised elements can be written as follows:

$$
\begin{aligned}
y_S &= y_{S,H_2S} \\
y_N &= y_{N,NH_3} \\
y_O &= y_{O,CO} + y_{O,CO_2} \\
y_C &= y_{C,CO} + y_{C,CO_2} + y_{C,CH_4} + y_{C,C_2H_4} \\
y_H &= y_{H,H_2S} + y_{H,NH_3} + y_{H,CH_4} + y_{H,C_2H_4} + y_{H,H_2}.
\end{aligned} \tag{16}
$$

Volatilised permanent gases are determined from the elemental balances.

2.7. Heat balance

The heat balance of the fuel decomposition is formulated based on theoretical reaction energies. The heat balance is modelled according to the following equations:

$$Q_{Reaction} = Q_{F,LHV} + Q_{F,H_2O} + Q_{Decomposition} \tag{17}$$

in which $Q_{F,LHV}$ is the lower heating value of fuel, Q_{F,H_2O} is evaporation of water, $Q_{Decomposition}$ is an external heat required by the decomposition and $Q_{Reaction}$ is combustion energy of decomposition products according to equation:

$$Q_{Reaction} = \sum_i W_{Char,i} Q_{Char,i} + \sum_j W_{PG,j} Q_{PG,j} + W_{Tar} Q_{Tar} \tag{18}$$

in which $W_{Char,i}$ is mass fraction of an char element, $W_{PG,j}$ is mass fraction of a gas specie, $Q_{Char,i}$ and $Q_{PG,j}$ are reaction heats of char elements and permanent gases, respectively. The energy balance is described in Fig. 2.

2.8. Overall balances of fuel model

The overall balances of the developed fuel model are summarised in Fig. 2. The mass and heat balances for fuel decomposition at 710 °C are presented. An example case based on a simulation is shown. Decomposition balances of fuel from the as-received state to individual gas species and solid char are presented.

2.9. Chemical reactions

Chemical reactions used in the model are summarised in Table 1. Chemical reactions are based on literature correlations for individual

Table 1
Chemical reactions.

Reaction	Equation	H (at 25 °C)	Ref.
Calcination	$CaCO_3(s) \rightarrow CaO(s) + CO_2(g)$		
	$R_{calc} = \rho_s k'_{calc} W^{2/3}_{s,CaCO_3} (C_{CO_2,eq} - C_{CO_2})$	178.3	[13–15]
	$k'_{calc} = 2057 \exp(-\frac{112400}{R_i T})$		
Carbonation	$CaO(s) + CO_2(g) \rightarrow CaCO_3(s)$		
	$R_{carb} = \rho_s k'_{carb} (W_{s,max} - W_{s,CaCO_3})(C_{CO_2} - C_{CO_2,eq})$	−178.3	[15–17]
	$k'_{carb} = 30$		
Sulphation	$CaO(s) + SO_2(g) + 0.5 O_2(g) \rightarrow CaSO_4(s)$		
	$R_{sulph} = \rho_s W_{s,CaO} k'_{sulph} W_{g,SO_2} W_{g,O_2}$	−502.1	[18]
	$k_{sulph} = 4.0(-3.843T + 5640)\exp(-\frac{8810}{T})$		
De-sulfation	$CaSO_4(s) + CO(g) \rightarrow CaO(s) + SO_2(g) + CO_2(g)$		
	$R_{desulph} = \rho_s W_{s,CaSO_4} k'_{desulp} C_{CO} A_{r,CaSO_4} M_{CaSO_4}$	219.2	[10]
	$k'_{desulph} = 0.005 \exp(-\frac{10000}{T})$		
Direct sulfation	$CaCO_3(s) + SO_2(g) + 0.5 O_2(g) \rightarrow CaSO_4(s) + CO_2(g)$		
	$R_{disulph} = \rho_s W_{s,CaCO_3} k'_{disulp} C^{0.9}_{SO_2} C^{0.75}_{CO_2} C^{0.001}_{O_2} A_{r,CaCO_3} M_{CaCO_3}$	−323.8	[10]
	$k'_{disulph} = 0.01 \exp(-\frac{3031}{T})$		
Boudouard	$C(s) + CO_2(g) \rightarrow 2CO(g)$		
	$R_{boud} = k_{boud} \rho_{char} W_{char,C}$	172.4	[19]
	$k_{boud} = 2.11 \cdot 10^7 \exp(-\frac{219000}{R_i T}) p^{0.36}_{CO_2}$ [bar]		
Water –gas	$C(s) + H_2O(g) \rightarrow CO(g) + H_2(g)$		
	$R_{wg} = k_{wg} \rho_{char} W_{char,C}$	131.3	[20]
	$k_{wg} = 1.23 \cdot 10^7 \exp(-\frac{198000}{R_i T}) p^{0.75}_{H_2O}$ [atm]		
Methanation	$C(s) + 2H_2(g) \rightarrow CH_4(g)$		
	$R_{meth} = k_{meth} \rho_{char} W_{char,C}$	-75.0	[5]
	$k_{meth} = 16.4 \exp(-\frac{94800}{R_i T}) p^{0.93}_{H_2}$ [MPa]		
Water –gas shift	$CO(g) + H_2O(g) \leftrightarrow H_2(g) + CO_2(g)$		
	$R_{wgs} = M_{CO} k'_{wgs} ((C_{CO} C_{H_2O}) - (C_{CO_2} C_{H_2})/K_{wgs})$	−41.1	[21,22]
	$k'_{wgs} = 2.78 \exp(-\frac{3965}{T})$		

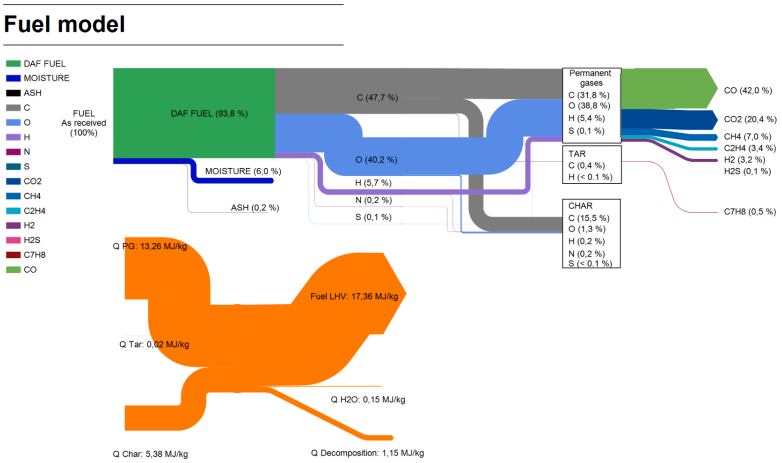

Fig. 2. Mass and heat balances of fuel model at 710 °C with $\gamma_1 = 0.764$ and $\gamma_2 = 0.642$.

chemical phenomena. Homogeneous and heterogeneous reactions are modeled as source terms of gas and solid phase mass balances. The balance equations and the main assumptions concerning the modelling of the chemical reactions in an SEG reactor are described elsewhere [9].

3. Experimental work

New experimental work focused on fuel decomposition was conducted to support the modelling. The experiments were carried out in the temperature range of 600–800 °C, which is the most relevant range for the SEG process. Wood pellets of the SEG gasification experiments were used to obtain proper boundary conditions for the fuel model. A brief description regarding the SEG gasification experiments is provided in this paper. The gasification experiments have been published in detail elsewhere [3].

3.1. Fuel decomposition experiments

Proximate analyses for wood pellets were carried out with a fixed bed reactor at temperatures of 650 °C, 700 °C, 750 °C, and 800 °C under atmospheric pressure. Wood pellets of ENplus A1-quality were used in the experiments. The mass of a single pellet was 15 g. The elemental composition of the pellets is presented in Table 2. The mass balances of the experiments are based on the fractions recovered from the reactor. The balances are shown in Table 3. The yields of the fractions are listed as received-based. Therefore, the liquid and solid yields in the table include the moisture and ash present in the fuel. The closures of the mass balances are reported as the sum of the measured fractions. The mass balances of the experiments were determined using the following procedure. The reactor was flushed by known N_2 flow, and the N_2 and other gases were collected in a bag. The permanent gas yield from the wood pellets was determined from a balance after gas chromatography analysis of the collected gases. The solid fraction was collected from the reactor after cooling. The liquid fraction was determined by weighing a condenser and various parts of the reactor where the liquid fraction can condense.

The permanent gas and liquid yields of the experiments represent the total volatile yield. The liquid fraction is formed from liquid organics and water, and it represents the tar fraction of the fuel [8]. The solid fraction is formed during devolatilisation. The solid fraction is in a stable state unless a reactive gasification agent is fed into the reactor. Distribution of the volatiles into the permanent gases and liquid varies by process conditions. The mass of the tar that is measured from a fluidised bed environment is much lower than from the fuel decomposition experiment. Therefore, the fraction given in Table 3 cannot be directly utilised in simulations of a fluidised bed without implementing reaction paths to decompose the tars to lighter gases. However, the solid fraction of the fuel from the experiments can be utilised in the analysis of a fluidised bed reactor.

3.2. Sorption-enhanced gasification experiments

Gasification experiments were conducted at a 200 kW_{th} dual fluidised bed (DFB) pilot facility at the Institute of Combustion and Power Plant Technology (IFK) at the University of Stuttgart [3]. The pilot facility consisted of a bubbling fluidised bed gasifier and a circulating fluidised bed combustor that were connected to each other. The pilot facility is shown in Fig. 3. Detailed information regarding the pilot facility is provided in [9]. The experimental work focused on varying the temperature of the SEG pilot by varying the bed material circulation rate from the combustor to the gasifier. Three steady-state operating points were selected from these experiments for further analysis with simulations. These operating points represent the most interesting operating range from the point of view of DME synthesis. The chemical composition of the wood pellets used is presented in Table 2. The operational parameters of the experiments are presented in Table 4. Additional boundary conditions were determined from solid samples for the simulations and are summarised in Table 5. The fuel decomposition fractions (char, tars, and permanent gases) were specified into the model as temperature-dependent. The fractions are summarised in Table 6. The tar fraction of the fuel was evaluated according to gravimetric tar measurements [23]. The char fraction was evaluated based on decomposition experiments presented in Table 3. The permanent gases were calculated from mass balance based on known tar and char fractions from Eq. 2. Moisture and ash content were specified in the model according to standard proximate analysis (Table 2) conducted for the fuel batch on the site. Elemental composition of biomass was specified in the model according to Table 2.

Table 2
Chemical composition of wood pellets used in gasification experiments.

Fuel	Wood pellets
C [wt.%,daf]	50.8
H [wt.%,daf]	6.1
N [wt.%,daf]	0.2
S [wt.%,daf]	0.1
O [wt.%,daf]	42.8
Moisture [wt.%,ar]	6.0
Ash [wt.%,ds]	0.2
LHV [MJ/kg,ar]	17.36

4. Simulation results and discussion

The aim of this work was to develop a fuel model and implement the model into an SEG model frame. By introducing the characteristics of the decomposition phenomena into the model frame, the overall model was able to capture the main characteristics of the SEG process, and aspects about the characteristics are discussed in this section.

4.1. Hydrodynamics and heat balances

The simulations were conducted by introducing the operating parameters of the pilot-scale process into the model with appropriate model equations describing phenomena that are present in the SEG process. A previously developed and validated hydrodynamic scheme was used in the current simulations [9]. Simulated temperature profiles against measurements of the gasifier are shown in Fig. 4. The temperature of the gasifier was adjusted during the experiments by varying the rate of bed material circulation from the combustor to the gasifier. The operating temperature of the gasifier was increased by increasing the circulation rate. Because of uncertainties in the applied boundary conditions, a heat balance correction term was applied to the bed of the gasifier to match local bed temperatures. The heat balance adjustments presented in Table 5 were applied to the bed. A constant heat loss [kW/m] was applied at the freeboard section according to Table 5. The freeboard heat loss was included in the adjustment. This approach is used to compensate for the impact of uncertainties such as devolatilization and uncertainty of the solid flow and temperature measurements in the energy balance.

4.2. Producer gas yield

The typical gas yield range of various SEG experiments is presented in Fig. 5 against the gas yield predicted by the model. The gas yield by the model matches with the typical range. The range is based on literature data [24]. The producer gas composition at the simulated operating points against measurements of the IFK's pilot facility from [3] are shown in Fig. 6. Furthermore, a typical producer gas composition range from various experiments is shown [24]. The range covers various operating conditions and was obtained from experiments with three different gasifiers. As can be seen from Fig. 6, some experiments can

Table 3
Fuel decomposition balances of wood pellets.

Wood pellets	Temperature °C	Liquid yield wt.%,ar	Solid/char yield wt.%,ar	Permanent gas yield wt.%,ar	Moisture wt.%,ar	Ash wt.%,ar	Closure wt.%,ar
	650	36.87	19.43	35.15	-	-	91.45
Temperature	700	31.90	19.52	40.48	-	-	91.90
variation	750	21.09	17.76	51.06	-	-	89.91
	800	20.53	17.28	55.94	-	-	93.75
Standard proximate	905	-	15.29	78.80	5.55	0.36	100

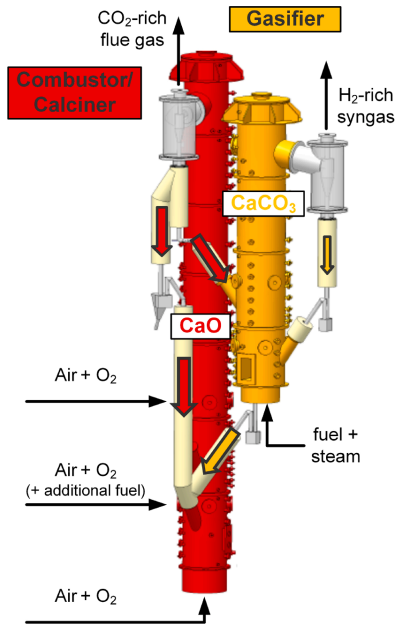

Fig. 3. 200 kW_{th} DFB pilot facility at IFK, University of Stuttgart [9].

Table 4
Operating parameters of gasification experiments.

Parameter	
Biomass feed [kg/h]	30
Steam flow [kg/h]	30.3
Steam temperature [°C]	146
Steam-to-Carbon ratio [mol/mol]	1.5

differ from this range because the producer gas composition is a result of the overall effect of various operating parameters, e.g. bed material circulation rate, steam-to-carbon ratio, and hydrodynamic conditions.

In Table 5, two model parameters for the fuel model are presented. The values for the parameters were determined from gasification experiments. Parameter γ_2 was set based on average distribution of hydrocarbons in the producer gas. Parameter γ_1 was calibrated to the methane concentration in Fig. 6, and a linear fit to the calibration was used.

The producer gas composition from the IFK pilot with respect to operating temperature is shown in Fig. 6. The model was able to predict the main temperature trends for the composition. Furthermore, the

Table 5
Simulation boundary conditions.

Parameter	OP 1.1	OP 1.2	OP 1.3
Operational temperature			
Bed temperature[1] [°C]	710	757	774
Solid circulation from combustor			
Solid flow[1] [kg/h]	498	570	694
Temperature[1] [°C]	734	787	809
Composition			
CaO[1] [wt.%]	93.3	91.2	96.0
$CaCO_3$ [1] [wt.%]	2.0	4.7	0.4
Ash[1] [wt.%]	4.7	4.1	3.6
N_2 sealing gas and purges			
Feed[1] [kg/h]	10.94	15.05	14.63
Temperature			
Freeboard [°C]	200	200	200
Dense Bed [°C]	650	650	650
Fuel model parameters			
γ_1	0.764	0.779	0.785
γ_2	0.642	0.642	0.642
Heat balance			
Freeboard loss [kW/m]	−2.4	−2.4	−2.4
Balance correction [kW/kW_{fuel}]	−0.037	0.072	0.105

[1] Measured value.

Table 6
Temperature-dependent fuel fractions used in the simulations.

OP		1.1	1.2	1.3
Temperature	°C	710	757	774
Tar	wt.%,ds	0.49	0.13	0.13
Char	wt.%,ds	18.33	17.56	17.28
Permanent gas	wt.%,ds	80.98	82.11	82.38
Moisture	wt.%,ar	6.0	6.0	6.0
Ash	wt.%,ds	0.2	0.2	0.2

simulation results with respect to the typical producer gas composition were good. However, there was a deviation between the simulations and measurements of the pilot for CO_2 and H_2 gases. There could be various reasons for the deviation. The modelling was limited within the main reactor, and chemical reactions outside the reactor, e.g. in the cyclones, were not considered. Thus, the modelling could not consider chemical reactions in the cyclones, such as carbonation of the bed material. Another explanation for the deviation could be that the reaction equilibrium of real limestone differs from the thermodynamic reaction equilibrium [25]. Consequently, the CO_2 capture in the pilot could be

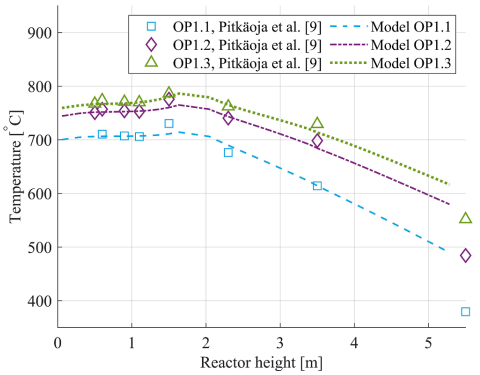

Fig. 4. Simulated temperature profiles against pilot's temperature measurements [9].

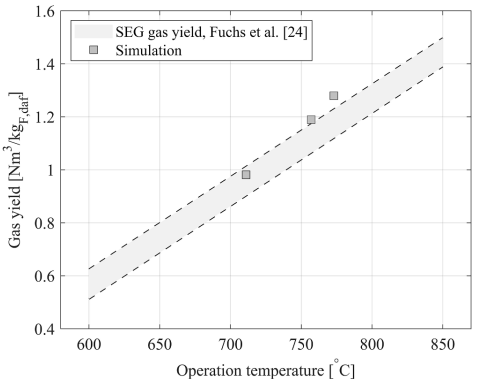

Fig. 5. Gas yield of various SEG experiments and simulated producer gas yield. The gas yield range is based on a data presented by [24].

larger than was predicted by the modelling. Because there is strong coupling of carbonation and water–gas shift, the higher H_2 fraction of the measurements could be explained by an enhanced water–gas shift reaction that was not captured by the modelling. In addition to explanations related to the CO_2 capture, the deviation could be caused by underestimated element transfer from the gasifier to the combustor in the simulations. There could have been material losses that were not included in the modelling and consequently, the model prediction for the CO_2 fractions was higher than the measurements.

The model was able to predict the producer gas composition of IFK experiments with reasonably good accuracy. As indicated, there were uncertainties in the boundary conditions of the experiments, which could explain the model's higher prediction of the CO_2 fractions. Nevertheless, the modelling results were in agreement with the general trends presented in Fig. 5 and Fig. 6. The modelling results were excellent in this respect.

4.3. Bed material CO_2 capture

Bed material CO_2 capture in the gasifier can be determined from the difference in $CaCO_3$ fractions of circulating solids. The bed material $CaCO_3$ mass fraction change in simulations is shown in Fig. 7, with the CO_2 capture determined from the fractions. The bed of the gasifier operated close to the thermodynamic reaction equilibrium. The bed elements with respect to the equilibrium are shown in Fig. 8. The reaction kinetics were fast enough to set the bed operating close to the equilibrium, and therefore the maximum transfer capacity for the CO_2 was attained in each case. Consequently, the operating temperature was the main process parameter to define the amount of carbon capture. The basic operating characteristics are shown in Fig. 7. The CO_2 capture decreases with increasing operating temperature because the maximum transfer capacity is limited by the equilibrium. When the operating temperature was increased to the level of OP 1.3, carbonation was no longer possible owing to thermodynamic limitations of the reaction. Thus, no carbon capture occurred according to Fig. 7. However, Fig. 8 shows that local carbon capture occurred at the upper parts of the bed, but the limestone was calcined before the bottom of the gasifier was reached.

4.4. Carbon balance

Carbon balances were formulated from the simulations for each operating point. The carbon balances were compared against carbon balance data from an SEG balance study [24]. The comparison is shown in Fig. 9. The carbon balances in the figure are presented as the carbon of fuel that is transported from the gasifier to the combustor. The carbon balances by [24] are based on general trends presented in Fig. 5 and Fig. 6.

The total carbon transport (in Fig. 9) was calculated by removing the carbon of the producer gas ($kg_{g,C}/kg_{F,daf,C}$) from the amount of carbon that was fed into the reactor. As a result, 60 wt.% to 40 wt.% of the total carbon was transported to the combustor in the simulations. The total carbon transport to the combustor is very similar in this study and in the study by [24], although there are differences in producer gas yield.

The total carbon transport can be divided among a solid carbon (carbon in char) and $CaCO_3$ to conduct more profound system analysis. The distribution of the carbon fractions is similar in this study and in the study by [24]. However, the simulation showed that the CO_2 transport to the combustor was not possible at the operating temperature of 774 °C owing to thermodynamic limitations. The char of the fuel was almost completely transported to the combustor owing to relatively low residence time in the reactor. Consequently, the carbon transport by the char followed closely the fuel's char fraction from the decomposition balances. Therefore, the elemental carbon concentration of producer gas was mainly the result of devolatilised carbon and carbon capture. This example highlights the importance of the decomposition process for the overall material balance of the SEG.

5. Conclusions

A fuel model for gasification was developed and implemented to an SEG model frame. The fuel model was suitable for various gasification processes and different operating temperatures. The model considered the major decomposition products of the fuel to model the main characteristics of the fuel decomposition. The main elemental balances and influence of temperature on the balances were considered.

The SEG model frame was previously developed based on specifications of a 200 kW_{th} SEG pilot plant [9]. The SEG pilot experiments were simulated with the model frame with the developed fuel model. The modelling focused on a temperature range between 710 °C and 770 °C, with a steam-to-carbon ratio of 1.5 [mol/mol]. This temperature range is the most interesting for the SEG process from the point of view of DME synthesis.

Elemental carbon balances, typical gas yield, and the producer gas composition range of an SEG reactor are presented by [24] for the investigated temperature range. The carbon balances of the simulations were consistent with [24]. Furthermore, the producer gas yield and

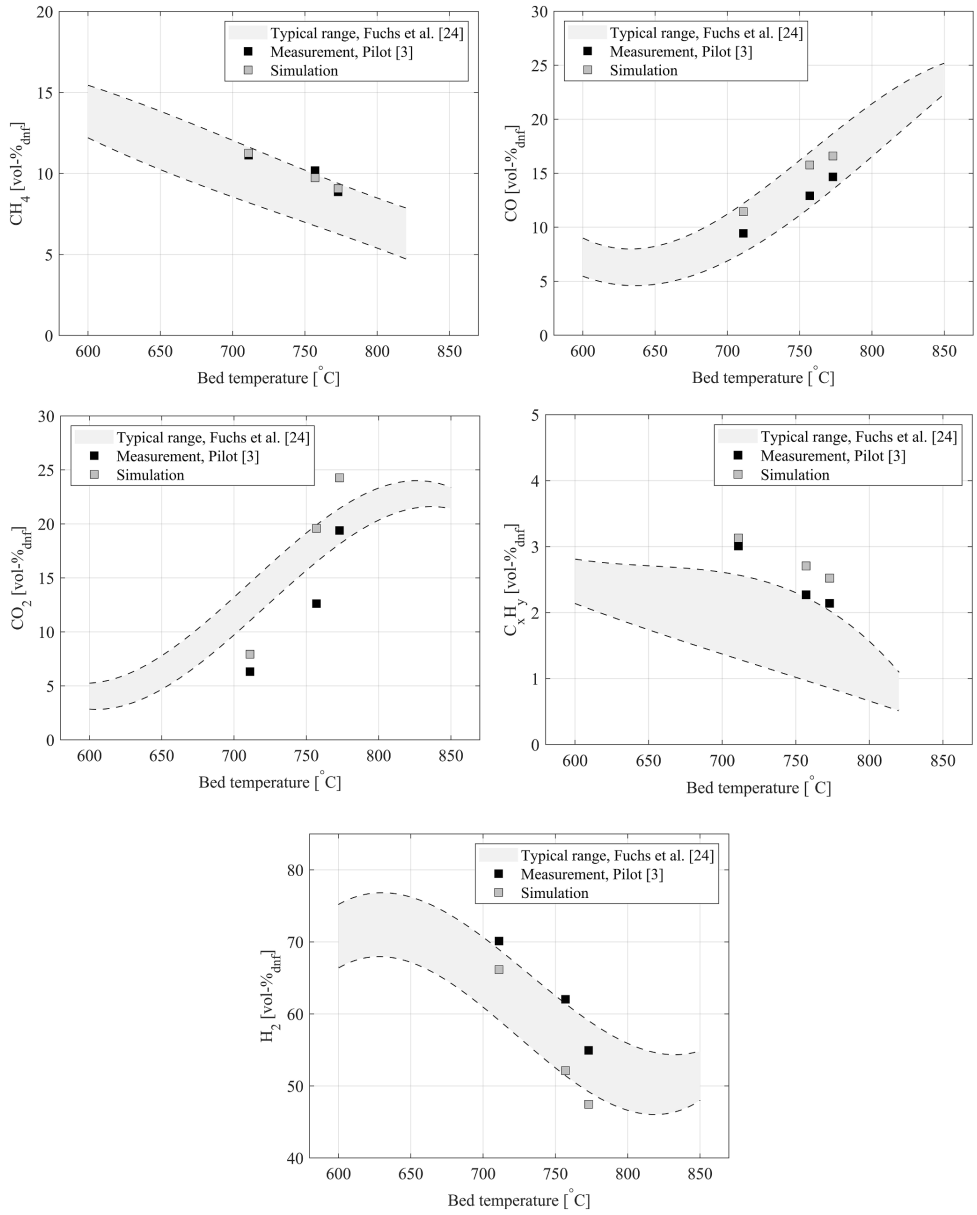

Fig. 6. Volume fractions of H_2, CO, CO_2, CH_4, and C_xH_y gas species of producer gas at the studied operating points of 200 kW_{th} pilot gasifier [3]. The typical range for the measurements is presented based on various SEG experiments [24].

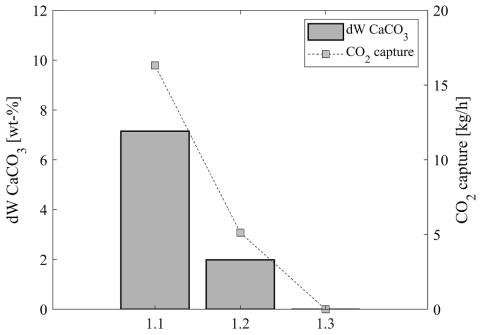

Fig. 7. Bed material $CaCO_3$ mass fraction change within the gasifier and CO_2 capture.The mass fraction change $dWCaCO_3$ is calculated as a difference of $CaCO_3$ fractions of solid inflow and solid outflow.

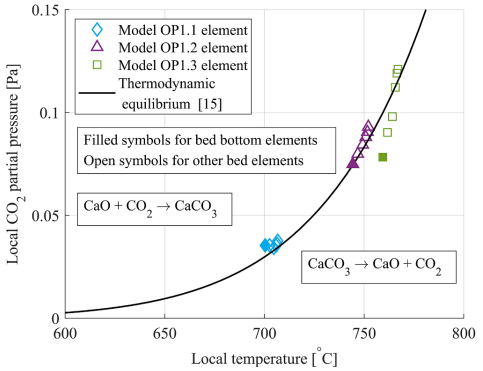

Fig. 8. Simulated local CO_2 partial pressure in the bed elements with respect to the local temperature. The pressure in emulsion is presented. The thermodynamic reaction equilibrium according to [15] is shown for comparison.

composition followed the typical trends. The heat balances of the model were in agreement with the trends from the IFK pilot reactor. Overall, the performance of the model was good. The model produced the main phenomena of the SEG process. Thus, the model can be used to study the operational characteristics of the process. The model predicted with reasonably good accuracy the CO, CO_2, C_xH_y, CH_4, and H_2 gas fractions of the IFK experiments. The simulated volume fractions of carbon-based gases were higher than the measurements. This indicates the carbon concentration of the producer gas to be higher than that of the pilot. This may be due to material losses during the experiments that were not specified in the model. Fuel decomposition balances played an important role in the overall balances of the process. Therefore, it is important to model the main phenomena of the fuel decomposition process. The decomposition has a significant impact on the element transfer between the reactors and for the composition of the producer gas.

To investigate material losses and fuel decomposition balances further, the element exchange between the gasifier and the combustor must be determined. The element exchange can be estimated by formulating a balance study. The known element exchange opens the possibility to evaluate the pilot system more profoundly and elucidates the uncertainties, such as the material losses.

The work presented in this paper improves the current

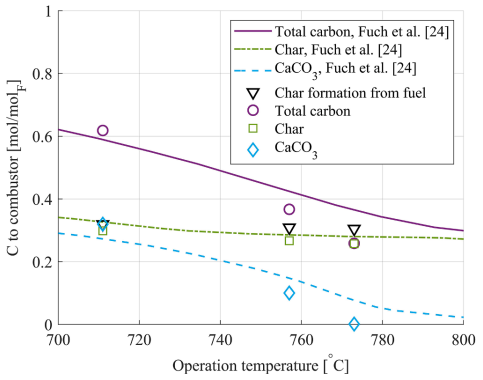

Fig. 9. Carbon transport to the combustor. The carbon transport of the model is presented against balances from an SEG balance study [24]. The overall carbon flow to the combustor is divided among char and $CaCO_3$. The char fraction of the fuel is shown for comparison.

understanding of the physical and chemical phenomena governing the SEG processes. Further investigations on this topic could include a balance study of the pilot SEG reactor system to evaluate the element exchange between the reactors. An understanding of material exchange in complex reactor systems is important for analysing the operation of the systems and for modelling the processes.

CRediT authorship contribution statement

Antti Pitkäoja: Methodology, Software, Formal analysis, Writing - original draft, Visualization, Validation. **Jouni Ritvanen:** Methodology, Software, Writing - review & editing, Supervision, Visualization. **Selina Hafner:** Investigation, Writing - review & editing, Visualization. **Timo Hyppänen:** Writing - review & editing, Supervision. **Günter Scheffknecht:** Writing - review & editing, Supervision.

Declaration of Competing Interest

The authors declare that they have no known competing financial interests or personal relationships that could have appeared to influence the work reported in this paper.

Acknowledgements

This work in FLEDGED project has received funding from the European Union's Horizon 2020 research and innovation programme under grant agreement No. 727600.

References

[1] Delbeke J, Vis P. EU Climate Policy Explained. Routledge; 2016.
[2] L. Pelkmans, European Union - 2018 update, Bioenergy policies and status of implementation, Technical Report, IEA Bioenergy, 2018. https://www.ieabioenergy.com/wp-content/uploads/2018/10/CountryReport2018_EU_final.pdf.
[3] Hafner S, Spörl R, Scheffknecht G. Sorption Enhanced Gasification: Process validation and investigations on the syngas composition in a 200 kW th dual fluidized bed facility. In: 23rd International Conference on Fluidized Bed Conversion; 2018. p. 826–32.
[4] Fiaschi D, Michelini M. A two-phase one-dimensional biomass gasification kinetics model. Biomass Bioenergy 2001;21:121–32.
[5] Hejazi B, Grace J, Bi X, Mahecha-Botero A. Kinetic Model of Steam Gasification of Biomass in a Bubbling Fluidized Bed Reactor. Energy Fuels 2017;31:1702–11.
[6] Kaushal P, Abedi J, Mahinpey N. A comprehensive mathematical model for biomass gasification in a bubbling fluidized bed reactor. Fuel 2010;89:3650–61.

[7] Di Blasi C, Signorelli G, Di Russo C, Rea G. Product Distribution from Pyrolysis of Wood and Agricultural Residues. Ind Eng Chem Res 1999;38:2216–24.
[8] Neves D, Thunman H, Matos A, Tarelho L, Gómez-Barea A. Characterization and prediction of biomass pyrolysis products. Progress Energy Combust Sci 2011;37:611–30.
[9] Pitkäoja A, Ritvanen J, Hafner S, Hyppänen T, Scheffknecht G. Simulation of a sorbent enhanced gasification pilot reactor and validation of reactor model. Energy Conversion Manage 2020;204:112318.
[10] Myöhanen K. Modelling of Combustion and Sorbent Reactions in Three-Dimensional Flow Environment of a Circulating Fluidized Bed Furnace. Acta Universitatis Lappeenrantaensis. Doctoral Dissertation, Lappeenranta 2011.
[11] Gómez-Barea A, Leckner B. Modeling of biomass gasification in fluidized bed. Progress Energy Combust Sci. 2010;36:444–509.
[12] Tuomi S, Kurkela E, Simell P, Reinikainen M. Behaviour of tars on the filter in high temperature filtration of biomass-based gasification gas. Fuel 2015;139:220–31.
[13] Martínez I, Grasa G, Murillo R, Arias B, Abanades J. Kinetics of calcination of partially carbonated particles in a Ca-looping system for CO2 capture. Energy Fuels 2012;26:1432–40.
[14] Fang F, Li Z-S, Cai N-S. Experiment and Modeling of CO 2 Capture from Flue Gases at High Temperature in a Fluidized Bed Reactor with Ca-Based Sorbents. Energy Fuels 2009;23:207–16.
[15] Stanmore B, Gilot P. Review-calcination and carbonation of limestone during thermal cycling for CO2 sequestration. Fuel Process Technol 2005;86:1707–43.
[16] Shimizu T, Hirama T, Hosoda H, Kitano K, Inagaki M, Tejima K. A Twin Fluid-Bed Reactor for Removal of CO2 from Combustion Processes. Chem Eng Res Des 1999;77:62–8.
[17] Alonso M, Rodríguez N, Grasa G, Abanades J. Modelling of a fluidized bed carbonator reactor to capture CO2 from a combustion flue gas. Chem Eng Sci 2009;64:883–91.
[18] Rajan R, Wen C. A comprehensive model for fluidized bed coal combustors. AIChE J 1980;26:642–55.
[19] Risnes H, Sorensen L, Hustad J. CO2 reactivity of chars from wheat, spruce and coal. In: Bridgewater A, editor. Progress in Thermochemical Biomass Conversion. Oxford: Blackwell Science; 2001. p. 61–72.
[20] Hemati M, Laguerie C. Determination of the kinetics of the sawdust steam-gasification of charcoal in a thermobalance. Entropie 1988;142:29–40.
[21] Biba V, Macák J, Klose E, Malecha J. Mathematical Model for the Gasification of Coal under Pressure. Ind Eng Chem Process Design Dev 1978;17:92–8.
[22] de Souza-Santos M. Comprehensive modelling and simulation of fluidized bed boilers and gasifiers. Fuel 1989;68:1507–21.
[23] Hafner S, Schmid M, Spörl R, Scheffknecht G. Experimental Investigation of the Sorption Enhanced Gasification of Biomass in a Dual Fluidized Bed Pilot Plant. In: 27th European Biomass Conference & Exhibition; 2019.
[24] Fuchs J, Schmid JC, Müller S, Mauerhofer AM, Benedikt F, Hofbauer H. The impact of gasification temperature on the process characteristics of sorption enhanced reforming of biomass. Biomass Conver Biorefinery 2019.
[25] Florin NH, Harris AT. Enhanced hydrogen production from biomass with in situ carbon dioxide capture using calcium oxide sorbents. Chem Eng Sci 2008;63:287–316.

Publication IV

Ritvanen, J., Myöhänen, K., Pitkäoja, A. and Hyppänen, T.
Modeling of industrial-scale sorption enhanced gasification process: One-dimensional simulations for operation of coupled reactor system

Reprinted with permission from
Energy
Vol. 226, 120387, pp. 1-14, 2021.
© 2021, Elsevier

Energy 226 (2021) 120387

Contents lists available at ScienceDirect

Energy

journal homepage: www.elsevier.com/locate/energy

Modeling of industrial-scale sorption enhanced gasification process: One-dimensional simulations for the operation of coupled reactor system

Jouni Ritvanen*, Kari Myöhänen, Antti Pitkäoja, Timo Hyppänen

Lappeenranta-Lahti University of Technology, LUT School of Energy Systems, P.O. Box 20, FI-53851, Lappeenranta, Finland

ARTICLE INFO

Article history:
Received 25 November 2020
Received in revised form
9 March 2021
Accepted 11 March 2021
Available online 23 March 2021

Keywords:
Sorption enhanced gasification
Biomass gasification
In-direct gasification
1D modelling
Dual fluidized bed
Coupled reactors

ABSTRACT

Sorption enhanced gasification (SEG) is a promising technology for producing gas derived from renewable feedstock to be used in biofuel synthesis processes. As a response to the growing need for renewable fuels, an SEG reactor design was developed for industrial-scale dimethyl ether (DME) production. A 100MW_{th} scale SEG reactor concept for wood pellets as a feedstock was created by a model-based approach. Thus, a 1D modeling tool for the coupled circulating fluidized beds was developed. The model was used to investigate the dual fluidized bed system's operation in the gasifier temperature range of 730−790°C. In this range, the optimal producer gas composition without external hydrogen for the downstream DME synthesis was achieved at gasifier temperature 730°C: 63 $\%_{vol,db}$ H_2, 11 $\%_{vol,db}$ CO, 13 $\%_{vol,db}$ CO_2. The model prediction was successfully compared against experimental data and modeling results from the literature. The developed 1D model enables the investigation of the composition and yield of the producer gas with different operating parameters, such as the part-load operation. This advanced capability can be used to develop new control strategies for the SEG system and investigate the impact of various operating parameters on the producer gas composition and yield.
© 2021 The Author(s). Published by Elsevier Ltd. This is an open access article under the CC BY license (http://creativecommons.org/licenses/by/4.0/).

1. Introduction

EU strategy for the transition to a low-carbon economy sets out a framework and mechanisms to address climate change. Greenhouse gas emissions from transportation account for almost a quarter of Europe's greenhouse gas emissions, and transportation is the primary source of air pollution in European cities [1]. The target of 14% renewable fuel usage in the transportation sector by 2030 has been set and, consequently, there is a pressing need to develop effective and cost-efficient ways to produce transportation fuels from renewable sources [2]. In recent decades, considerable research attention has been devoted to the study of conventional biomass gasification. However, in recent years, more advanced processes, such as dual fluidized bed gasifiers, have become the subject of increased research interest to produce tailored syngas for transportation biofuel production [3]. Sorbent enhanced gasification (SEG) is a dual fluidized bed technology that improves the syngas' quality compared to conventional gasification [4]. The SEG is an indirect steam gasification process operated at temperatures between 600 and 800°C, and the process is enhanced by limestone, which captures CO_2 from the gasification process. The removal of CO_2 from the gasifier enhances hydrogen production through the water-gas shift reaction. The schematic of the SEG process is illustrated in Fig. 1.

By the SEG operation, producer gas composition can be adjusted. The operating parameters affecting producer gas yield and composition are steam to carbon ratio, biomass feed rate to the combustor, solid inventories in the reactors, solids carrying capacity of CO_2, and solids circulation rate between the reactors. By these parameters, the reactors' temperature levels can be controlled, resulting in the target reaction environment. The gasifier temperature level is the most dominant controlling variable, which defines the limestone CO_2 capture yield by the carbonation reaction equilibrium.

The SEG and similar absorption enhanced reforming (i.e., AER) processes have been studied previously experimentally and in numerical simulations. The experimental investigations have mainly been carried out using pilot-scale test equipment from TU Wien [5,6] and the University of Stuttgart [7]. In these facilities, the

* Corresponding author.
E-mail address: jouni.ritvanen@lut.fi (J. Ritvanen).

https://doi.org/10.1016/j.energy.2021.120387
0360-5442/© 2021 The Author(s). Published by Elsevier Ltd. This is an open access article under the CC BY license (http://creativecommons.org/licenses/by/4.0/).

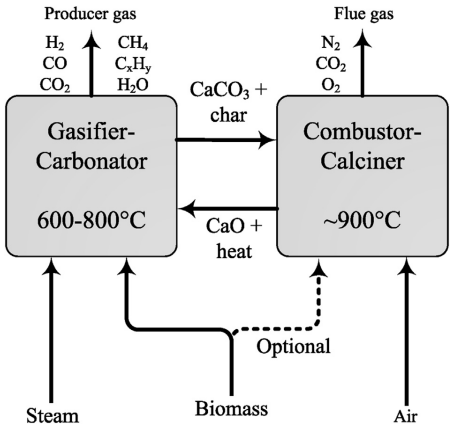

Fig. 1. Schematic of the SEG process.

gasifier is operated in bubbling fluidized bed (BFB) mode, and the combustor is operated in circulating fluidized bed (CFB) mode. Experimental results from these facilities are summarized in a review by Fuchs et al. [8]. The test results show the operation range of the SEG process in the temperature range of 600 – 850°C, which results in the corresponding H_2 gas concentrations 75 – 50%$_{db}$, CO gas concentrations 5 – 22%$_{db}$ and CO_2 gas concentrations 3 – 24%$_{db}$, respectively. The test results show the SEG process's controllability, enabling the flexible production of producer gas suitable for downstream processes. By adjusting the process, it is possible to maximize hydrogen production or, accordingly, to produce the desired ratio of gas components. Coupled SEG reactors have also been investigated numerically using simple lumped reaction equilibrium models [9,10], and kinetic reaction models [11,12] in a 1D simulation frame. These macroscopic models of coupled reactors have been implemented with the BFB gasifier and the CFB combustor on a pilot scale.

In this work, coupled SEG process is simulated on an industrial-scale using CFB technology in both reactors considering the reactors' hydrodynamics and using kinetic modeling for the reactions. These novel model approach and reactor combination have not been considered in the earlier studies. Here, CFB reactors have been selected, which are often more favorable and are used in larger industrial units due to their better mixing properties and smaller land area footprint. A model frame for the SEG process with CFB reactors was developed based on a semi-empirical 1D-approach. The model frame contains the gasification and the combustion reactors, coupled together to form a complete SEG process. Fundamental balance equations for mass and energy are implemented in the reactor model frame. This modeling approach involves coupled heat capacity flows from hydrodynamics that determines reactor temperatures. The model also considers solids' conversion degree between reactors obtained from a combination of solids inventories, reaction rates, and residence times. Transport phenomena and chemical reactions are modeled using empirical model equations validated with pilot-scale experiments and literature data. Reactor design with geometry and boundary condition data for the SEG system using biomass (i.e., wood pellets) as feedstock is proposed in this study. SEG model in a scale of 100MW$_{th}$ is used to estimate SEG operation in the gasifier temperature range of 730 – 790°C. The lower value of the temperature range is selected according to producer gas suitability for downstream Dimethyl ether (DME) synthesis with producer gas Module (M) of 2. The Module M is determined according to Eq. (1), using the ratio of the H_2, CO and CO_2 concentrations of the producer gas.

$$M = \frac{y_{H_2} - y_{CO_2}}{y_{CO} + y_{CO_2}} \quad (1)$$

The temperature range's upper value is based on the mixing of additional hydrogen from an external source with producer gas to make the producer gas suitable for DME synthesis. SEG system operation and performance values are investigated within the operation range of M = 2.17…0.7. This is the most interesting operation range for the DME synthesis. The model approach evaluates aspects of process operation and optimization that influence the process and plant design and form the basis for evaluating process performance and costs. One objective is to create a model frame that can investigate the process conditions outside of this study, such as different biomass feedstock.

2. One-dimensional SEG model

2.1. Reactor model frame

The overall 1D model frame can simulate a system of several interconnected reactors, each of which is discretized vertically into one-dimensional control volumes. The physical reactor scale is not limited: it can range from laboratory and pilot-scale to industrial scale. The effect of the scale is naturally considered in fundamental physical submodels or included in the empirical submodels and correlations. Fig. 2 presents the 1D-model for one CFB reactor including the cyclone-standpipe-loop seal system.

The overall model frame can contain several reactor models, which exchange solid material with each other. Time-dependent conservation equations for mass, energy, and gas and solid material fractions have written using the first-order difference method and the forward Euler method. The convective flows are differentiated with the upwind method, and the diffusion of energy is differentiated with the central difference method. These equations are solved in the Matlab Simulink environment using built-in ordinary differential equation (ODE) solvers. The reactor models are capable of using constant and variable time steps with ODE solvers. In this study, simulations are continued until the steady-state is reached for the SEG system.

The discretization scheme has three regions related to the chosen reactor geometry, namely straight bottom and freeboard sections, and a conical frustum part between these sections. The user-defined number of discretization elements with geometry data can be set for all regions independently. Elevation to exit channel defines the exit channel location, and the model collects and averages flow properties from discretized 1D elements located next to the exit channel. The gas phase's main boundary conditions include primary gas feed, and a user-defined number of secondary gas feeds with feed point elevation data. The fuel is numerically decomposed into char, ash, volatile, tar, and moisture fractions. In CFB conditions, volatile, tar, and moisture fractions are released in the reactor's bottom section, where larger fuel particles settle after the feeding. In the model's steady-state conditions, the rates of released components in the bottom section equal to the amount of components in the fuel feeding. Therefore, in the model, the total amount of volatile, tar, and moisture fractions in the fuel feed are released to the gas phase in the bottom section, which typically consists of 2–4 lowest elements of the reactor model. The

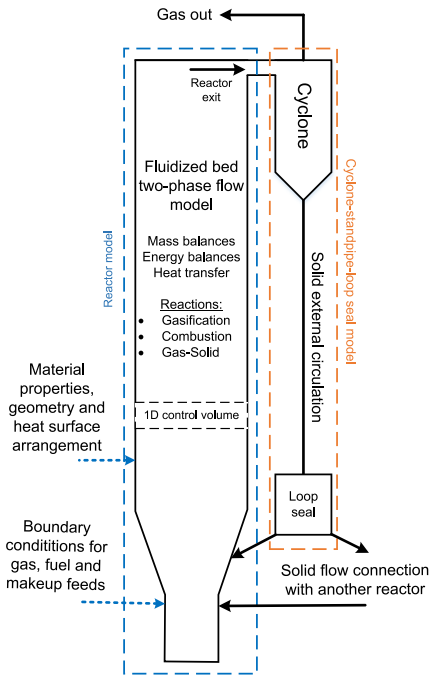

Fig. 2. Overview of the 1D model frame for the CFB reactor.

heterogeneous reactions connect gas-phase mass balance with solid-phase mass balance. Thirteen gas species (O_2, N_2, CO_2, H_2O, NH_3, H_2S, CO, CH_4, C_2H4, H_2, NO, SO_2 and tars) are solved in gas phase with heterogeneous and homogeneous reaction schemes. The solid phase is divided into char and primary solid material with separate reactor-level inventory balances. The primary solid's consists of four solid materials: CaO, $CaCO_3$, $CaSO_4$ and ash. The primary solid's main boundary conditions include a user-given solid inlet flow profile, fuel ash, and makeup flow sources. A separate solid purge can be used to control the primary solid inventory in the reactor. In connection with the material purge, char is removed at the discharge location in proportion to the materials' concentrations. Fuel ash source, makeup flow, and solid purge are located at the bottom of the reactor (i.e., in the first element). Char has the reactor-level mass inventory to which char from the fuel is added. Primary solid and char inventories are distributed to the reactor by the vertical density profiles. The solid-phase flow scheme includes wall layer flow (i.e., 1.5D-model) used in larger reactors to model horizontal and vertical mixing in the reactor. The mass balance of the char includes char combustion and gasification reactions. The Ca-containing materials are solved with the dominant reaction schemes for calcitic limestone. The ash is assumed inert. According to mass balances, gas and solids flow rates combined with local reactions determine the gas species' concentration profiles and solids material fraction profiles. The general form of the mass balance for material j and discretized element i is given in Eq. (2).

$$\frac{dm_{j,i}}{dt} = \sum_{in} q_{m,j,i} - \sum_{out} q_{m,j,i} + \sum_{reaction} r_{j,i}, \tag{2}$$

where $q_{m,j}$ represents the mass flow rate of material j and $r_{j,i}$ represents the change of mass due to chemical reactions. The energy balance scheme includes input and output streams of gas and solid, reaction heats, heat transfer to cooling surfaces, and energy dispersion between adjacent control volumes to model energy mixing. Heat transfer to cooling surfaces has three main options. Reactor configuration with refractory linings can be modeled with heat conduction through the wall. Also, a heat transfer to a plain reactor wall can be modeled. An internal plain wall heat surfaces can also be included in the model with location and heat surface area data. The general form of the energy balance for element i is given in Eq. (3).

$$\frac{dE_i}{dt} = \sum_{solid} q_{adv,i} + \sum_{gas} q_{adv,i} + \sum_{solid} q_{disp,i} + \sum q_{ht,i} + \sum q_{r,i}, \tag{3}$$

where q_{adv} is advection, q_{disp} is energy dispersion between adjacent elements, q_{ht} is the heat transfer to the cooling surfaces and q_r is reaction heat. The energy dispersion term represents the mixing of energy between adjacent control volumes, and it is written by applying the central difference method to Fick's law of diffusion.

A large number of continuous state variables are included in the model. The reactor's general state variables are total solid mass, total char mass, and total volatile and tar release rates. Also, state profiles with n_{tot} (i.e., the total number of 1D elements) variables for solid density, char density, the concentration of gas species, core temperature, wall layer temperature, wall layer solid density, and solid material fractions in core and wall layer are solved. Furthermore, two-dimensional state variables are included in the model for refractory lining temperatures. As a model input, amounts and compositions of primary and secondary gases, fuel, and solid makeup flow are given. The primary gas is inserted into the first control volume, and secondary gases can be inserted into any control volumes based on the secondary gas feed elevation. The solids input is divided to enter the selected control volumes according to design and exits the reactor from the control volumes located at the exit. Surface temperatures of heat surfaces are given as an input. The inputs are given as a time-vector to the Matlab Simulink solver. The solver requires the initial state values for each continuous variable, read from the state file.

2.2. Fuel decomposition

According to the fuel's proximate analysis, the fuel decomposition model divides the fuel into moisture, ash, volatiles, char, and tar. Elements C, N, O, H and S are divided between tar, char, and volatiles based on fuel analysis data. Submodels for char material fractions with tar composition are used to divide elements into volatile, tar, and char. For tar, C_7H_8 hydrocarbon is used as a model component to represent overall tar composition. The C_7H_8 hydrocarbon was selected to describe tars based on SEG test results [13] to represent the measured ratio of Carbon and Hydrogen and satisfy the elemental material balance. The fuel decomposition model generates reactive gas and solid fractions with theoretical reaction heats. This reaction heat is balanced with moisture latent heat and volatilization heat to obtain a measured lower heating value (LHV) of the fuel for the model.

In a standard laboratory analysis (DIN 51720), the sample's devolatilization temperature is 900°C. The actual process temperature inside the gasifier is below 800°C. A lower process

temperature is considered in the primary fuel decomposition, and temperature-dependent decomposition for volatiles, char, and tars is used instead of standard proximate data. For fuel moisture and amount of ash, a standard proximate data is used, shown with fuel's ultimate data in Table 1.

In the analysis, the volatile content was determined according to DIN 51720, but at temperatures 650…800°C. Within this range, char formation represents a process conditions of the SEG. With this data, the char fraction of the fuel was obtained in a function of a gasification temperature T_{gasif} in °C. An empirical correlation for char formation is given in Eq. (4).

$$x_{char,ds} = \max\left[-1.72\times10^{-4}T_{gasif} + 0.3037, 0.17\right], [\mathrm{kg_{char}}/\mathrm{kg_{ds}}] \quad (4)$$

The amount of the formed tars during the fuel decomposition is modeled by combining the measured tar yield from SEG experiments [13] and producer gas yield reported by Fuchs et al. [8]. Linear dependency for tar formation is assumed in the investigated temperature range. Empirical correlation for tar formation is presented in Eq. (5).

$$x_{tar,ds} = -2.0\times10^{-5}T_{gasif} + 2.92\times10^{-2}, [\mathrm{kg_{tar}}/\mathrm{kg_{ds}}] \quad (5)$$

The volatile fraction of the fuel is calculated from the following Eg. 6.

$$x_{vol,ds} = 1 - x_{char,ds} - x_{tar,ds} - x_{ash,ds} \quad (6)$$

In the fuel decomposition model, empirical correlations by Neves et al. [14] are used for Carbon (Eq. (7)) and Hydrogen (Eq. (8)) fractions in char, and empirical correlations by Myöhänen [15] are used for fractions of Nitrogen (Eq. (9)) and Sulphur (Eq. (10)) in char. Correlations for C and H composition of the char are according to Neves et al. [14]:

$$x_{char,\mathrm{C}} = 0.93 - 0.92\exp\left(-4.2\times10^{-3}T_{gasif}\right) \quad (7)$$

$$x_{char,\mathrm{H}} = -4.1\times10^{-3} + 0.1\exp\left(-2.4\times10^{-3}T_{gasif}\right). \quad (8)$$

N and S elements are assumed to follow correlations by Myöhänen [15]:

$$x_{char,\mathrm{N}} = 8.8\times10^{-2}x_{F,\mathrm{N}}x_{char,daf}^{0.6}\left(\frac{x_{F,\mathrm{N}}}{x_{F,\mathrm{C}}}\right)^{-0.6} \quad (9)$$

$$x_{char,\mathrm{S}} = 0.14x_{F,\mathrm{S}}x_{char,daf}^{0.2}\left(\frac{x_{F,\mathrm{H}}}{x_{F,\mathrm{C}}}\right)^{-0.6}, \quad (10)$$

where $x_{F,i}$ is fraction an element of char's parent fuel according to the ultimate analysis. The oxygen fraction of the char is calculated from the Eq. (11).

Table 1
Chemical composition of wood pellets.

Fuel	Wood pellets
C [wt-%,daf]	51.82
H [wt-%,daf]	6.15
N [wt-%,daf]	0.2
S [wt-%,daf]	0.02
O [wt-%,daf]	41.81
Moisture [wt-%,ar]	15.0
Ash [wt-%,ds]	1.15
LHV [MJ/kg,ar]	16.37

$$x_{char,\mathrm{O}} = 1 - x_{char,\mathrm{C}} - x_{char,\mathrm{H}} - x_{char,\mathrm{N}} - x_{char,\mathrm{S}} \quad (11)$$

The volatiles' elemental composition is calculated from the balance (Eq. (12)) using the ultimate analysis data and compositions of char and tar.

$$x_{vol,i} = x_{F,i} - x_{char,daf}x_{char,i} - x_{tar,daf}\frac{M_{tar,i}}{M_{tar}} \quad (12)$$

Based on stoichiometry NH_3, H_2S, CO, CO_2, CH_4, C_2H_4 and H_2 gases are formed from volatilized elements. The stoichiometric composition can be adjusted with model parameters γ_1 and γ_2:

$$\gamma_1 = \frac{n_{\mathrm{CO}}}{n_{\mathrm{CO}} + n_{\mathrm{CO_2}}} \quad (13)$$

$$\gamma_2 = \frac{n_{\mathrm{CH_4,C}}}{n_{\mathrm{CH_4,C}} + n_{\mathrm{C_2H_4,C}}} \quad (14)$$

For the formation of the volatile species, following procedure is applied:

1. Volatile S and N are used to form H_2S and NH_3, respectively.
2. Volatile O is used to form CO and CO_2 in a ratio of γ_1, defined in Eq. (13).
3. Leftover Carbon after step 2. is used to form hydrocarbons CH_4 and C_2H_4 in a ratio of γ_2, defined in Eq. (14).
4. Leftover Hydrogen after steps 1. and 3. is used to form H_2

Measured Hydrocarbon concentrations from SEG experiments [13] and producer gas yield reported by Fuchs et al. [8] were used to develop empirical correlations for γ_i, which are presented in Eqs. (15) and (16).

$$\gamma_1 = 1.626\times10^{-4}T_{gasif} + 0.703 \quad (15)$$

$$\gamma_2 = -4.38\times10^{-8}T_{gasif}^2 + 8.142\times10^{-5}T_{gasif} + 0.612 \quad (16)$$

2.3. Reactions

In this study, homogeneous gas reactions and heterogeneous reactions for limestone and char are considered. Limestone and gasification reactions are summarized in Table 2.

In oxidation conditions, a combustion reaction is applied for char with reaction rate by Basu [25]. The different combustible gaseous species produced from fuel decomposition, tar release, char combustion, and gasification will react in the presence of oxygen. The kinetic reaction rates of homogeneous combustion reactions are determined with the generic correlation given in Eq. (17).

$$r_{gas} = A_0T^{a_1}C_{gas}^{a_2}C_{\mathrm{O_2}}^{a_3}C_{\mathrm{H_2O}}^{a_4}\exp\left(\frac{-T_e}{T}\right), \left[\mathrm{mol}\,/\left(\mathrm{m^3 s}\right)\right] \quad (17)$$

The modeled homogeneous reaction equations with reaction rate parameters are given in Table 3.

2.4. Solid hydrodynamics

The vertical distribution of solid material in the reactor is solved by dividing the total solid mass into the reactor with a semi-empirical correlation presented in Eq. (18) by Johnsson and Leckner [32].

Table 2
Limestone and gasification reactions. Heterogeneous reactions in $R_i = [\mathrm{kg}/(\mathrm{m^3 s})]$ and homogeneous reactions in $r_i = [\mathrm{mol}/(\mathrm{m^3 s})]$.

Reaction	Equation	ΔH_{298K} [kJ/mol]	Ref.
Calcination	$CaCO_3(s) \rightarrow CaO(s) + CO_2(g)$	178.2	
	$R_{calc} = k_{calc}\rho_s W_{CaCO_3}^{0.67}(C_{CO_2,eq} - C_{CO_2})$		[16]
	$k_{calc} = 2057\exp\left(-\frac{112400}{RT}\right)$		[17]
	$C_{CO_2,eq} = \frac{4.137\times10^{12}}{RT}\exp\left(-\frac{20474}{T}\right)$		[18]
Carbonation	$CaO(s) + CO_2(g) \rightarrow CaCO_3(s)$	−178.2	
	$R_{carb} = k_{carb}\rho_s(W_{CaCO_3,max} - W_{CaCO_3})^{0.67}(C_{CO_2} - C_{CO_2,eq})$		[19]
	$k_{carb} = 0.3429 f_{carb}\exp\left(-\frac{2309}{T}\right)$		[19]
	$f_{carb} = 0.9$		
Sulphation	$CaO(s) + SO_2(g) + 0.5O_2(g) \rightarrow CaSO_4(s)$	−502.3	
	$R_{sulp} = k_{sulp}\rho_s W_{CaO} W_{SO_2} W_{O_2}$		[20]
	$k_{sulp} = 4.0(-3.843T + 5640)\exp\left(-\frac{8810}{T}\right)$		[20]
Direct Sulphation	$CaCO_3(s) + SO_2(g) + 0.5O_2(g) \rightarrow CaSO_4(s) + CO_2$	−324.1	
	$R_{dirs} = k_{dirs}\rho_s W_{CaCO_3} C_{SO_2}^{0.9} C_{CO_2}^{-0.75} C_{O_2}^{0.001}$		[15]
	$k_{dirs} = 0.01\exp\left(-\frac{3031}{T}\right) A_{m,CaCO_3} M_{CaCO_3}$		[15]
	$A_{m,CaCO_3} = 300\ [\mathrm{m^2/kg}]$		[15]
Desulphation	$CaSO_4(s) + CO(g) \rightarrow CaO(s) + SO_2 + CO_2$	219.3	
	$R_{desu} = k_{desu}\rho_s W_{CaSO_4} C_{CO}$		[15]
	$k_{desu} = 0.005\exp\left(-\frac{10000}{T}\right) A_{m,CaSO_4} M_{CaSO_4}$		[15]
	$A_{m,CaSO_4} = 100\ [\mathrm{m^2/kg}]$		[15]
Boudouard	$C(s) + CO_2(g) \rightarrow 2CO(g)$	172.4	
	$R_{boud} = k_{boud}\rho_{char} W_{char,C}$		[21]
	$k_{boud} = 2.11\times10^7\exp\left(-\frac{219000}{RT}\right) p_{CO_2}^{0.36}[\mathrm{bar}]$		[21]
Water-gas	$C(s) + H_2O(g) \rightarrow CO(g) + H_2(g)$	131.3	
	$R_{wg} = k_{wg}\rho_{char} W_{char,C}$		[22]
	$k_{wg} = 1.23\times10^7\exp\left(-\frac{198000}{RT}\right) p_{H_2O}^{0.75}[\mathrm{atm}]$		[22]
Methanation	$C(s) + 2H_2(g) \rightarrow CH_4(g)$	−74.6	
	$R_{mf} = k_{mf}\rho_{char} W_{char,C}$		[23]
	$k_{mf} = 16.4\exp\left(-\frac{94800}{RT}\right) p_{H_2}^{0.93}[\mathrm{MPa}]$		[23]
Water-gas-Shift	$CO(g) + H_2O(g) \rightarrow H_2(g) + CO_2(g)$	−41.1	
	$r_{wgs} = k_{wgs}(C_{CO}C_{H_2O} - C_{CO_2}C_{H_2}/K_{wgs})f_{wgs}$		[24]
	$k_{wgs} = 2.78\exp\left(-\frac{12560}{RT}\right)$		[24]
	$K_{wgs} = 0.0265\exp\left(\frac{3956}{T}\right)$		[23]
	$f_{wgs} = 0.075$		

Table 3
Reaction rate parameters for homogeneous combustion reactions.

Reaction equation	ΔH_{298K} [kJ/mol]	gas	A_0	a_1	a_2	a_3	a_4	T_e	Ref.
$C_2H_4 + 3O_2 \rightarrow 2CO + 2H_2$	−1323.2	C_2H_4	6.3×10^7	0.0	0.1	1.65	0.0	15106	[26]
$CH_4 + 0.5O_2 \rightarrow CO + 2H_2$	−802.6	CH_4	3.6×10^{11}	−1.0	1.0	1.0	0.0	15700	[27]
$H_2S + 1.5O_2 \rightarrow SO_2 + H_2O$	−518.0	H_2S	2.8×10^9	0.0	1.074	1.084	0.0	18956	[28]
$CO + 0.5O_2 \rightarrow CO_2$	−283.0	CO	7.3×10^{14}	0.0	1.0	0.25	0.5	34745	[29]
$H_2 + 0.5O_2 \rightarrow H_2O$	−241.8	H_2	1.6×10^9	−1.5	1.5	1.0	0.0	3430	[30]
$C_7H_8 + 3.5O_2 \rightarrow 7CO + 4H_2$	−3772.0	C_7H_8	5.0×10^6	0.0	0.1	1.85	0.0	15106	[26]
$NH_3 + 1.25O_2 \rightarrow NO + 1.5H_2O$	−902.1	NH_3	1.9×10^9	0.0	0.86	1.04	0.0	19655	[31]

$$\rho_s(h) = [\rho_b - \rho_e\exp(Kh_e)]\exp(-ah) + \rho_e\exp[K(h_e - h)], \quad (18)$$

where ρ_b is the bottom density, ρ_e is the exit density at the elevation h_e, a represents the splash zone decay coefficient and K represents the transport zone decay coefficient. Empirical correlations for decay coefficients a and K [32] are given in Eqs. (19) and (20), respectively.

$$a = \frac{4u_t}{u_{grid}} \quad (19)$$

$$K = \frac{0.23}{u - u_t}, \quad (20)$$

where u is the superficial gas velocity at the transport zone, u_t is the terminal velocity of the particle, and u_{grid} is the superficial gas

velocity at the grid. Solid density at the exit is calculated with a linear function according to Eq. (21).

$$\rho_e = \rho_{s,av}\frac{u - u_t}{u_{pn} - u_t} \tag{21}$$

where $\rho_{s,av}$ is the average solid density in the reactor, and u_{pn} represents the corresponding transport velocity of the gas. The solid mass flow rate out from the reactor is approximated with a semi-empirical correlation given in Eq. (22) by Ylätalo [33].

$$q_{m,s,e} = 0.85 u A_e \rho_e^{0.8} \tag{22}$$

3. Simulation setup for coupled SEG reactor system

The SEG configuration was built by coupling two CFB reactors together. The reactor coupling was done by connecting solid streams from the reactor to another. The coupled reactor system is illustrated in Fig. 3. Both reactors have a circular cross-section, straight bottom and freeboard sections, and a conical frustum between these sections. On design basis, 100 MW_{th} fuel power and superficial gas velocity of 5 m/s in both reactor were used. Steam to Carbon ratio (S/C) on a molar basis was fixed to 1.5.

The dimensions of the reactors and material properties for char and limestone are given in Table 4.

Ten operation points were investigated, covering the SEG operation range for producer gas Module from 2 to 0.7. Definition for producer gas module M is given in the Eq. (1). The SEG operation was investigated with a temperature limit of 950°C for the combustor. A constant heat loss of 20.0 kW/m was applied to model a heat loss of the reactors. Cyclone efficiencies after the reactors were set for limestone, ash, and char separately with values of 0.999, 0.995, and 0.99, respectively. The maximum carbonation degree for the limestone was set to 0.25 as mass-based. Boundary conditions for the operation points are presented in Table 5.

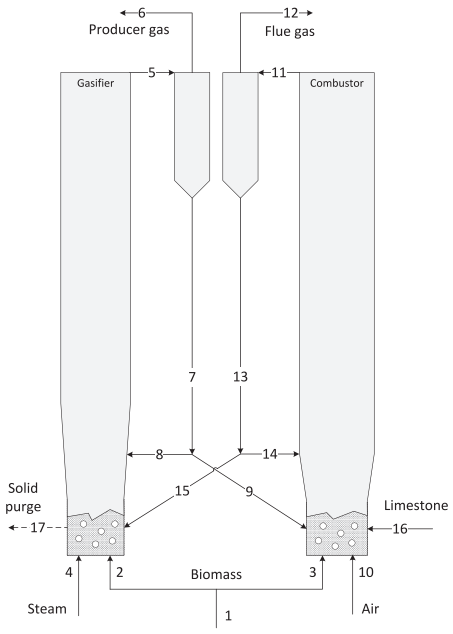

Fig. 3. SEG configuration with connection streams.

Table 4
Dimensions of the SEG reactors and solid material properties.

	Gasifier	Combustor
Height of the bottom section, m	2.3	2.2
Height of the frustum section, m	4.00	2.00
Height of the reactor, m	20.00	20.00
Diameter of the grid, m	2.35	2.51
Diameter of the freeboard, m	2.88	3.09
Number of nodes in bottom section	5	5
Number of nodes in frustum section	8	4
Number of nodes in freeboard section	27	31
Elevation of secondary gas feed, m	1.0	1.0
Elevation of tertiary gas feed, m	2.0	2.0
Elevation of input solid flow channel, m	0–0.9	0–0.9
Elevation of external circulation channel, m	0–0.9	0–0.9
Solid exit to another reactor, m	18.00	18.00
Limestone particle diameter, μm	150	150
Limestone particle density, kg/m^3	3000	3000
Limestone specific heat, J/kgK	1050	1050
Char particle diameter, μm	300	300
Char particle density, kg/m^3	550	550
Wood pellet particle diameter, mm	6	6

4. Results and discussion

1D simulation results for the industrial-scale SEG system is shown in ten operating points (OP) covering an operational range for producer gas M value from 2.17 (OP1) to 0.7 (OP10). The Module range is achieved within the gasifier temperature range of 730°C (OP1) to 786°C (OP10). 1D simulation results for producer gas yield and composition are compared against experimental results [13] and an SEG review study by Fuchs et al. [8]. Simulated temperature range and solid's circulation rates in the SEG system are illustrated in Fig. 4.

The temperature range is achieved by changing the fuel feed ratio to the combustor and controlling the temperature difference between the reactors with system hydrodynamics. Increasing the solid's inventory or gas velocity will lead to a higher solid's circulation rate and a smaller temperature difference between the reactors. In the SEG system, the gasifier's temperature is the most dominant factor in defining SEG performance. The gasifier temperature will determine the producer gas yield and composition by carbonation and water-gas shift reactions. Simulated producer gas yield is presented in Fig. 5, which is consistent with the SEG range by review work of Fuchs et al. [8].

Simulation results for the main produced gas concentrations and corresponding producer gas module M are presented in Fig. 6. All the main gas concentrations are consistent with the SEG range by review work of Fuchs et al. [8] and with experimental data for wood pellets [13] with steam to carbon ratio of 1.5. Estimation for producer gas module *M* was achieved within the investigated temperature range.

In the current simulation approach, hydrocarbons are considered only in gaseous form and are divided into three groups: 1) methane CH_4 2) light hydrocarbons C_2H_4 and 3) heavy hydrocarbons (i.e., tars) C_7H_8. Simulation results for hydrocarbons in producer gas are illustrated in Fig. 7. Amounts of the hydrocarbons in the producer gas are consistent with the SEG range by review work of [8] and with experimental data [13].

Table 5
Boundary conditions for the SEG simulations. Stream numbers (S#) refer to numbering in Fig. 3.

	S#	OP1	OP2	OP3	OP4	OP5	OP6	OP7	OP8	OP9	OP10
Fuel feed, kg/s	1	6.644									
Fuel feed, MW	1	108.8									
Fuel to combustor, %	3	1	2	3	4	5	6	6	6	6	6
S/C, mol/mol	4/2	1.5									
CO_2 feed[a], kg/s	4	0.2									
CO_2 feed[a], °C	4	25									
Steam, °C	4	200	200	200	200	200	200	300	400	400	400
O_2, v − $\%_{db}$	12	3.0	3.0	3.0	3.0	3.0	3.0	3.5	4.7	4.7	4.7
Air, °C	10	250									
$CaCO_3$, kg/s	16	0.5									
$CaCO_3$, °C	16	20									
Grid over pressure[b], Pa	4,10	4500	4500	4500	4500	4500	4500	4500	4750	5000	5250
Exit pressure, kPa	6,12	143									
Solid purge, kg/s	17	0.163	0.156	0.150	0.144	0.138	0.131	0.122	0.097	0.088	0.080

[a] Sealing gas.
[b] Pressure difference caused by the solid material in the reactor.

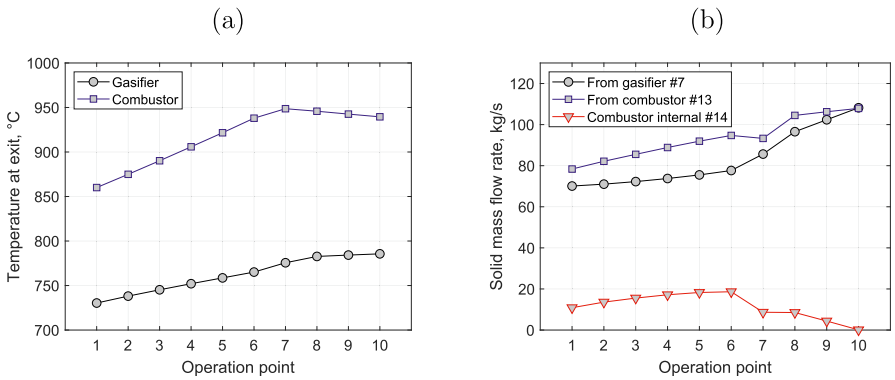

Fig. 4. Simulated temperatures (a) and mass flow rates (b) from the gasifier and the combustor.

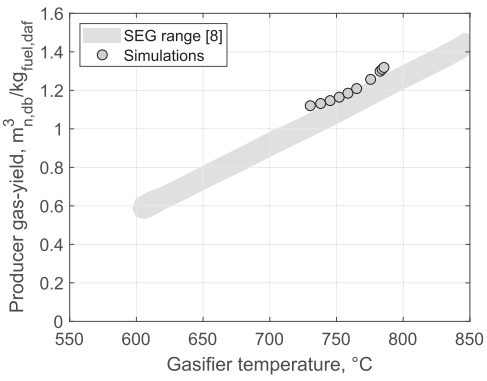

Fig. 5. Producer gas yields a function of gasifier peak temperature.

Overall performance indicators for the SEG system can be derived using a producer gas yield and composition data. Cold gas efficiency (CGE) values have been derived for the producer gas considering different gas species. The general form for CGE in lower heating value basis is given in Eq. (23).

$$\mathrm{CGE} = \frac{q_{m,pg} \sum x_i \mathrm{LHV}_i}{P_{fuel}} \tag{23}$$

where $q_{m,pg}$ is the producer mass flow rate, x_i is mass fraction of gas species i with lower heating value LHV_i, and P_{fuel} is fuel power fed to the gasifier in LHV basis. Simulated CGE values with and without methane and light hydrocarbons are illustrated in Fig. 8.

In the CGE calculations, tars are excluded. Maximum CGE = 75.4% with methane and light hydrocarbons is obtained at OP10 in the gasifier temperature of 786°C. Throughout the investigated temperature range, the methane and light hydrocarbon part in the CGE are approximately 29%-units. Methane and light hydrocarbons should be exploited in downstream processes to capture fuel power most efficiently. Carbon conversion (CC) into the producer gas, tar, char, and $CaCO_3$ is investigated and determined by the Eq. (24), considering the effect of CO_2 sealing gas.

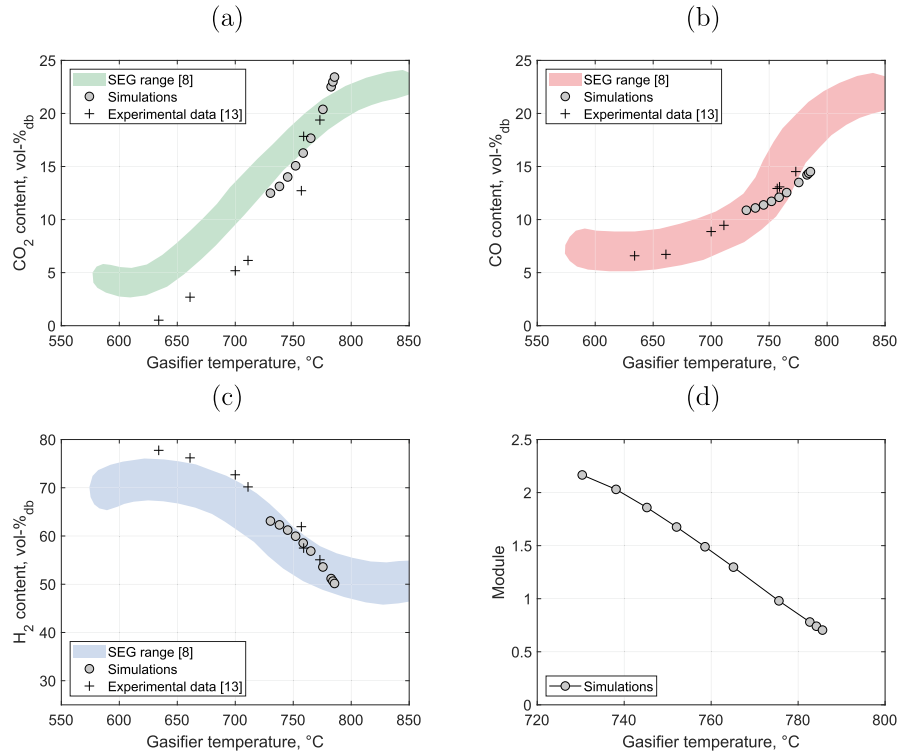

Fig. 6. Concentrations of main producer gas species (a) CO_2, (b) CO, (c) H_2 and corresponding module M in (d).

$$CC_i = \frac{q_{m,C,i}}{q_{m,C,fuel} + q_{m,C,CO_2}} \tag{24}$$

Carbon conversion and carbon transport to combustor are presented in Fig. 9.

The carbon conversion to char is slightly decreasing as the temperature is increased. This is mainly caused by the fuel decomposition model that forms less char in higher temperatures, and there is a slight increase in char gasification on the elevated temperatures. Carbon conversion to Calcium material is reduced significantly on the elevated temperatures shifting the carbon conversion towards producer gas. On the elevated temperatures, gasifier operation approaches the carbonation equilibrium reducing the CO_2 capture. The carbon transport from the gasifier to the combustor is compared with the model prediction by Fuchs et al. [8]. Simulation results are consistent with the model prediction by Fuchs et al. [8].

Carbonation and water-gas shift reactions are the most dominant SEG reactions, and these reactions mainly define the overall system performance. For these reactions, reaction rate definitions according to Table 2 are used. As a result of reaction kinetics in local system conditions, both reactions approach the thermodynamic equilibrium as operating temperature increases. The deviation from the equilibrium is determined by the expression given in Eq. (25).

$$p\delta_{eq} = \log_{10}\left[\frac{\prod_i p_i^{\nu_i}}{K_p(T)}\right] \tag{25}$$

The deviation from the equilibrium for the water-gas shift and the carbonation reactions are shown in Fig. 10.

In addition to the overall SEG results, the model provides 1D profile results for the reactors. Temperature profiles along the reactor height are presented in Fig. 11 for OP1 and OP10. Almost uniform temperature is predicted for both reactors with respect to the reactor height in the investigated operation range. The maximum of 50°C temperature difference was predicted inside the reactors.

Carbonation, calcination, and water-gas-shift reaction are the most dominant SEG reactions to determine the local gas concentrations inside the reactors. Reaction rates for these reactions are illustrated in Fig. 12, at OP1 and OP10.

At OP1, the gasifier is entirely on the carbonation side, and the combustor is fully on the calcination side. At OP10, the bottom part of the gasifier is on the calcination side. Above 5 m, carbonation occurs until the top of the gasifier. The actual carbonation rate at OP10 is smaller compared to OP1, resulting smaller amount of $CaCO_3$ to be transferred to the combustor. At OP10, $CaCO_3$ fed to the reactor is fully calcined already at the bottom part of the combustor.

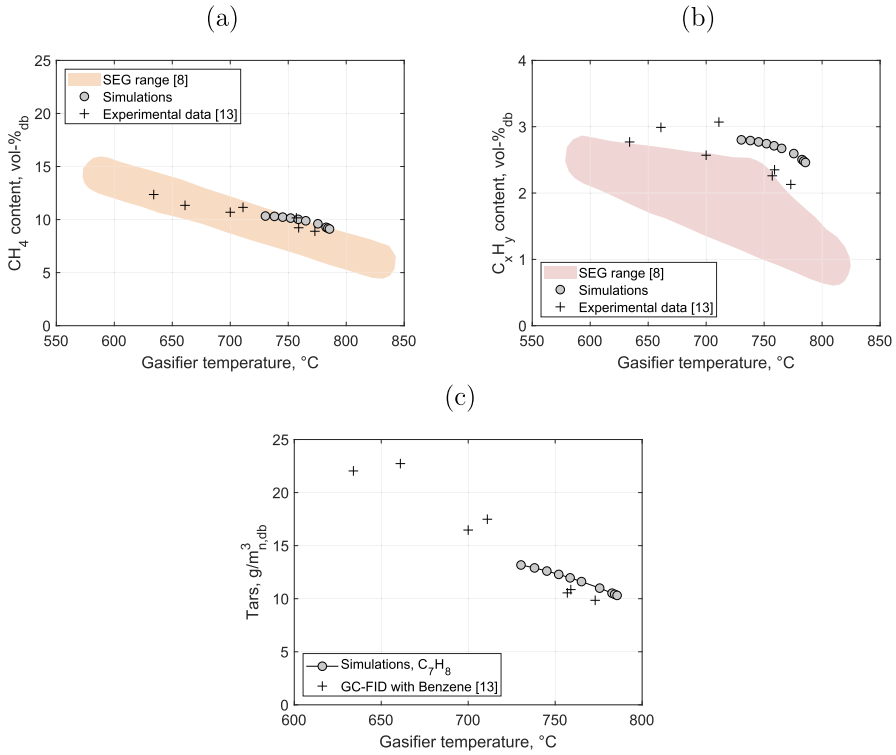

Fig. 7. Concentrations of hydrocarbons in producer gas. (a) methane CH_4, (b) light hydrocarbons C_xH_y and (c) tars C_7H_8.

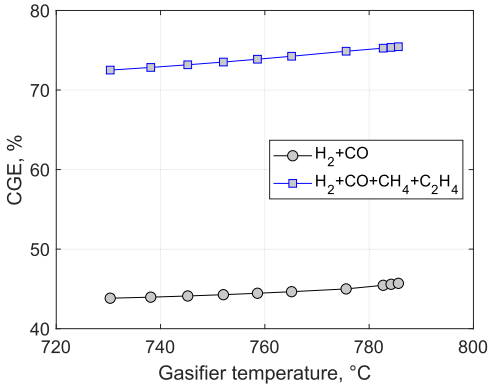

Fig. 8. Cold gas efficiencies (CGE) in a function of gasifier temperature. Simulation data with and without methane and light hydrocarbons.

In both operating points, water-gas shift reaction rate profiles are on a similar magnitude. A shift of the carbonation-calcination reaction direction at OP10 is illustrated in Fig. 13, where the local CO_2 concentration is plotted against local temperature that crosses the reaction equilibrium curve.

At OP1, combustor temperature is closer to the carbonation equilibrium resulting in slow calcination and partially calcined limestone material transfer to the gasifier. Increasing the combustor temperature at OP1 would increase the calcination rate leading to the fully calcined material output.

Simulated conversion degree profiles for $CaCO_3$ are presented in Fig. 14 for OP1 and OP10.

Minimal $CaCO_3$ content at the combustor bottom is observed at OP10. This is due to the low CO_2 capture on the gasifier side, leading to a low $CaCO_3$ concentration in the solids flow, as well as the relatively high combustor temperature. The low $CaCO_3$ concentration in the solids input stream keeps the $CaCO_3$ level very low on the combustor side. The high temperature of the combustor accelerates the calcination reaction, leading to the disappearance of the $CaCO_3$ fraction above the lower reaction zone. At OP1, about 1 m-% of $CaCO_3$ is estimated at combustor exit. On the gasifier side, small $CaCO_3$ content is observed at OP10 due to operation near the carbonation equilibrium. Maximum $CaCO_3$ conversion is observed at OP1 in the gasifier's exit with a value of 11 m-%. That is much

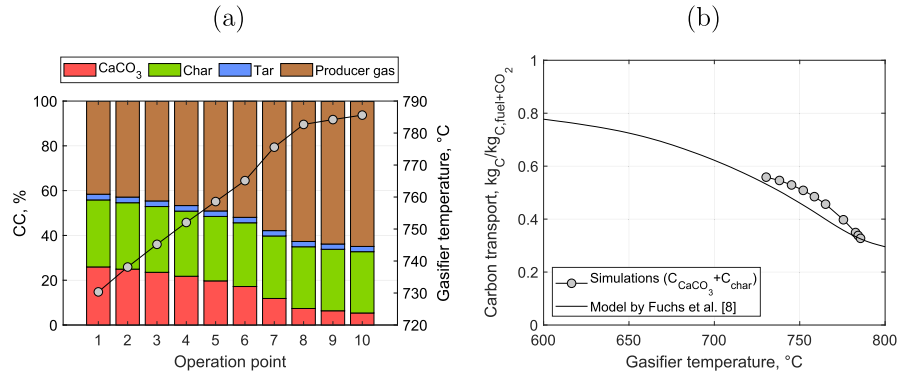

Fig. 9. (a) Carbon conversion to produced gas, tar, char and $CaCO_3$. Gasifier temperature presented with circles. (b) Carbon transport to combustor with char and $CaCO_3$.

smaller compared to the maximum $CaCO_3$ conversion degree of 25 m-%, set for the limestone material. A negligible amount of $CaSO_4$ was observed within the lime.

As a result of the reaction scheme connected with mass and energy balances, gas concentration profiles are obtained. The gas concentration profiles for the main gas species and both reactors are illustrated in Fig. 15.

In operation points OP1 and OP10, the effect of water-gas shift reaction can be observed. The water-gas shift reaction will reduce the CO and H_2O contents along with the reactor height. At the same time, H_2 and CO_2 contents are increasing. At OP1, H_2 content is increasing with a higher rate than CO_2. The formed CO_2 by the water-gas shift is captured and reduced by the carbonation reaction. At OP10, reduced CO_2 content at the combustor side is observed due to reduced CO_2 capture on the gasifier side. Gas concentrations on the gasifier side start to remain constant after 15 m and on the combustor side after 10 m of height.

The water-gas shift reaction balance profile is determined by using the gas concentration profiles of the gasifier. The water-gas shift reaction balance values in a function of corresponding local temperature are presented in Fig. 16 with the theoretical reaction equilibrium.

The water-gas shift reaction approaches the equilibrium but will not reach it. The water-gas shift reaction balance values for the gasifier output are shown in Fig. 10 expressed as a logarithmic distance from the equilibrium.

5. Conclusions

In this work, sorption enhanced biomass gasification on an industrial scale was studied. A 1D modeling tool for coupled reactors was used to design and investigate the SEG process on a $100MW_{th}$ scale. Based on the simulations, it was possible to demonstrate the wide operating range of the SEG process, where it is possible to produce producer gas with different compositions suitable for downstream biofuel syntheses. The optimal producer gas composition without external hydrogen for the downstream DME synthesis was achieved at gasifier temperature 730°C: 63 $\%_{vol,db}$ H_2, 11 $\%_{vol,db}$ CO, 13 $\%_{vol,db}$ CO_2, corresponding Module value of 2.1. The modeling method used took into account the hydrodynamic solids profiles and flow rates between the reactors. The thermal capacity

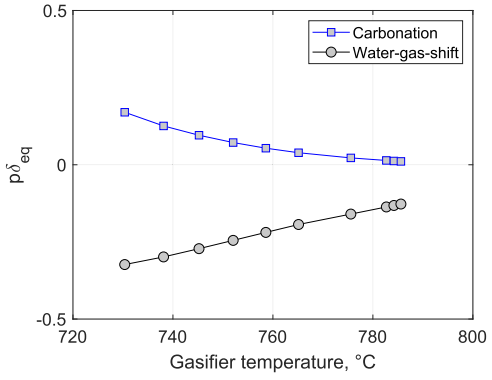

Fig. 10. Deviation of the equilibrium for carbonation and water-gas shift reactions.

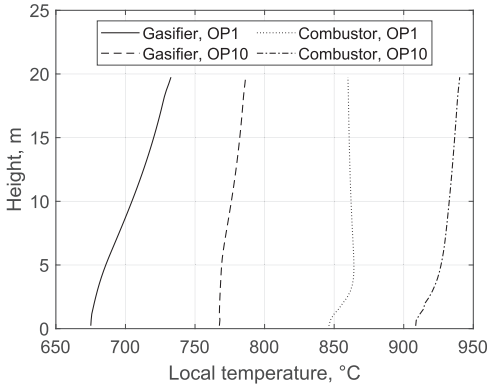

Fig. 11. OP1 and OP10 temperature profiles for both reactors along with the reactor height.

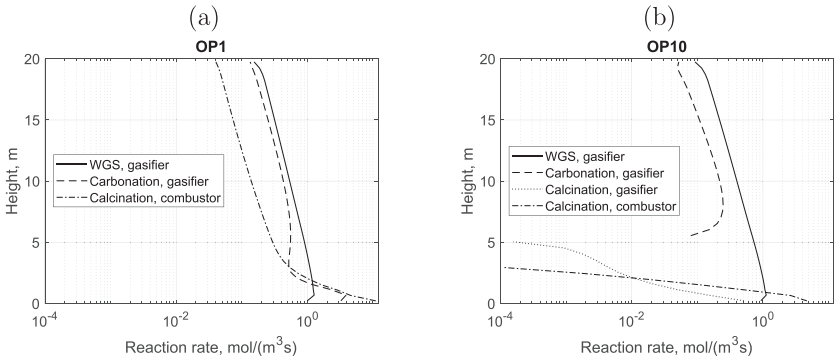

Fig. 12. Reaction rates for carbonation, calcination, and water-gas-shift along the reactor height. (a) OP1 and (b) OP10.

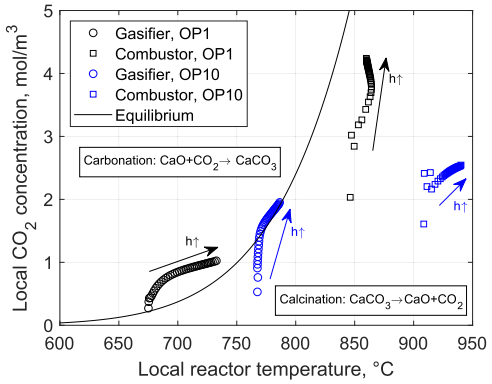

Fig. 13. Local CO_2 concentration in a function of local temperature with carbonation-calcination reaction equilibrium. Arrows show the direction of the reactor's vertical axes.

flows according to the solids flow rates were taken into account in the connected reactors' energy balances, giving an accurate physical description of the reactor temperature levels. Also, the flow rates of solids, including their conversion degrees, provided a sound basis for considering heterogeneous reactions in reactors with sufficient accuracy. Unlike before, the modeling used a temperature-dependent fuel decomposition model, which gave a more detailed description of the fuel's behavior under the conditions of the reactors. This was able to guarantee more accurate source terms for the reaction descriptions, and ultimately a reliable prediction of the yield and composition of the product gas was achieved. This also included a forecast for the yields of light and heavy hydrocarbons to obtain more accurate predictions for the elemental distribution of producer gas. The simulation results obtained correspond to the results presented in the literature for a similar type of process. The work was also able to demonstrate the suitability of CFB-CFB for SEG processes using a simulation model. In the future, this investigation can be extended to part load cases where the total fuel feed to the SEG process is changed. In this way, it is possible to consider lower and higher gasifier temperatures, whereby the yield and composition of the product gas can be controlled over a broader range. Concerning the physical sub-

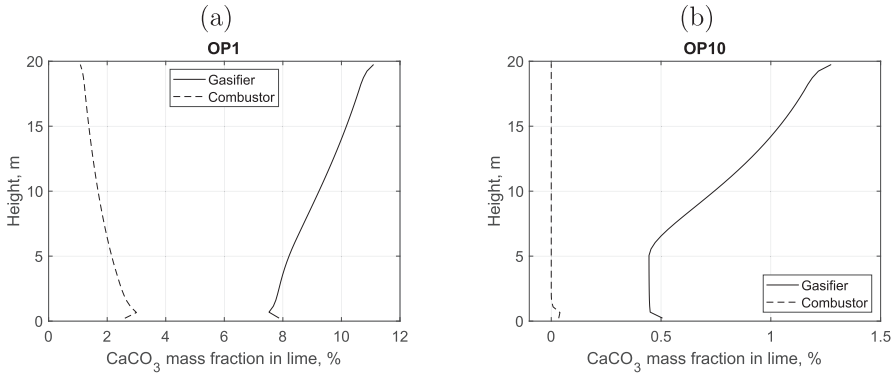

Fig. 14. Local $CaCO_3$ conversion degrees. (a) OP1 and (b) OP10.

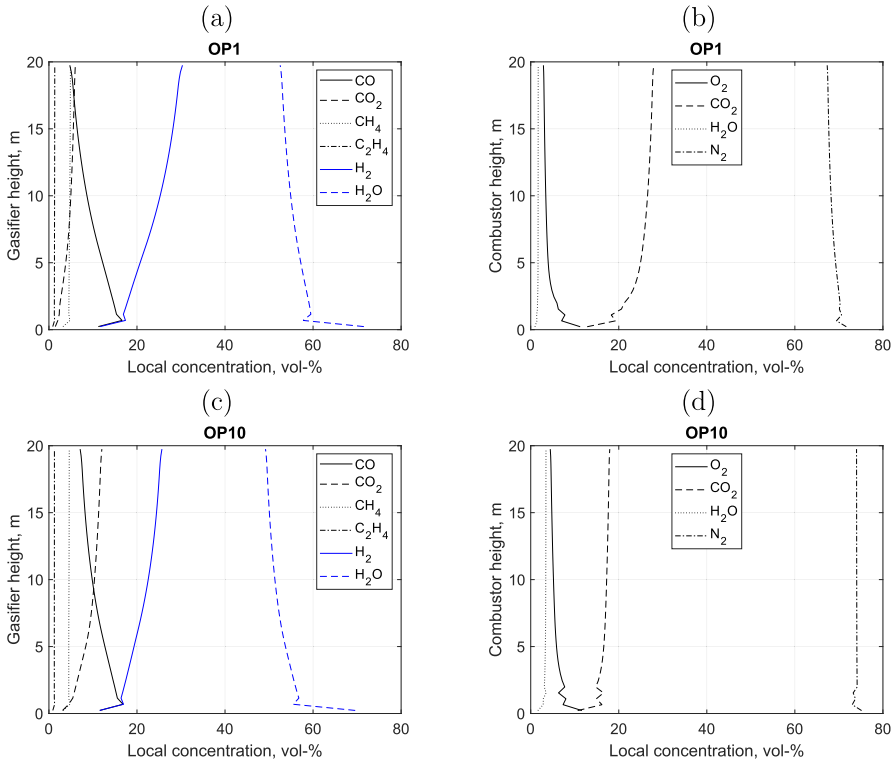

Fig. 15. Gas concentration profiles for both reactors at (a) OP1 and (b) OP10.

processes, it was found that the lime reactions and the water-gas shift reaction were the most significant reactions together with the decomposition of the fuel, which affect the yield and composition of the product gas. For lime reactions, an appropriate temperature level must be obtained for the carbonation in the gasifier in order to be able to control the CO_2 capture and water-gas shift reactions that ultimately determine the quality of the producer gas. A sufficiently high-temperature level must be reached on the combustor side so that the calcination is as efficient as possible, and the degree of lime material conversion will not limit the CO_2 capture in the gasifier. For the water-gas shift reaction, it is noted that the reaction does not reach equilibrium under SEG conditions, and this should be taken into account when using simplified reaction equilibrium modeling techniques. One important model development area is related to the hydrodynamics of the CFB reactor. For hydrodynamics, computational fluid dynamics can provide a good model development support. More accurate hydrodynamic submodels can provide a better prediction for intra- and inter-reactor flows, giving a more accurate model result for heat capacity flows. This also leads to a better and physically valid estimation for the operation of the whole process. The presented modeling method also provides an opportunity to study and compare different biomasses' suitability for the SEG process based on dual bed arrangement. However, this requires adequate preliminary data and physical sub-models for different biomasses' behavior under SEG conditions. The modeling method presented in this

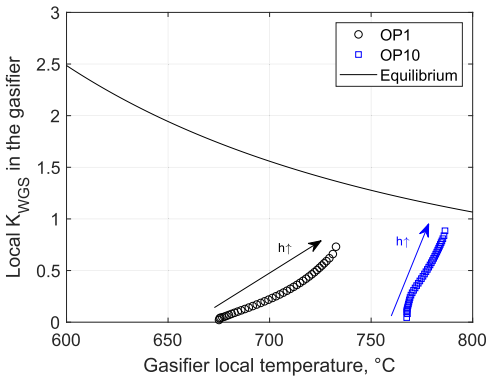

Fig. 16. Local water-gas shift reaction balance value in a function of local temperature. Arrows show the direction of the reactor's vertical axes.

work does not place constraints on the biomass under consideration, as long as it is possible to find and use sufficiently accurate descriptions of fuel decomposition at different temperatures, as well as main reaction descriptions. An industrial-scale plant's operating values presented in this work provide essential information to support plant design and assess plant operating performance and costs.

Author statement

Jouni Ritvanen: Conceptualization, Methodology, Software, Formal analysis, Visualization, Writing – original draft. Kari Myöhänen: Methodology, Writing – review & editing, Antti Pitkäoja: Visualization, Methodology, Writing – review & editing, Timo Hyppänen: Supervision, Writing – review & editing

Declaration of competing interest

The authors declare that they have no known competing financial interests or personal relationships that could have appeared to influence the work reported in this paper.

Acknowledgements

This work in FLEDGED project has received funding from the European Union's Horizon 2020 research and innovation programme under grant agreement No 727600.

Nomenclature

γ_i	Fuel decomposition model parameter, [−]
ρ	Density, [kg/m^3]
ρ_b	Bottom density, [kg/m^3]
ρ_e	Exit density, [kg/m^3]
A	Cross section area of the reactor, [m^2]
a, K	Decay parameters
C	Molar concentration, [mol/m^3]
E	Energy, [J]
f	Calibration factor, [−]
h	Height, [m]
i	Index, [−]
j	Index, [−]
k	Reaction rate factor, [1/s]
M	Module, $M = (y_{H_2} - y_{CO_2})/(y_{CO} + y_{CO_2})$
m	Mass, [kg]
M_i	Molar mass, [g/mol]
n_{tot}	Total number of 1D elements, [−]
P	Power, [W]
p	Pressure, [bar, atm, Pa]
$p\delta_{eq}$	Deviation from the reaction equilibrium, [−]
q_m	Mass flow rate, [kg/s]
q_r	Reaction heat, [W]
q_{adv}	Advection, [W]
q_{disp}	Energy dispersion, [W]
q_{ht}	Heat transfer, [W]
R	Universal gas constant, [J/(molK)]
R_i	Reaction rate, [kg/(m^{3}s)]
r_i	Reaction rate, [mol/(m^{3}s)]
$r_{j,i}$	Reaction rate, [kg/s]
T	Temperature, [K]
t	Time, [s]
T_{gasif}	Average gasifier temperature, [°C]
u	Gas superficial velocity, [m/s]
u_t	Terminal velocity, [m/s]
u_{pn}	Transport velocity, [m/s]
W	Solid's mass fraction, [−]
x	Mass fraction, [−]
ar	As-received fuel
av	Average
BFB	Bubbling fluidized bed
boud	Boudouard reaction
calc	Calcination reaction
carb	Carbonation reaction
CC	Carbon conversion
CFB	Circulating fluidized bed
CGE	Cold gas efficiency
daf	Dry ash free fuel
db	Dry basis
desu	Desulphation reaction
dirs	Direct sulphation reaction
DME	Dimethyl ether
ds	Dry fuel
eq	Equilibrium
F	Fuel
LHV	Lower heating value, [MJ/kg]
mf	Methanation reaction
pg	Producer gas
S/C	Steam to carbon ratio, [mol/mol]
SEG	Sorption enhanced gasification
sulp	Sulphation reaction
vol	Volatile
wg	Water-gas reaction
wgs	Water-gas shift reaction

References

[1] European commission A. European strategy for low-Emission Mobility 2016. 2016.
[2] Pelkmans, L. European Union - 2018 update, Bioenergy policies and status of implementation. 2018.
[3] Corella J, Toledo JM, Molina G. A review on dual fluidized-bed biomass gasifiers. Ind Eng Chem Res 2007;46:6831–9. https://doi.org/10.1021/ie0705507.
[4] Pfeifer C. 22 - sorption-enhanced gasification. In: Scala F, editor. Fluidized bed technologies for near-zero emission combustion and gasification. Woodhead Publishing Series in Energy; Woodhead Publishing; 2013, ISBN 978-0-85709-541-1. p. 971–1001. https://doi.org/10.1533/9780857098801.4.971.
[5] Fuchs J, Schmid JC, Benedikt F, Müller S, Hofbauer H, Stocker H, Kieberger N, Bürgler T. The impact of bed material cycle rate on in-situ CO2 removal for sorption enhanced reforming of different fuel types. Energy 2018;162:35–44. https://doi.org/10.1016/j.energy.2018.07.199.
[6] Benedikt F, Schmid J, Fuchs J, Mauerhofer A, Müller S, Hofbauer H. Fuel flexible gasification with an advanced 100 kW dual fluidized bed steam gasification pilot plant. Energy 2018;164:329–43. https://doi.org/10.1016/j.energy.2018.08.146.
[7] Schweitzer D, Beirow M, Gredinger A, Armbrust N, Waizmann G, Dieter H, Scheffknecht G. Pilot-scale demonstration of oxy-SER steam gasification: production of syngas with pre-combustion CO2 capture. Energy Procedia 2016;86:56–68. https://doi.org/10.1016/j.egypro.2016.01.007.
[8] Fuchs J, Schmid JC, Müller S, Mauerhofer AM, Benedikt F, Hofbauer H. The impact of gasification temperature on the process characteristics of sorption enhanced reforming of biomass. Biomass Conversion and Biorefinery; 2019. https://doi.org/10.1007/s13399-019-00439-9.
[9] Hejazi B, Grace JR, Bi X, Mahecha-Botero A. Steam gasification of biomass coupled with lime-based CO2 capture in a dual fluidized bed reactor: a modeling study. Fuel 2014;117:1256–66. https://doi.org/10.1016/j.fuel.2013.07.083.
[10] Detchusananarda T, Ponpesha P, Saebeab D, Authayanunc S, Arpornwichanopa A. Modeling and analysis of sorption enhanced chemical looping biomass gasification. Chemical Engineering Transactions 2017;57:103–8. https://doi.org/10.3303/CET1757018.
[11] Beirow M, Parvez A, Schmid M, Scheffknecht G. A detailed one-dimensional hydrodynamic and kinetic model for sorption enhanced gasification. Appl Sci 2020;10(17). https://doi.org/10.3390/app10176136.
[12] Yan L, Cao Y, He B, Li X. Calcium looping enhanced biomass steam gasification in a two-stage fluidized bed gasifier. Energy Fuels 2018;32(8):8462–73. https://doi.org/10.1021/acs.energyfuels.8b01414.
[13] Hafner S, Schmid M. FLEDGED Deliverable D3.4 - Final experimental results on SEG process experiments at pilot (TRL5) scale for stationary and flexible operating regimes. 2020.
[14] Neves D, Thunman H, Matos A, Tarelho L, Gómez-Barea A. Characterization

and prediction of biomass pyrolysis products. Prog Energy Combust Sci 2011;37(5):611–30. https://doi.org/10.1016/j.pecs.2011.01.001.
[15] Myöhänen K. Modelling of combustion and sorbent reactions in three-dimensional flow environment of a circulating fluidized bed furnace. Ph.D. thesis; Lappeenranta University of Technology; 2011. http://urn.fi/URN:ISBN:978-952-265-161-7.
[16] Fang F, Li ZS, Cai NS. Experiment and modeling of CO2 capture from flue gases at high temperature in a fluidized bed reactor with Ca-based sorbents. Energy Fuels 2009;23(1):207–16. https://doi.org/10.1021/ef800474n.
[17] Martínez I, Grasa G, Murillo R, Arias B, Abanades JC. Kinetics of calcination of partially carbonated particles in a Ca-looping system for CO2 capture. Energy Fuels 2012;26(2):1432–40. https://doi.org/10.1021/ef201525k.
[18] Silcox GD, Kramlich JC, Pershing DW. A mathematical model for the flash calcination of dispersed calcium carbonate and calcium hydroxide particles. Ind Eng Chem Res 1989;28(2):155–60. https://doi.org/10.1021/ie00086a005.
[19] Grasa G, Murillo R, Alonso M, Abanades JC. Application of the random pore model to the carbonation cyclic reaction. AIChE J 2009;55(5):1246–55. https://doi.org/10.1002/aic.11746.
[20] Rajan RR, Wen CY. A comprehensive model for fluidized bed coal combustors. AIChE J 1980;26(4):642–55. https://doi.org/10.1002/aic.690260416.
[21] Risnes H, Sorensen L, Hustad J. CO2 reactivity of chars from wheat, spruce and coal. In: Bridgewater A, editor. Progress in thermochemical biomass conversion. Oxford: Blackwell Science; 2001. p. 61–72.
[22] Hemati M, Laguerie C. Determination of the kinetics of the sawdust steam-gasification of charcoal in a thermobalance. Entropie 1988;142:29–40.
[23] Hejazi B, Grace J, Bi X, Mahecha-Botero A. Kinetic model of steam gasification of biomass in a bubbling fluidized bed reactor. Energy Fuels 2017;31(2):1702–11. https://doi.org/10.1021/acs.energyfuels.6b03161.
[24] Biba V, Macák J, Klose E, Malecha J. Mathematical model for the gasification of coal under pressure. Ind Eng Chem Process Des Dev 1978;17(1):92–8. https://doi.org/10.1021/i260065a017.
[25] Basu P. Combustion and gasification in fluidized beds. CRC Press; 2006.
[26] Ansys® Fluent. Release 2020;19.2.
[27] Adánez J, Miranda J, Gavilán J. Kinetics of a lignite-char gasification by CO2. Fuel 1985;64(6):801–4. https://doi.org/10.1016/0016-2361(85)90013-4.
[28] Oguma A, Yamada N, Furusawa T, Kunii D. Preprint for the 11th fall meeting of the soc. Of chem. Eng. Japan 1977:121.
[29] Sergeant GD, Smith IW. Combustion rate of bituminous coal char in the temperature range 800 to 1700 K. Fuel 1973;52(1):52–7. https://doi.org/10.1016/0016-2361(73)90012-4.
[30] Gibson M, Euker C. Mathematical modelling of fluidized bed coal gasification. In: AIChE meeting; 1975.
[31] Johnson J. Kinetics of coal gasification. New York: John Wiley; 1979.
[32] Johnsson F, Leckner B. Vertical distribution of solids in a CFB-furnace. In: Proceedings of the 13th international conference on fluidized bed combustion. Orlando, USA: ASME; 1995. p. 671–9.
[33] Ylätalo J. Model based analysis of the post-combustion calcium looping process for carbon dioxide capture. Ph.D. thesis. Lappeenranta University of Technology; 2013. http://urn.fi/URN:ISBN:978-952-265-521-9.

Publication V

Pitkäoja, A., Ritvanen, J., Hafner, S., Hyppänen, T. and Scheffknecht, G.
Modeling of Sorbent Enhanced Gasification Utilizing Waste-Derived Fuel

Reprinted with permission from
Proceedings of 13th International Conference on Fluidized Bed Technology,
Vancouver - Virtual event, Canada, 10.-14.05.2021,
© 2021, 13th International Conference on Fluidized Bed Technology

MODELING OF SORBENT ENHANCED GASIFICATION UTILIZING WASTE-DERIVED FUEL

Antti Pitkäoja[1], Jouni Ritvanen[1], Selina Hafner[2], Timo Hyppänen[1] and Günter Scheffknecht[2]

[1] *LUT School of Energy Systems, Lappeenranta-Lahti University of Technology, Yliopistonkatu 34, PO. Box 20, FI-53851 Lappeenranta, Finland*

[2] *Institute of Combustion and Power Plant Technology (IFK), University of Stuttgart, Pfaffenwaldring 23, 70569 Stuttgart, Germany*

*Email: antti.pitkaoja@lut.fi

Abstract

EU strategy for transition to a low-carbon economy sets out a framework and mechanisms to address climate change. A target of 14% renewable fuels usage in the transportation sector by 2030 has been set and, consequently, there is a pressing need to develop effective and cost-efficient ways to produce transportation fuels from renewable sources. Efficient use of existing resources such as a low value waste reduces need of fresh resources and reduces consumption of non-renewable sources. Sorbent enhanced gasification (SEG) is a promising technology for replacing conventional gasification for providing feedstock gas for fuel synthesis processes. The SEG process has been demonstrated at a pilot scale. A 1D bubbling fluidized bed (BFB) gasification reactor model developed for the pilot SEG process is utilized for simulation of waste-derived fuel. Empirical equations for local gas-solid interaction and gasification chemistry have been employed in the model. Process conditions at the bubbling bed and the freeboard sections of the gasification reactor are estimated with the developed model. The modeling results compared against experimental investigations of 200kW_{th} dual fluidized bed facility are with good agreement. The conducted model validation improved understanding of bed material behavior, gasification chemistry and hydrodynamics and their role in SEG reactors under waste gasification conditions.

INTRODUCTION

The Paris climate agreement sets out a framework for EU strategy to transition to low-carbon economy to address climate change. The aim of the EU strategy is to keep average global warming below 2°C compared to the pre-industrial temperatures (Delbeke and Vis, 2016). A target of 14% renewable fuels usage in the transportation sector by 2030 has been set and, consequently, there is a pressing need to develop effective and cost-efficient ways to produce transportation fuels from renewable sources. Efficient use of existing resources such as a low value waste reduces needs of fresh resources and reduces consumption of non-renewable sources. Greenhouse gas emissions from transportation account for almost one quarter of Europe's greenhouse gas emissions and transportation is the main source of air pollution in European cities (European commission, 2016). The majority of emissions from traditional liquid fuels comprises CO_2, NO_X and small particulate emissions. However, gaseous fuels such as dimethyl ether (DME) are free from small particle emissions, which makes them as attractive alternative.

Indirect gasification comprises two interconnected reactors with continuous exchange of material flows. In sorbent enhanced gasification (SEG) reactive bed material is circulated between the reactors. Limestone is commonly used as the bed material and the limestone is carbonated in the gasifier with CO_2 formed in the gasification process and calcined in the combustion reactor. The producer gas of the gasifier can be tailored by changing CO_2 capture of the bed, which influences the yield of the water-gas shift reaction at lower operating

temperatures. Typical operation range for the SEG reactor is between 600-800°C. Feedstock gas of DME synthesis requires certain composition from the producer gas that can be achieved with a certain operating temperature. The capability to tailor the producer gas facilitates flexible use of various solid feedstocks with varying properties.

A 1D BFB gasification model for biomass SEG process has been developed in Pitkäoja et al. (2020). The previously published model is improved to take into account heavy hydrocarbons. The improved model is used to simulate SEG process operating with waste-derived fuel. The purpose of model validation is to provide a better understanding of phenomena's and their role in the SEG process, which can be applied for predicting operation of process under different process conditions. The validation of the model is carried out with steady-state simulations against experimental data published by Hafner et al. (2020) from a dual fluidized bed facility located at the Institute of Combustion and Power Plant Technology (IFK) of the University of Stuttgart.

MODEL DESCRIPTION

The model frame for the BFB SEG process has been developed based on a semi-empirical 1D-approach in Pitkäoja et al. (2020). Fundamental conservation equations for mass and energy for gas and solid phases are implemented in the gasification model frame. The model frame is implemented in Matlab's Simulink environment, where reactor code is resolved using Simulink's embedded computational engine. Spatial derivatives of the reactor model are discretized using a first order upwind scheme for convection terms and time derivatives are resolved using an explicit solver in Simulink. A hydrodynamic model was previously derived in Pitkäoja et al. (2020) based on Kunii and Levenspiel (1991). Heavy hydrocarbons "Tars" were not included in this previous model frame. To model appropriate elemental distribution of the producer gas, it is important to also consider the heavy hydrocarbons. In the current study, the existing model frame is further developed to take into account the heavy hydrocarbon fractions by using a model component. Additional balance was added in the model for the heavy hydrocarbons. The model component for the heavy fractions was selected as C_8H_{10} and C_2H_4 for the light hydrocarbons based on biomass studies. The hydrocarbons (C_2 and C_8) are assumed to be inert gas species only affecting the elemental distribution. The decomposition of the fuel as permanent gases and hydrocarbons is according to following chemical equation:

$$FUEL \rightarrow NH_3 + H_2S + CO + CO_2 + CH_4 + C_2H_4 + C_8H_{10} + H_2 \quad (1)$$

Chemical reactions are modeled according to Table 1. A detailed discussion about the chemical reactions is provided in Pitkäoja et al. (2020).

MODELLING SETUP

Modeling setup is done based on the specification of the pilot gasifier. Only the gasifier is modeled. The facility including gasifier (yellow) and combustor (red) is shown in Fig. 1. For modeling, the gasifier is divided into 40 discrete elements from which 3 were placed on the conical bottom.

Experimental investigations were conducted by Hafner et al. (2020). Two similar batches of waste pellets were used in experiments and characterization of the fuel is provided in Table 2. The gasifier was operated with constant operational parameters that are summarized in Table 3. Simulation boundary conditions, which are summarized in Table 3, were determined from online process measurements and samples of solid material extracted from loop seals. Maximum solid conversion for calcium carbonate is selected as 30m-% based on previous studies on calcium looping process (Ylätalo, 2013).

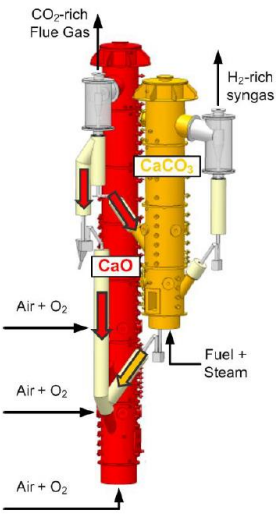

Fig. 1. 200 kWth dual fluidized bed facility at IFK, University of Stuttgart (Hafner et al., 2018).

Table 1. Chemical reactions.

Reaction	Chemical equation	*H* (at 25°C) [J/kg]	Ref
Boudouard	$C(s)+CO_2(g)\rightarrow 2CO(g)$	172400	van den Aarsen et al. (1985)
Water-gas	$C(s)+H_2O(g)\rightarrow H_2(g)+CO(g)$	131300	Nandi and Onischak (1985)
Methanation	$C(s)+2H_2(g)\rightarrow CH_4(g)$	-75000	Hejazi et al. (2017)
Water-gas shift	$CO(g)+H_2O(g)\leftrightarrow CO_2(g)+H_2(g)$	-41100	Biba et al. (1978)
Steam methane reforming	$CH_4(g)+H_2O(g)\leftrightarrow CO(g)+H_2(g)$	206200	Jones and Lindstedt (1988)
Calcination	$CaCO_3(s)\rightarrow CaO(s)+CO_2(g)$	178300	Martinez (2012)
Carbonation	$CaO(s)+CO_2(g)\rightarrow CaCO_3(s)$	-178300	Alonso et al. (2009), Shimizu et al. (1999)
Sulphation	$CaO(s)+SO_2(g)+0.5O_2(g)\rightarrow CaSO_4(s)$	-502100	Rajan and Wen (1980)
De-sulphation	$CaSO_4(s)+CO(g)\rightarrow CaO(s)+SO_2(g)+CO_2(g)$	219200	Myöhänen (2011)
Direct sulphation	$CaCO_3(s)+SO_2(g)+0.5O_2(g)\rightarrow CaSO_4(s)+CO_2(g)$	-323800	Myöhänen (2011)

Table 2. Chemical composition of two batches of pellets used in experimental investigations of the SEG process.

Batch	Proximate analysis				Ultimate analysis					
	Moisture	Ash	Volatiles	Fixed carbon	C	H	N	S	Cl	LHV
	m-%, ar	m-%, ds			m-%, daf					MJ/kg, ar
1	8.0	33.2	60.2	6.7	53.9	6.4	2.5	0.6	1.0	11.6
2	10.7	26.2	65.4	8.4	51.6	6.7	2.6	0.6	1.0	12.7

SIMULATION RESULTS

Validation of the developed reactor model was conducted by introducing the measured operation parameters into the model with appropriate model equations for physical and chemical phenomena. Model equations for chemical reactions were used according to Table 1. Hydrocarbons that were measured from the gasifier were mainly assumed to form during devolatilization (Neves et al., 2011). The devolatilization yield for hydrocarbons were set according to this assumption. Heaviest hydrocarbons were set according to tar measurement (Hafner et al., 2020) and light hydrocarbons according to CH_4 yield of the gasifier. Hydrodynamics scheme is described in details in Pitkäoja et al. (2020). The hydrodynamics scheme was set against pressure measurements of the reactor.

Experimental and simulated temperature profiles are shown in Fig. 2 a). Good match was gained between the simulations and experimental temperatures. A heat source term was applied for the reactor bed to match local temperatures. The heat balance adjustment according to Table 3 is applied for the bed of the gasifier. A constant heat loss was applied at the freeboard in each simulations case. The freeboard heat loss is included in the energy balance adjustment. The approach was used to compensate impacts of uncertainties, such as devolatilization process, solid flow measurement and temperature measurements in the energy balance. A suitable match for temperatures between the simulations and measurements in the bed section is important for model validation, since chemical kinetics are influenced by the local temperature.

The measured producer gas composition against simulation results is shown in Fig. 2 b)-f). Good agreement between the measured producer gas composition and the simulation was achieved at higher temperatures. The model prediction capability on the higher temperatures is more important, since optimal gas composition for DME synthesis is achieved at higher operating temperatures. The relation of gas species is described with module:

$$M = (y_{H_2} - y_{CO_2})/(y_{CO} + y_{CO_2}) \quad (2)$$

The optimal value of the module for DME synthesis is 2 (Hafner et al., 2018), which is achieved at operating temperatures similar to OP 1.3, which is shown in Fig. 2 g).

Table 3. Experimental operation conditions and simulation boundary conditions.

Parameter	OP 1.1	OP 1.2	OP 1.3
Experimental operation conditions			
Fuel feed [kg/h]	45	30	30
Primary gas [kg/h]	30	20	20
Primary gas temperature [°C]		146	
S/C [mol/mol]		1.5	
Fuel batch	1	2	2
Solid make-up to gasifier/combustor [kg/h]	20/0	0/20	0/20
Simulation boundary conditions			
Solid flow from combustor [kg/h]	430	370	520
Temperature of solid flow [°C]	760	770	810
Solid make-up to gasifier ($CaCO_3$)	20	0	0
Material mass fractions at circulation inlet [%]			
CaO	85.4	84.0	65.7
$CaCO_3$	0.5	0.3	0.0
$CaSO_4$	0.0	0.0	0.0
Ash	14.1	15.8	34.3
Solid heat capacity [J/(kg K)]	1000		
Heat balance adjustment [kW/kW_{fuel}]	14.1	15.8	15.8
Heat loss of freeboard [kW/m]	1.5	1.2	1.2

Common for steam gasification processes such as SEG is a low wet CO_2 partial pressure in the reactor. The SEG reactor is operated as carbonator, where the CO_2 is captured by the CaO of the bed material. The low CO_2 partial pressure with reactive bed material produces special operation characteristics for the SEG process, where the gasification process is enhanced by the reactive bed material. The bed material carbonation was measured for each operation point from the pilot process, and in Fig. 2 h), the simulated carbonation is compared against the measurement. Thermodynamic reaction equilibrium according to Stanmore and Gilot (2005) was shifted towards calcination 22°C according to limestone equilibrium modification of Pitkäoja et al (2020). Actual limestone does not follow exactly the theoretical reaction equilibrium in real process conditions because of impurities of the limestone. This remark can be determined from measurements of Hajaligol et al.(1988). The reaction equilibrium plays an important role in the pilot reactor, since the bed of the pilot reactor operates close by the equilibrium, which causes the temperature to govern the carbonation reaction in the bed. Four solid material fractions (CaO, $CaCO_3$, $CaSO_4$ and ash) were included in simulations and material fraction profiles were modeled for each fraction with separate balances for wake and emulsion in the bed. In the pilot reactor high in-bed solid mixing is induced by pilot reactor design, which evens differences in the solid material fractions on vertical direction of the dense bed, which is shown in Fig. 2 i) for $CaCO_3$. The high mixing of solids causes the bed to behave as ideally mixed bed without significant material fraction differences.

CONCLUSIONS

Validation of the 1D BFB gasification model was done at steady-state conditions for a waste-derived fuel. The model was able to capture the most important characteristics of the SEG process and an influence of hydrocarbons to the elemental distribution was considered. The improved model was capable of predicting temperature profiles, bed material conversion and producer gas composition at higher operating temperatures, which is more important than prediction capability of lower operating temperatures, since producer gas composition at higher temperatures is favourable for DME synthesis.

Model validation provided detailed information regarding different phenomena. The current understanding of bed material behaviour in the reactor was improved. Reaction kinetics and reaction equilibrium were included in the model to take into account reversibility of carbonation and calcination. The reaction equilibrium between the two reactions played an important role,

since the bed of the gasifier operated close by the reaction equilibrium. At particular operation conditions the process temperature was governing the quantity of carbonation.

The modeling results compared against the measurements show a good agreement. However, further refinement and comprehensive validation of the gasification model with additional data from the pilot reactor is required.

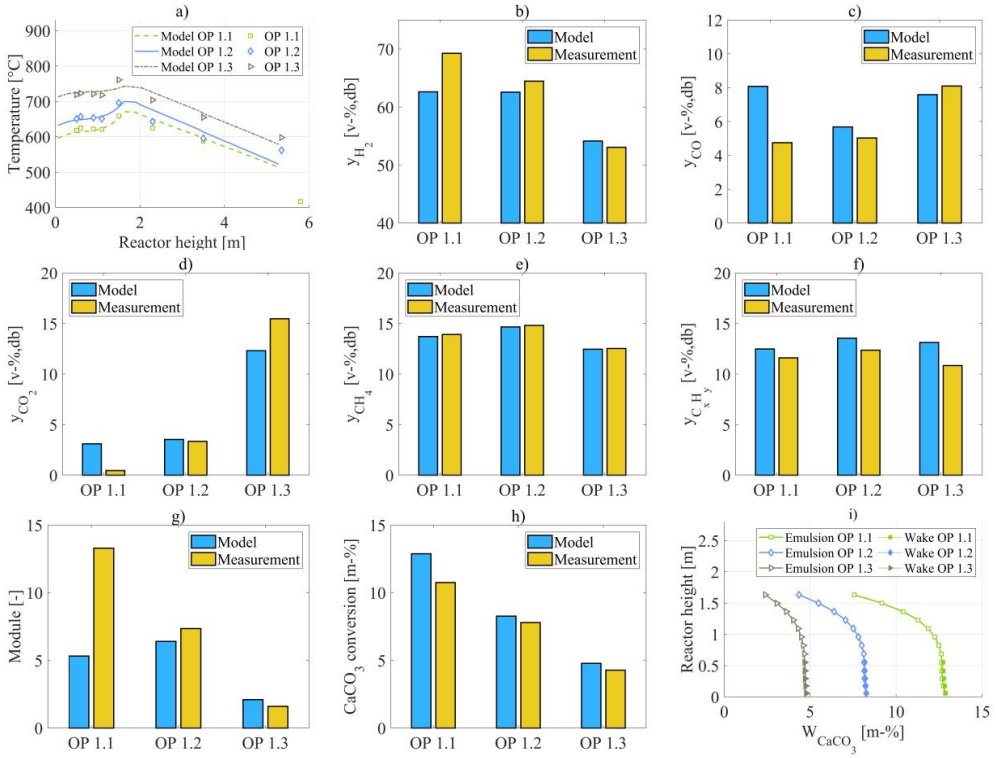

Fig. 2. Simulation results. In Fig. 2 a) Simulated temperature profiles and process measurements from the pilot gasifier. Fig. 2 b) H_2, –c) CO, –d) CO_2, –e) CH_4, and –f) C_xH_y volume fractions of producer gas are shown. Fig. 2 g) Module of producer gas is shown. Producer gas volume fractions are presented as N_2, NH_3, H_2S and tar free and dry basis. In Fig. 2 h) Bed material conversion in the gasifier from CaO to $CaCO_3$ is shown. The bed material conversion was determined from solid samples extracted from loop seals. The conversion is calculated as difference of $CaCO_3$ mass fractions. In Fig. 2 i) Local material fractions for $CaCO_3$ below bed material feeding point is shown.

ACKNOWLEDGEMENT

This work in FLEDGED project has received funding from the European Union's Horizon 2020 research and innovation programme under grant agreement No 727600 .

REFERENCES

Alonso, M., Rodríguez, N., Grasa, G., Abanades, J.C., 2009. Modelling of a fluidized bed carbonator reactor to capture CO2 from a combustion flue gas. Chem. Eng. Sci. 64, 883–891. https://doi.org/10.1016/J.CES.2008.10.044

Biba, V., Macák, J., Klose, E., Malecha, J., 1978. Mathematical Model for the Gasification of Coal under Pressure. Ind. Eng. Chem. Process Des. Dev. 17, 92–98.

Delbeke, J., Vis, P., 2016. EU climate policy explained [WWW Document]. URL https://ec.europa.eu/clima/sites/clima/files/eu_climate_policy_explained_en.pdf

European commission, 2016. A European Strategy for Low-Emission Mobility [WWW Document]. URL https://ec.europa.eu/transparency/regdoc/rep/1/2016/EN/1-2016-501-

EN-F1-1.PDF
Hafner, S., Schmid, M., Scheffknecht, G., 2020. Investigation of the Sorption Enhanced Gasification Process in a Dual Fluidized Bed Pilot Plant Using a Waste-Derived Fuel. Proceeding 13th Int. Conf. Fluid. Bed Technol.
Hafner, S., Spörl, R., Scheffknecht, G., 2018. Sorption Enhanced Gasification : Process validation and investigations on the syngas composition in a 200 kW th dual fluidized bed facility. 23rd Int. Conf. Fluid. Bed Convers. 826–832.
Hajaligol, M.R., Longwell, J.P., Sarofim, A.F., 1988. Analysis and Modeling of the Direct Sulfation of CaCO3. Ind. Eng. Chem. Res. 27, 2203–2210.
Hejazi, B., Grace, J.R., Bi, X., Mahecha-Botero, A., 2017. Kinetic Model of Steam Gasification of Biomass in a Bubbling Fluidized Bed Reactor. Energy and Fuels 31, 1702–1711.
Jones, W.P., Lindstedt, R.P., 1988. Global reaction schemes for hydrocarbon combustion. Combust. Flame 73, 233–249. https://doi.org/10.1016/0010-2180(88)90021-1
Kunii, D., Levenspiel, O., 1991. Fluidization engineering, 2nd ed. Butterwoth-Heinemann.
Martínez, I., Grasa, G., Murillo, R., Arias, B., Abanades, J.C., 2012. Kinetics of calcination of partially carbonated particles in a Ca-looping system for CO2 capture. Energy and Fuels 26, 1432–1440. https://doi.org/10.1021/ef201525k
Myöhanen, K., 2011. Modelling of Combustion and Sorbent Reactions in Three-Dimensional Flow Environment of a Circulating Fluidized Bed Furnace. Acta Universitatis Lappeenrantaensis. Doctoral Dissertation, Lappeenranta.
Nandi, S.P., Onischak, M., 1985. Gasification of Chars Obtained from Maple and Jack Pine Woods, in: Overend, R.P., Milne, T.A., Mudge, L.K. (Ed.), Fundamentals of Thermochemical Biomass Conversion. Springer, Dordrecht, p. 1159.
Neves, D., Thunman, H., Matos, A., Tarelho, L., Gómez-Barea, A., 2011. Characterization and prediction of biomass pyrolysis products. Prog. Energy Combust. Sci. 37, 611–630.
Pitkäoja, A., Ritvanen, J., Hafner, S., Hyppänen, T., Scheffknecht, G., 2020. Simulation of a sorbent enhanced gasification pilot reactor and validation of reactor model. Energy Convers. Manag. 204, 112318. https://doi.org/10.1016/j.enconman.2019.112318
Rajan, R.R., Wen, C.Y., 1980. A comprehensive model for fluidized bed coal combustors. AIChE J. 26, 642–655. https://doi.org/https://doi.org/10.1002/aic.690260416
Shimizu, T., Hirama, T., Hosoda, H., Kitano, K., Inagaki, M., Tejima, K., 1999. A Twin Fluid-Bed Reactor for Removal of CO2 from Combustion Processes. Chem. Eng. Res. Des. 77, 62–68. https://doi.org/10.1205/026387699525882
Stanmore, B.R., Gilot, P., 2005. Review—calcination and carbonation of limestone during thermal cycling for CO2 sequestration. Fuel Process. Technol. 86, 1707–1743.
van den Aarsen, F., Beenackers, A., van Swaaij, W., 1985. Wood pyrolysis and carbon dioxide char gasification kinetics in a fluidized bed, in: Overend, R.P., Milne, T.A., Mudge, L.K. (Ed.), Fundamentals of Thermochemical Biomass Conversion. Springer, Dordrecht, p. 1159. https://doi.org/https://doi.org/10.1007/978-94-009-4932-4_36
Ylätalo, J., 2013. Model Based Analysis of the Post- Combustion Calcium Looping Process for Carbon Dioxide Capture. Acta Universitatis Lappeenrantaensis. Doctoral Dissertation, Lappeenranta.

ACTA UNIVERSITATIS LAPPEENRANTAENSIS

958. KÄRKKÄINEN, HANNU. Analysis of theory and methodology used in determination of electric motor drive system losses and efficiency. 2021. Diss.

959. KIM, HEESOO. Effects of unbalanced magnetic pull on rotordynamics of electric machines. 2021. Diss.

960. MALYSHEVA, JULIA. Faster than real-time simulation of fluid power-driven mechatronic machines. 2021. Diss.

961. SIEVINEN, HANNA. Role of the board of directors in the strategic renewal of later-generation family firms. 2021. Diss.

962. MENDOZA MARTINEZ, CLARA. Assessment of agro-forest and industrial residues potential as an alternative energy source. 2021. Diss.

963. OYEWO, AYOBAMI SOLOMON. Transition towards decarbonised power systems for sub-Saharan Africa by 2050. 2021. Diss.

964. LAHIKAINEN, KATJA. The emergence of a university-based entrepreneurship ecosystem. 2021. Diss.

965. ZHANG, TAO. Intelligent algorithms of a redundant robot system in a future fusion reactor. 2021. Diss.

966. YANCHUKOVICH, ALEXEI. Screening the critical locations of a fatigue-loaded welded structure using the energy-based approach. 2021. Diss.

967. PETROW, HENRI. Simulation and characterization of a front-end ASIC for gaseous muon detectors. 2021. Diss.

968. DONOGHUE, ILKKA. The role of Smart Connected Product-Service Systems in creating sustainable business ecosystems. 2021. Diss.

969. PIKKARAINEN, ARI. Development of learning methodology of additive manufacturing for mechanical engineering students in higher education. 2021. Diss.

970. HOFFER GARCÉS, ALVARO ERNESTO. Submersible permanent-magnet synchronous machine with a stainless core and unequal teeth widths. 2021. Diss.

971. PENTTILÄ, SAKARI. Utilizing an artificial neural network to feedback-control gas metal arc welding process parameters. 2021. Diss.

972. KESSE, MARTIN APPIAH. Artificial intelligence : a modern approach to increasing productivity and improving weld quality in TIG welding. 2021. Diss.

973. MUSONA, JACKSON. Sustainable entrepreneurial processes in bottom-of-the-pyramid settings. 2021. Diss.

974. NYAMEKYE, PATRICIA. Life cycle cost-driven design for additive manufacturing: the frontier to sustainable manufacturing in laser-based powder bed fusion. 2021. Diss.

975. SALWIN, MARIUSZ. Design of Product-Service Systems in printing industry. 2021. Diss.

976. YU, XINXIN. Contact modelling in multibody applications. 2021. Diss.

977. EL WALI, MOHAMMAD. Sustainability of phosphorus supply chain – circular economy approach. 2021. Diss.

978. PEÑALBA-AGUIRREZABALAGA, CARMELA. Marketing-specific intellectual capital: Conceptualisation, measurement and performance. 2021. Diss.

979. TOTH, ILONA. Thriving in modern knowledge work: Personal resources and challenging job demands as drivers for engagement at work. 2021. Diss.

980. UZHEGOVA, MARIA. Responsible business practices in internationalized SMEs. 2021. Diss.

981. JAISWAL, SURAJ. Coupling multibody dynamics and hydraulic actuators for indirect Kalman filtering and real-time simulation. 2021. Diss.

982. CLAUDELIN, ANNA. Climate change mitigation potential of Finnish households through consumption changes. 2021. Diss.

983. BOZORGMEHRI, BABAK. Finite element formulations for nonlinear beam problems based on the absolute nodal coordinate formulation. 2021. Diss.

984. BOGDANOV, DMITRII. Transition towards optimal renewable energy systems for sustainable development. 2021. Diss.

985. SALTAN, ANDREY. Revealing the state of software-as-a-service pricing. 2021. Diss.

986. FÖHR, JARNO. Raw material supply and its influence on profitability and life-cycle assessment of torrefied pellet production in Finland – Experiences from pilot-scale production. 2021. Diss.

987. MORTAZAVI, SINA. Mechanisms for fostering inclusive innovation at the base of the pyramid for community empowerment - Empirical evidence from the public and private sector. 2021. Diss.

988. CAMPOSANO, JOSÉ CARLOS. Integrating information systems across organizations in the construction industry. 2021. Diss.

989. LAUKALA, TEIJA. Controlling particle morphology in the in-situ formation of precipitated calcium carbonate-fiber composites. 2021. Diss.

990. SILLMAN, JANI. Decoupling protein production from agricultural land use. 2021. Diss.

991. KHADIM, QASIM. Multibody system dynamics driven product processes. 2021. Diss.

992. ABDULKAREEM, MARIAM. Environmental sustainability of geopolymer composites. 2021. Diss.

993. FAROQUE, ANISUR. Prior experience, entrepreneurial outcomes and decision making in internationalization. 2021. Diss.

994. URBANI, MICHELE. Maintenance policies optimization in the Industry 4.0 paradigm. 2021. Diss.

995. LAITINEN, VILLE. Laser powder bed fusion for the manufacture of Ni-Mn-Ga magnetic shape memory alloy actuators. 2021. Diss.

LUT University

ISBN 978-952-335-746-4
ISBN 978-952-335-747-1 (PDF)
ISSN-L 1456-4491
ISSN 1456-4491
Lappeenranta 2021